DYNAMIC MECHANICAL BEHAVIOR OF RECYCLED AGGREGATE CONCRETE

LI LONG

PhD

The Hong Kong Polytechnic University

This programme is jointly offered by The Hong Kong Polytechnic University and Tongji University

2018

The Hong Kong Polytechnic University
Department of Civil and Environmental Engineering

Tongji University
Department of Structural Engineering

Dynamic Mechanical Behavior of Recycled Aggregate Concrete

LI LONG

A thesis submitted in partial fulfillment of the requirements for the degree of Doctor of Philosophy

August 2017

CERTIFICATE OF ORIGINALITY

I hereby declare that this thesis is my own work and that, to the best of my knowledge and belief, it reproduces no material previously published or written, nor material that has been accepted for the award of any other degree or diploma, except where due acknowledgement has been made in the text.

_________________(Signed)

LI LONG (Name of student)

ABSTRACT

Using recycled aggregate concrete (RAC) is generally considered as one of the most effective measures to solve the problem of waste concrete. At present, most of the researches on RAC are about its static mechanical behaviors, and only a few are about its dynamic mechanical behaviors. In this study, the dynamic mechanical behaviors of RAC were studied.

Firstly, based on cylindrical RAC specimens and modeled recycled aggregate concrete (MRAC) specimens, the dynamic mechanical behaviors of RAC under uniaxial compressive loadings at low strain rates (10^{-5}/s to 10^{-1}/s) were experimentally studied. The strain-rate sensitivity of RAC and the influence of recycled coarse aggregate (RCA) replacement percentage, the static strength, and the moisture condition were studied. The results showed that with the increase in strain rate, the peak stress and elastic modulus of RAC increased, the peak strain fluctuated around a constant value, while the failure pattern had no obvious difference. The strain-rate sensitivity of RAC with lower static strength was more significant. The strain-rate sensitivity of RAC with 100% RCA was larger than that of natural aggregate concrete (NAC). There was no significant difference between the strain-rate sensitivity of RAC under wet and air-dry conditions.

Secondly, based on the cylindrical RAC specimens, the dynamic mechanical behaviors of RAC under uniaxial compressive loadings at high strain rates (10^{1}/s ~ 10^{2}/s) were experimentally studied by using a Split Hopkinson Pressure Bar (SHPB). The strain-rate sensitivity of RAC and the influences of the RCA replacement percentage and moisture condition were explored. The results showed that at high strain rates, the peak stress and elastic modulus of RAC increased with the increase in strain rate and the increase was more significant than that at low strain rates, the peak strain fluctuated around a constant value with the increase in strain rate, there were more fractured aggregates than that at low strain rates, the strain-rate sensitivity of RAC was slightly larger when RCA replacement percentage was higher, and the moisture condition had no significant influence on the strain-rate sensitivity of RAC.

Thirdly, MRAC specimens were used to study the effect of carbonation on the mesoscopic properties of RCA and the static mechanical behavior of RAC. The effect of using carbonated RCA on the dynamic mechanical behaviors of RAC at low strain rates was studied based on the cylindrical specimens. The results showed that the old ITZ and old mortar in RCA were enhanced

after carbonation, the static and dynamic peak stress and elastic modulus of RAC with carbonated RCA increased, while the strain-rate sensitivity of RAC with carbonated RCA decreased.

Based on the test results, the relation between the dynamic increase factor of peak strain (DIF_f) of RAC and the strain rate ranging from 10^{-5}/s to 10^{2}/s was established, and the mechanism of strain-rate sensitivity of RAC was discussed. It showed that Stefan effect, inertia force effect and cracking development were not the main cause of the strain-rate sensitivity of RAC at low strain rates; at high strain rates, Stefan effect and transverse inertia effect had no significant influence on the strain-rate sensitivity of RAC, while longitudinal inertia effect had some influence on the strain-rate sensitivity of RAC but it was still not the leading factor. The strain-rate dependence of crack propagation resistance of meso-phase materials may be the leading factor of strain-rate sensitivity of RAC when the strain rate varied from 10^{-5}/s to 10^{2}/s. In addition, a static and dynamic model of RAC was established, which explained the reason why the strain-rate sensitivity of RAC with 100% RCA was larger than that of NAC.

Finally, finite element model based on the MRAC was established. Considering the strain-rate sensitivity of all meso-phase materials (i.e. mortar, ITZ, and aggregate), the overall strain-rate sensitivity of RAC was studied. The influences of the strain-rate sensitivity of each meso-phase material on the overall strain-rate sensitivity of RAC were also studied. Moreover, the influence of RCA replacement percentage and the strength of the new mortar and the old mortar on the strain-rate sensitivity of RAC were studied. The simulation results showed that the peak stress and elastic modulus of RAC increased almost linearly with the increase in strain rate, and the increasing of elastic modulus was more uniform. When compared with ITZ and aggregate, the strain-rate sensitivity of RAC were mainly decided by the strain-rate sensitivity of the mortar in RAC. There was no clear relationship between the RCA replacement percentage and the strain-rate sensitivity of peak stress, while the strain-rate sensitivity of elastic modulus was larger when the RCA replacement percentage was larger. When the strength of the new mortar or the old mortar was lower, the strain-rate sensitivity of elastic modulus was greater, but the strain-rate sensitivity of peak stress did not show a strict increase.

Key Words: Recycled aggregate concrete (RAC), strain-rate sensitivity, recycled coarse aggregate (RCA) replacement percentage, moisture condition, carbonation.

PUBLICATIONS ARISING FROM THE THESIS

Academic Journal Papers:

[1] **Li Long**, Xiao Jianzhuang, Poon Chi Sun. Effect of carbonation of recycled coarse aggregate on the mechanical properties of recycled aggregate concrete [J]. *Cement & Concrete Composites*, 2018, 89: 169-180. (SCI, EI)

[2] **Li Long**, Poon Chi Sun, Xiao Jianzhuang, Xuan Dongxing. Effect of carbonated recycled coarse aggregate on the dynamic compressive behavior of recycled aggregate concrete [J]. Construction and Building Materials, 2017, 151: 52-62. (SCI, EI)

[3] **Li Long**, Xiao Jianzhuang, Huang Kaiwen. Simulation on strain-rate sensitivity of mechanical properties of recycled aggregate concrete [J]. *Journal of Southeast University (Natural Science Edition)*, 2017, 47(4): 776-784. (in Chinese) (EI)

[4] **Li Long**, Xiao Jianzhuang, Poon Chi Sun. Dynamic compressive behavior of recycled aggregate concrete [J]. Materials and Structures, 2016, 49:4451-4462. (SCI, EI)

[5] Wang Chunhui, Xiao Jianzhuang, Zhang Guanzhen, **Li Long**. Interfacial properties of modeled recycled aggregate concrete modified by carbonation [J]. Construction and Building Materials , 2016, (105)：307-320. (SCI, EI)

[6] Xiao Jianzhuang, **Li Long**, Shen Luming, Poon Chi Sun. Compressive behaviour of recycled aggregate concrete under impact loading [J]. Cement and Concrete Research, 2015, 71: 46-55. (SCI, EI)

[7] Xiao Jianzhuang, **Li Long**, Shen Luming, Yuan Junqiang. Effects of strain rate on mechanical behavior of modeled recycled aggregate concrete under uniaxial compression [J]. Construction and Building Materials, 2015, 93: 214-222. (SCI, EI)

[8] Xiao Jianzhuang, **Li Long**, Tam Vivian W.Y., Li Hong. The state of the art regarding the long-term properties of recycled aggregate concrete. Structural Concrete. 2014, 15(1):3-12. (SCI, EI)

[9] Xiao Jianzhuang, Huang Kaiwen, **Li Long**. Numerical simulation on static force and fatigue behaviors of modeled recycled aggregate concrete under uniaxial compression [J]. *Journal of*

Southeast University (Natural Science Edition), 2016, 46(3): 552-558. (in Chinese). (EI)

[10] Xiao Jianzhuang, Yuan Junqiang, **Li Long**. Experimental study on dynamic mechanical behavior of modeled recycled aggregate concrete under uniaxial compression [J]. *Journal of Building Structures*, 2014, 35(3): 201-207. (in Chinese) (EI)

[11] Xiao Jianzhuang, Li Hong, **Li Long**. Investigation on fatigue behavior of recycled aggregate concrete under flexure loading [J]. *Journal of Southeast University (Natural Science Edition)*, 2012(42): 340-345. (in Chinese) (EI)

Conference Paper:

[1] Xiao Jianzhuang, **Li Long**. Review on Recycled Aggregate Concrete in the Past 15 Years in China [C]. *Third International Conference on Sustainable Construction Materials and Technologies*, Japan, 2013.

[2] **Li Long**, Xiao Jianzhuang. Discussion on dynamic behavior of recycled aggregate concrete [C]. *The 3rd National Academic Conference on Recycled Concrete*, Beijing, 2012. (in Chinese)

[3] Yuan Junqiang, Xiao Jianzhuang, **Li Long**. Review of concrete dynamic properties and analysis of compressive strength of recycled aggregate concrete under different loading rate [C]. *The 3rd National Academic Conference on Recycled Concrete*, Beijing, 2012. (in Chinese)

ACKNOWLEDGEMENT

First, I would like to express sincere thanks to my chief supervisor, Prof. Poon Chi Sun, for his patient guidance in research and his care in my daily life. When I am Hong Kong, Prof. Poon has given me largest support so that I can enjoy the research without pressure. I am also vey grateful to my chief supervisor in Tongji University, Prof. Xiao Jianzhuang, for his guidance and care no matter I am in Shanghai or in Hong Kong.

I would like to acknowledge the Joint PhD Programme Leading to Dual Awards between Tongji University and The Hong Kong Polytechnic University. I would like to acknowledge the financial support from the National Natural Science Foundation of China (51325802) and The Hong Kong Polytechnic University (Asian University Cluster - Centre of Excellence in Civil Engineering)

I would like to thank Prof. Wu Xutao for his guidance and help in the test, I would like to thank Prof. Ren Xiaodan for his help in the test, I would like to thank Prof. Li Jie, Prof. Zhao Ming, Prof. Chen Jun, Prof. Chen Jianbin and Prof Xie Qiang for their suggestions to me.

I would like to thank Mr. Yuan Junqiang for his preliminary research work. I would like to thank Dr. Xuan Dongxing and Dr. Zhan Baojian for their advice for my research. I would like to thank Mr. Zheng Shitong, Mr. Zhang Kaijian, Mr. Xie Qinghai, and so on, for their help in my expeiment. I would like to thank Mr. Wong K.H. for his assistance in my experiment.

I would like to thank Dr. Guo Mingzhi, Dr. Duan Zhenhua, Dr. Tu Zhenju, Mr. Wang lei and all other colleagues in my research group in PolyU for their help and care in my life. I also would like to thank all the colleagues in my research group in Tongji University for their help and care in my life. It's my pleasure to meet them in my life and become friends with them.

I would like to thank Mr. Chang, Ms. Peng and Ms Zhang who instructs me to understand the foundation, the value and the direction of life and also the meaning of research. I would like to thank my colleagues for their companions and encouragement.

Finally, special thanks to my parents and relatives, their selfless love and silence support are my shield wherever I am, whatever I do.

CONTENTS

LIST OF FIGURES

LIST OF TABLES

LIST OF ABBREVIATIONS

AVG	Average value
C&DW	Construction and demolition waste
CRAC	Carbonated recycled aggregare concrete
CRCA	Carbonated recycled coarse aggregare
C-S-H	Calcium-Silicate-Hydrate
DIF_E	Dynamic increase fortor of elastic modulus
DIF_f	Dynamic increase fortor of peak stress
DIF_{f_c}	Dynamic increase fortor of compressive strength
DIF_{f_t}	Dynamic increase fortor of tensile strength
DIF_ε	Dynamic increase fortor of peak strain
DIF_t	Dynamic increase factor of toughness
ITZ	Interface transition zone
LVDT	Linear variable differential transformer
MNAC	Modeled natural aggregate concrete
MNCA	Modeled natural coarse aggregare
MRAC	Modeled recycled aggregare concrete
MRCA	Modeled recycled coarse aggregare
NAC	Natural aggregate concrete
NCA	Natural coarse aggregare
PVC	Polyvinylchloride
RAC	Recycled aggregare concrete
RCA	Recycled coarse aggregare
SD	Standard deviation
SHPB	Split Hopkinson Pressure Bar
w/c	Water to cement ratio

Chapter 1 Introduction

1.1 Research background and significance

With the rapid growth in the world's population, the process of urbanization in the world is also very rapid. As one of the pillars of the national economy, the construction industry is also flourishing. More than 3 billion tons of raw materials per year are used to produce building materials, accounting for about 40% to 50% of the global economy (Sagoe-Crentsil et al. 2001). But at the same time, huge quantities of construction and demolition waste (C&DW) are produced. Over the past 20 years, the amount of C&DW produced in China increased continuously, as shown in Fig. 1-1. The amount of C&DW is particularly shocking, and it is still increasing with the pace of urbanization. It is expected that the amount of C&DW generated in China will reach its peak around 2020. In China, the amount of C&DW has accounted for 30% to 40% of the total amount of urban waste (Xiao 2008).

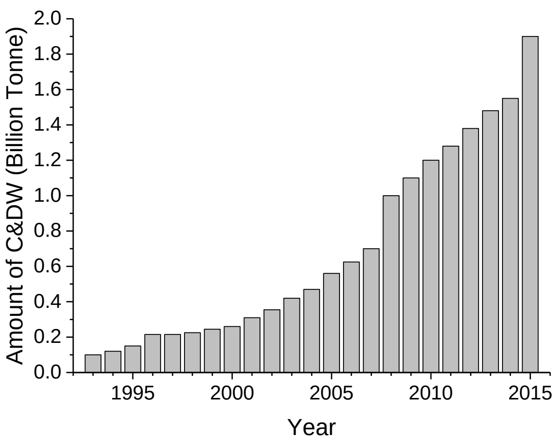

Fig. 1-1 Amount of C&DW in China

Earthquakes, tsunamis and hurricanes and other natural disasters also lead to the generation of a huge amount of demolition waste. For example, in the Wenchuan earthquake, there were about 6.8 million collapsed houses, 2300 million damaged houses of which about 50% were demolished (Xiao et al. 2008), and construction waste generated from the collapsed houses and the demolition of the dangerous houses was up to 500 million tonnes. In 2010, the construction waste generated in the Yushu earthquake was also more than 4 million tonnes. The 2010 Haiti earthquake damaged almost half of the buildings in the Haitian Republic, producing about 15 million m^3 of construction waste (Li 2013). In the United States, the total amount of construction waste generated by natural disasters is 5 to 15 times the average annual amount of construction waste generation in the affected area (Basnayake et al. 2006).

Such a large volume of C&DW will have a serious impact on our environment. The dumping of C&DW will take up a lot of land, and damage the structure of the soil and degrade the quality of the soil. At the same time, it will pollute the surrounding water and soil which have an adverse effect on the city appearance and the environment. As a result, various policies have been adopted in the world to deal with the problem of C&DW, including actively promoting the use of C&DW. According to the relevant statistics (Xiao 2008), in the current composition of the C&DW, waste concrete accounts for the largest proportion, which is up to 41%. Therefore, the reuse of waste concrete is an important part of the utilization of C&DW, and it can play a significant role in the sustainable development strategy in China.

Using concrete produced with recycled aggregate, which is also called recycled aggregate concrete (RAC), is usually considered as one of the most effective measures to solve the problem of waste concrete. The utilization of RAC can not only solve the disposal problem of waste concrete, but also reduce the consumption of natural aggregates, thereby reducing the damage to the natural environment resulting from the gravel mining. Therefore, the development of RAC technology has been regarded as one of the important measures to develop green ecological concrete and realize the sustainable uses of construction resources.

Because of the Second World War, many countries almost turned into ruins. After that, it needed a lot of reconstruction in which the construction waste disposal was also a big problem. Therefore, after the Second World War, the former Soviet Union, Japan, Germany and other countries began to carry out research on the waste concrete treatment and recycling (Nixon 1978; Topcu 1995). Subsequently, the United States, South Korea, Austria, the Netherlands and many other countries have proposed requirements or approaches for the reuse of C&DW. So far, RILEM has held five international conferences on the recycling of waste concrete. In 2002, the ACI approved the evaluation and treatment of waste concrete that could be used for recycling (ACI Committee 555 2002). In recent years, researchers in China have also carried out a lot of studies on RAC. Up to the present, four national meetings on the RAC have been held in China. At the same time, the government of China is actively promoting the implementation of specifications and standards on the RAC. In general, although up till now RAC has not been widely used and it is rarely used in engineering structure, the structural RAC technology are being studied and promoted worldwide.

As we know, concrete structures are likely to suffer from earthquakes, impacts, explosions and other dynamic loadings in their life cycles. It has been generally accepted that the concrete material shows different properties under different dynamic loadings. In other words, it is a strain-rate sensitive material, i.e., its strength, elastic modulus and other properties change with the strain rate. Therefore, in the dynamic design or safety evaluation of concrete structure, the strain-rate sensitivity of concrete should be considered. As a special kind of concrete, RAC is also strain-rate sensitive under dynamic loading. But so far, most studies on the RAC have been limited to the static properties, and very few researches on the dynamic properties of RAC can be found. Therefore, it is essential to study the dynamic mechanical properties of RAC to promote its application in the engineering structure. Moreover, the study of the dynamic mechanical properties of RAC has other significances which are shown as follows.

First, wars or natural disasters will cause large-scale structures failure or even collapse. In the reconstruction process, the use of RAC will reduce a lot of construction waste clean-up work, and also overcome the shortage of local natural aggregate. Also, the structures in war or natural disaster prone areas may suffer from wars or natural disasters again. Therefore, it is essential to consider the dynamic properties of RAC in these areas. In addition, it is known that the static mechanical properties of RAC are generally inferior to that of conventional concrete because of the larger number of weak interface transition zone (ITZ). However, because the influence of ITZ on the dynamic mechanical properties of concrete is smaller (Du & Jin 2015), the dynamic mechanical properties of RAC may be more close to that of conventional concrete, which is an advantage to promote the application of RAC.

1.2 Reviews on the static mechanical properties of RAC

At present, a large number of researchers have carried out studies on the static mechanical properties of RAC under tensile, compressive, bending and shear loadings. It is shown that the properties of recycled aggregate and natural aggregate are different, leading to the difference between the mechanical properties of RAC and NAC. Therefore, there are a lot of researches on the modification of recycled aggregate or RAC. In this paper, the static mechanical properties of

RAC are briefly introduced from the aspects of compressive properties, tensile properties, flexural properties and modification of RAC.

1.2.1 Compressive properties of RAC

1.2.1.1 Compressive strength

Compressive strength is one of the most important mechanical properties of concrete, a large number of studies have shown that the compressive strength of RAC is lower than that of natural aggregate concrete (NAC) with same water-to-cement ratio (w/c). Nixon (1978) showed that the compressive strength of RAC was 20% lower than that of NAC. Ravidrarajah (1985) reported that the compressive strength of RAC was reduced by about 8% to 24%. Gerardu (1985) pointed out that the compressive strength of RAC was about 95% or more of NAC. Hu et al. (2009) founded that the cube compressive strength of RAC with 100% recycled coarse aggregate (RCA) was about 11% lower than the corresponding strength of NAC. However, some researchers have found that the compressive strength of RAC may be higher than that of NAC, such as Yoda and Yoshikane (1988). The test results reported by Xiao et al. (2004) showed that the compressive strength of RAC with 30%, 70% and 100% RCA were 24%, 28% and 30% lower than that of NAC, respectively, but the compressive strength of RAC with 50% RCA was higher than that of NAC.

The reason why different researchers have different conclusions is that there are many factors that affect the compressive strength of RAC, including the RCA replacement percentage, w/c, brick content, the sources of RCA and so on (Xiao 2008).

1.2.1.2 Elastic modulus

In general, the elastic modulus of RAC decreases with the increase in RCA replacement percentage. That is because there are more old mortar attached to the surface of RCA and also more micro-cracks produced in the crushing process in RAC with higher RCA replacement percentage. The results reported by Kou et al. (2007) showed that the elastic modulus of RAC decreases with the increase in RCA replacement percentage. When the RCA replacement percentage is 100%, the elastic modulus of RAC is 40% lower than that of NAC. Xiao et al. (2005) reported that the elastic modulus of RAC with 100% RCA is reduced by as much as 45%. Frondistou-Yannas (1977), Wesche and Schulz (1982) showed that decreasing rate were 33% and 19%, respectively. The results of Domingo-Cabo (2009) show that the elastic modulus of RAC decreases with the increase in RCA replacement percentage, but when the RCA replacement percentage was 50%, the elastic modulus of RAC is larger than that of RAC with 20% RCA.

1.2.1.3 Peak strain

Some researchers studied the effect of the RCA replacement percentage on the peak strain of RAC. The results show that the peak strain of RAC with the same w/c is larger than that of NAC. Xiao et al. (2005) studied the compressive stress-strain curves of RAC with different RCA replacement percentages. It was found that the peak strain of RAC increased with the increase in the RCA replacement percentage. When the RCA replacement percentage is 100%, the peak strain was 20% higher than that of NAC. In addition, Deng et al (2008), Du et al. (2010) also pointed out that the peak strain of RAC is greater than the peak strain of the corresponding NAC.

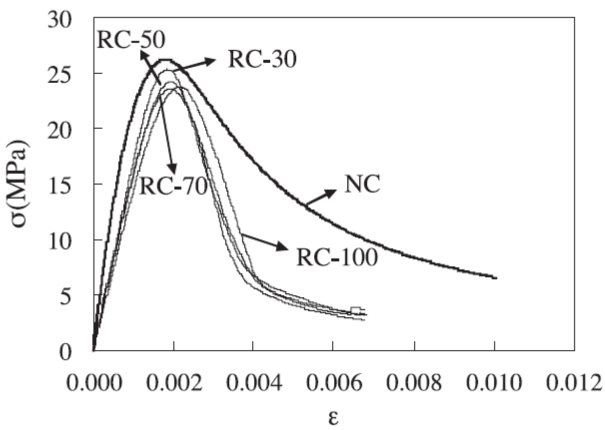

Fig. 1-2 Typical stress-strain curve of RAC under uniaxial compression (Xiao et al. 2005)

1.2.1.4 Compressive stress-strain curve

The stress-strain curve of concrete can comprehensively reflect its characteristics. So far, scholars have conducted a lot of researches on the stress-strain relationship of NAC, but the researches on the stress-strain curve of RAC are few. As early as the 1980s, Henrichshen and Jensen Xiao et al (1989) studied the stress-strain curve of RAC, it was found that the stress-strain curve of RAC was similar to that of NAC. Topcu (1995) studied the stress-strain curve of RAC with different RCA replacement percentage, it was found that the compressive strength and elastic modulus of RAC decreased with the increase in RCA replacement percentage. Xiao et al. (2007) and Xiao (2007) studied the stress-strain curve of RAC under uniaxial compression and showed that the overall shape of stress-strain curve of RAC is similar to that of NAC, but the stress and strain values at the important points in the curve are different, as shown in Fig. 1-2.

1.2.2 Tensile properties of RAC

Ravindrarajah and Tam (1985) found that the splitting tensile strength of RAC cylinders was not significantly different from that of NAC. Gerardu and Hendriks (1985) reported that the splitting tensile strength of RAC was about 10% lower than that of NAC. Ikeda and Yamane (1988) showed that the tensile strength of RAC is about 6% lower than that of RAC. Liu et al. (2011) found that the tensile strength of RAC was similar to that of NAC with the same w/c. Gupta (2001) pointed out that when the w/c was low, the tensile strength of RAC was lower than that of NAC, but the tensile strength of RAC was higher than that of NAC when the w/c was high. The variation inin the tensile strength of RAC with the age is the same as that of NAC. Xiao and Lan (2006) showed that the tensile strength of RAC was lower than that of NAC, and when the RCA replacement percentage was 100 %, the tensile strength of RAC is about 30% lower than that of NAC. Moreover, the tensile stress-strain curve of RAC is similar to that of NAC. When the RCA replacement percentage increases, the tensile peak strain increases slightly, but the tensile strength and elastic modulus decrease as shown in Fig. 1-3.

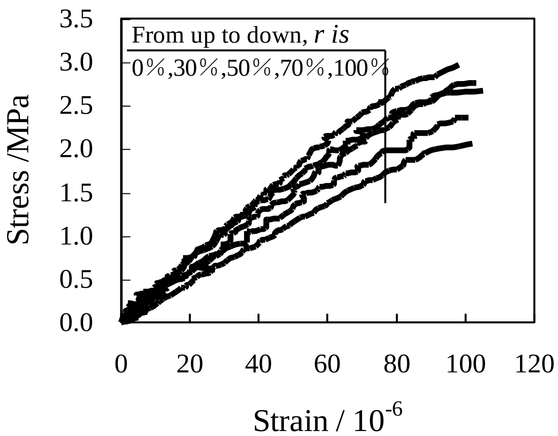

Fig. 1-3 Typical stress-strain curve of RAC under uniaxial tensile loading (Xiao & Lan 2006)

1.2.3 Flexural strength of RAC

Kawamura et al. (1988), Xiao et al. (2005) and Cheng et al. (2005) showed that the flexural strength of RAC was almost the same as that of NAC. Ravindrarajah and Tam (1987) reported that the flexural strength of RAC is 10% lower than that of NAC. The results of Mandal and Gupta (2002) showed that the flexural strength of RAC is lower than that of NAC, and the average decrease is 12%. Topçu et al. (2004) pointed out that with the increase in RCA replacement percentage, the flexural strength of RAC decreases. In addition, B.C.S.J (1978) found that the flexural strength of RAC is about 1/5 ~ 1/8 of its compressive strength, which is similar to that of NAC.

1.2.4 Modification methods for RAC

Because of the presence of the adhered old mortar, the porosity and water absorption of RCA are larger than that of natural coarse aggregate (NCA). The high water absorption of RCA may lead to a loose and porous ITZ between the RCA and the new cement mortar in RAC (Poon et al. 2004). In addition, the micro-cracks present in the RCA will weaken the properties of RAC. It is for these reasons, the application of RAC was limited and it was seldom used in structural concrete. To extend the application of RAC, it is essential to conduct pretreatment work to enhance the properties of RCA and thus improve the properties of RAC.

Therefore, many researchers began to conduct investigations on the techniques of RCA pretreatment to improve the properties of RAC. Kou and Poon (2010) reported that polyvinyl alcohol (PVA) solution can be used to improve the properties of RCA and thus increase the strength and durability of RAC. Otsuki et al. (2003), Tam et al. (2005) and Elhakam et al. (2012) pointed out that using a two-stage mixing approach could enhance the properties of RAC, that is because the RCA will be coated with mortar of a lower water-binder ratio in the premix process, which can lead to a stronger ITZ. Elhakam et al. (2012) proposed two other types of methods which can also improve the mechanical properties of RAC. One is the self-healing method by immersing the RCA in water up to 30 days which increased the property of RCA because the unhydrated cement particles will react again with water, the other is adding silica fume as a cement admixture which can enhance the ITZ and also the RCA itself. In addition, it has been recently reported that the mechanical properties of RAC can be improved when using the carbonated RCA (CRCA) (Kou et al. 2014; Zhan et al. 2014; Xuan et al. 2016; Zhang et al. 2015) because the carbonation process can improve the properties of RCA. Moreover, the carbonation approach is lower in cost and it is more environmentally friendly when compared with other approaches due to CO_2 sequestration by RCA (Monkman & Shao 2010).

1.2.5 Modeled recycled aggregate concrete (MRAC)

In the past, many researchers have attempted to study the complex mechanical properties of concrete from simplified concrete models. Shah et al. (1966) studied the mechanical properties and crack development of concrete using a structural element analysis model, which was a thin plate specimen made of cylindrical aggregate and mortar. Buyukozturk et al. (1971), Liu and Nilson (1978), Tasuji et al. (1972) used concrete models to study the stress-strain relationship and failure mechanism of concrete under uniaxial and biaxial stress. Guo and Shi (2003) reported that using a square plate specimen (127mm×127mm×12.7mm) in the concrete test was helpful to make the specimen close to the ideal plane stress state, and it was easier to get the information of crack development. In 2007, Corr et al. (2007) studied the ITZ and the fracture process of concrete using concrete models with a single or two aggregates. In 2006, Tregger et al. (2006) adopted concrete models with one or three aggregates to study the effect of randomness at the mesoscale scale on the fracture properties of concrete.

Based on the nine aggregates concrete model proposed by Buyukozturk et al. (1971), Xiao et al. (2011) proposed the concept of modeled RAC (MRAC). Compared with the natural aggregate, the modeled RCA (MRCA) has a layer of old mortar and old ITZ outside the parent natural aggregate, so there are many old mortar and old ITZ in the MRAC. Li et al. (2011), Li et al. (2012), Xiao et al. (2012) used the nine aggregates MRAC to carry out experimental study on the static mechanical behaviors of RAC. It was shown to be an effective method to study the mechanical behavior of RAC. Numerical studies were also conducted to investigate the compressive mechanical behavior of RAC and the failure mechanism of the RAC.

1.3 Reviews on the dynamic mechanical properties of NAC

The dynamic mechanical properties of concrete mainly refer to the strength and deformation properties of concrete under various dynamic loadings. The concrete structures are likely to suffer from dynamic loadings during their life cycle, for example, high-rise buildings need to withstand wind loads, dams need to withstand hydrodynamic pressure, ocean platforms need to withstand waves, and various structures are likely to suffer from seismic loads, terrorist attacks or accidents caused by the explosive load, so a lot of interest has been paid on studying the dynamic mechanical properties of concrete. Especially in recent years, earthquakes, tsunamis and other natural disasters become more frequent, more and more terrorist attacks arise around the world, the study on the dynamic mechanical properties of concrete become more urgent.

The strain rate of the concrete structure under different load shows a large variation. It is less than 10^{-6} /s under creep load, between 10^{-6} /s and 10^{-5} /s under quasi-static load, between 10^{-4} /s and 10^{-2} /s under earthquake load, when under impact load it is usually between 10^{0} /s and 10^{2} /s, and under explosive load it is above10^{2} /s, as shown in Fig. 1-4. A lot of studies have shown that concrete is a strain-rate sensitive material. Therefore, if using the static mechanical properties of concrete to calculate the response of concrete structure under dynamic loadings, it will produce a large error or even the wrong results. In the current seismic design of concrete structures, it is done by increasing the static mechanical properties of concrete to a certain percentage to consider the dynamic mechanical properties, but this approach is too rough. Therefore, in order to carry out more accurate dynamic design and safety evaluation of concrete structures, it is urgently needed to study the dynamic mechanical properties of concrete and its mechanism, and establish a more accurate dynamic constitutive model.

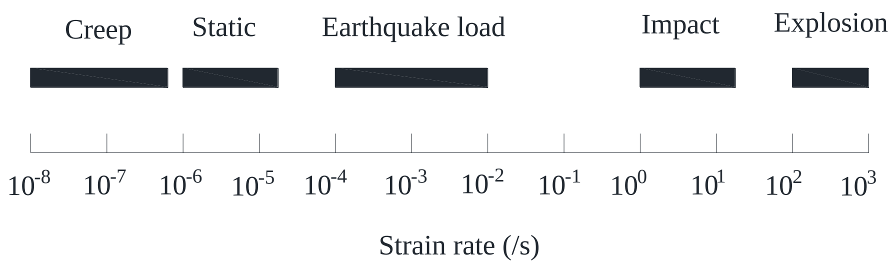

Fig. 1-4 The strain rate corresponding to different loadings

1.3.1 Testing technology for dynamic loading

Because the variation inin strain rate is very large, there is still no test equipment to test the dynamic mechanical properties of concrete under various strain rates, which is a limitation on the research on the dynamic mechanics of concrete. At present, there are several common dynamic test equipments: hydraulic test system, drop hammer, and Split Hopkins Pressure Bar (SHPB). These test equipments have different sources of power, which produce loads with different loading rates. The following will be a brief introduction to these test equipments.

1.3.1.1 Hydraulic test system

The hydraulic testing system is one of the most commonly used mechanical test equipments. It is a testing system that uses liquid as the driving force to transmit the medium. This type of test equipment is usually used for static loading, and it can achieve a load of which the corresponding strain rate is usually in the range of 10^{-6} /s to 10^{-2} /s. However, with the development of testing technology, it can achieve a higher loading rate by adding a rapid response pump and a valve, which can be used for dynamic testing. This type of test equipment has many advantages: it has the flexibility to control the load, accurately measure the load and deformation values, and also achieve a relatively constant strain rate or loading rate during the loading process. But the cost of such equipment is high, and it is difficult to achieve higher strain rates.

Many researchers have used this type of testing system to study the dynamic compressive or tensile behavior of concrete. Xiao et al. (2001, 2002) used a MTS hydraulic servo fatigue testing machine for dynamic compression and tensile test of concrete materials. The strain rate is in the range of 10^{-5} /s ~ 10^{-2} /s in the tensile tests, and it is in the range of 10^{-5} /s ~ 10^{-1} /s in the compression tests. Yan et al. (2006a, 2006b) also carried out dynamic mechanical tests by the 810NEW electrohydraulic servo testing machine on concrete materials with a strain rate range of about 10^{-5} /s ~ 10^{-2} /s in the compression tests and about 10^{-5} /s ~ $10^{-0.3}$ /s in the tensile tests. Dong et al. (1997) used the MTS 815.02 electro-hydraulic servo testing system to carry out dynamic compression tests on the cylindrical concrete specimens with a strain rate range of 10^{-5} /s ~ 10^{2} /s. Zeng and Li (2013) and Zeng et al. (2013) studied the dynamic mechanical properties of concrete using a MTS 815.04 testing machine, and the strain rates in the compression and tensile tests varied from 10^{-5} /s to 3.5×10^{-2} /s.

1.3.1.2 Drop hammer

A drop hammer is a loading device that controls the magnitude of the strain rate actually applied to the specimen by setting the weight of the hammer, the drop height, the thickness of cushion for landing collision, and so on. Using this testing system, a higher loading rate than the hydraulic testing system can be obtained, and the strain rate range is usually about 1 /s to 10 /s. A typical drop hammer testing system is given by Rao et al. (2011), shown in Fig. 1-5. The advantage of the testing system is that the equipment is simple, the cost is low, and a higher strain rate can be obtained. The disadvantage is that it is difficult to accurately measure the load and the deformation of the specimen, and it is difficult to achieve a constant loading rate.

There are also many researchers using drop hammer to study the dynamic properties of concrete. Watstein (1953) conducted an impact test with a 63.56 kg weight drop from 1.68 m height on the concrete specimens with size Φ76.2 mm × 152.4 mm, the strain rate was from 10^{-6} /s to 10 /s. Atchley and Furr (1967) conducted an impact test on the concrete with a drop hammer from 6.10 m height, they found the dynamic strength increased by up to 1.6 times. Sukontasukkul et al. (2004) used a 578 kg hammer to perform impact load on the Φ100mm × 200mm concrete specimen, the speed was 2.21m/s and 3.13m/s respectively when the height of the drop hammer was 250mm and 500mm, and the strain rate was in the range of about 1 /s ~ 10 /s. Elfahal et al. (2005) used this testing system to perform impact tests on cylindrical concrete specimens of different sizes at an impact velocity of 5 m/s and 7 m/s, with a corresponding strain rate of about 1 /s to 10 /s.

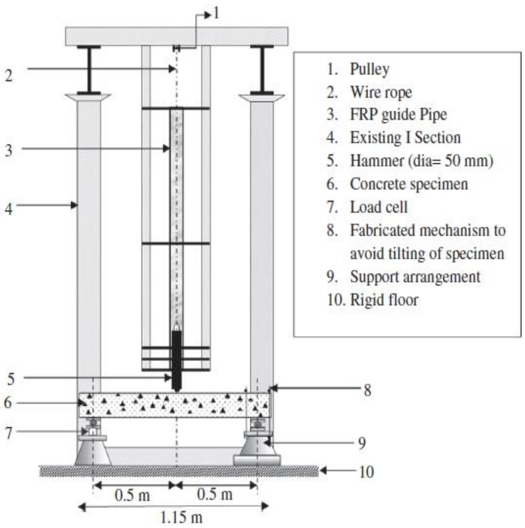

Fig. 1-5 Typical drop hammer testing system (Sukontasukkul et al. 2004)

1.3.1.3 Split Hopkinson Pressure Bar (SHPB)

The SHPB testing system is considered to be the most effective method to measure the dynamic mechanical properties of solid materials at high strain rate which is usually in the range of 10^1 /s ~10^3 /s. It is also the most common method to study the dynamic mechanical properties of concrete. The experimental technique was proposed by Hopkinson (1914), and after its improvement by Kolsky (1949), its basic composition is still used today. A typical SHPB test device is displayed in the study by Grote et al. (2001), as shown in Fig. 1-6. The experimental principle will be introduced in chapter 4. The subtlety of the SHPB testing system is the decoupling of the stress wave effect and the strain rate effect, as described in the literatureWang (2005). In addition, the testing system has the advantage of being a simple structure, accurate measurement method, easy to control the loading waveform, and provide a wide range of strain rate etc. However, there are some limitations when using the SHPB testing system to test the dynamic properties of concrete. On the one hand, in the SHPB test, it is assumed that the internal stress and strain of the specimen is uniform, but in reality it is difficult for the concrete material to satisfy this assumption. On the other hand, because the aggregate size of the concrete is large, and there are many initial cracks in concrete. In order to ensure accuracy, it is normally required that the concrete specimen has a larger size, so it is neccesary to adopt a larger size SHPB test machine, which is more difficult to biuld.

Many researchers (e.g., Grote et al. 2001; Ross et al. 1995, 1996; Chen et al. 2013; Xiao et al. 2009; Wang et al. 2008) used the SHPB to test the impact compression properties of concrete. There are also some researchers (e.g., Brara et al. 2004; Asprone et al. 2009; Cadoni et al. 2009) using the SHPB test device to test the axial tensile properties of concrete. Some scholars (e.g., Ross et al. 1995; Tedscoet al. 1993; Lambert et al. 2000) and Chen et al. (2014) have used the device to test the dynamic splitting performance of concrete. In addition to the experimental study, some numerical studies (e.g., Wu et al. 2010; Brara et al. 2001; Li et al. 2003) on the dynamic mechanical properties of concrete through the use of SHPB devices were conducted to explore the problems using this type of test device for dynamic tests on concrete.

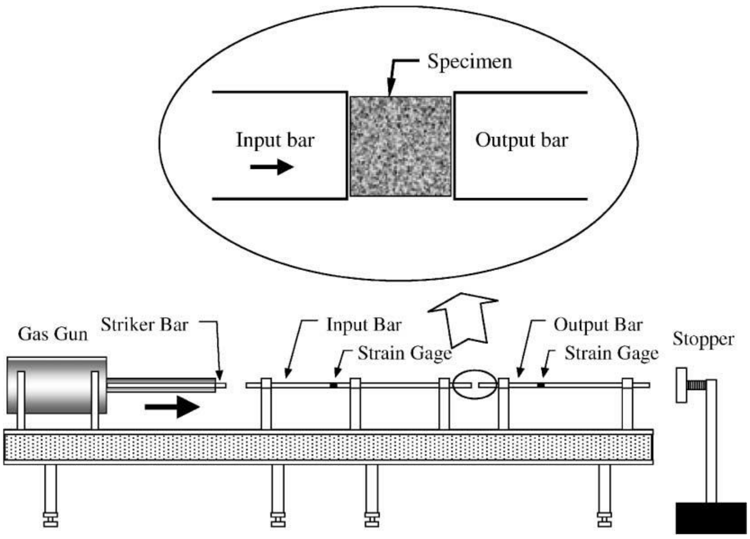

Fig. 1-6 Typical SHPB testing system (Grote et al. 2001)

1.3.2 Strain-rate sensitivity of concrete

1.3.2.1 Strain-rate effect on stress-strain curve of concrete

Many researchers have studied the stress-strain curves under dynamic loadings and there are two different points of view. One is that, as the strain rate increases, the stress-strain curve is similar in shape and the elastic modulus does not change. For example, Dong et al. (1997) studied the stress-strain curve of a cylindrical specimen with a strain rate of 10^{-5} /s ~ 10^{2} /s. The results show that the peak stress and peak strain increased with the strain rate while the elastic modulus was not changed. The other is that with the increase in strain rate, the stress-strain curve is similar in shape while the elastic modulus increases with the increase in strain rate. For example, Xiao et al. (2010) studied the stress-strain curves of concrete under strain rates of 10^{-5} /s ~ 10^{-2} /s, and the results showed that the peak stress and elastic modulus increased with the increase in the strain rate while the peak strain decreased. Zeng et al. (2013) also showed that the elastic modulus increased with the increase in strain rate. Grote (2001) studied the stress-strain curve of a mortar at high strain rate and the results also showed that the elastic modulus increased with the increase in strain rate.

1.3.2.2 Strain-rate effect on uni-axial compressive strength of concrete

Abrams (1917) found that the compressive strength of concrete was sensitive to loading rate, and after that the dynamic mechanical properties of concrete at different strain rates were studied extensively. Watstein (1953) studied the dynamic properties of concrete with nominal strength of 2500 psi and 4650 psi under strain rates from 10^{-6} /s to 10 /s by a drop hammer, and the experimental results showed that the dynamic strength of the two specimens increased by 84% and 85%, respectively. Atchley and Furr (1967) studied the dynamic mechanical properties of Φ6in × 12in cylindrical concrete specimens, and the results show that when the stress rate varied between 2000 psi and 106 psi, the increase in concrete strength was 25%, and when the stress rate varied between 106 psi and 107 psi, the strength increment were 38 %. Bischoff and Perry (1991) conducted a review of the dynamic compressive behavior of concrete, giving the relationship between dynamic compressive strength of concrete and strain rate, as shown in Fig. 1-7 (Bischoff and Perry 1991).

It can be seen that with the increase in strain rate, the compressive strength of concrete increases, and the relative increase in compressive strength is below 1.5 when the strain rate is 10^{-5} /s ~ 10^{-1}

/s. After the strain rate reaches 10^0 /s ~ 10^1 /s, the strength increases faster, and the dynamic strength is more than twice the static strength when the strain rate reaches 10^2 /s.

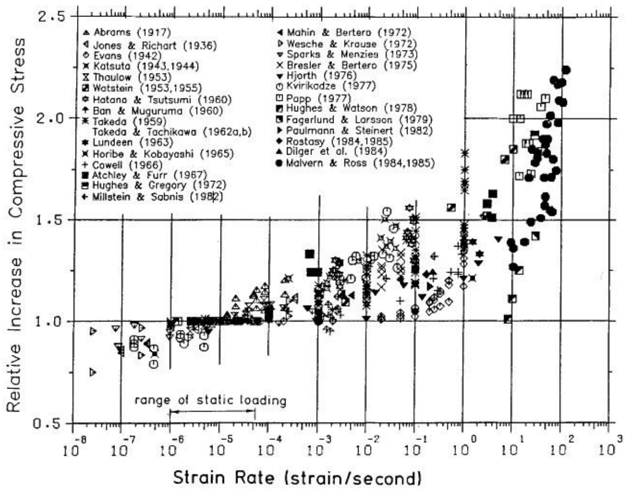

Fig. 1-7 Relationship between compressive strength of concrete and strain rate (Bischoff and Perry 1991)

Then, a large number of scholars continued to study the dynamic compressive strength of concrete. Ross et al. (1995) conducted dynamic tests on the cylinder concrete specimens with different water contents under lower strain rates (10^{-7}/s ~10^{-3}/s) and under higher strain rates (1/s ~300/s) using a hydraulic testing system and a SHPB equipment respectively, the results showed that the dynamic increase factor of compressive strength (DIF_{f_c}) of concrete with different water content were about 2.5 as the strain rate reached 300/s, and the critical strain rate was about 60/s. In 1997, Tedesco et al. (1997) carried out uniaxial compression tests on concrete specimens under strain rates of 10^{-1}/s ~ 10^3/s by using a SHPB device, and obtained the stress-strain curves of concrete under uniaxial compression, based on which the constitutive model of concrete in ADINA was improved to consider the increase in concrete strength under high strain rate. Zheng et al. (1999) used an extended SHPB device to carry out the dynamic compression tests to the cylindrical specimens, studied the stress-strain relationship, established the uniaxial constitutive model on the basis of the damage delay, and also constructed the dynamic failure criterion. Grote (2001) used SHPB to study the dynamic properties of concrete under high strain rates with lateral pressure, and the results showed that the compressive strength of concrete and mortar was obviously improved with the increase in strain rate and hydrostatic pressure; The compressive strength of the mortar at a strain rate of 1700 /s was about four times that of the static strength. Cadoni et al. (2009) used a large-sized SHPB device to perform uniaxial compression tests on 200 mm side-length cube specimens, and obtained the stress-strain curve at a strain rate of 10 /s. The results showed that the compressive strength of the large-size concrete specimen was about 2 times of the static strength at 10 /s.

After entering the 21st century, the studies in this field by Chinese scholars have increased rapidly, and achieved a lot of results. Shang et al. (1994) used a MTS hydraulic testing system to perform uniaxial compression tests on cube concrete specimens and uniaxial tensile tests on dumbbell-shaped concrete specimens, analyzed the effect of aggregate size and specimen size on the dynamic properties of concrete, established a viscoelastic damage dynamic constitutive model. Dong et al. (1997) used a MTS815.02 hydraulic testing system to study the compressive stress-strain curves of cylindrical concrete specimens with strain rates varing from 10^{-5} /s to 10^{2} /s, and the results showed that the compressive strength of concrete increased linearly with the increase in strain rate, and there was no critical strain rate. Hu et al. (2001) used an improved SHPB equipment to carry out the impact compressive loading on concrete cylinders, and the strain rate was about 10 /s ~ 85 /s. It is concluded that the concrete not only showed the strain rate effect but also showed obvious damage softening effect. Hu et al. (2002) studied the dynamic damage evolution of concrete. In 2005, Yan et al. (2005) studied the uniaxial compression performance of concrete using a large static and a dynamic real triaxial electro-hydraulic servo testing system with strain rates of 10^{-5} /s ~ 10^{-2} /s. In 2006, Yan et al. (2006) studied the compressive behavior of concrete under different conditions. Xiao et al. (2010) used a large-scale electro-hydraulic servo testing system to study the uniaxial compressive properties of concrete with strain rates of 10^{-5} /s ~ 10^{-2} /s, analyzed the relationship between the compressive strength, elastic modulus and critical strain of concrete under dynamic loadings and strain rates. They also conducted some other researches on the dynamic compressive properties of concrete Xiao et al. (2002, 2011). Zeng and Li (2013) studied the constitutive relationship of concrete under uniaxial compression with strain rates varing from 10^{-5} /s to 3.5×10^{-2} /s. The results showed that the compressive strength of the specimen was about 1.2 times of quasi-static strength when the strain rate was 3.5×10^{-2} /s.

In general, it has been accepted that the uniaxial compressive strength of concrete increase with the increase in strain rate. However, there is no definite conclusion on whether there is a critical strain rate at which the uniaxial compressive strength of concrete increases faster after the critical strain rate is reached. Moreover, the results of different researchers show that there is no consistent conclusion on the magnitude of the increase in dynamic compressive strength because it is affected by many factors.

The strain rate effect on concrete compressive strength was considered in the CEB standard (1993), and the relationship between the dynamic increase factor of compressive strength (DIF_{f_c}) of concrete and the strain rate was expressed as:

$$DIF_{f_c} = \begin{cases} (\dot{\varepsilon} / \dot{\varepsilon}_s)^{1.026\alpha} & \text{for } \dot{\varepsilon} \le 30\text{s}^{-1} \\ \gamma(\dot{\varepsilon} / \dot{\varepsilon}_s)^{1/3} & \text{for } \dot{\varepsilon} > 30\text{s}^{-1} \end{cases} \tag{1-1}$$

$$\gamma = 10^{(6.156\alpha\text{-}2)} \tag{1-2}$$

$$\alpha = 1/(5+9f_{cm}/f_{cmo}) \tag{1-3}$$

Where f_{cm} is the average compressive strength of concrete; f_{cmo} is equal to 10MPa; $\dot{\varepsilon}_s$ is the quasi-static strain rate, which is taken as -30 × 10^{-6} /s; $\dot{\varepsilon}$ is the strain rate.

1.3.2.3 Strain-rate effect on uni-axial tensile strength of concrete

In 1966, Mellinger and Birkimer (1966) conducted an uniaxial tension test on Φ2in × 0.25in cylindrical concrete, and the experimental results showed that the dynamic increase factor of tensile strength (DIF_{f_t}) was between 5.1 and 6.5 when the strain rate was 20 /s. When the strain rate was 23 /s, the DIF_{f_t} was between 4.5 and 8.1. Yon et al. (1992) used a three-point bending fracture test to study the tensile strength, elastic modulus and fracture energy of concrete, the results showed that the tensile strength and elastic modulus of concrete increased with the increase in loading rate, but the fracture energy did not change with the loading rate . Rossi et al. (1994) carried out a dynamic tensile test on concrete specimens with different water contents, and the results showed that the strain-rate sensitivity of the tensile strength in the dry state was lower than that in the wet state. Ross et al. (1995, 1996) and Tedeseo & Ross (1991) had done a lot of research on the dynamic tensile properties of concrete. For example, Ross et al. (1995) used a SHPB equipment to perform direct tensile and splitting tests on cylindrical concrete specimens at the strain rate of 10^{-7} /s to 20 /s. The results showed that when the strain rate was 17.8 /s, the DIF_{f_t} was 6.47. The critical strain rate was about 5 /s. Ross et al. (1995) conducted dynamic splitting tests on concrete specimens with different water contents, the results showed that the critical strain rate varired between 1 /s and 10 /s. Cadoni et al. (2000, 2001, 2009) also conducted a lot of experimental studies on the dynamic tensile properties of concrete. For example, Cadoni et al. (2000) studied the dynamic tensile properties of concrete at high strain rates using a SHPB, and the results showed that the tensile strength, ductility and energy absorption capacity of the concrete increased with the increase in strain rate. Cadoni et al. (2000) used the SHPB to study the dynamic tensile properties of concrete specimens with different relative humidity, and explained the mechanism of tensile strain-rate sensitivity based on the microscopic characteristics of the concrete and the theory of stress waves. Cadoni et al. (2009) also studied the dynamic tensile properties of large-size aggregate concrete specimens. Brara et al. (2006) used a modified SHPB to study the dynamic tensile tests of concrete at strain rates of about 10 /s to 120 /s, the results showed that when the strain rate reached 120 /s, the DIF_{f_t} was larger than 10, which was higher than the results of other investigators.

In China, in the mid-1980s, Tsinghua University (1996) began to study the dynamic properties of reinforced concrete, it showed that the increase in dynamic strength of high strength concrete was about 20% when the strain rate was about 4×10^{-4} /s. Yan and Lin (2006) used a hydraulic testing system to perform dynamic tensile tests on dumbbell-shaped concrete specimens with a strain rate of 10^{-5} /s ~ $10^{-0.3}$ /s, the results showed that the dynamic tensile strength of concrete was 1.67 times of the static strength when the strain rate was $10^{-0.3}$ /s. Xiao (2001) used a MTS fatigue machine to study the uniaxial tensile properties of concrete when the strain rate varied from 10^{-5} /s to 10^{-2} /s, the test results showed that the tensile strength of concrete increased linearly with the logarithm of the strain rate. Zeng (2012) studied the dynamic tensile properties of concrete with different strength at strain rate of 10^{-5} /s ~ 3×10^{-2} /s, the results showed that the effect of strength on strain-rate sensitivity of concrete showed no clear trend.

In 1998, Malvar and Ross (1998) summarized the effect of strain rate on the dynamic tensile strength of concrete under uniaxial loading and illustrated the relationship between the dynamic tensile strength and the strain rate, as shown in Fig. 1-8 (Malvar and Ross 1998). In general, the tensile strength increased with the increase in loading rate; the strain-rate sensitivity of tensile strength is higher than the strain-rate sensitivity of compressive strength.

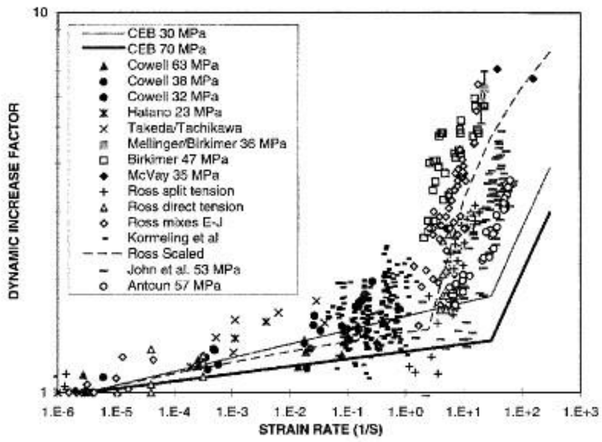

Fig. 1-8 The relationship between the dynamic tensile strength and strain rate (Malvar and Ross 1998)

The DIF_{f_t} proposed by CEB model code (1993) for concrete is recalled as follows:

$$DIF_{f_t} = \begin{cases} (\dot{\varepsilon} / \dot{\varepsilon}_s)^{1.016\alpha} & \text{for } \dot{\varepsilon} \le 30\text{s}^{-1} \\ \beta_s (\dot{\varepsilon} / \dot{\varepsilon}_s)^{1/3} & \text{for } \dot{\varepsilon} > 30\text{s}^{-1} \end{cases} \tag{1-4}$$

$$\gamma = 10^{(6.156\alpha\text{-}2)} \tag{1-5}$$

$$\alpha = 1/(5 + 9 f_c / 10) \tag{1-6}$$

Where, f_c is the static compressive strength.

1.3.2.4 Strain-rate effect on elastic modulus of concrete

Many studies have also been conducted on the dynamic elastic modulus of concrete. In general, the secant modulus of concrete exhibits an increasing trend as the strain rate increases. Dhir (1972) conducted dynamic tests on concrete when the strain rate increased from 5.0×10^{-5}/s to 2.5×10^{-4}/s, it showed that the secant modulus at 50% of compressive strength increased by 22%; Yan (2006) [**Error! Bookmark not defined.**] carried out dynamic tensile and compressive tests on concrete, and the results showed that the tensile secant modulus of C10 concrete at 50% peak stress increased by 18% at a strain rate of $10^{-0.3}$ /s, while the tensile secant modulus of C20 concrete increased by 12.1%; the compressive secant modulus of C10 increased by 12.1% at a strain rate of 10^{-2} /s, while the compressive secant modulus of C20 concrete increased by 11.6%. However, there is no consistent trend on the influence of strain rate on the initial tangent modulus. Some researchers (Wetsein 1953; Xiao et al. 2002; Shkolnik et al. 2008) reported that the initial tangent modulus of concrete increased with the increase in strain rate, while some others (Takeda et al. 1972; Dilger et al. 1984; Ahmad et al. 1985) reported that strain rate had no effect on the initial elastic modulus of concrete.

CEB (1993) recommended that the dynamic increase factor of elastic modulus (DIF_E) could be determined according to the following equation:

$$DIF_E = (\dot{\varepsilon} / \dot{\varepsilon}_s)^{0.026} \tag{1-7}$$

1.3.2.5 Strain-rate effect on peak strain of concrete

The peak strain is defined as the strain corresponding to the peak stress, which is also an important indicator of the deformation characteristics of concrete. A large number of studies have shown that the effect of strain rate on the peak strain of concrete is not conclusive. Some researchers (Dilger et al. 1984; Hughes et al. 1985; Xiao and Zhang 2010) reported that with the increase in strain rate, the peak strain of concrete reduced. For example, Xiao and Zhang (2010) studied the dynamic compressive properties of concrete, the results showed that the peak strain of concrete decreased from 1108 με at a strain rate of 10^{-5} /s to 1011 με at a strain rate of 10^{-2} /s. Some researchers (Hatano et al. 1960; Cowell et al. 1966; Lv and Song 2002; Yan and Lin 2006) showed that with a change inin the strain rate, the peak strain of concrete did not show obvious change. In addition, some researchers (Grote 2001; Takeda et al. 1972; Rostasy et al. 1984; Cadoni et al. 2000) reported that with the increase in strain rate, the peak strain of concrete increased. For example, Takeda (1972) tested several types of concrete specimens and found that the peak strain of concrete increased by a maximum of 40% when the strain rate was 1 /s.

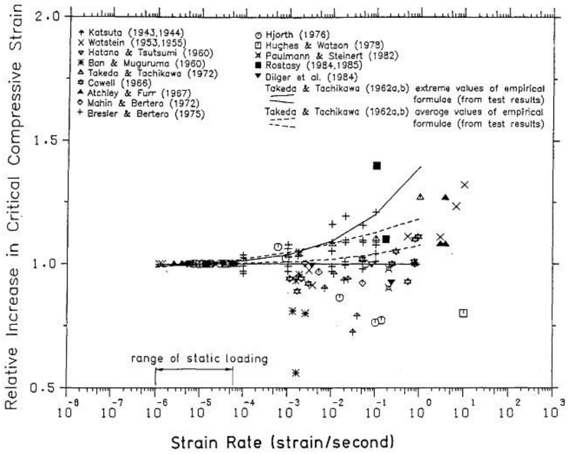

Fig. 1-9 Relationship between the strain rate and relative increase in peak strain (Bischoff and

Perry 1991)

Bischoff and Perry (1991) studied the relationship between the strain rate and the peak strain of concrete based on the results of a large number of researchers, as shown in Fig. 1-9. It can be seen that the peak strain showed different trends as the strain rate increased.

CEB (1993) recommended that the dynamic increase factor of peak strain (DIF_{ε}) strain could be determined according to the following equation:

$$DIF_{\varepsilon} = (\dot{\varepsilon} / \dot{\varepsilon}_s)^{0.020} \tag{1-8}$$

1.3.2.6 Strain-rate effect on the failure mode of concrete

There are only a few studies on the effect of strain rate on the failure modes of concrete. It can be seen from the limited literature that there were some consistent conclusions about the effects of strain rates on the failure mode of concrete, and there were also some inconsistent results. Many researchers have found that the failure mode was similar to that under the static loads as the strain rate increased, but the cracks at a higher strain rate were straighter and the number of cracks in the concrete specimen passing through the aggregate increases. For example, Lambert et al. (2000) used a SHPB testing system to perform concrete splitting tests and photographed the failure of the specimens under high-speed impact loading with a high-speed camera. It was found that the cracks were mostly linearly oriented and passed through some coarse aggregates. Yan (2006) studied the dynamic properties of dumbbell-shaped concrete specimen under different strain rates and found that the tensile fracture surface became more flat with the increase in strain rate. Lv et al. (2002) reported that the failure mode of concrete under dynamic stresses was similar to that under the static state, but the number of fractured aggregates on the concrete cracking surface increased with the increase in strain rate.

With regard to the effect of strain rates on the number of cracks in the concrete specimens, the results are also not consistent. Some researchers believed that as the strain rate increased, the total number of cracks increased. For example, Harsh (1990) pointed out that the number of cracks in the specimen was larger at a higher strain rate when studying the effect of strain rate on the compressive behavior of mortar. Some other researchers suggested that the total number of cracks was reduced as the strain rate increased. For example, Zeng (2012) reported that the number of major cracks in concrete specimens at a high strain rate was smaller. Li et al. (2010) pointed out that with the increase in the strain rate, the cracks in the concrete specimen under the same stress were reduced.

For the failure mode of direct tensile specimen under the static load, the fracture is often at the weakest surface. However, the result may be different at high strain rates. Brara et al. (2001) used a SHPB device with a diameter of 50.8 mm to perform direct tensile tests on specimens with a size of Φ 50.8 mm × 50.8 mm and a high speed camera to capture the failure of the specimens. The results showed that there were two failure modes, one with only one fracture surface, one with two fracture surfaces, and the fracture surface was essentially perpendicular to the specimen axis.

In addition, Du et al. (2014) studied the effect of ITZ on the failure mode of concrete under different strain rates. The results showed that the mechanical properties of the ITZ had a significant effect on the tensile and bending failure mode and the macroscopic mechanical properties when the loading rate was small. When the loading rate was larger than 50 /s, the dynamic tensile and bending failure mode of concrete beams were not affected by the mechanical properties of ITZ.

1.3.3 Mechanism of strain-rate sensitivity of concrete

Because the constitutive materials in concrete have a high degree of variability, coupled with the difference in the test conditions and methods, there are different opinions to explain the mechanism of strain-rate sensitivity of concrete.

In 2010, Li et al. (2010) explained the physical mechanism of the strain-rate sensitivity of concrete from three aspects based on interpretations of some previous studies (e.g., Bischoff and perry 1991; Rossi et al. 1990, 1991, 1992, 1996; Li and Meng 2003). The first aspect is from the viscous effect. That is, the presence of a viscous liquid in concrete will resist the localization and the expansion of cracks under dynamic loadings, so that the tensile strength of concrete increases. The second aspect is from the crack development. On the one hand, the propagation path of a single crack becomes straighter and more single cracks pass through the aggregate with an increase in loading rate, but on the other hand, the crack number in the concrete specimen are reduced under the same stress as the loading rate increases. These two factors indicate that the strength of the concrete increases with the increase in loading rate. The third aspect is from the inertial effect. On one hand, the inertia force caused by the dynamic loading always tends to resist the deformation caused by the external load. When the loading rate is large, the existence of the inertial force can significantly increase the dynamic strength of the material. On the other hand, the constraint effect caused by the inertial force makes the specimen to be in a three-axis compression stress state, so that the compressive strength is improved.

Wang and Li (2006) reported that the free water in the crack can reach the tip of the micro cracks of the concrete specimen at lower strain rates, the wedge of the free water accelerates the expansion of the crack and thus reduces the strength of the concrete. In the case of higher strain rate, the propagation speed of the crack is very fast, so that the free water in the crack does not have enough time to reach the tip of crack. As a result, the dynamic compressive strength of a saturated concrete will increase because of the negative pressure of the pore water, the free water viscosity and the Stefan effect. Zhang et al. (2015) also argued that at higher strain rates, free water does not easily reach the tip due to the surface tension and capillary action under the rapid expansion of the crack, but move inwards to the crack with a relative velocity, resulting in significant Stefan effect, as shown in Fig. 1-10.

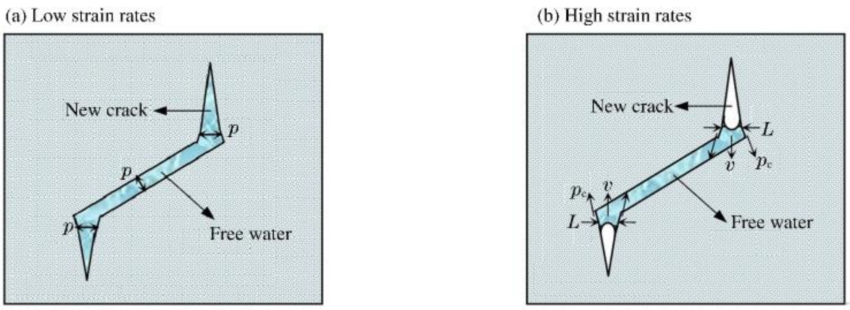

Fig. 1-10 Force of water in saturated concrete cracks at different strain rates (Zhang et al. 2015)

Qi and Qian (2003) studied the physical mechanism of brittle materials such as rocks from low strain rate to high strain rates. It is believed that the strain-rate sensitivity of the materials' strength is the result of the competition of the thermal activation mechanism and the macroscopic viscosity mechanism. They argued that the strain-rate sensitivity is controlled by the thermal activation mechanism in the range of low strain rates, which is called the thermal activation control zone. As the strain rate increases, the macroscopic viscous mechanism of the material become more obvious and gradually occupy the dominant position, this range is called the phonon damping area. At higher strain rates such as in explosions and impact loading, the inertia effect of the material is very large, and different sizes of defects begin to grow. At the same time, the thermal activation mechanism caused the broken of atomic bonds where there is no defects. At that time, the thermal activation mechanism has re-emerged. This range is called a high strain zone.

Wu et al. (2010) studied the mechanism of dynamic tensile strength of concrete from the microscopic point of view, established a unified model of dynamic tensile strength of concrete, and divided the mechanism of the strain-rate sensitivity of concrete into three parts, i.e., solid material effect, free water effect and inertia effect. The solid material effect reflects the effect of the microstructure and loading rate on the strength of concrete. The free water effect reflects the capillary suction and the Stefan effect of free water, which has a great influence on the dynamic strength at high strain rates. The inertial effect reflects the influence of the inertial force, which is the dominant factor influencing the strength of concrete at high strain rates.

In addition, Li et al. (2000, 2001) proposed a mechanism of the strain-rate sensitivity of rocks, that is, the strain rate dependence of the propagation speed of micro-cracks and the fracture toughness lead to the strain-rate sensitivity of the strength of rocks.

1.4 Research objectives and contents

Up to now, a large number of researchers have studied the dynamic mechanical properties of conventional concrete, and obtained a good understanding. Thus, we can also have a general understanding of the dynamic mechanical properties of RAC which is also a type of concrete. However, as mentioned earlier, the static mechanical properties of RAC are significantly different fromfrom that of conventional concrete. Therefore, it is necessary to study the dynamic mechanical properties of RAC which may also be different fromfrom that of conventional concrete. However, research on the dynamic mechanical properties of RAC is still rare. Only Lu et al. (2014) conducted a preliminary study on the impact properties of RAC and Rao et al. (2011) studied the impact properties of recycled concrete beams with different RCA replacement percentages. Therefore, this thesis aims to have a better understanding of the dynamic mechanical properties of RAC based on the experimental and theoretical studies. The main focus of this thesis are summarized as follows:

(1) The strain-rate sensitivity of RAC varing from low strain rates (10^{-5}/s~10^{-1}/s) to high strain rates (10^{1}/s ~ 10^{2}/s) will be studied. The effect of RCA replacement percentages on the strain-rate sensitivity of RAC will be studied in order to explore the difference between the dynamic mechanical properties of RAC and conventional concrete. The RAC specimens with different

moisture conditions will be used to o explore the influence of Stefan effect on the strain-rate sensitivity of RAC. The effect of using carbonated RCA on the dynamic compressive behavior of RAC will be studied. Based on the test results, the mechanism of the strain-rate sensitivity of RAC will be discussed.

(2) The modeled recycled aggregate concrete (MRAC) will be used to study the dynamic properties of RAC. On one hand, it provides a simplified model to study the dynamic properties of RAC. On the other hand, it is a convenient method to study the relationship between the strain-rate sensitivity of RAC and its meso-phase materials by comparing the dynamic properties of the modeled mortar with that of MRAC.

(3) Based on the data obtained from the dynamic tests on MRAC, numerical simulation of the MRAC will be carried out to further understand the dynamic mechanical properties of RAC.

According to the above, the main contents and the arrangement of the thesis are displayed as follows:

(1) In chapter 2, the stress-strain curves of the MRAC and modeled mortar (MM) with a size of 150mm × 150mm × 30mm were experimentally studied at low strain rates (10^{-5} /s ~ 10^{-1} /s) using the MTS815.02 electro-hydraulic servo test system. The effects of strain rate on the peak stress, peak strain, elastic modulus and failure mode were analyzed to study the strain-rate sensitivity of RAC. At the same time, the effects of RCA replacement percentage and the strength of new mortar on the strain-rate sensitivity of RAC were studied.

(2) In chapter 3, the stress-strain curves of RAC specimens with a size of Φ70mm × 140mm were experimentally studied at low strain rates (10^{-5} /s ~ 10^{-1} /s) using the MTS815.02 electro-hydraulic servo test system. The effects of strain rate on the peak stress, peak strain, elastic modulus, energy absorption capacity and failure mode were analyzed to study the strain-rate sensitivity of RAC. At the same time, the effects of RCA replacement percentage and the moisture condition of the specimen on the strain-rate sensitivity of RAC were studied.

(3) In chapter 4, the stress-strain curve of RAC specimens with the size of Φ70mm × 35mm was experimentally studied under impact loadings using the a SHPB test system. The strain rates are in the range 10^1 /s ~ 10^2 /s. The effects of strain rate on the peak stress, peak strain, elastic modulus and failure mode were analyzed to study the strain-rate sensitivity of RAC. At the same time, the effects of RCA replacement percentage and the moisture condition of the specimens on the strain-

rate sensitivity of RAC under impact loading were studied.

(4) In chapter 5, the dynamic compressive behavior of RAC prepared with RCA modified by carbonation (CRAC) was studied and compared with that of RAC.

(5) In chapter 6, based on the experimental results in the above chapters, the mechanism of the strain-rate sensitivity of RAC was discussed from three aspects: Stefan effect, inertial effect and crack development effect. Based on the microscopic stochastic fracture model of ordinary concrete, a simplified model of RAC under static and dynamic loading is established. Based on this model, the reason why the strain-rate sensitivity of RAC is higher than that of conventional concrete is analyzed.

(6) In chapter 7, a finite element model of MRAC was established. By considering the strain-rate sensitivity of meso-phase materials including aggregate, mortar and ITZ, the strain-rate sensitivity of the MRAC was studied and compared with the experimental results. At the same time, the influence of strain-rate sensitivity of the mesoscopic materials on the strain-rate sensitivity of MRAC is studied. In addition, the effects of RCA replacement percentage, the strength of new mortar and old mortar on the strain-rate sensitivity of MRAC were also studied.

Chapter 2 Dynamic mechanical behavior of MRAC at low strain rates

The model recycled coarse concrete (MRAC) is a simplified model of RAC, which consisting of a certain size of cylindrical aggregates at fixed locations with cement mortar around the cylindrical aggregates. The use of MRAC has some advantages. First, the use of MRAC can reduce the randomness of RAC resulting from the size, shape, location and distribution of RCA, so it is easier to study the mechanical behavior of RAC. Second, the application of MRAC can simplify the stress state of RAC, which is approximated to a plane stress state. In this way, we can clearly see the interface between the aggregate and the mortar, so we can easily record the crack development. In addition, it is easier to establish finite element model when utilizing MRAC. As mentioned in Chapter 1, many scholars have used the MRAC to study the mechanical properties of RAC, which shows that this simplified model is a good way to study the mechanical behavior of RAC.

In this chapter, the mechanical properties of RAC at low strain rates ranging from 10^{-5} /s ~ 10^{-1} /s were studied under uniaxial compressive loading based on the MRAC. The effects of strain rate on the stress-strain curve, failure mode, peak stress, peak strain and elastic modulus of RAC were studied. The influences of the RCA replacement percentage and the static compressive strength on the dynamic mechanical properties of RAC were also investigated to explore the main factors affecting the strain-rate sensitivity of RAC. In addition, the mortar specimens were designed to study the dynamic mechanical properties of the main meso-phase materials of RAC. The difference between the strain-rate sensitivity of RAC and its main meso-phase materials were compared. It can provide an experimental basis for the numerical simulation of the dynamic mechanical properties of RAC.

2.1 Test design

2.1.1 Materials

The cement used in this study was ordinary 42.5 Grade Portland cement. The water was tap water. The fine aggregate was fine river sand of which the modulus of fineness is 1.9. The modeled natural coarse aggregate (MNCA) was cylindrical granite aggregates with 30 mm in diameter and 30 mm in height (Fig. 2-1(a)), based on which the MRCA was made, as shown in Fig. 2-1(b). Three types of mortars, which were marked with M20, M30 and M40, were used for the MRAC specimens. The mixture proportions of the mortars are listed in Table 2-1. Their water, sand and cement proportions were designed to produce concrete with three different nominal compressive strengths grades, i.e. C20, C30, and C40, when mixed with the granite aggregates. The symbols of different types of mortar do not stand for the real strength grade of the mortar. In fact, the test results showed that the strength of the mortars marked with M30 and M40 were similar. The average results of compressive strengths of M20, M30 and M40 measured from 70mm×70mm×70mm mortar cubes were 37.9 MPa, 68.5 MPa and 68.8 MPa, respectively. The elastic modulus of M20, M30 and M40 from 100mm×100mm×300mm mortar prisms were 27.7 GPa, 32.1 GPa and 28.0 GPa, respectively.

(a) **MNCA**

(b) MRCA

Fig. 2-1 The modeled coarse aggregate

Table 2-1 Mixture proportions of the mortars

Type	w/c	Quantity (Kg/m^3)		
		Water	Cement	Sand
M20	0.58	160	275.9	589.2
M30	0.45	160	355.6	565.3
M40	0.36	190	527.8	403.7

2.1.2 Specimen design and preparation

Five types of MRAC specimens (i.e., MRAC20, MRAC30, MRAC40, MRACP30 and MNAC30) were prepared and classified by different types of new mortar and MRCA replacement ratio, as described in Table 2-2. There were in total 15 specimens for each type of MRAC for 5 strain rates (three specimens for each strain rate). The geometric dimensions of the MRAC specimens are given in Fig. 2-2.

Table 2-2 Classification of MRAC specimens

Specimen	Old mortar	New mortar	Replacement ratio of MRCA
MRAC20	M30	M20	100%
MRAC30	M30	M30	100%
MRAC40	M30	M40	100%
MRACP30	M30	M30	55%
MNAC30	--	M30	0%

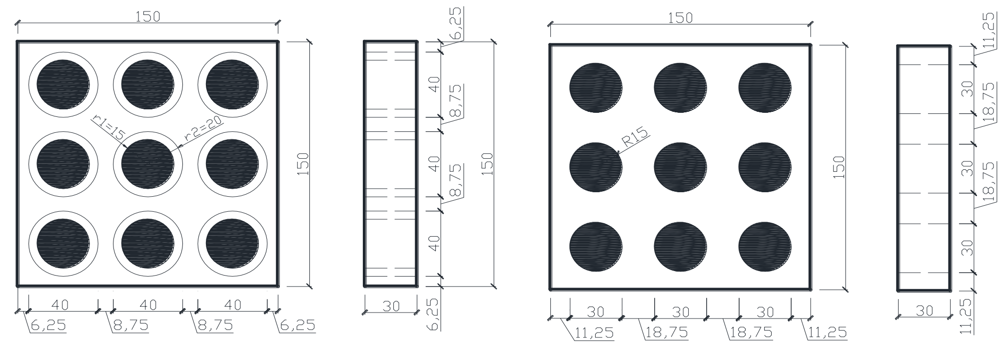

(a) MRAC20, MRAC30, MRAC40

(b) MNAC30

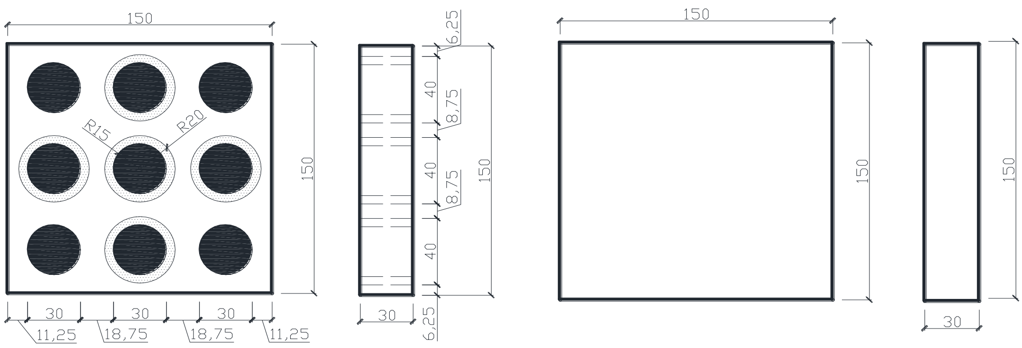

(c) MRACP30

(d) MM30

Fig. 2-2 Geometry dimensions of the different types of MRAC specimens

The followings are the procedures for producing MRAC specimens. Firstly, the cylindrical granite aggregates were placed vertically in wooden molds, and then the mortar was filled around the aggregates. The poured plate was kept in the molds during the first 24 hours, and was then removed from the molds and stored in a curing room with a controlled temperature of 20 ^{o}C and relative humidity of 95% for 28 days. After it had been taken out of the curing room for one day, MRCA samples of 40 mm diameter were cored out with a bench drill from the plate with the mortar adhering to the cylindrical granite aggregates, and the thickness of the mortar layer was about 5 mm. The MRCAs were soaked in water for 1 day to prevent excessive water absorption from the mortar matrix during casting, and then air-dried for approximately 1 hour before the casting of

MRAC. When casting the MRAC specimens, nine MRCAs were placed vertically and uniformly in the steel molds with strips of wood on the top to keep them fixed when filling the new mortar around them. The size of the steel molds is 150 mm×150 mm×30 mm. After one day curing in the laboratory, the specimens were removed from the steel molds and kept in a curing room with a controlled temperature of 20 ^{o}C and a relative humidity of 95% for one year before testing. Prior to testing, the top and bottom of the specimens were polished to reduce friction induced shear confinement at the loading platen/specimen interface.

2.1.3 Experimental setup and testing

The specimens were loaded in uniaxial compression using a stiff-framed servo-hydraulic testing machine (MTS815.02), as shown in Fig. 2-3, with a compressive load capacity of 2,700kN. This system could provide sufficient stiffness (the stiffness is 9.0×10^{9} N/m) to prevent the specimens from sudden rupture and thus it is able to acquire the descending part of the stress-strain curve. Displacement-controlled loading with a constant loading velocity being as fast as 30mm/s could be achieved with this system. There is an internal force transducer in the system for accurate measurement of the load applied to the specimen. The displacements of the actuator were recorded via the internal linear variable differential transformer (LVDT) fixed in the test setup. Two extensometers were fixed at mid-height on opposite faces of the specimens by strings to measure the average axial longitudinal strain, as shown in Fig. 2-4. In order to reduce the frictional constraints, two Teflon sheets, 0.1mm in thickness, were used at the top and bottom of the specimens (Van et al. 1997).

Fig. 2-3 MTS815.02 testing system

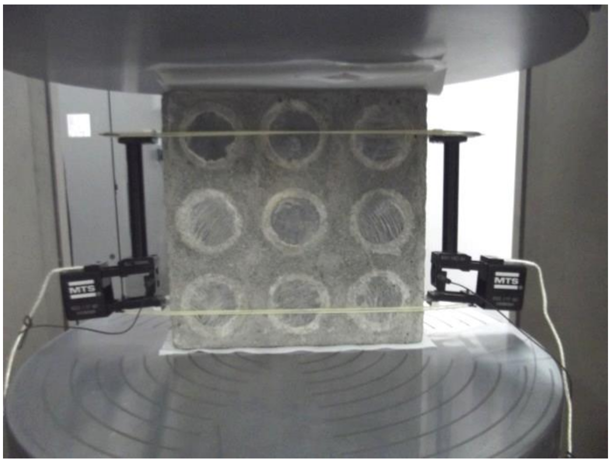

Fig. 2-4 Strain measuring by extensometer

Because the height of the specimens was 150 mm, constant strain rate up to 2×10^{-1} /s could be achieved using this test setup. Here, the strain of specimen used to calculate the strain rate was nominal global strain which was calculated by dividing the total displacement from LVDT data by the specimen height. The specimens were loaded at five constant velocities ranging from 1.5×10^{-3} mm/s to 15mm /s in steps by a factor of 10 (one order of magnitude), corresponding to a strain rate ranging from 10^{-5} /s to 10^{-1} /s. The tests were terminated when the displacements of the actuator reached about 1.5 mm to obtain enough data for the complete stress-strain curves, including the ascending and descending portions. The specimens failed in about 17 minutes when loaded at the slowest strain rate of 10^{-5} /s, which is considered as quasi-static loading, while the specimens failed in about 0.1s at the fastest strain rate of 10^{-1} /s.

2.2 Data processing method

On the one hand, after the load exceeded the peak load, as the deformation of the specimen increased, the visible cracks appeared and gradually passed through the specimen. At this time, i the specimen as a whole did not carry the load, and some portions might have lost load carrying ability. As a result, the strain data after the peak load measured by the extensometer became either larger or smaller. Therefore, it might not reflect the true strain of the specimen. Moreover, even in the ascending section, the strain data of many specimens measured by the extensometer rebounded, which may be because that the extensometers was moving on the surface of specimens. It indicated that not all of strain data measured by extensometer can accurately reflect the true strain of the specimens. On the other hand, the displacement data measured by the internal LVDT were stable. Therefore, the displacement data measured by the LVDT was used to calculate the strain of the specimens. However, the displacement data measured by the LVDT under a certain load actually consistsed of the displacement of the specimen and the additional displacement which was the total of the displacement of the friction-reducing layer and the machine. Therefore, calibration tests which will be described in the following paragraph were conducted to obtain the relationship of the additional displacement and the load under different strain rates.

In the calibration test, a steel specimen of the same size as the MRAC specimen was used and more rubber bands were used to prevent the extensometers sliding on the surface of the steel specimen, as shown in Fig. 2-5. Other conditions were kept unchanged with that for the MRAC.

There were five loading rates, i.e. 0.0015 mm/s, 0.015 mm/s, 0.15 mm/ s, 1.5 mm/s and 15 mm/s. The tests were stopped when the load reached 500 KN. This loading range was selected because the peak loads for all MRAC specimens were below 500 KN, and the steel specimen was still in the elastic phase within this load range.

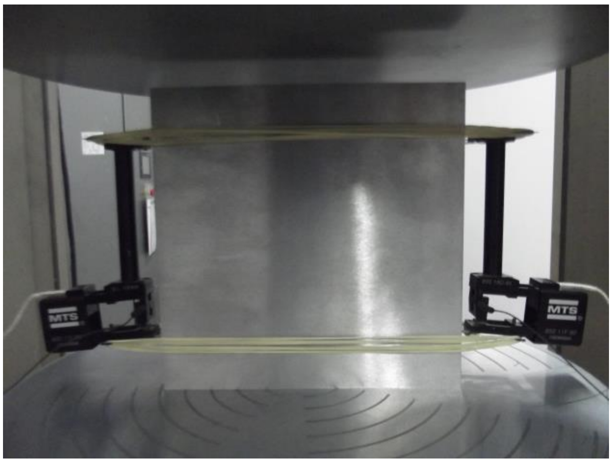

Fig. 2-5 The specimen and the extensometer in the calibration test

In the calibration test, at a certain strain rate, the total displacement (d_{total}) corresponding to the force (F) is equal to the sum of the additional displacement (d_{add}) and the displacement of steel specimen (d_{steel}), that is

$$d_{total} = d_{add} + d_{steel} \tag{2-1}$$

Because the elastic modulus of the steel specimen is known, the displacement of the steel specimen can be calculated according to the load. Therefore, d_{add} corresponding to the force could be obtained by subtracting d_{steel} by d_{total}, that is

$$d_{add} = d_{total} - d_{steel} \tag{2-2}$$

In this study, it is assumed that the relationship between d_{add} and F is constant. Therefore, by fitting the test results, the relationship between F and d_{add} can be determined, which can be shown as

$$d_{add} = f(F) \tag{2-3}$$

Taking the condition when the strain rate is 1.0×10^{-1}/s as an example, $d_{total} - F$, $d_{steel} - F$, $d_{add} - F$ relationships are shown in Fig. 2-6.

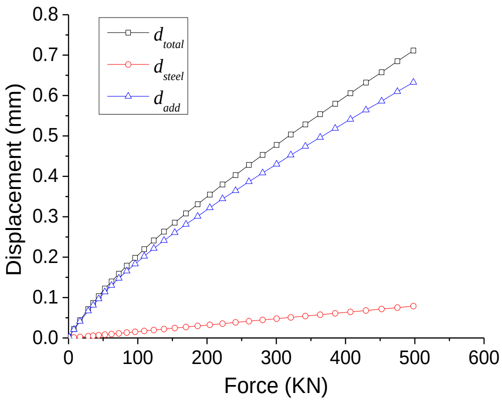

Fig. 2-6 Data in calibration test

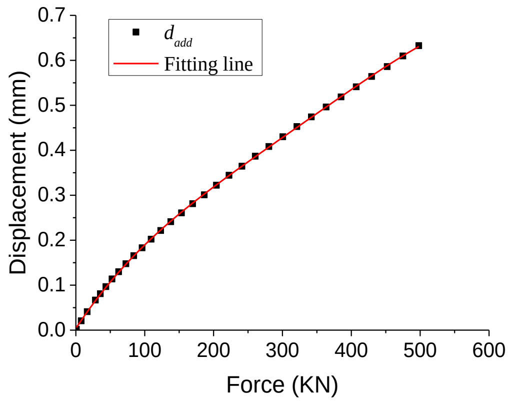

Fig. 2-7 Fitting line of the $d_{add} - F$ relation

The $d_{add} - F$ relation was fitted with four polynomials by the origin software, as shown in Fig. 2-7. The result shows that the fitting curve was in good agreement with the experimental data. Therefore, it is reasonable to use four polynomials to describe the $d_{add} - F$ relationship. The $d_{add} - F$ relationships at all studied strain rates can be expressed as:

$$d_{add} = \mathrm{a} + \mathrm{b} \times F + \mathrm{c} \times F^2 + \mathrm{d} \times F^3 + \mathrm{e} \times F^4 \tag{2-4}$$

Where, F is the load; a, b, c, d, e are constant coefficients, which are different at different strain rates. Using the above method, the $d_{add} - F$ relationships at all studied strain rates were determined and their constant coefficients are shown in Table 2-3.

Table 2-3 Constant coefficients in $d_{add} - F$ relationships

Strain rate (/s)	a	b	c	d	e
1.0×10^{-5}	0.01117	0.00264	-7.1612×10^{-6}	1.4882×10^{-8}	-1.1527×10^{-11}
1.0×10^{-4}	0.01093	0.00285	-9.8831×10^{-6}	2.6104×10^{-8}	-2.6311×10^{-11}
1.0×10^{-3}	0.00702	0.00273	-9.1559×10^{-6}	2.3598×10^{-8}	-2.3095×10^{-116}
1.0×10^{-2}	0.00274	0.00256	-7.4254×10^{-6}	1.6709×10^{-8}	-1.1472×10^{-126}
1.0×10^{-1}	0.00371	0.00230	-5.4375×10^{-6}	1.0581×10^{-8}	-7.7322×10^{-126}

According to the $d_{add} - F$ relationships at all the strain rates studied determined in calibration tests, the displacement of each MRAC specimen (d_{MRAC}) at any load can be obtained by subtracting the corresponding d_{add} from the total displacement in MRAC tests (d_{total}), that is

$$d_{MRAC} = d_{total}^{'} - d_{add} \tag{2-5}$$

In addition, it was found that the load-strain curves of the steel specimens remained almost unchanged at different strain rates during the elastic phase, as shown in Fig. 2-8. It indicated that the elastic modulus of steel did not change obviously with the increase in strain rate.

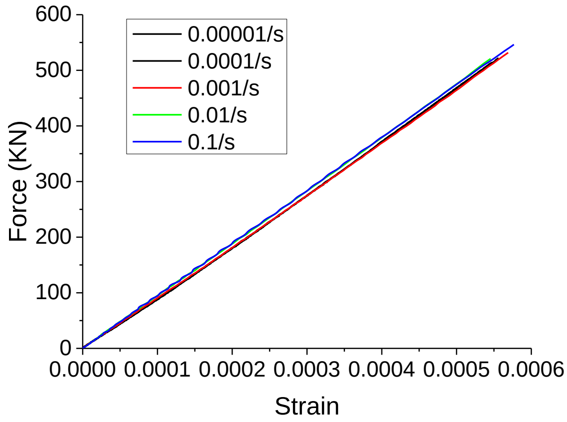

Fig. 2-8 Load-strain curves of steel specimen at different strain rate

2.3 Test results

In this part, the stress-strain curves and failure patterns of the mortar specimens and MRAC specimens were obtained. The dynamic mechanical properties of the specimens were analyzed from the following aspects: peak stress, elastic modulus, peak strain. Without special reasons, in each condition the stress-strain curve of the specimen whose peak stress was in the middle was considered as the typical stress-strain curve. Peak stress is the maximum stress in the stress-strain curve. The peak strain is the strain corresponding to the peak stress. The secant slope between 5 to 20 percent of peak stress in the stress-strain curve is considered as the elastic modulus, because concrete-like materials could be regarded as linear elastic in this range (Harsh et al. 1990).

2.3.1 MM30 specimens

2.3.1.1 Stress-strain curves of MM30 at different strain rates

The stress-strain curves of MM30 specimens at all the strain rates studied are shown in Fig. 2-9. The results show that the stress-strain curves of MM30 specimens were similar in shape at different strain rates. After the stress reached to about 80% of the peak stress, the stress-strain curves show obvious nonlinearity. As the strain rate was increased, the peak stress of MM30 increased, but the increase was not uniform. The elastic modulus of MM30 also showed an increasing trend as the strain rate increases, but in some cases the elastic modulus at a higher strain rate reduced. However, the peak strain of MM30 did not show a clear trend with the increase in strain rate. The peak stress, peak strain and elastic modulus of all the specimens are shown in Table 2-4.

Table 2-4 Peak stress, peak strain and elastic modulus of MM30

Strain rate (/s)	No.	Peak stress (MPa)	DIF_f	Peak strain (10^{-6})	DIF_ε	Elastic modulus (GPa)	DIF_E
10^{-5}	1	53.5	1.118	2797	1.067	25.7	1.148
	2	42.3	0.883	2330	0.889	21.7	0.969
	3	47.9	0.999	2736	1.044	19.7	0.883
	AVG	**47.9**	**1.000**	**2621**	**1.000**	**22.4**	**1.000**
10^{-4}	1	49.7	1.037	2592	0.989	21.5	0.961
	2	50.8	1.061	2497	0.953	24.3	1.085
	3	50.2	1.047	2776	1.059	20.3	0.906
	AVG	**50.2**	**1.049**	**2622**	**1.000**	**22.0**	**0.984**
10^{-3}	1	57.8	1.207	2467	0.941	30.6	1.367
	2	59.3	1.237	2417	0.922	29.6	1.324
	3	61.0	1.274	2520	0.961	29.6	1.324
	AVG	**59.4**	**1.239**	**2468**	**0.942**	**29.9**	**1.338**
10^{-2}	1	58.4	1.219	3005	1.147	22.4	1.003
	2	61.9	1.293	2673	1.020	28.4	1.271
	3	60.5	1.263	2877	1.098	24.1	1.078
	AVG	**60.3**	**1.258**	**2852**	**1.088**	**25.0**	**1.117**
10^{-1}	1	68.3	1.425	2826	1.078	30.3	1.357
	2	69.1	1.442	3166	1.208	26.7	1.196
	3	69.5	1.450	2884	1.100	28.2	1.263
	AVG	**68.9**	**1.439**	**2959**	**1.129**	**28.4**	**1.272**

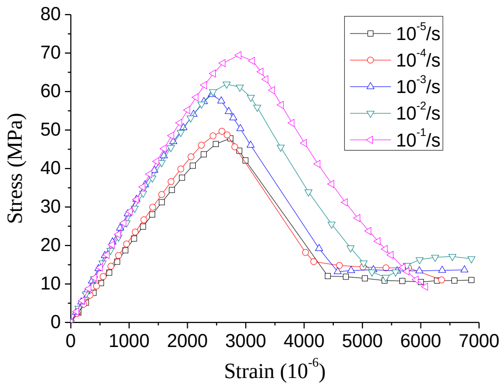

Fig. 2-9 Stress-strain curves of MM30 at different strain rates

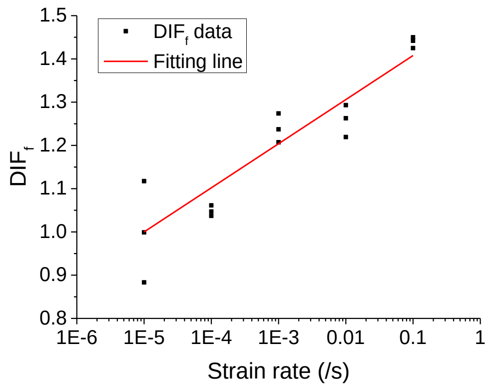

Fig. 2-10 Relationship between the DIF_f of MM30 and strain rate

2.3.1.2 Effect of strain rate on peak stress of MM30

According to Table 2-4, it can be seen that the average peak stress of MM30 increased with the increase in strain rate, but the increase was not uniform, the peak stress shows more obvious increase when the strain rate was from 10^{-2} /s to 10^{-1} /s. The relationship between the dynamic increase factor of peak stress (DIF_f) of MM30 and strain rate is shown in Fig. 2-10, the fitting line could be displayed as

$$DIF_f = 1 + 0.102 \cdot \lg(\dot{\varepsilon} / \dot{\varepsilon}_s) \tag{2-6}$$

Where, DIF_f is defined as the ratio of the peak stress at different strain rate to the quasi-static peak stress; $\dot{\varepsilon}$ is the current strain rate; $\dot{\varepsilon}_0$ is quasi-static strain rate, which is 10^{-5} /s in this study.

2.3.1.3 Effect of strain rate on peak strain of MM30

The results from Table 2-4 show that the average peak strain of MM30 firstly increased and then decreased with the increase in strain rate, but in general they were around a constant value. Moreover, the dispersion of the peak strain was large. Therefore, it is considered that the peak strain of mortar shows a fluctuation with the increase in strain rate. The relationship between the dynamic increase factor of peak strain (DIF_ε) of MM30 and strain rate is shown in Fig. 2-11, the fitting curve could be displayed as

$$DIF_\varepsilon = 1 + 0.022 \cdot \lg(\dot{\varepsilon} / \dot{\varepsilon}_s) \tag{2-7}$$

Where, DIF_ε is defined as the ratio of the peak strain at different strain rate to the quasi-static peak strain.

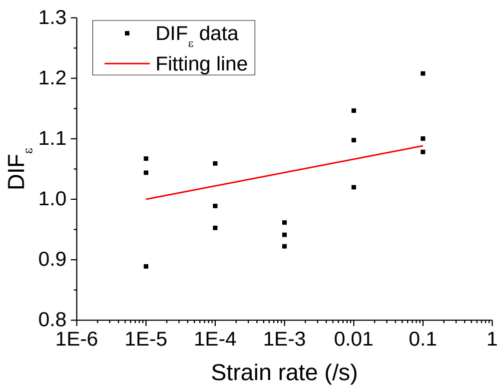

Fig. 2-11 Relationship between the DIF_ε of MM30 and strain rate

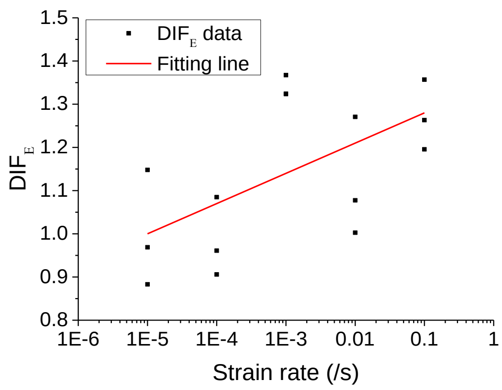

Fig. 2-12 Relationship between the DIF_E of MM30 and strain rate

2.3.1.4 Effect of strain rate on elastic modulus of MM30

According to Table 2-4, the average elastic modulus increased with the increase in strain rate. Moreover, the dispersion of the peak strain was large. With the increase in strain rate, the increasing rate of elastic modulus was smaller than that of peak stress. The relationship between the dynamic increase factor of elastic modulus (DIF_E) of MM30 and strain rate is shown in Fig. 2-12, the fitting line could be displayed as

$$DIF_E = 1 + 0.070 \cdot \lg(\dot{\varepsilon} / \dot{\varepsilon}_s) \tag{2-8}$$

Where, DIF_E is defined as the ratio of the elastic modulus at different strain rate to the quasi-static elastic modulus;

2.3.1.5 Effect of strain rate on failure pattern of MM30

The failure patterns of MM30 specimens at all the strain rates studied are shown in Fig. 2-13. The results show that there were vertical cracks parallel to the loading direction in MM30 specimens at all the strain rates studied. With the increase in strain rate, there was no significant difference in the number of cracks. It indicated that the influence of strain rate on the failure pattern of the mortar is not significant.

(a) 10^{-5}/s (b) 10^{-5}/s (c) 10^{-5}/s (d) 10^{-5}/s (e) 10^{-5}/s

Fig. 2-13 The failure patterns of MM30 specimens at different strain rates

Table 2-5 Peak stress, peak strain and elastic modulus of MRAC20

Strain rate (/s)	No.	Peak stress (MPa)	DIF_f	Peak strain (10^{-6})	DIF_ε	Elastic modulus (GPa)	DIF_E
10^{-5}	1	26.1	0.859	3218	1.203	8.6	0.657
	2	33.6	1.106	3065	1.146	11.9	0.910
	3	31.5	1.036	1738	0.650	18.7	1.434
	AVG	**30.4**	**1.000**	**2674**	**1.000**	**13.1**	**1.000**
10^{-4}	1	41.0	1.349	2519	0.942	24.9	1.907
	2	33.2	1.091	3718	1.390	11.8	0.902
	3	32.1	1.057	2030	0.759	16.9	1.292
	AVG	**35.4**	**1.165**	**2756**	**1.031**	**17.9**	**1.367**
10^{-3}	1	36.5	1.202	2401	0.898	19.7	1.509
	2	39.9	1.311	2072	0.775	22.9	1.751
	3	42.3	1.389	2382	0.891	23.7	1.812
	AVG	**39.6**	**1.301**	**2285**	**0.855**	**22.1**	**1.690**
10^{-2}	1	49.6	1.632	2213	0.828	31.0	2.371
	2	48.2	1.585	2922	1.093	24.3	1.864
	3	48.4	1.591	2361	0.883	25.3	1.937
	AVG	**48.7**	**1.602**	**2499**	**0.935**	**26.9**	**2.057**
10^{-1}	1	40.4	1.330	1764	0.660	31.2	2.389
	2	43.7	1.437	2572	0.962	23.6	1.804
	3	50.3	1.653	2661	0.995	28.7	2.194
	4	48.0	1.579	2125	0.795	31.1	2.378
	5	45.7	1.503	1939	0.725	32.4	2.483
	AVG	**45.6**	**1.500**	**2212**	**0.827**	**29.4**	**2.250**

2.3.2 MRAC20 specimens

2.3.2.1 Stress-strain curves of MRAC20 at different strain rates

The stress-strain curves of MRAC20 specimens at all the strain rates studied are shown in Fig.

2-14. The results show that with the increase in strain rate, the stress-strain curves of the MRAC20 specimens were similar in shape. When the stress reached about 80% of the peak stress, the stress-strain curves showed obvious nonlinearity. With the increase in strain rate, the peak stress and elastic modulus of MRAC20 increased, but it did not show a strict increase. The peak strain of MRAC20 specimens fluctuated around a constant value with the increase in strain rate. The peak stress, peak strain and elastic modulus of all the specimens are shown in Table 2-5.

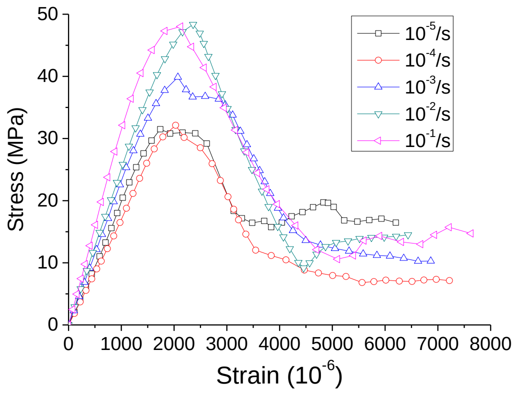

Fig. 2-14 Stress-strain curves of MRAC20 at different strain rates

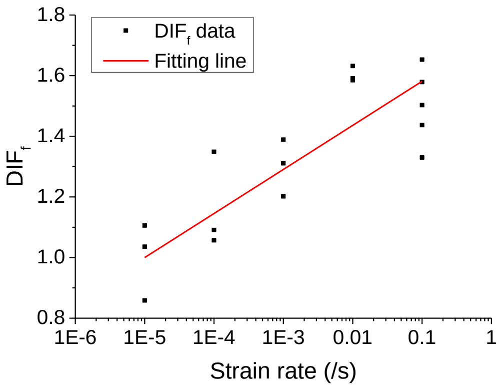

Fig. 2-15 Relationship between the DIF_f of MRAC20 and strain rate

2.3.2.2 Effect of strain rate on peak stress of MRAC20

According to Table 2-5, the average peak stress of MRAC20 generally increased with the increase in strain rate, but variations occurred at 10^{-2} /s, i.e., the peak stress of MRAC20 at 10^{-2} /s was higher than that at other strain rates, which may be a result of experimental dispersion. The relationship between the DIF_f of MRAC20 and strain rate is shown in Fig. 2-15, the fitting curve could be displayed as

$$DIF_f = 1 + 0.145 \cdot \lg(\dot{\varepsilon} / \dot{\varepsilon}_s) \tag{2-9}$$

2.3.2.3 Effect of strain rate on peak strain of MRAC20

The results from Table 2-5 show that the average peak strain of MRAC20 fluctuated around a constant value with the increase in strain rate. The relationship between the DIF_ε of MRAC20 and strain rate is shown in Fig. 2-16, the fitting curve could be displayed as

$$DIF_\varepsilon = 1\text{-}0.040 \cdot \lg(\dot{\varepsilon} / \dot{\varepsilon}_s) \tag{2-10}$$

It indicates that the fitting line of peak strain of MRAC20 exhibits a decreasing trend in general, but this trend is most likely due to the fact that the average peak strain of MRAC20 at a strain rate of 10^{-5} /s is larger than the actual value, which makes the value of DIF_ε smaller. Therefore, it was not very suitable to make conclusion based on the fitting line because the data of peak strain are very scatter.

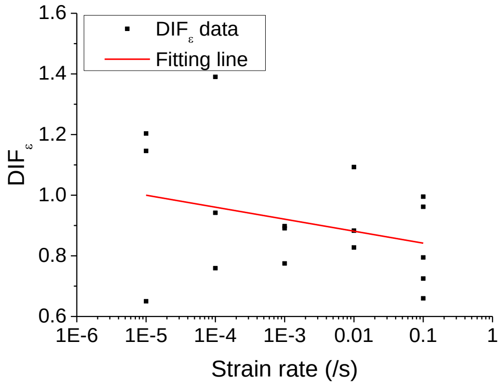

Fig. 2-16 Relationship between the DIF_ε of MRAC20 and strain rate

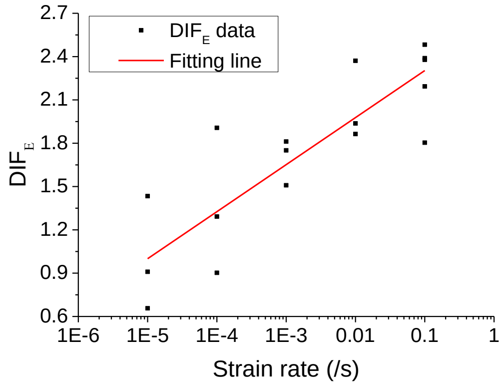

Fig. 2-17 Relationship between the DIF_E of MRAC20 and strain rate

2.3.2.4 Effect of strain rate on elastic modulus of MRAC20

According to Table 2-5, it can be seen that the average elastic modulus of MRAC20 increased with the increase in strain rate, but the dispersion of elastic modulus was large. Moreover, the increasing rate of elastic modulus of MRAC20 was larger than that of peak stress. The relationship between the DIF_E of MRAC20 and strain rate is shown in Fig. 2-17, the fitting line could be displayed as

$$DIF_{\mathrm{E}} = 1 + 0.326 \cdot \lg(\dot{\varepsilon} / \dot{\varepsilon}_s) \tag{2-11}$$

2.3.2.5 Effect of strain rate on failure pattern of MRAC20

The failure patterns of MRAC20 specimens at all the strain rates studied are shown in Fig. 2-18. The results show that there were vertical splitting cracks parallel to the loading direction in MRAC20 specimens at all the strain rates studied, and most of the cracks passed through the specimens along the old or the new interface. At a higher strain rate, the width of the cracks was larger, and there were several main cracks leading to the failure of the specimen. Moreover, more cracks were found in the new interface than in the old interface. In general, there was no significant difference in the number of cracks when the strain rate was changed.

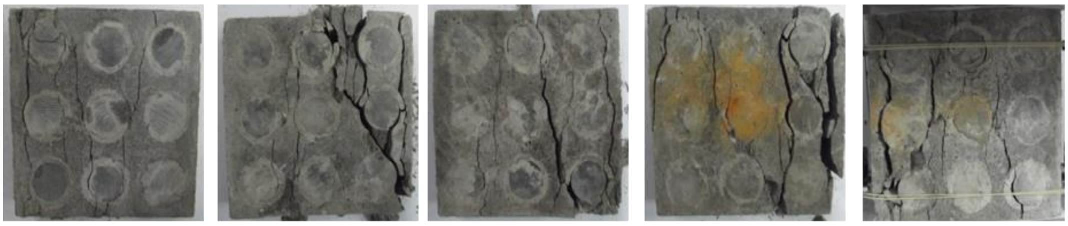

(a) 10^{-5}/s (b) 10^{-5}/s (c) 10^{-5}/s (d) 10^{-5}/s (e) 10^{-5}/s

Fig. 2-18 The failure patterns of MRAC20 specimens at different strain rates

2.3.3 MRAC30 specimens

2.3.3.1 Stress-strain curves of MRAC30 at different strain rates

The stress-strain curves of MRAC30 specimens at all the strain rates studied are shown in Fig. 2-19. The results show that the stress-strain curves of the MRAC30 specimens were similar in shape. Compared with MRAC20, the nonlinearity of both the ascending part and the descending part of the stress-strain curve were smaller. With the increase in strain rate, the peak stress of MRAC30 increased, but the elastic modulus and peak strain did not show a clear trend. The peak stress, peak strain and elastic modulus of all the specimens are shown in Table 2-6.

Table 2-6 Peak stress, peak strain and elastic modulus of MRAC30

Strain rate (/s)	No.	Peak stress (MPa)	DIF_f	Peak strain (10^{-6})	DIF_ε	Elastic modulus (MPa)	DIF_E
10^{-5}	1	42.9	0.941	2100	0.974	29.6	1.061
	2	48.7	1.067	2573	1.194	23.5	0.845
	3	45.3	0.992	1793	0.832	30.5	1.094
	AVG	**45.6**	**1.000**	**2155**	**1.000**	**27.9**	**1.000**
10^{-4}	1	40.0	0.876	2932	1.361	13.6	0.488
	2	49.3	1.081	2833	1.315	21.2	0.762
	3	51.1	1.120	2363	1.097	26.2	0.939
	AVG	**46.8**	**1.026**	**2709**	**1.257**	**20.3**	**0.730**
10^{-3}	1	45.7	1.002	2357	1.094	22.5	0.809
	2	50.1	1.098	1870	0.868	32.8	1.177
	3	47.1	1.032	2120	0.984	25.5	0.915
	AVG	**47.6**	**1.044**	**2116**	**0.982**	**27.0**	**0.967**
10^{-2}	1	53.4	1.170	2015	0.935	34.7	1.245
	2	51.6	1.131	2241	1.040	27.6	0.991
	3	55.6	1.218	2176	1.010	31.5	1.132
	AVG	**53.5**	**1.173**	**2144**	**0.995**	**31.3**	**1.123**
10^{-1}	1	57.0	1.249	2945	1.367	17.7	0.634
	2	58.7	1.287	2832	1.314	19.4	0.695
	3	54.7	1.200	2462	1.142	20.2	0.726
	4	66.0	1.446	2420	1.123	39.7	1.423
	AVG	**59.1**	**1.295**	**2665**	**1.237**	**24.2**	**0.870**

2.3.3.2 Effect of strain rate on peak stress of MRAC30

According to Table 2-6, the average peak stress of MRAC30 generally increased with the increase in strain rate, the increasing rate was larger when the strain rate is from 10^{-3} /s to 10^{-1} /s. The relationship DIF_f of MRAC30 and strain rate is shown in Fig. 2-20, the fitting curve could be displayed as

$$DIF_f = 1 + 0.062 \cdot \lg(\dot{\varepsilon} / \dot{\varepsilon}_s) \tag{2-12}$$

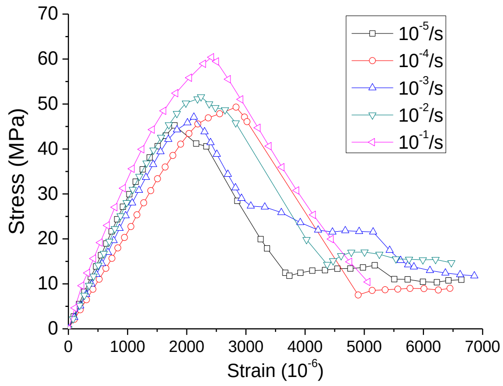

Fig. 2-19 Stress-strain curves of MRAC30 at different strain rates

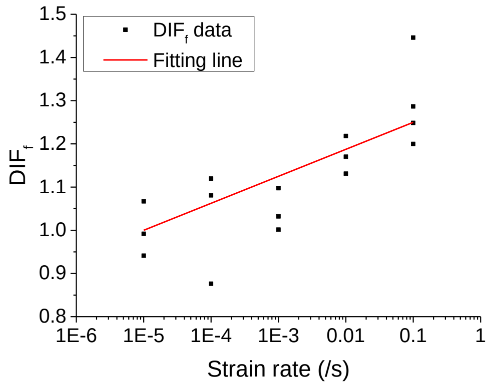

Fig. 2-20 Relationship between the DIF_f of MRAC30 and strain rate

2.3.3.3 Effect of strain rate on peak strain of MRAC30

According to Table 2-6, the average peak strain of the MRAC30 specimens were 22155με, 2709με, 2116με, 2144με and 2665με respectively when the strain rate were 10^{-5} /s, 10^{-4} /s, 10^{-3} /s, 10^{-2} /s and 10^{-1} /s. The corresponding dynamic increase factors were 1.000, 1.257, 0.982, 0.995 and 1.237 respectively. The results show the average peak strain of MRAC30 fluctuated with the increase in strain rate. The relationship DIF_ε of MRAC30 and strain rate is shown in Fig. 2-21, the fitting line could be displayed as

$$DIF_\varepsilon = 1 + 0.042 \cdot \lg(\dot{\varepsilon} / \dot{\varepsilon}_s) \tag{2-13}$$

2.3.3.4 Effect of strain rate on elastic modulus of MRAC30

The results from Table 2-6 show that the elastic modulus did not show a clear trend with the increase in strain rate. The relationship between the DIF_E of MRAC30 and strain rate is shown in Fig. 2-22, the fitting line could be displayed as

$$DIF_{\mathrm{E}} = 1 - 0.019 \cdot \lg(\dot{\varepsilon} / \dot{\varepsilon}_s) \tag{2-14}$$

We can see that the elastic modulus of MRAC30 showed a decreasing trend in general with the increase in strain rate. This phenomenon is contradictory to the previous research. It is believed that this is because the quasi-static elastic modulus of MRAC30 is larger than the real value, so that the value of DIF_E is less than 1.0 when the strain rate is increased.

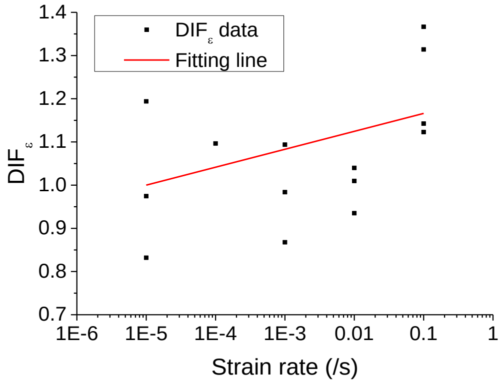

Fig. 2-21 Relationship between the DIF_ε of MRAC30 and strain rate

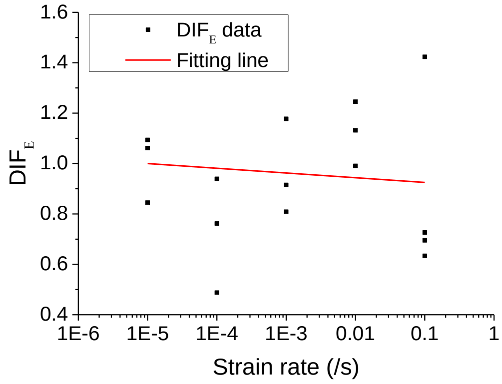

Fig. 2-22 Relationship between the DIF_E of MRAC30 and strain rate

2.3.3.5 Effect of strain rate on failure pattern of MRAC30

The failure patterns of MRAC30 specimens at all the strain rates studied are shown in Fig. 2-23. The results show that there were vertical cracks parallel to the loading direction at all the strain rates studied, and most of the cracks passed through the specimens along the old or the new interface. At a higher strain rate, the width of the cracks was larger, and there were several main cracks leading to the failure of specimen. At a lower strain rate, the cracks propagated along both the old and new interface, while the cracks just propagated along the old or new interface at a higher strain rate. Moreover, the cracks in the old and new interface were similar in number. In general, the number of cracks had no significant change when the strain rate was changed.

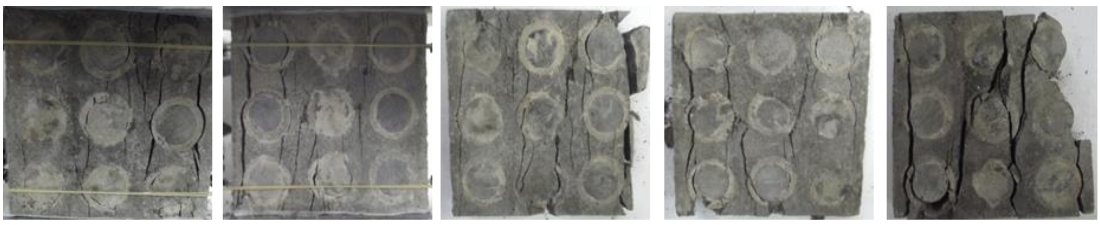

(a) 10^{-5}/s (b) 10^{-5}/s (c) 10^{-5}/s (d) 10^{-5}/s (e) 10^{-5}/s

Fig. 2-23 The failure patterns of MRAC30 specimens at different strain rates

2.3.4 MRAC40 specimens

2.3.4.1 Stress-strain curves of MRAC40 at different strain rates

The stress-strain curves of MRAC40 specimens at all studied strain rates are shown in Fig. 2-24. The results show that the stress-strain curves of the MRAC40 specimens were similar in shape.

With the increase in strain rate, the degree of nonlinearity of the ascending part decreased while the degree of nonlinearity of the descending part did not show significant change. The peak stress and elastic modulus of MRAC40 increased with the increase in strain rate, while the peak strain did not show a clear trend. The peak stress, peak strain and elastic modulus of all specimens are shown in Table 2-7.

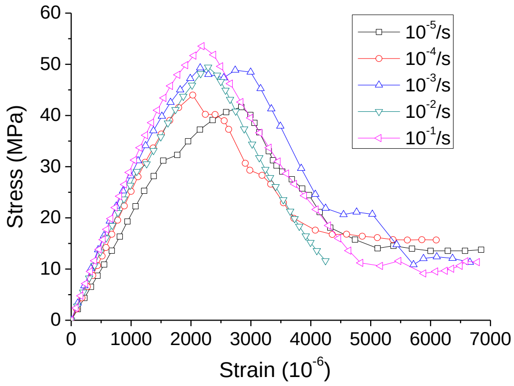

Fig. 2-24 Stress-strain curves of MRAC40 at different strain rates

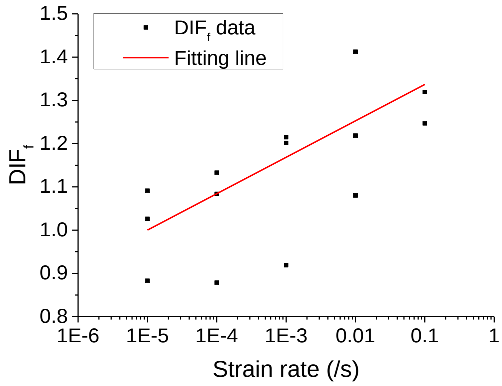

Fig. 2-25 Relationship between the DIF_f of MRAC40 and strain rate

Table 2-7 Peak stress, peak strain and elastic modulus of MRAC40

Strain rate (/s)	No.	Peak stress (MPa)	DIF_f	Peak strain (10^{-6})	DIF_ε	Elastic modulus (MPa)	DIF_E
10^{-5}	1	44.3	1.091	1945	0.800	28.3	1.362
	2	35.8	0.883	2504	1.030	14.3	0.686
	3	41.7	1.026	2840	1.169	19.8	0.952
	AVG	**40.6**	**1.000**	**2430**	**1.000**	**20.8**	**1.000**
10^{-4}	1	44.0	1.084	2029	0.835	24.3	1.171
	2	46.0	1.133	1877	0.772	35.9	1.726
	3	35.7	0.879	1914	0.788	21.0	1.013
	AVG	**41.9**	**1.032**	**1940**	**0.798**	**27.1**	**1.303**
10^{-3}	1	37.3	0.919	1681	0.692	24.8	1.196
	2	48.8	1.202	1939	0.798	31.9	1.533
	3	49.3	1.215	2154	0.886	30.6	1.474
	AVG	**45.1**	**1.112**	**1925**	**0.792**	**29.1**	**1.401**
10^{-2}	1	57.3	1.412	2276	0.937	32.8	1.581
	2	49.5	1.219	2287	0.941	27.4	1.321
	3	43.8	1.080	2317	0.953	28.7	1.379
	AVG	**50.2**	**1.237**	**2317**	**0.953**	**28.7**	**1.379**
10^{-1}	1	65.1	1.604	2391	0.984	36.1	1.740
	2	53.6	1.319	2184	0.899	29.8	1.434
	3	50.6	1.247	2243	0.923	26.2	1.260
	AVG	**56.4**	**1.390**	**2273**	**0.935**	**30.7**	**1.478**

2.3.4.2 Effect of strain rate on peak stress of MRAC40

According to Table 2-7, the average peak stress of the MRAC40 specimens were 40.59MPa, 41.88MPa, 45.13MPa, 50.21MPa and 56.42MPa respectively when the strain rate were 10^{-5} /s, 10^{-4} /s, 10^{-3} /s, 10^{-2} /s and 10^{-1} /s. It indicates that the average peak stress of MRAC30 generally increased with the increase in strain rate. The relationship between the DIF_f of MRAC40 and strain rate is shown in Fig. 2-25, the fitting line could be displayed as

$$DIF_f = 1 + 0.084 \cdot \lg(\dot{\varepsilon} / \dot{\varepsilon}_s) \tag{2-15}$$

2.3.4.3 Effect of strain rate on peak strain of MRAC40

The results from Table 2-7 show that the average peak strain of MRAC40 decreased firstly and then increases with the increase in strain rate. The relationship between the DIF_ε of MRAC30 and strain rate is shown in Fig. 2-26, the fitting curve could be displayed as

$$DIF_\varepsilon = 1\text{-}0.035 \cdot \lg(\dot{\varepsilon} / \dot{\varepsilon}_s) \tag{2-16}$$

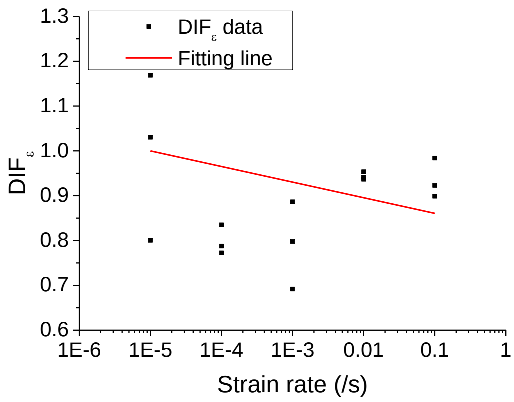

Fig. 2-26 Relationship between the DIF_ε of MRAC40 and strain rate

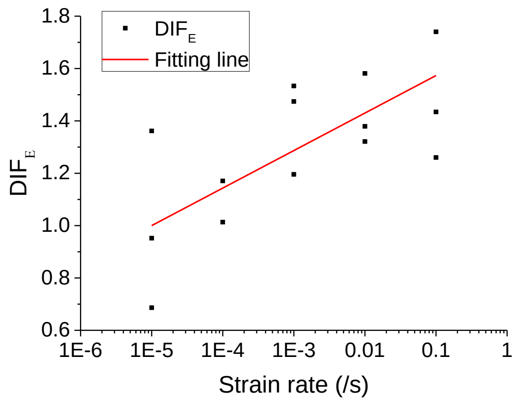

Fig. 2-27 Relationship between the DIF_E of MRAC40 and strain rate

2.3.4.4 Effect of strain rate on elastic modulus of MRAC40

According to Table 2-7, the average elastic modulus of the MRAC30 specimens are 20772MPa, 27074MPa, 29103MPa, 28651MPa and 30705MPa respectively when the strain rate were 10^{-5} /s, 10^{-4} /s, 10^{-3} /s, 10^{-2} /s and 10^{-1} /s. The results show that the average elastic modulus showed an increasing trend with the increase in strain rate, but the dispersion was large. The relationship between the DIF_E of MRAC40 and strain rate is shown in Fig. 2-27, the fitting curve could be displayed as

$$DIF_E = 1\text{+}1.143 \cdot \lg(\dot{\varepsilon} / \dot{\varepsilon}_s) \tag{2-17}$$

2.3.4.5 Effect of strain rate on failure pattern of MRAC40

The failure patterns of MRAC40 specimens at all the strain rates studied are shown in Fig. 2-28. The results show that most of the cracks passed through specimens along the old or the new interface. Some short cracks appeared in the mortar matrix, but it did not pass through the whole specimen. At a higher strain rate, the width of the cracks was larger, and there were several main cracks leading to the failure of the specimen. Moreover, the cracks in the old and the new interface were similar in number. In general, the number of cracks showed no significant change when the strain rate was changed.

(a) 10^{-5}/s (b) 10^{-5}/s (c) 10^{-5}/s (d) 10^{-5}/s (e) 10^{-5}/s

Fig. 2-28 The failure patterns of MRAC40 specimens at different strain rates

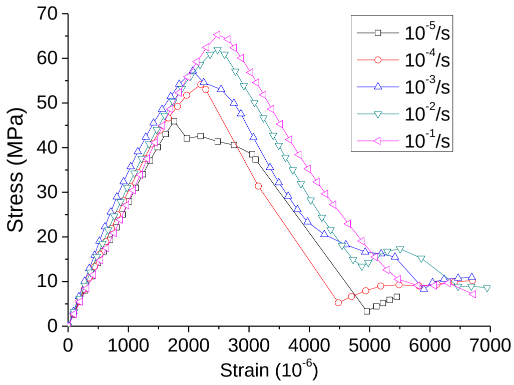

Fig. 2-29 Stress-strain curves of MRACP30 at different strain rates

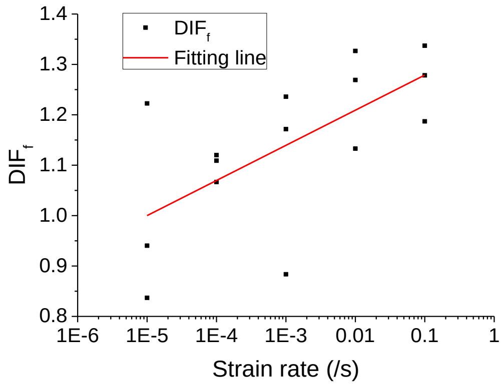

Fig. 2-30 Relationship between the DIF_f of MRACP30 and strain rate

2.3.5 MRACP30 specimens

2.3.5.1 Stress-strain curves of MRACP30 at different strain rates

The stress-strain curves of MRACP30 specimens at all the strain rates studied are shown in Fig. 2-29. The results show that the stress-strain curves of the MRACP30 specimens were similar in shape. The degree of nonlinearity of the ascending part was small. The peak stress and the elastic modulus of MRAC40 increased with the increase in strain rate, while the peak strain did not show a clear trend. The peak stress, peak strain and elastic modulus of all the specimens are shown in Table 2-8.

Table 2-8 Peak stress, peak strain and elastic modulus of MRACP30

Strain rate (/s)	No.	Peak stress (MPa)	DIF_f	Peak strain (10^{-6})	DIF_ε	Elastic modulus (MPa)	DIF_E
10^{-5}	1	40.9	0.837	2728	1.162	19.3	0.743
	2	45.9	0.940	1758	0.749	28.7	1.105
	3	59.7	1.223	2559	1.090	30.0	1.152
	AVG	**48.8**	**1.000**	**2348**	**1.000**	**26.0**	**1.000**
10^{-4}	1	52.1	1.067	2021	0.861	30.9	1.189
	2	54.7	1.120	2061	0.878	29.1	1.121
	3	54.1	1.109	2200	0.937	30.8	1.186
	AVG	**53.6**	**1.099**	**2094**	**0.892**	**30.3**	**1.165**
10^{-3}	1	57.2	1.172	2068	0.881	36.8	1.417
	2	60.3	1.236	2351	1.001	34.0	1.308
	3	43.1	0.884	2409	1.026	21.6	0.830
	AVG	**53.6**	**1.097**	**2276**	**0.969**	**30.8**	**1.185**
10^{-2}	1	55.3	1.133	2521	1.074	30.1	1.159
	2	62.0	1.269	2479	1.056	32.7	1.257
	3	64.8	1.327	2321	0.989	34.0	1.306
	AVG	**60.7**	**1.243**	**2440**	**1.039**	**32.3**	**1.241**
10^{-1}	1	62.4	1.278	2748	1.170	29.6	1.140
	2	58.0	1.187	2346	0.999	29.1	1.120
	3	65.3	1.337	2481	1.057	27.4	1.052
	AVG	**61.9**	**1.268**	**2525**	**1.075**	**28.7**	**1.104**

2.3.5.2 Effect of strain rate on peak stress of MRACP30

According to Table 2-8, the average peak stress of the MRACP30 specimens were 48.82MPa, 53.63MPa, 53.56MPa, 60.68MPa and 61.88MPa respectively when the strain rate were 10^{-5} /s, 10^{-4} /s, 10^{-3} /s, 10^{-2} /s and 10^{-1} /s. It indicates that the peak stress of MRAC30 generally increased with the increase in strain rate. The dispersion of peak stress was large when the strain rates are 10^{-5} /s and 10^{-3} /s. The relationship between the DIF_f of MRACP30 and strain rate is shown in Fig. 2-30, the fitting line could be displayed as

$$DIF_f = 1 + 0.0697 \cdot \lg(\dot{\varepsilon} / \dot{\varepsilon}_s) \tag{2-18}$$

2.3.5.3 Effect of strain rate on peak strain of MRACP30

The results from Table 2-8 show that the average peak strain of MRAC40 decreased firstly and then increased with the increase in strain rate. The relationship between the DIF_ε of MRACP30 and strain rate is shown in Fig. 2-31, the fitting curve could be displayed as

$$DIF_\varepsilon = 1 + 0.0083 \cdot \lg(\dot{\varepsilon} / \dot{\varepsilon}_s) \tag{2-19}$$

2.3.5.4 Effect of strain rate on elastic modulus of MRACP30

According to Table 2-8, the average elastic modulus of the MRACP30 specimens were

26003MPa, 30303MPa, 30817MPa, 32258MPa and 28709MPa respectively when the strain rate were 10^{-5} /s, 10^{-4} /s, 10^{-3} /s, 10^{-2} /s and 10^{-1} /s. The results show that the elastic modulus showed an increasing trend with the increase in strain rate except when the strain rate was 10^{-1} /s. The dispersion of elastic modulus of MRACP30 was large. The relationship between the DIF_E of MRACP30 and strain rate is shown in Fig. 2-32, the fitting line could be displayed as

$$DIF_{\mathrm{E}} = 1 + 0.0558 \cdot \lg(\dot{\varepsilon} / \dot{\varepsilon}_s) \tag{2-20}$$

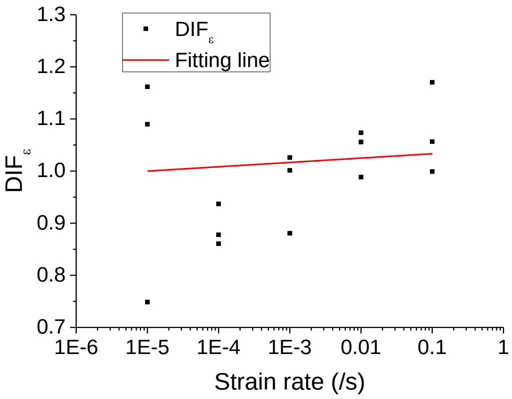

Fig. 2-31 Relationship between the DIF_ε of MRACP30 and strain rate

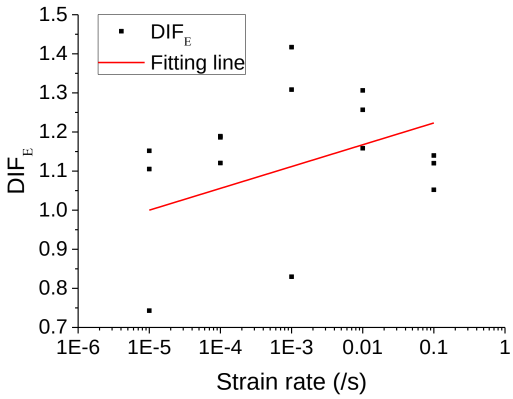

Fig. 2-32 Relationship between the DIF_E of MRACP30 and strain rate

2.3.5.5 Effect of strain rate on failure pattern of MRACP30

The failure patterns of MRACP30 specimens at all the strain rates studied are shown in Fig. 2-33. The results show that there were vertical cracks parallel to the loading direction at all the strain rates studied, and most of the cracks passed through the specimens along the old or the new interface. At a higher strain rate, the width of the cracks was larger, and there were several main cracks leading to the failure of the specimen. The number of cracks in the old interface and the new interface were similar. In general, there is no significant change in the number of cracks when the strain rate was changed.

(a) 10^{-5}/s (b) 10^{-5}/s (c) 10^{-5}/s (d) 10^{-5}/s (e) 10^{-5}/s

Fig. 2-33 The failure patterns of MRACP30 specimens at different strain rates

2.3.6 MNAC30 specimens

2.3.6.1 Stress-strain curves of MNAC30 at different strain rates

The stress-strain curves of MNAC30 specimens at all the strain rates studied are shown in Fig. 2-34. The results show that the stress-strain curves of the MNAC30 specimens at different strain rates were similar in shape. The degree of nonlinearity of the ascending part was not obvious. With the increase in strain rate, the peak stress of MNAC30 increased, but the elastic modulus and peak strain did not show a clear trend. The peak stress, peak strain and elastic modulus of all the specimens are shown in Table 2-9.

Table 2-9 Peak stress, peak strain and elastic modulus of MNAC30

Strain rate (/s)	No.	Peak stress (MPa)	DIF_f	Peak strain (10^{-6})	DIF_ε	Elastic modulus (MPa)	DIF_E
10^{-5}	1	56.1	1.001	2334	1.032	28.0	0.848
	2	56.2	1.004	2079	0.920	33.9	1.026
	3	55.7	0.995	2370	1.048	37.2	1.126
	AVG	**56.0**	**1.000**	**2261**	**1.000**	**33.0**	**1.000**
10^{-4}	1	51.9	0.926	1950	0.862	29.1	0.880
	2	54.3	0.970	1584	0.701	45.1	1.365
	3	51.6	0.921	2165	0.958	27.1	0.821
	AVG	**52.6**	**0.939**	**1900**	**0.840**	**33.7**	**1.022**
10^{-3}	1	66.3	1.185	2241	0.991	31.5	0.953
	2	70.6	1.260	3585	1.586	19.2	0.581
	3	53.4	0.954	2469	1.092	28.5	0.862
	AVG	**63.5**	**1.133**	**2765**	**1.223**	**26.4**	**0.799**
10^{-2}	1	69.6	1.242	3119	1.379	28.6	0.867
	2	56.8	1.014	2259	0.999	30.0	0.909
	3	77.0	1.375	2449	1.083	41.4	1.254
	AVG	**67.8**	**1.211**	**2609**	**1.154**	**33.4**	**1.010**
10^{-1}	1	69.4	1.238	1829	0.809	44.9	1.359
	2	64.1	1.145	2335	1.033	25.9	0.784
	3	53.4	0.954	2509	1.110	19.1	0.577
	AVG	**62.3**	**1.113**	**2224**	**0.984**	**29.9**	**0.907**

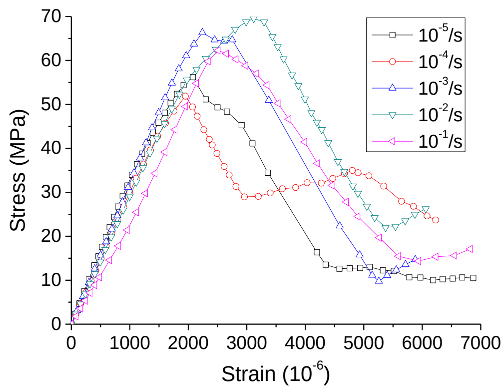

Fig. 2-34 Stress-strain curves of MNAC30 at different strain rates

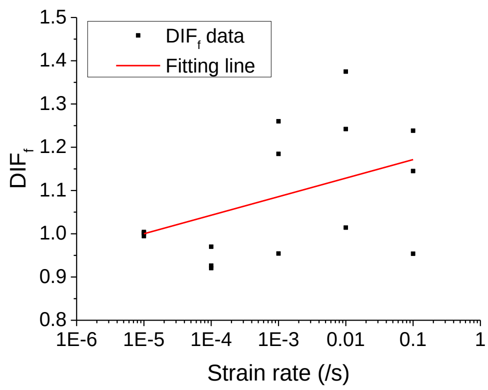

Fig. 2-35 Relationship between the DIF_f of MNAC30 and strain rate

2.3.6.2 Effect of strain rate on peak stress of MNAC30

According to Table 2-9, the average peak stress of the MNAC30 specimens were 56.00MPa, 52.59MPa, 63.45MPa, 67.79MPa and 62.30MPa respectively when the strain rate were 10^{-5} /s, 10^{-4} /s, 10^{-3} /s, 10^{-2} /s and 10^{-1} /s. It indicates that the peak stress of MNAC30 generally increased with the increase in strain rate. The relationship between the DIF_f of MNAC30 and strain rate is shown in Fig. 2-35, the fitting line could be displayed as

$$DIF_f = 1 + 0.0429 \cdot \lg(\dot{\varepsilon} / \dot{\varepsilon}_s) \tag{2-21}$$

2.3.6.3 Effect of strain rate on peak strain of MNAC30

According to Table 2-9, the average peak strain of the MNAC30 specimens were 2261με, 1900με, 2765με, 2609με and 2224με respectively when the strain rate are 10^{-5} /s, 10^{-4} /s, 10^{-3} /s, 10^{-2} /s and 10^{-1} /s. The results show the average peak strain of NRAC30 fluctuated with the increase in strain rate. The relationship between the DIF_ε of MRACP30 and strain rate is shown in Fig. 2-36, the fitting line could be displayed as

$$DIF_\varepsilon = 1 + 0.0228 \cdot \lg(\dot{\varepsilon} / \dot{\varepsilon}_s) \tag{2-22}$$

2.3.6.4 Effect of strain rate on elastic modulus of MNAC30

According to Table 2-9, the average elastic modulus of the MNAC30 specimens were 33025MPa, 337443MPa, 26378MPa, 33359MPa and 29939MPa respectively when the strain rate were 10^{-5} /s, 10^{-4} /s, 10^{-3} /s, 10^{-2} /s and 10^{-1} /s. The results show that the elastic modulus did not show a clear trend with the increase in strain rate. The dispersion of elastic modulus of MNAC30 was large. The relationship between the DIF_E of MNAC30 and strain rate is shown in Fig. 2-37, the fitting line could be displayed as

$$DIF_E = 1 - 0.0241 \cdot \lg(\dot{\varepsilon} / \dot{\varepsilon}_s) \tag{2-23}$$

The results show that the DIF_E of MNAC30 showed a decreasing trend with the increase in strain rate, which is contradictory to the general conclusion. It is believed that it is due to the large dispersion of elastic modulus.

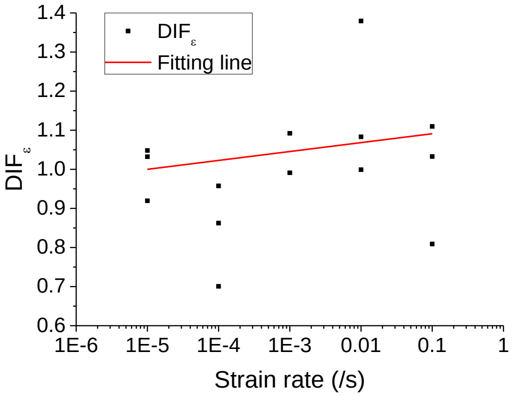

Fig. 2-36 Relationship between the DIF_ε of MNAC30 and strain rate

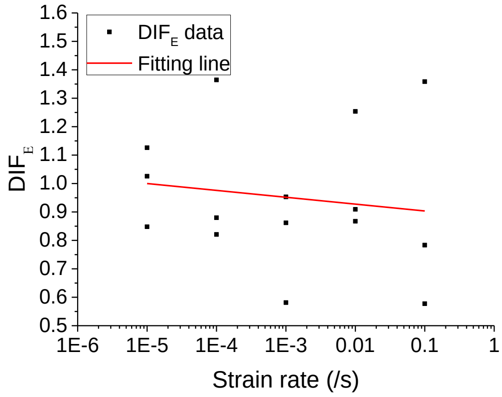

Fig. 2-37 Relationship between the DIF_E of MNAC30 and strain rate

2.3.6.5 Effect of strain rate on failure pattern of MNAC30

The failure patterns of MNAC30 specimens at all the strain rates studied are shown in Fig 2-38. The results show that there were vertical cracks parallel to the loading direction in MNAC30 specimens at all the strain rates studiedrates and most of the cracks passed through the specimens along the old or the new interface. At a higher strain rate, the width of the cracks was larger, and there were several main cracks leading to the failure of the specimen. In general, the number of cracks showed no significant change when the strain rate was changed. Due to the absence of old mortar in MNAC30, the number of cracks is less than other types of specimens.

(a) 10^{-5}/s (b) 10^{-5}/s (c) 10^{-5}/s (d) 10^{-5}/s (e) 10^{-5}/s

Fig. 2-38 The failure patterns of MNAC30 specimens at different strain rates

2.4 Analysis and Discussion

According to the above test results, the strain-rate sensitivity of RAC will be analyzed in the following section by evaluating the effect of strain rate on the peak stress, peak strain, elastic modulus and failure pattern. At the same time, the effect of static strength and RCA replacement ratio will also be analyzed to explore the main factors influencing the strain-rate sensitivity of RAC. In addition, the strain-rate sensitivity of the mortar which is the main meso-phase materials of concrete will be compared with that of NAC and RAC.

2.4.1 Strain-rate sensitivity of MRAC at low strain rates

2.4.1.1 Effect of strain rate on peak stress of MRAC

Fig. 2-39 show the variations of the average peak stress of all types of MRAC specimens with strain rate. The results show that the average peak stress of all types of MRAC specimens increases with the increase in strain rate. Moreover, the MRAC whose quasi-static strength is larger also has larger peak stress at all the strain rates studied. The variations of the DIF_f of all types of MRAC specimens with strain rate are shown in Fig. 2-40. The results show that the rates of increase in the DIF_f of different MRAC specimens are different, indicating that their strain-rate sensitivities are different.

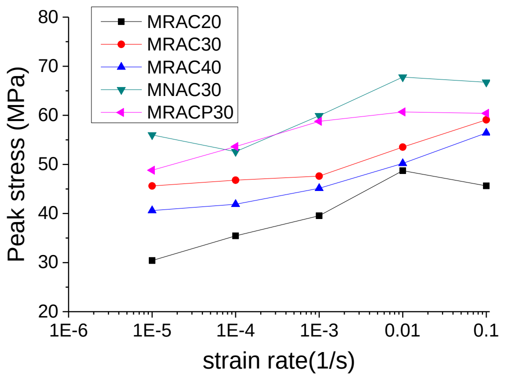

Fig. 2-39 Effect of strain rate on the peak stress of MRAC

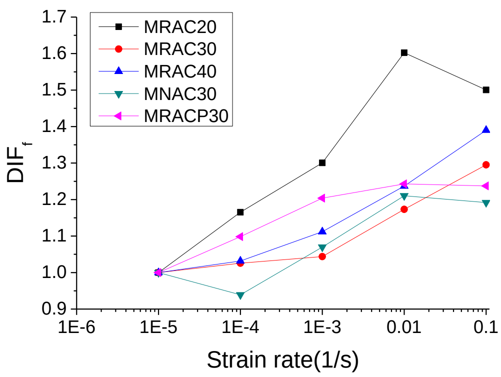

Fig. 2-40 Effect of strain rate on the DIF_f of MRAC

2.4.1.2 Effect of strain rate on peak strain of MRAC

Fig. 2-41 shows the variations of the average peak strain of all types of MRAC specimens with strain rate. The results show that the average peak strain of all types of MRAC specimens fluctuates around a constant value with the increase in strain rate. The variations of the DIF_ε of all types of MRAC specimens with strain rate are shown in Fig. 2-42. The results show that the values of DIF_ε of all MRAC specimens fluctuates around 1.0. Therefore, it is considered that the peak strain of MRAC does not change with the increase in strain rate, and the fluctuation is caused by the dispersion of the test.

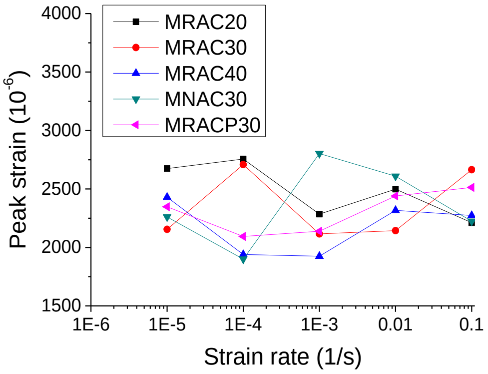

Fig. 2-41 Effect of strain rate on the peak strain of MRAC

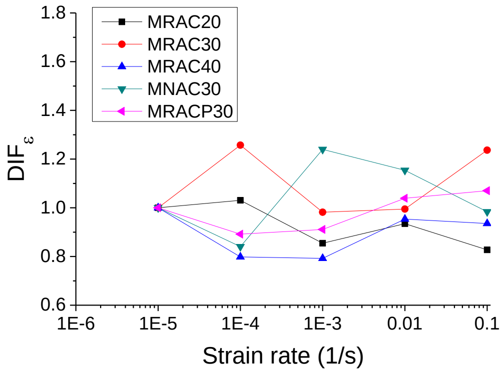

Fig. 2-42 Effect of strain rate on the DIF_ε of MRAC

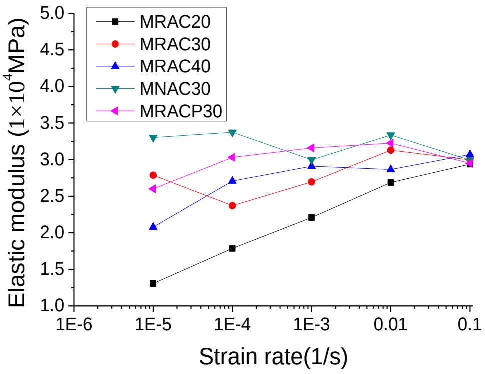

Fig. 2-43 Effect of strain rate on the elastic modulus of MRAC

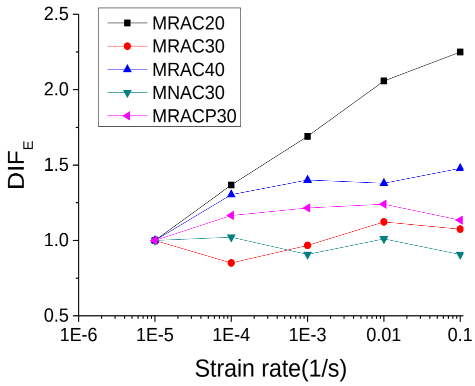

Fig. 2-44 Effect of strain rate on the DIF_E of MRAC

2.4.1.3 Effect of strain rate on elastic modulus of MRAC

Fig. 2-43 and Fig. 2-44 show the variations of the average elastic modulus and the DIF_E of all types of MRAC specimens with strain rate. The results show that the elastic modulus of the majority of MRAC specimens shows an increasing trend with the increase in strain rate. However, the elastic modulus of MNAC30 specimen decreases with the increase in strain rate. Although it is not clear whether this trend is true or not, it can be explained that the dispersion of elastic modulus is large when MRAC is used to study the dynamic behavior of RAC. Generally, it is believed that the elastic modulus of MRAC increases with the increase in strain rate, while the increasing rate is different for different types of MRAC.

2.4.1.4 Effect of strain rate on failure pattern of MRAC

According to the above description of the failure patterns of different types of MRAC specimens, we can see that there are common features among them. At each strain rate, the cracks appeared at the interfaces and gradually developed to the mortar, finally the cracks passed through the specimens. There was no significant change in the number of cracks with the increase in strain rate. However, at higher strain rates, the cracks developed faster and the main cracks were less in number and larger in width. Overall, it is considered that the strain rate has little influence on the failure pattern of RAC under the low strain rates.

2.4.2 Effect of static strength on strain-rate sensitivity of MRAC

In this section, the dynamic mechanical properties of MRAC with different static strengths are compared and analyzed from the aspects of peak stress, peak strain, elastic modulus and failure pattern. It should be noted that the static strength of MRAC30 in this test is higher than that of MRAC40. According to the static strength from low to high, the sequence is MRAC20, MRAC40 and MRAC30.

2.4.2.1 Effect of static strength on peak stress and DIF_f of MRAC

The peak stresses of MRAC20, MRAC30 and MRAC40 at all the strain rates studied are compared in Fig. 2-45. The results show that the MRAC whose static strength is larger has a higher dynamic peak stress. However, the difference between the different types of MRAC is narrowed, indicating that the peak stress of the lower strength MRAC increases rapidly with the increase in strain rate. According to the Eq. (2-9), Eq. (2-12) and Eq. (2-15), the increasing rates of the peak stress of MRAC20, MRAC30 and MRAC40 specimens are 14.5%, 6.2% and 8.4%, respectively. According to Fig. 2-45, the DIF_f of the lower static strength MRAC is larger. This feature is consistent with the result of CEB model. The test results and the results calculated by CEB model are compared in Fig. 2-46. It can be noted that the DIF_f of MRAC30 and MRAC40 are close to those of CEB model, while the DIF_f of MRAC20 is much larger than that of CEB model. In conclusion, it is considered that the DIF_f of lower strength MRAC is higher, indicating its strain-rate sensitivity is more significant.

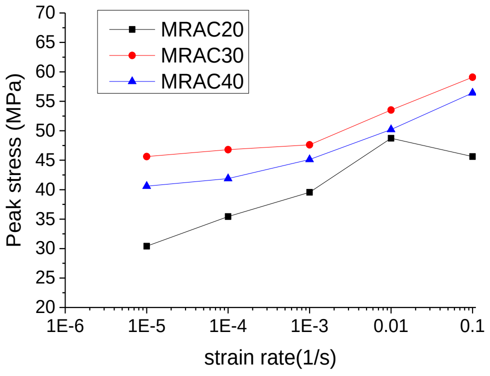

Fig. 2-45 Effect of static strength on the dynamic peak stress of MRAC

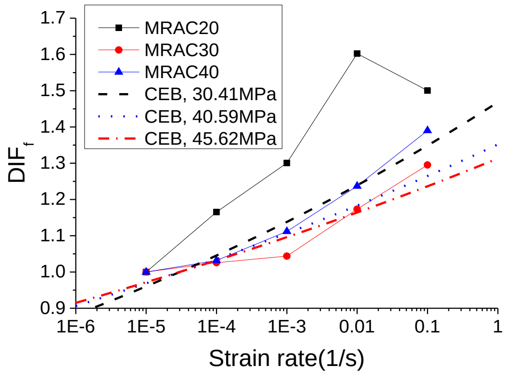

Fig. 2-46 Effect of static strength on the DIF_f of MRAC

2.4.2.2 Effect of static strength on peak strain and DIF_ε of MRAC

The peak strains of MRAC20, MRAC30 and MRAC40 at all the strain rates studied are compared in Fig. 2-47. The results show that the peak strain of each type of MRAC has no obvious trend with the increase in strain rate, which may be due to the dispersion of the peak strain. So the effect of static strength on dynamic peak strain is also not clear. The value of DIF_ε of MRAC20, MRAC30 and MRAC40 at all the strain rates studied are compared in Fig. 2-48, the results show that the influence of static strength on DIF_ε is also not clear.

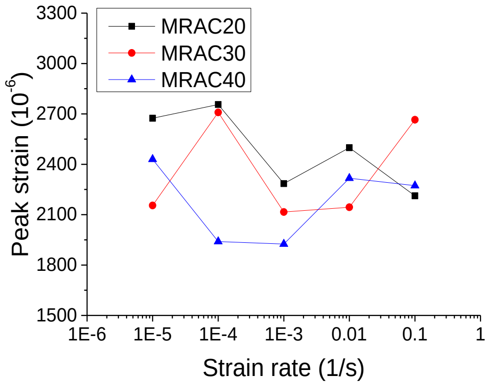

Fig. 2-47 Effect of static strength on the dynamic peak strain of MRAC

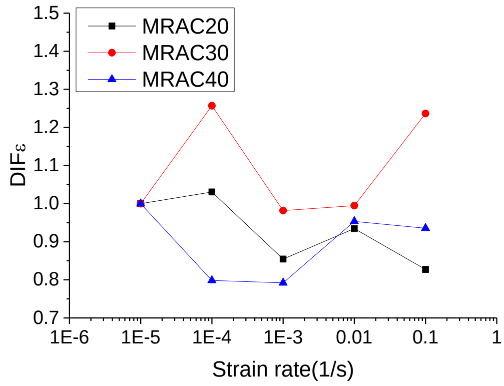

Fig. 2-48 Effect of static strength on the DIF_ε of MRAC

2.4.2.3 Effect of static strength on elastic modulus and DIF_E of MRAC

The elastic modulus of MRAC20, MRAC30 and MRAC40 at all the strain rates studied are compared in Fig. 2-49. The results show that the MRAC with larger static strength has a higher dynamic elastic modulus. However, the relationships between the dynamic elastic modulus of MRAC30 and MRAC40 and strain rate are not obvious due to the large dispersion of the data itself.

The values of DIF_E of MRAC20, MRAC30 and MRAC40 at all the strain rates studied are compared in Fig. 2-50. The results show that the elastic modulus of the lower static strength MRAC increases more rapidly with the increase in strain rate, further indicating that the strain-rate sensitivity of lower strength MRAC is more significant.

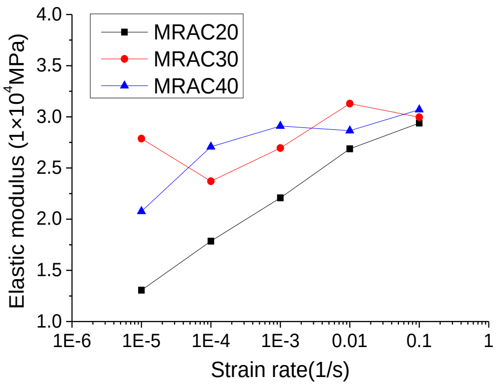

Fig. 2-49 Effect of static strength on the dynamic elastic modulus of MRAC

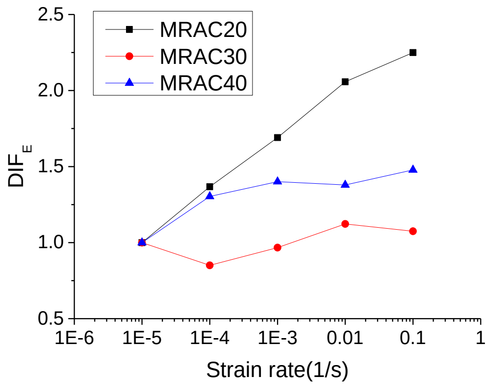

Fig. 2-50 Effect of static strength on the DIF_E of MRAC

2.4.2.4 Effect of static strength on failure pattern of MRAC

Comparing the failure patterns of the MRAC20, MRAC30 and MRAC40 at each strain rate as described above, It can be noted that the three types of MRAC specimens have both common features and differences. The common characteristics are displayed as follows. At each strain rate, the cracks appeared in the interfaces and finally passed through both old interfaces and new interfaces. As the strain rate increases, there was no significant difference in the number of cracks. At a higher strain rate, the main cracks were less in number and larger in width. There were also some different features. For MRAC20, there were more cracks in the new interfaces than in the old interfaces. This is because the strength of the new mortar is lower than that of old mortar in MRAC20. For MRAC30, the cracks appeared firstly in the old interface, and finally the number of cracks in the new interface and the old interface had no significant difference. This is because the elastic modulus of the mortar and the granite is quite different, leading to more obvious stress concentration between the granite and the old mortar. As a result, the cracks formed firstly in the old interface. After failure, the number of cracks in the new interface and old interface was similar because the strength of the old mortar and the new mortar was similar. For MRAC40, the failure characteristic was similar to that of MRAC30 because the strength and elastic modulus of M40 and M30 was similar.

2.4.3 Effect of RCA replacement percentage on strain-rate sensitivity of MRAC

In this section, the dynamic mechanical properties of MRAC with different RCA replacement percentages are compared and analyzed from the aspects of peak stress, peak strain, elastic modulus and failure pattern. Here, MNAC30, MRACP30 and MRAC30 represent the MRACs of which the RCA replacement percentages are 0%, 55% and 100%, respectively.

2.4.3.1 Effect of RCA replacement percentage on peak stress and DIF_f of MRAC

The peak stresses of MNAC30, MRACP30 and MRAC30 at all the strain rates studied are compared in Fig. 2-51. It can be noted that the peak stress of MRAC decreased with the increase in RCA replacement percentage at each strain rate. The value of DIF_f of MNAC30, MRACP30 and MRAC30 at all the strain rates studied are compared in Fig. 2-52, the results show that the growth rate of the MRAC with 55% RCA is largest, and the second is the MRAC with 100% RCA. The smallest one is the MRAC with 0% RCA. According to the Eq. (2-21), Eq. (2-18) and Eq. (2-12), the trend can also be found. Namely, the peak stress of MNAC30, MRACP30 and MRAC30 increased by 4.29%、6.9%、6.2% when the strain rate increase by a factor of 10. However, when the DIF_f of MNAC30, MRACP30 and MRAC30 at the strain rate of 10^{-1} /s are compared, It can be noted that the DIF_f of MRAC with 100% RCA is largest, which means its strain-rate sensitivity is most significant. Overall, it can be concluded that the strain-rate sensitivity of MRAC is more significant than that of MNAC, but the effect of the RCA replacement percentage on the strain-rate sensitivity of MRAC is not very clear.

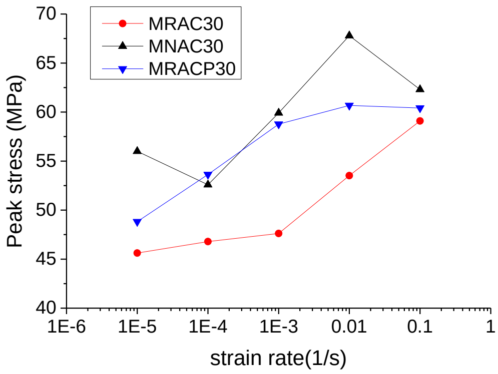

Fig. 2-51 Effect of RCA replacement percentage on the dynamic peak stress of MRAC

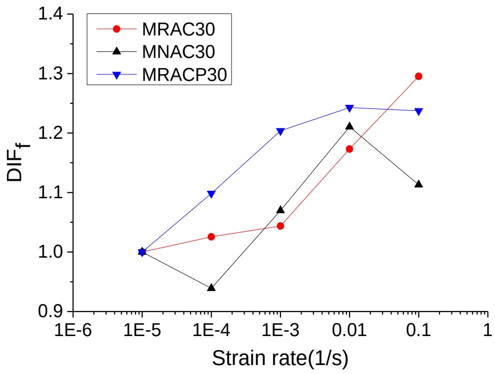

Fig. 2-52 Effect of RCA replacement percentage on the DIF_f of MRAC

2.4.3.2 Effect of RCA replacement percentage on peak strain and DIF_ε of MRAC

The peak stresses of MNAC30, MRACP30 and MRAC30 at all the strain rates studied are compared in Fig. 2-53. The results show that there is no clear relationship between the RCA replacement percentage and the peak strain of MRAC at each strain rate. The value of DIF_ε of MNAC30, MRACP30 and MRAC30 at all the strain rates studied are compared in Fig. 2-54, the results show that there is also no clear relationship between the RCA replacement percentage and the DIF_ε of MRAC at each strain rate. In general, the peak strain tends to be unchanged as the strain rate increases for MRAC with all RCA replacement percentages.

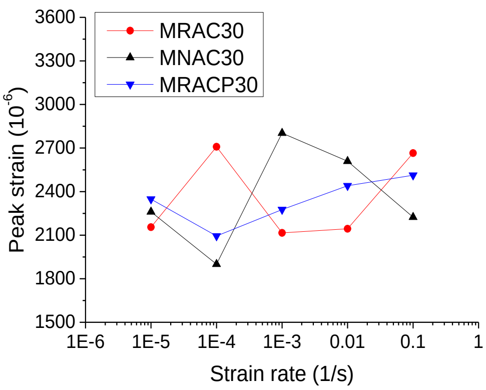

Fig. 2-53 Effect of RCA replacement percentage on the dynamic peak strain of MRAC

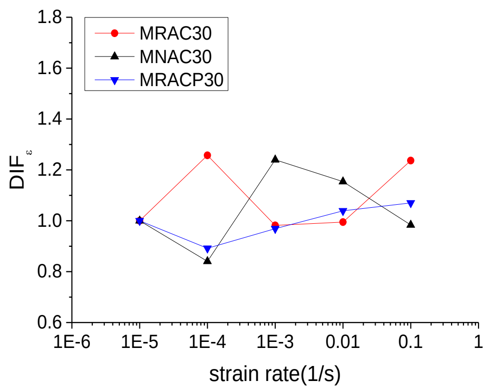

Fig. 2-54 Effect of RCA replacement percentage on the DIF_ε of MRAC

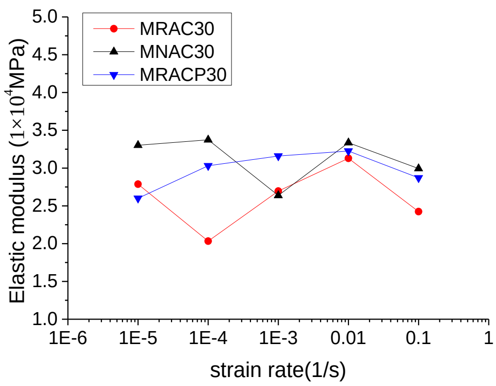

Fig. 2-55 Effect of RCA replacement percentage on dynamic elastic modulus of MRAC

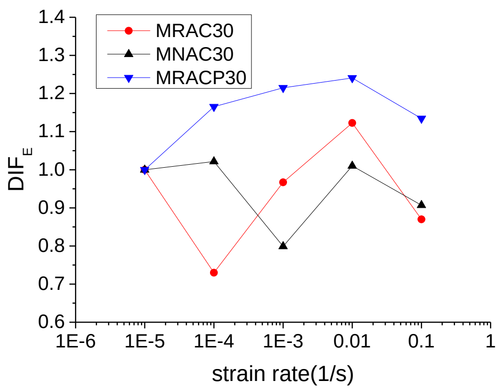

Fig. 2-56 Effect of RCA replacement percentage on the DIF_E of MRAC

2.4.3.1 Effect of RCA replacement percentage on elastic modulus and DIF_E of MRAC

The elastic modulus of MNAC30, MRACP30 and MRAC30 at all the strain rates studied are compared in Fig. 2-55. It can be noted that the elastic modulus of MRAC generally decreases with the increase in RCA replacement percentage at each strain rate. However, due to the large dispersion of the elastic modulus data in this test, abnormalities occur at the strain rate of 10^{-5} /s and 10^{-3} /s. The value of DIF_E of MNAC30, MRACP30 and MRAC30 at all the strain rates studied are compared in Fig. 2-56, it indicates that the strain-rate effect of the elastic modulus of MRACP30 is more significant than that of MRAC30 and MNAC30. However, because the dispersion of the elastic modulus in this test is large, it is not clear whether this phenomenon is a real conclusion.

2.4.4 Comparison on the dynamic property of MM30, MRAC30 and MNAC30

2.4.4.1 Comparison on peak stress, peak strain and elastic modulus

The peak stresses, peak strain and elastic modulus of MM30, MRAC30 and MNAC30 at all the strain rates studied are compared in Fig. 2-57, Fig. 2-58, and Fig. 2-59. The results show that under the same strain rate, the dynamic peak stress of MNAC30 is the largest, followed by MM30, the smallest one is MRAC30. At the same strain rate, the dynamic peak strain of MM30 is larger, and the relationship between the dynamic peak strain MNAC30 and MRAC30 is not clear. When the strain rate is the same, the elastic modulus of NAC is the largest, followed by RAC, and the elastic modulus of the mortar is the least. This is because the elastic modulus of the natural aggregate is much larger than that of the mortar.

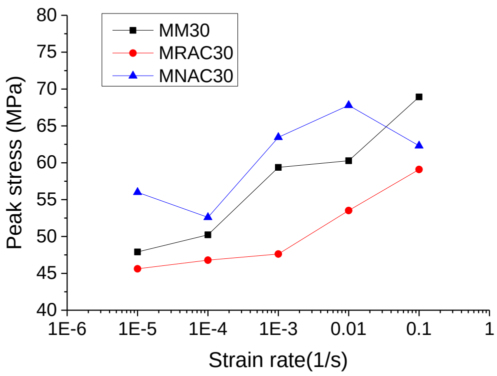

Fig. 2-57 Comparison of the peak stress of MM30, MRAC30 and MNAC30

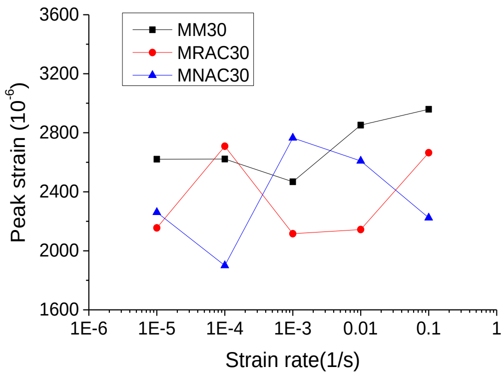

Fig. 2-58 Comparison of the peak strain of MM30, MRAC30 and MNAC30

2.4.4.2 Comparison on strain-rate sensitivity

The relationship between the DIF_f of MM30, MRAC30 and MNAC30 and the strain rate is shown in Fig. 2-60. The results show that the DIF_f of MM30 is larger and it increases at the fastest rate with the increase in strain rate. The relationship between the value of DIF_f of MRAC30 and MNAC30 is not clear due to the discrepancy of the experimental results. Overall, the rate of increase in DIF_f of MRAC30 is faster than that of MNAC30. From the Eq. (2-6), Eq. (2-12) and Eq. (2-21), as the strain rates are increases by a factor of 10, the peak stresses of MM30, MRAC30 and MNAC30 are also increased by 10.2%, 6.2% and 4.29% respectively. Therefore, it can be inferred that the mortar is the most sensitive to the strain rate, followed by RAC, and NAC is the least. This is because NAC and RAC contain natural aggregate, which is less strain-rate sensitive than the mortar, making the strain-rate sensitivity of NAC and RAC less significant than the mortar. Moreover, the content of mortar in RAC is higher than that of NAC, which makes the strain-rate sensitivity of RAC higher than that of NAC.

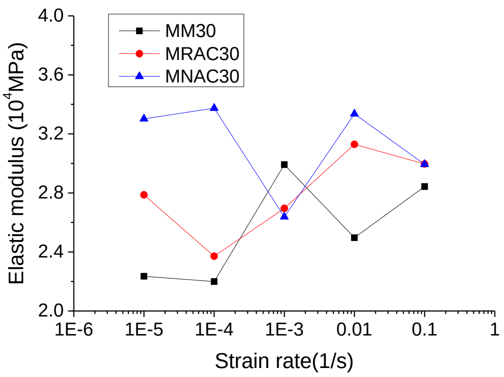

Fig. 2-59 Comparison of the elastic modulus of MM30, MRAC30 and MNAC30

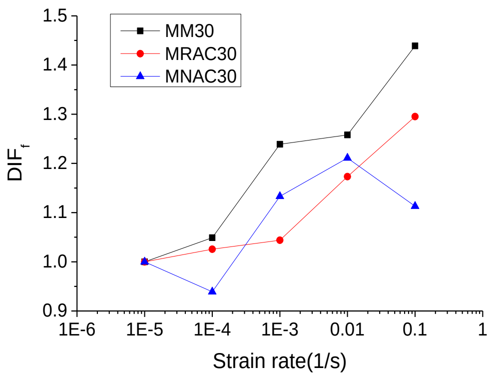

Fig. 2-60 Comparison of the DIF_f of MM30, MRAC30 and MNAC30

2.5 Summary

In this chapter, the stress-strain curves of the modeled recycled aggregate concrete (MRAC) and mortar were experimentally studied under low strain rates (i.e., 10^{-5} /s ~ 10^{-1} /s). By analyzing the effect of strain rate on peak stress, peak strain, elastic modulus and failure pattern, the strain-rate sensitivity of MRAC and mortar were studied. At the same time, the effects of the recycled coarse aggregate (RCA) content and the static strength on the strain-rate sensitivity of MRAC were discussed. In summary, the main conclusions are displayed as follows:

(1) With the increase in the strain rate, the peak stress and elastic modulus of MRAC increased, and the peak strain fluctuated around a constant value, and the failure pattern did not change obviously.

(2) The dynamic peak stress and elastic modulus of the lower strength MRAC were smaller than the higher strength MRAC. The value of DIF_f and DIF_E of the lower strength MRAC were larger than that of the higher strength MRAC, indicating that the strain-rate sensitivity of RAC is more significant when its static strength is lower.

(3) Regardless of static loading or dynamic loading, the peak stress and elastic modulus of MRAC

decreased with the increase in RCA replacement percentage under the same strain rate, while the relationship between the peak stain and the RCA replacement percentage was not clear. The strain-rate sensitivity of RAC with 100% RCA was more significant than that of NAC, but the relationship between the strain-rate sensitivity and the RCA replacement percentage did not show a clear trend.

(4) The mortar was most sensitive to strain rate, followed by RAC, and NAC was least sensitive to strain rate.

Chapter 3 Dynamic mechanical behavior of RAC at low strain rates

In the previous chapter, the dynamic mechanical properties of RAC under uniaxial compression were studied based on the MRAC. However, because it is a simplified model of RAC, it may not fully reflect the properties of RAC in some aspects. Therefore, the results in the previous chapter need to be compared with the real RAC to ensure the rationality of using MRAC to study the dynamic properties of RAC. In order to understand the dynamic mechanical properties of RAC more accurately and verify the rationality of using MRAC, the dynamic mechanical properties of real RAC under uniaxial compressive loading at low strain rates (i.e., 10^{-5} /s ~ 10^{-1} /s) were studied in this chapter.

In this chapter, the stress-strain curves and failure modes of RAC under different strain rates were studied. The strain-rate sensitivity of RAC was studied by evaluating the effect of strain rate on peak stress, peak strain, elastic modulus, energy absorption capacity and failure mode. The effect of RCA replacement percentage on the strain-rate sensitivity of RAC was also investigated. In addition, considering that the free water in concrete was considered as one of the important factors causing the strain-rate sensitivity of concrete, the effect of the moisture condition on the strain-rate sensitivity of RAC was also studied.

3.1 Test design

3.1.1 Materials

The cement used was an ordinary Portland cement of 42.5 Grade. River sand was used as the fine aggregate, of which the fineness modulus was 2.6. The selected coarse aggregates were natural coarse aggregates (NCA) from a local aggregate production plant and RCA derived from waste concrete which were obtained from a local RCA manufacturing plant in Shanghai, China. The physical properties of the NCA and the RCA were determined according to the Chinese specification GB T14685-2011 (2011), as given in Table 3-1. The grading of RCA conformed to the requirement of coarse aggregate prescribed in ASTM C33/C33M–13 (2013), as shown in Fig. 3-1.

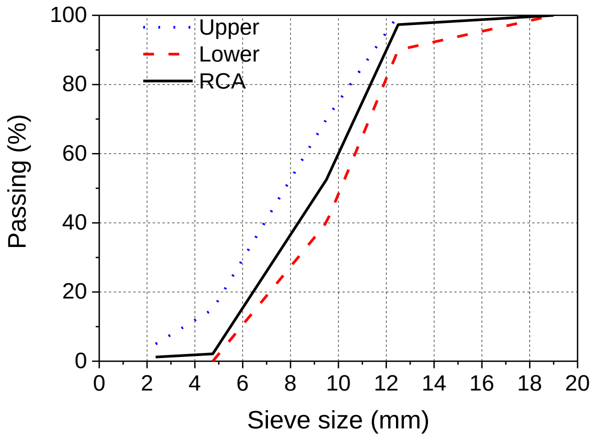

Fig. 3-1 The grading curve of RCA

Five RAC replacement percentages, i.e., 0%, 30%, 50%, 70% and 100%, were used to prepared RAC for the tests; the corresponding specimens were named NAC, RAC30, RAC50, RAC70 and RAC100. The mix proportions of RAC are listed in Table 3-2. In this study, RCA in an air-dry condition was used when casting RAC specimens. Here, considering the high water absorption of RCA, additional amounts of water was added to assure the same effective w/c. Additional water of RCA was measured according to the water absorbed from air-dry condition to saturated surface dry condition.

Table 3-1 Physical properties of NCA and RCA

Type	Size (mm)	Bulk density (kg/m^3)	Apparent density (kg/m^3)	Crushing index (%)	Water absorption (%)
NCA	5-12.5	1395	2634	5.0	0.95
RCA	5-12.5	1290	2620	12.4	6.30

Table 3-2 Mix proportions of concretes

Specimen	effective w/c	Cement (kg/m^3)	Sand (kg/m^3)	NCA (kg/m^3)	RCA (kg/m^3)	Mixing water (kg/m^3)	Additional water (kg/m^3)
NAC	0.45	467	582	1082	0	210	0
RAC30	0.45	467	574	746	320	210	12.8
RAC50	0.45	467	568	528	528	210	21.12
RAC70	0.45	467	562	313.5	731.5	210	29.26
RAC100	0.45	467	554	0	1029	210	41.46

Table 3-3 Number and distribution of the specimens

Strain rate (/s)	Number of specimen				
	NAC	RAC30	RAC50	RAC70	RAC100
10^{-5}	3+3	3	3	3	3+3
10^{-4}	3	0	0	0	3
10^{-3}	3+3	3	3	3	3+3
10^{-2}	3	0	0	0	3
10^{-1}	3+3	3	3	3	3+3

3.1.2 Specimen design and preparation

Cylindrical RAC specimens with a size of Φ70mm × 140mm were designed in the test. Among them, there were 15 NAC and RAC100 specimens which were tested in five groups at different strain rates. For RAC30, RAC50 and RAC70, there were 9 specimens which were prepared for three different strain rates. In addition, in order to explore the influence of the moisture condition on the strain-rate sensitivity of RAC, nine additional wet NAC and RAC100 specimens were prepared for three different strain rates. The number and distribution of the specimens are shown in Table 3-3.

The specimens were first cast in polyvinylchloride (PVC) pipes (Diameter (D)=75mm, Length (L)=320 mm). The diameter of the specimens was about 70 mm, and the specimens were demoulded after 24 hours and put in a curing room (RH=95%, T=20°C) for 28 days. Then, the specimens were cut by a diamond saw, to produce two types of cylindrical specimens with different lengths, i.e. L_1=35mm and L_2=140mm. The cut surfaces were ground to ensure they were smooth. The first type of specimens (L/D=0.5) were for the Split Hopkinson Pressure Bar (SHPB) test and the results will be introduced in the next chapter, as shown in Fig. 3-2 (a). The second type of specimens, with the same diameter as those for the SHPB test and an L/D of 2, were used for axial loading tests with the strain rates from $10^{-5}s^{-1}$ to $10^{-1}s^{-1}$, as shown in Fig. 3-2 (b). Wang *et al*. (2011) suggested that cylinders with the same diameter as those of the SHPB but with L/D=2 are suitable for determining the static strength to be used in the Dynamic Increase Factor (DIF) computations.

(a) Φ70mm×35mm (b) Φ70mm×140mm

Fig. 3-2 RAC specimens

The prepared specimens were kept under indoor conditions for 1 year after casting to ensure an air-dry condition was reached before testing. Certain number of RAC100 and NAC specimens, named RAC100(wet) and NAC(wet) respectively, were further immersed in water under an indoor environment for 2 days before testing in order to study the effect of moisture condition on the dynamic compressive behavior of the RAC.

3.1.3 Experimental setup and testing

The testing machine is the same as that used in chapter 2. The specimens were loaded with five different loading velocities ranging from 1.4×10^{-3} mm/s to 14mm/s, with each increment by a factor of 10, corresponding to the strain rate varing from $10^{-5}s^{-1}$ to $10^{-1}s^{-1}$. In order to reduce the frictional constraints, two Teflon sheets with a thickness of 0.1 mm were used both at the top and bottom of the specimens (1997). The tests were terminated when the displacements reached about 1.2 mm which was sufficient to cover the complete stress-strain curves, including the ascending and descending portions. The specimens failed in about 15 min when loaded at the slowest strain rate of $10^{-5}s^{-1}$, which could be considered as a quasi-static loading, while the specimens failed in about 0.1s when the fastest strain rate of $10^{-1}s^{-1}$ was used. The loads applied to the specimens were measured by the internal force transducer in the system. The displacements of the loading platen, which consists of the displacement of specimens, Teflon sheets and testing machine, were recorded via the internal linear variable differential transformer (LVDT) attached to the test setup.

3.2 Data processing method

In order to obtain the stress-strain curve of the RAC specimens, it is necessary to know the displacement of the RAC specimen itself. However, as described in Chapter 2, the displacement measured by the machine's internal LVDT actually contains the displacement of specimen and additional displacement (d_{add}), which should be obtained from calibration test.

In chapter 2, it has already been described a means to obtain the relationship between the d_{add} and the force F at different strain rates by the calibration test, and thus to correct the total displacement data measured by the LVDT, it will not be repeated here. However, it was found from the calibration tests that when different sizes of steel blocks were used, the $d_{add} - F$ relationships were different. Fig. 3-3 compares the $d_{add} - F$ relationships when using two different sizes of steel blocks, which are 150mm × 150mm × 30mm and 100mm × 100mm × 300mm, respectively. The results show that the difference between them was large. The possible reason is that the rigidity of the machine itself is quite different from that of the steel block in both cases. The rigidity of the machine represents the sum of the stiffness of all devices except the specimen, including the machine frame, loading plates, force sensor and Teflon sheets and so on. The d_{add} refers to the sum of the deformations of all devices except the specimen. When the first type of steel block is used, more plates are required, which makes the total rigidity of the machine smaller. It is speculated that the height of the specimen (determined by the number of plates) has a large influence on the rigidity of the machine. Therefore, the $d_{add} - F$ relationship obtained by the calibration test using the first type of steel block was used in this chapter because the height RAC specimen was closer to the steel block. However, because the testing condition, the rigidity of the machine is certainly different, so some adjustments are needed.

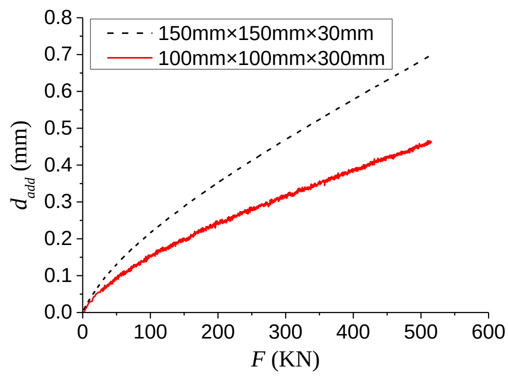

Fig. 3-3 The $d_{add} - F$ relationships using different steel blocks in calibration test

According to the testing condition, the $d_{add} - F$ relationship obtained by the calibration test using the first type of steel block is adjusted by adding a reduction coefficient which is 0.85. Moreover, the same $d_{add} - F$ relationship is used at different strain rates to reduce the error accumulation. This $d_{add} - F$ relationship can be expressed as:

$$d_{add} = \mathrm{a} + \mathrm{b} \times F + \mathrm{c} \times F^2 + \mathrm{d} \times F^3 + \mathrm{e} \times F^4 \qquad (3\text{-}1)$$

Where, a is 0.00315, b is 0.00196, c is 4.6219×10^{-6}, d is 0.8994×10^{-8} , e is 6.572×10^{-12}.

3.3 Test results

In this part, the stress-strain curves and failure patterns of RAC specimens were obtained. The dynamic mechanical properties of RAC were analyzed from peak stress, elastic modulus, and peak strain. The stress-strain curve of the specimen whose peak stress was in the middle was considered as typical stress-strain curve. Peak stress is the maximum stress in the stress-strain curve. The peak strain is the strain corresponding to the peak stress. The secant slope between 20% and 40% of peak stress in the stress-strain curve is considered as elastic modulus.

3.3.1 NAC Specimen

3.3.1.1 Stress-strain curves of NAC at different strain rates

The stress-strain curves of NAC at all the strain rates studied are shown in Fig. 3-4. The results show that the stress-strain curves of NAC were similar at all the strain rates studied, and the nonlinearity of stress-strain curves became obvious when the stress is close to the peak stress. The stress after the peak stress decreased faster with the increase in strain rate. As the strain rate is increased, the peak stress and the elastic modulus showed an increasing trend, while the change inin the peak strain was not obvious. The peak stress, peak strain and elastic modulus of NAC specimens are shown in Table 3-4.

Table 3-4 The peak stress, peak strain and elastic modulus of NAC specimens

Strain rate （/s）	No.	Peak stress (MPa)	DIF_f	Peak strain (10^{-6})	DIF_ε	Elastic modulus (GPa)	DIF_E
10^{-5}	1	34.8	0.988	1706	1.001	28.8	0.989
	2	35.2	0.998	1725	1.012	28.4	0.975
	3	35.7	1.011	1684	0.988	30.2	1.036
	AVG	**35.3**	**1.000**	**1705**	**1.000**	**29.1**	**1.000**
10^{-4}	1	38.3	1.086	1682	0.987	34.2	1.172
	2	37.7	1.069	1553	0.911	29.1	0.998
	3	43.2	1.223	1592	0.934	40.2	1.380
	AVG	**39.7**	**1.126**	**1609**	**0.944**	**34.5**	**1.183**
10^{-3}	1	45.8	1.298	1391	0.816	41.0	1.408
	2	44.3	1.255	1917	1.124	32.2	1.104
	3	43.2	1.225	1520	0.891	39.5	1.354
	AVG	**44.4**	**1.259**	**1609**	**0.944**	**37.6**	**1.289**
10^{-2}	1	40.0	1.135	1502	0.881	38.7	1.327
	2	-	-	-	-	-	-
	3	43.7	1.239	1522	0.893	36.9	1.265
	AVG	**41.9**	**1.187**	**1512**	**0.887**	**37.8**	**1.296**
10^{-1}	1	49.1	1.392	1723	1.011	46.9	1.608
	2	46.8	1.326	1549	0.909	43.0	1.476
	3	46.1	1.308	1484	0.870	42.0	1.440
	AVG	**47.3**	**1.342**	**1585**	**0.930**	**43.9**	**1.508**

3.3.1.2 Effect of strain rate on peak stress of NAC

According to Table 3-4, the average peak stress of the NAC specimens are 35.27MPa, 39.72MPa, 44.41MPa, 41.87MPa and 47.34MPa respectively when the strain rate are 10^{-5} /s, 10^{-4} /s, 10^{-3} /s, 10^{-2} /s and 10^{-1} /s. It indicates that the peak stress of NAC increased with the increase in strain rate in general, while abnormal point appeared at the strain rate of 10^{-2} /s. The relationship between the DIF_f of NAC and strain rate is shown in Fig. 3-5, the fitting curve could be expressed as

$$DIF_f = 1 + 0.0884 \cdot \lg(\dot{\varepsilon} / \dot{\varepsilon}_s) \tag{3-2}$$

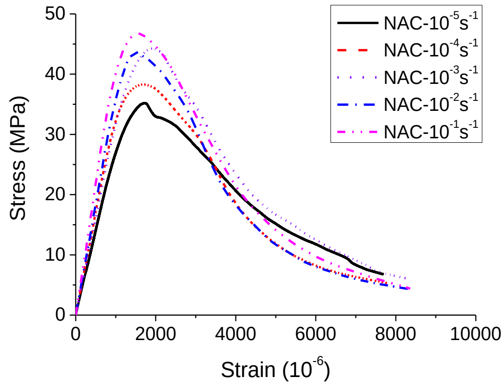

Fig. 3-4 Stress-strain curves of NAC at different strain rates

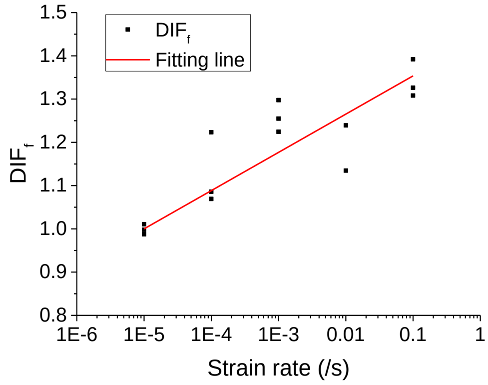

Fig. 3-5 Relationship between the DIF_f of NAC and strain rate

3.3.1.3 Effect of strain rate on peak strain of NAC

According to Table 3-4, the average peak strain of the NAC specimens were 1705με, 1609με, 1609με, 1512με and 1585με respectively when the strain rate are 10^{-5} /s, 10^{-4} /s, 10^{-3} /s, 10^{-2} /s and 10^{-1} /s. It shows that the peak strain of NAC showed a slightly decreasing tendency with the increase in strain rate in general. The relationship between the DIF_ε of NAC and strain rate is shown in Fig. 3-6. The fitting line could be expressed as

$$DIF_\varepsilon = 1\text{-}0.0250 \cdot \lg(\dot{\varepsilon} / \dot{\varepsilon}_s) \tag{3-3}$$

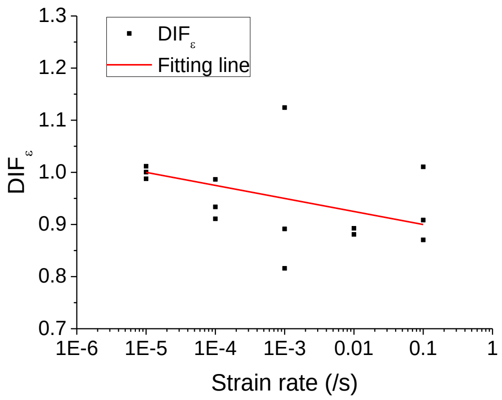

Fig. 3-6 Relationship between the DIF_ε of NAC and strain rate

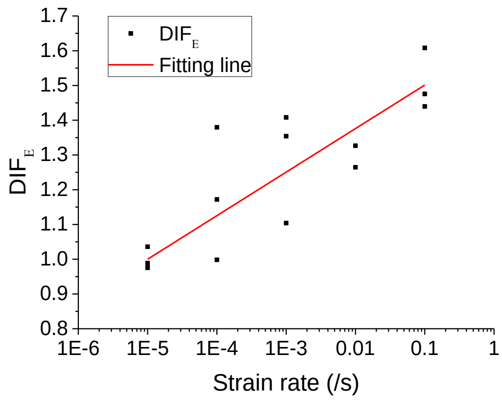

Fig. 3-7 Relationship between the DIF_E of NAC and strain rate

3.3.1.4 Effect of strain rate on elastic modulus of NAC

According to Table 3-4, the average elastic modulus of the NAC specimens were 29.14GPa, 34.48GPa, 37.55GPa, 37.76GPa and 43.94GPa respectively when the strain rate are 10^{-5} /s, 10^{-4} /s, 10^{-3} /s, 10^{-2} /s and 10^{-1} /s. The corresponding DIF_E of NAC were 1, 1.183, 1.289, 1.296 and 1.508, respectively. It shows that the elastic modulus of NAC increased with the increase in strain rate in general. The relationship between the DIF_E of NAC and strain rate is shown in Fig. 3-7, the fitting curve could be expressed as

$$DIF_E = 1 + 0.1253 \cdot \lg(\dot{\varepsilon} / \dot{\varepsilon}_s) \tag{3-4}$$

3.3.2 RAC30 Specimen

3.3.2.1 Stress-strain curves of RAC30 at different strain rates

The stress-strain curves of RAC30 at all the strain rates studied are shown in Fig. 3-8. The results show that the stress-strain curves were similar at all the strain rates studied, and the nonlinearity of stress-strain curves became obvious when the stress was close to the peak stress. As the strain rate was increased, the peak stress and the elastic modulus increase, while the peak strain showed a slight increase. The peak stress, peak strain and elastic modulus of RAC30 specimens are shown in Table 3-5.

Table 3-5 The peak stress, peak strain and elastic modulus of RAC30 specimens

Strain rate (/s)	No.	Peak stress (MPa)	DIF_f	Peak strain (10^{-6})	DIF_ε	Elastic modulus (GPa)	DIF_E
10^{-5}	1	39.4	1.088	1532	0.981	29.3	1.031
	2	35.8	0.989	1707	1.093	25.9	0.912
	3	33.3	0.922	1448	0.927	30.0	1.057
	AVG	**36.2**	**1.000**	**1562**	**1.000**	**28.4**	**1.000**
10^{-3}	1	38.7	1.070	1663	1.065	32.2	1.133
	2	37.7	1.043	1901	1.217	27.5	0.967
	3	41.7	1.154	1644	1.052	36.6	1.290
	AVG	**39.4**	**1.089**	**1736**	**1.111**	**32.1**	**1.130**
10^{-1}	1	43.9	1.214	1771	1.134	34.4	1.211
	2	43.3	1.197	1402	0.898	39.0	1.372
	3	44.3	1.226	1694	1.085	36.7	1.293
	AVG	**43.9**	**1.212**	**1622**	**1.038**	**36.7**	**1.292**

3.3.2.2 Effect of strain rate on peak stress of RAC30

According to Table 3-5, the average peak stress of the RAC30 specimens were 36.17MPa, 39.39MPa and 43.85MPa respectively when the strain rate were 10^{-5} /s, 10^{-3} /s and 10^{-1} /s. The corresponding DIF_f of RAC30 were 1, 1.089 and 1.212 respectively. It indicates that the peak stress of RAC30 increased with the increase in strain rate. The relationship between the DIF_f of RAC30 and strain rate is shown in Fig. 3-9. The fitting line could be expressed as

$$DIF_f = 1 + 0.0514 \cdot \lg(\dot{\varepsilon} / \dot{\varepsilon}_s) \quad (3\text{-}5)$$

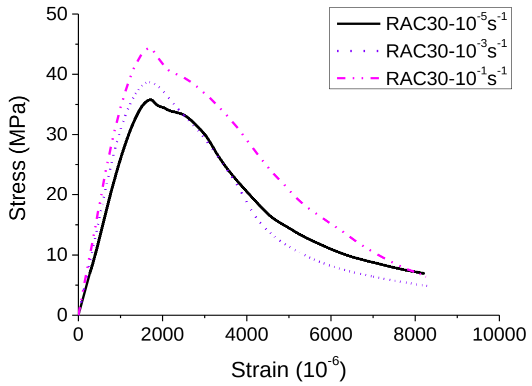

Fig. 3-8 Stress-strain curves of RAC30 at different strain rates

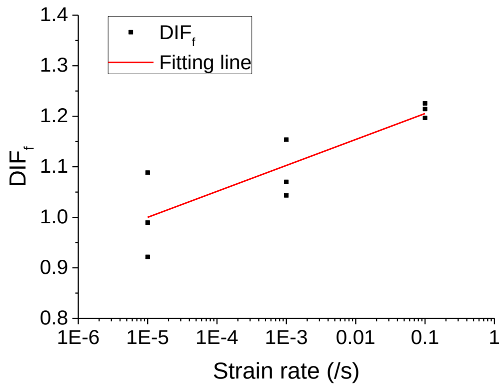

Fig. 3-9 Relationship between the DIF_f of RAC30 and strain rate

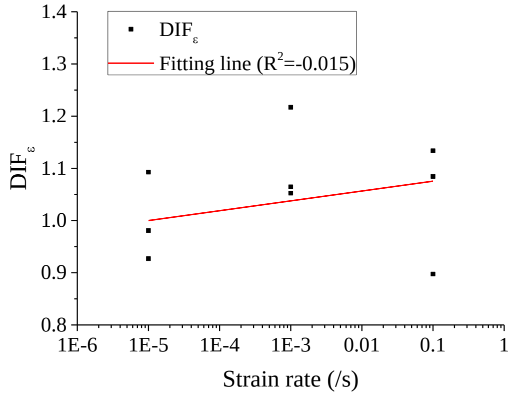

Fig. 3-10 Relationship between the DIF_ε of RAC30 and strain rate

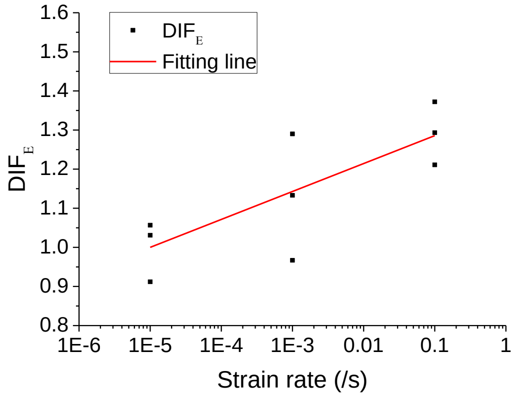

Fig. 3-11 Relationship between the DIF_E of RAC30 and strain rate

3.3.2.3 Effect of strain rate on peak strain of RAC30

According to Table 3-5, the average peak strain of the RAC30 specimens were 1562με, 1736με and 1622με respectively when the strain rate were 10^{-5} /s, 10^{-3} /s and 10^{-1} /s. The corresponding DIF_ε of RAC30 were 1.000, 1.111 and 1.038, respectively. It shows that the peak strain of RAC30 firstly increased and then decreased with the increase in strain rate. The relationship between the DIF_ε of RAC30 and strain rate is shown in Fig. 3-10. The fitting line could be expressed as

$$DIF_\varepsilon = 1{+}0.0187 \cdot \lg(\dot{\varepsilon} / \dot{\varepsilon}_s) \quad (3\text{-}6)$$

It shows that the R^2 of regression line for peak strain is very low which indicates that the variation of the peak strain were large, and it was not very suitable to make conclusion based on the fitting line.

3.3.2.4 Effect of strain rate on elastic modulus of RAC30

According to Table 3-5, the average elastic modulus of the RAC30 specimens were 28.40GPa, 32.09GPa and 36.70GPa respectively when the strain rate were 10^{-5} /s, 10^{-3} /s and 10^{-1} /s. The corresponding DIF_E of RAC30 were 1.000, 1.130 and 1.292, respectively. It shows that the elastic modulus of RAC30 increased with the increase in strain rate in general. The relationship between the DIF_E of RAC30 and the strain rate is shown in Fig. 3-11, the fitting curve could be expressed as

$$DIF_E = 1 + 0.0714 \cdot \lg(\dot{\varepsilon} / \dot{\varepsilon}_s) \tag{3-7}$$

Table 3-6 The peak stress, peak strain and elastic modulus of RAC50 specimens

Strain rate (/s)	No.	Peak stress (MPa)	DIF_f	Peak strain (10^{-6})	DIF_ε	Elastic modulus (GPa)	DIF_E
10^{-5}	1	33.7	0.953	1515	0.866	28.1	0.993
	2	38.0	1.074	2018	1.153	27.9	0.987
	3	34.4	0.973	1718	0.982	28.8	1.019
	AVG	**35.3**	**1.000**	**1750**	**1.000**	**28.2**	**1.000**
10^{-3}	1	35.7	1.011	1582	0.904	27.1	0.961
	2	34.2	0.967	-	-	-	-
	3	41.6	1.177	1700	0.971	28.5	1.008
	AVG	**37.2**	**1.052**	**1641**	**0.938**	**27.8**	**0.984**
10^{-1}	1	45.9	1.300	2055	1.174	37.1	1.313
	2	45.7	1.292	1837	1.050	34.2	1.210
	AVG	**45.8**	**1.296**	**1946**	**1.112**	**35.6**	**1.262**

3.3.3 RAC50 Specimen

3.3.3.1 Stress-strain curves of RAC50 at different strain rates

The stress-strain curves of RAC50 at all the strain rates studied are shown in Fig. 3-12. The results show that the stress-strain curves were similar all the strain rates studied, and the nonlinearity of stress-strain curves became obvious when the stress was close to the peak stress. The decreasing trend of the descending part of the all stress-strain curves was similar. As the strain rate is increased, the peak stress and the elastic modulus increase, while the peak strain also showed an increasing trend. The peak stress, peak strain and elastic modulus of RAC50 specimens are shown in Table 3-6.

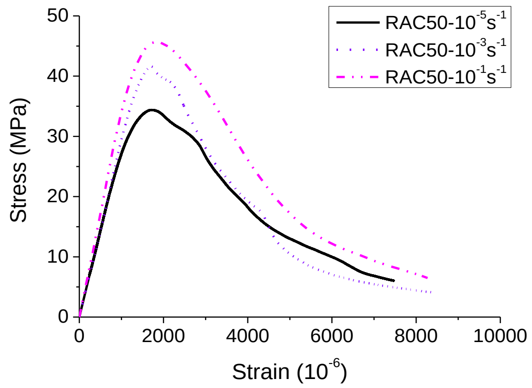

Fig. 3-12 Stress-strain curves of RAC50 at different strain rates

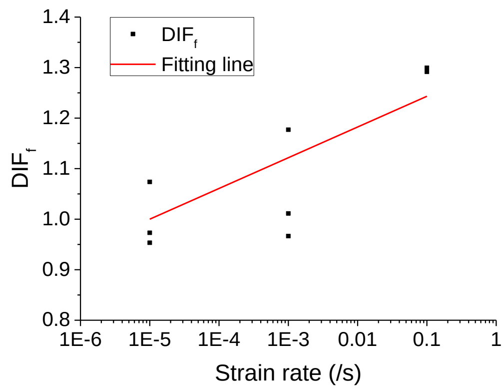

Fig. 3-13 Relationship between the DIF_f of RAC50 and strain rate

3.3.3.2 Effect of strain rate on peak stress of RAC50

According to Table 3-6, the average peak stress of the RAC50 specimens were 35.34MPa, 37.17MPa and 45.79MPa respectively when the strain rate were 10^{-5} /s, 10^{-3} /s and 10^{-1} /s. The corresponding DIF_f were 1, 1.052 and 1.296 respectively. It indicated that the peak stress of RAC50 increased with the increase in strain rate and it increased faster after a strain rate of 10^{-3} /s. The relationship between the DIF_f of RAC50 and strain rate is shown in Fig. 3-13. The fitting line could be expressed as

$$DIF_f = 1 + 0.0608 \cdot \lg(\dot{\varepsilon} / \dot{\varepsilon}_s) \tag{3-8}$$

3.3.3.3 Effect of strain rate on peak strain of RAC50

According to Table 3-6, the average peak strain of the RAC50 specimens were 1750με, 1641με and 1946με respectively when the strain rate were 10^{-5} /s, 10^{-3} /s and 10^{-1} /s. The corresponding DIF_ε are 1, 0.938 and 1.112, respectively. It shows that the peak strain of RAC50 firstly decreased and then increased with the increase in strain rate. The relationship between the DIF_ε of RAC50 and strain rate is shown in Fig. 3-14. The fitting line could be expressed as

$$DIF_\varepsilon = 1 + 0.0162 \cdot \lg(\dot{\varepsilon} / \dot{\varepsilon}_s) \tag{3-9}$$

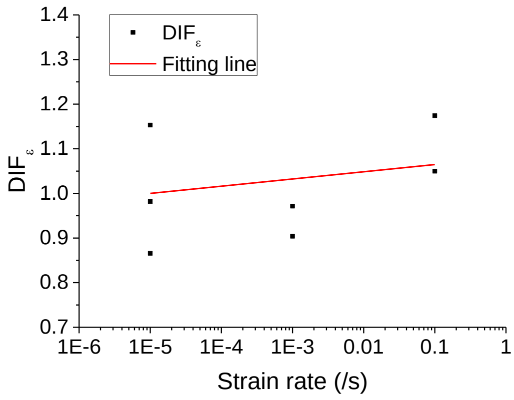

Fig. 3-14 Relationship between the DIF_ε of RAC50 and strain rate

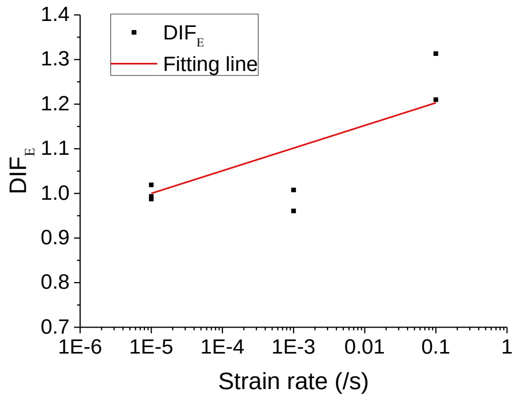

Fig. 3-15 Relationship between the DIF_E of RAC50 and strain rate

3.3.3.4 Effect of strain rate on elastic modulus of RAC50

According to Table 3-6, the average elastic modulus of the RAC50 specimens were 28.24GPa, 27.80GPa and 35.63GPa respectively when the strain rate were 10^{-5} /s, 10^{-3} /s and 10^{-1} /s. The corresponding DIF_E of RAC50 were 1, 0.984 and 1.262, respectively. It shows that the elastic modulus of RAC50 at a strain rate of 10^{-3} /s was lower than that at a strain rate of 10^{-5} /s. However, in general, the elastic modulus of RAC50 increased with the increase in strain rate. The relationship between the DIF_E of RAC50 and strain rate is shown in Fig. 3-15. The fitting curve could be expressed as

$$DIF_{\mathrm{E}} = 1 + 0.0508 \cdot \lg(\dot{\varepsilon} / \dot{\varepsilon}_s) \tag{3-10}$$

3.3.4 RAC70 Specimen

3.3.4.1 Stress-strain curves of RAC70 at different strain rates

The stress-strain curves of RAC70 at all the strain rates studied are shown in Fig. 3-16. The results show that the stress-strain curves were similar at all the strain rates studied, and the nonlinearity of stress-strain curves became obvious when the stress was close to the peak stress. The decreasing rate of the descending part of the all stress-strain curves was larger at a higher strain rate. As the strain rate is increased, the peak stress and the elastic modulus increased, while the peak strain did not show a clear trend. The peak stress, peak strain and elastic modulus of RAC70 specimens are shown in Table 3-7.

Table 3-7 The peak stress, peak strain and elastic modulus of RAC70 specimens

Strain rate (/s)	No.	Peak stress (MPa)	DIF_f	Peak strain (10^{-6})	DIF_ε	Elastic modulus (GPa)	DIF_E
10^{-5}	1	35.4	1.035	2904	1.310	13.8	0.640
	2	32.6	0.952	1932	0.872	22.7	1.056
	3	34.7	1.013	1812	0.818	28.0	1.304
	AVG	**34.2**	**1.000**	**2216**	**1.000**	**21.5**	**1.000**
10^{-3}	1	32.9	0.962	2078	0.938	26.4	1.229
	2	35.3	1.032	2068	0.933	25.4	1.182
	3	38.5	1.127	2305	1.040	20.3	0.944
	AVG	**35.6**	**1.040**	**2150**	**0.970**	**24.0**	**1.118**
10^{-1}	1	44.9	1.312	2086	0.941	33.2	1.547
	2	42.3	1.237	1917	0.865	33.0	1.536
	3	39.6	1.159	2007	0.906	27.7	1.290
	AVG	**42.3**	**1.236**	**2003**	**0.904**	**31.3**	**1.457**

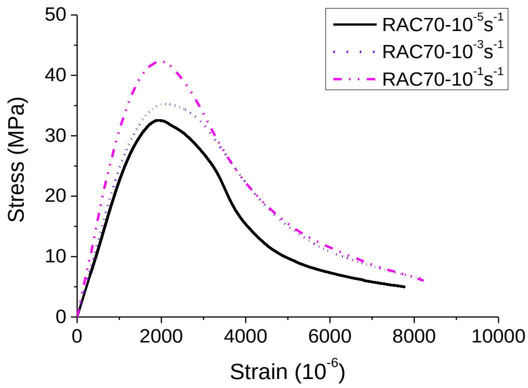

Fig. 3-16 Stress-strain curves of RAC70 at different strain rates

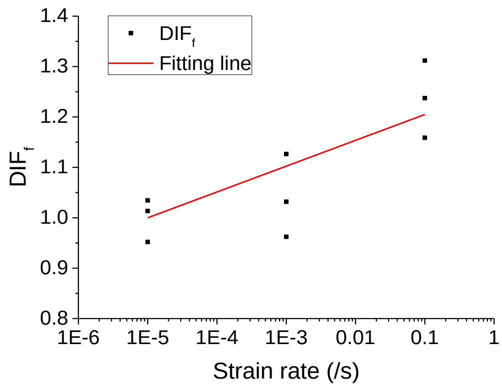

Fig. 3-17 Relationship between the DIF_f of RAC70 and strain rate

3.3.4.2 Effect of strain rate on peak stress of RAC70

According to Table 3-7, the average peak stress of the RAC70 specimens were 34.2Mpa, 35.58MPa and 42.27MPa respectively when the strain rate were 10^{-5} /s, 10^{-3} /s and 10^{-1} /s. The corresponding DIF_f are 1, 1.040 and 1.236 respectively. It indicates that the peak stress of RAC70 increased with the increase in strain rate and the increase was more obvious after a strain rate of 10^{-3} /s. The relationship between the DIF_f of RAC70 and strain rate is shown in Fig. 3-17. The fitting line could be expressed as

$$DIF_f = 1 + 0.0512 \cdot \lg(\dot{\varepsilon} / \dot{\varepsilon}_s) \tag{3-11}$$

3.3.4.3 Effect of strain rate on peak strain of RAC70

According to Table 3-7, the average peak strain of the RAC70 specimens were 2216με, 2150με and 2003με respectively when the strain rate were 10^{-5} /s, 10^{-3} /s and 10^{-1} /s. The corresponding

DIF_ε are 1, 0.970 and 0.904, respectively. It shows that the peak strain of RAC70 showed a decreasing trend with the increase in strain rate. The relationship between the DIF_ε of RAC70 and strain rate is shown in Fig. 3-18, the fitting curve could be expressed as

$$DIF_\varepsilon = 1\text{-}0.0221 \cdot \lg(\dot{\varepsilon} / \dot{\varepsilon}_s) \tag{3-12}$$

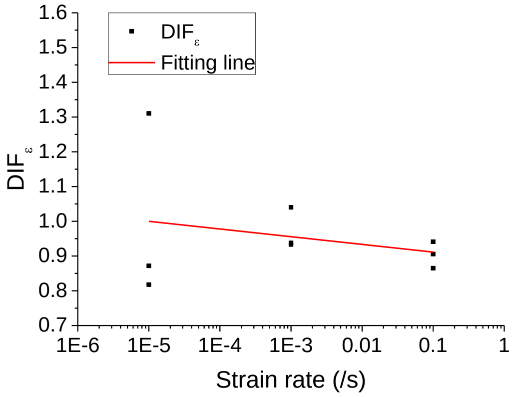

Fig. 3-18 Relationship between the DIF_ε of RAC70 and strain rate

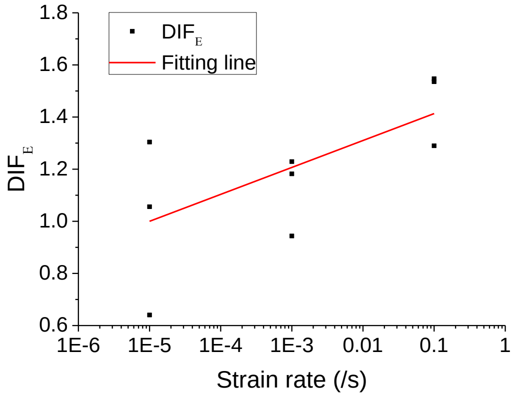

Fig. 3-19 Relationship between the DIF_E of RAC70and strain rate

3.3.4.4 Effect of strain rate on elastic modulus of RAC70

According to Table 3-7, the average elastic modulus of the RAC70 specimens are 21.47GPa, 24.01GPa and 31.29GPa respectively when the strain rate are 10^{-5} /s, 10^{-3} /s and 10^{-1} /s. The corresponding DIF_E are 1, 1.118 and 1.457, respectively. It shows that the elastic modulus of RAC70 increases with the increase in strain rate. The relationship between the DIF_E of RAC70 and strain rate is shown in Fig. 3-19. The fitting line could be expressed as

$$DIF_E = 1+0.1033 \cdot \lg(\dot{\varepsilon} / \dot{\varepsilon}_s) \tag{3-13}$$

3.3.5 RAC100 Specimen

3.3.5.1 Stress-strain curves of RAC100 at different strain rates

The stress-strain curves of RAC70 at all the strain rates studied are shown in Fig. 3-20. The results show that the stress-strain curves were similar at all the strain rates studied, and the nonlinearity of the stress-strain curves became obvious when the stress was close to the peak stress. The decreasing trend of the descending part of the all stress-strain curves was similar. As the strain rate was increased, the peak stress and the elastic modulus increase, while the peak strain showed no clear trend. The peak stress, peak strain and elastic modulus of RAC100 specimens are shown in Table 3-8.

Table 3-8 The peak stress, peak strain and elastic modulus of RAC100 specimens

Strain rate (/s)	No.	Peak stress (MPa)	DIF_f	Peak strain (10^{-6})	DIF_ε	Elastic modulus (GPa)	DIF_E
10^{-5}	1	32.7	1.079	2439	1.035	21.09	1.016
	2	30.1	0.994	2276	0.965	20.42	0.984
	3	28.1	0.927	-	-	-	-
	AVG	**30.3**	**1.000**	**2357.5**	**1.000**	**20.76**	**1.000**
10^{-4}	1	34.7	1.147	2197	0.932	22.91	1.104
	2	32.5	1.074	2282	0.968	21.33	1.027
	3	30.3	1.001	2115	0.897	22.99	1.107
	AVG	**32.5**	**1.074**	**2198**	**0.932**	**22.41**	**1.079**
10^{-3}	1	35.6	1.177	2268	0.962	19.98	0.962
	2	35.5	1.173	2066	0.876	25.74	1.240
	3	34.7	1.147	2097	0.890	22.76	1.096
	AVG	**35.3**	**1.166**	**2144**	**0.909**	**22.83**	**1.100**
10^{-2}	1	36.4	1.204	2080	0.882	27.53	1.326
	2	36.1	1.193	2118	0.898	23.9	1.151
	3	38.3	1.264	2187	0.928	24.59	1.184
	AVG	**36.9**	**1.220**	**2128**	**0.903**	**25.34**	**1.221**
10^{-1}	1	39.7	1.312	2155	0.914	28.02	1.350
	2	39.7	1.312	2300	0.976	23.34	1.124
	3	48.7	1.609	2186	0.927	32.81	1.580
	AVG	**42.7**	**1.411**	**2214**	**0.939**	**28.06**	**1.352**

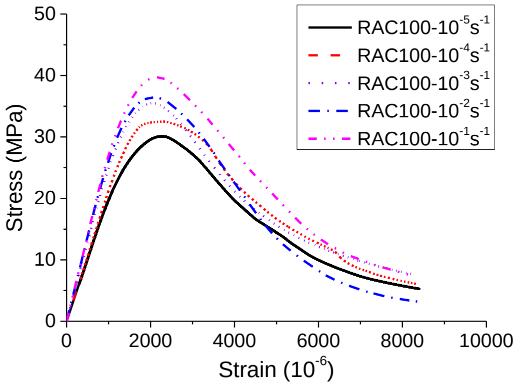

Fig. 3-20 Stress-strain curves of RAC100 at different strain rates

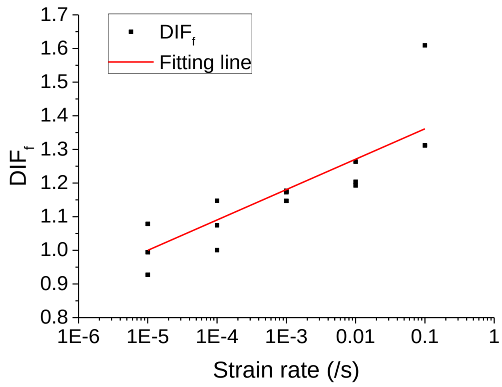

Fig. 3-21 Relationship between the DIF_f of RAC100 and strain rate

3.3.5.2 Effect of strain rate on peak stress of RAC100

According to Table 3-8, the average peak stress of the RAC100 specimens were 30.27MPa, 32.51MPa, 35.28MPa, 36.93MPa and 42.71MPa respectively when the strain rate were 10^{-5} /s, 10^{-4} /s, 10^{-3} /s, 10^{-2} /s and 10^{-1} /s. The corresponding DIF_f were 1, 1.074, 1.166, 1.220 and 1.411 respectively. It indicates that the peak stress of NAC increased with the increase in strain rate in general, it increased slowly before 10^{-2} /s and the increase was uniform, but it increased faster after 10^{-2} /s. The relationship between the DIF_f of RAC100 and strain rate is shown in Fig. 3-21. The fitting line could be expressed as

$$DIF_f = 1 + 0.0903 \cdot \lg(\dot{\varepsilon} / \dot{\varepsilon}_s) \tag{3-14}$$

3.3.5.3 Effect of strain rate on peak strain of RAC100

According to Table 3-8, the average peak strain of the RAC100 specimens were 2357.5με, 2198με, 2144με, 2128με and 2214με respectively when the strain rate were 10^{-5} /s, 10^{-4} /s, 10^{-3} /s, 10^{-2} /s and 10^{-1} /s. The corresponding DIF_ε were 1, 0.932, 0.909, 0.903 and 0.939, respectively. It shows that the peak strain of RAC100 showed a slightly decreasing tendency with the increase in strain rate before 10^{-2} /s, but it increased after 10^{-2} /s. The relationship between the DIF_ε of RAC100 and strain rate is shown in Fig. 3-22, the fitting curve could be expressed as

$$DIF_\varepsilon = 1\text{-}0.0262 \cdot \lg(\dot{\varepsilon} / \dot{\varepsilon}_s) \tag{3-15}$$

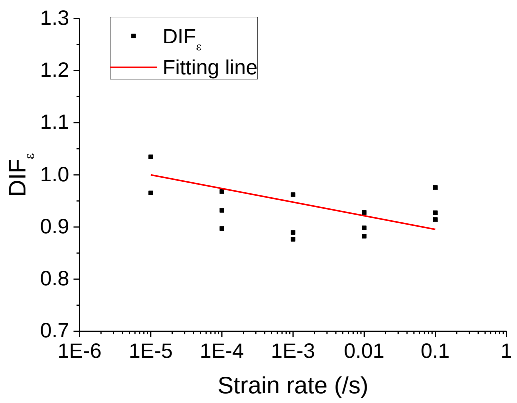

Fig. 3-22 Relationship between the DIF_ε of RAC100 and strain rate

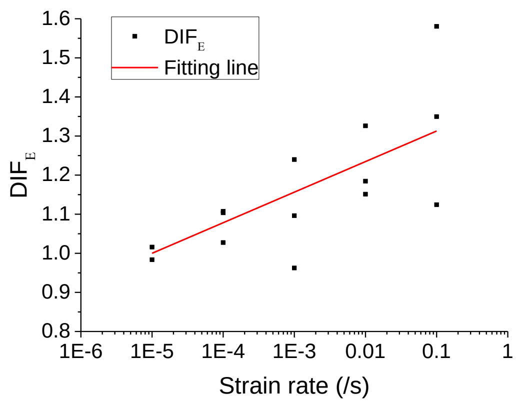

Fig. 3-23 Relationship between the DIF_E of RAC100 and strain rate

3.3.5.4 Effect of strain rate on elastic modulus of RAC100

According to Table 3-8, the average elastic modulus of the RAC100 specimens were 20.76GPa, 22.41GPa, 22.83GPa, 25.34GPa and 28.06GPa respectively when the strain rate were 10^{-5} /s, 10^{-4} /s, 10^{-3} /s, 10^{-2} /s and 10^{-1} /s. The corresponding DIF_E were 1, 1.079, 1.100, 1.221 and 1.352, respectively. It shows that the elastic modulus of RAC100 increased with the increase in strain rate in general. The relationship between the DIF_E of RAC100 and strain rate is shown in Fig. 3-23. The fitting line could be expressed as

$$DIF_E = 1 + 0.0782 \cdot \lg(\dot{\varepsilon} / \dot{\varepsilon}_s) \quad (3\text{-}16)$$

3.3.6 NAC(wet) Specimen

3.3.6.1 Stress-strain curves of NAC(wet) at different strain rates

The stress-strain curves of NAC(wet) at all the strain rates studied are shown in Fig. 3-24. The results show that the stress-strain curves are similar in all the strain rates studied, and the nonlinearity of the stress-strain curves became obvious when the stress is close to the peak stress. As the strain rate is increased, the peak stress increase, the elastic modulus showed an increasing tendency, the peak strain also showed an increasing tendency. The peak stress, peak strain and elastic modulus of NAC(wet) specimens are shown in Table 3-9.

Table 3-9 The peak stress, peak strain and elastic modulus of NAC(wet) specimens

Strain rate (/s)	No.	Peak stress (MPa)	DIF_f	Peak strain (10^{-6})	DIF_ε	Elastic modulus (GPa)	DIF_E
10^{-5}	1	31.9	1.032	1618	1.027	28.3	1.019
	2	29.1	0.944	1624	1.030	23.5	0.845
	3	31.6	1.025	1486	0.943	31.6	1.137
	AVG	**30.9**	**1.000**	**1576**	**1.000**	**27.8**	**1.000**
10^{-3}	1	32.4	1.048	1834	1.164	27.0	0.972
	2	33.8	1.094	1767	1.121	25.1	0.903
	3	35.0	1.134	1498	0.951	29.8	1.073
	AVG	**33.7**	**1.092**	**1700**	**1.079**	**27.3**	**0.982**
10^{-1}	1	38.2	1.237	1456	0.924	39.0	1.401
	2	40.4	1.307	1600	1.015	37.4	1.346
	3	43.1	1.397	1772	1.124	37.0	1.331
	AVG	**40.6**	**1.314**	**1609**	**1.021**	**37.8**	**1.359**

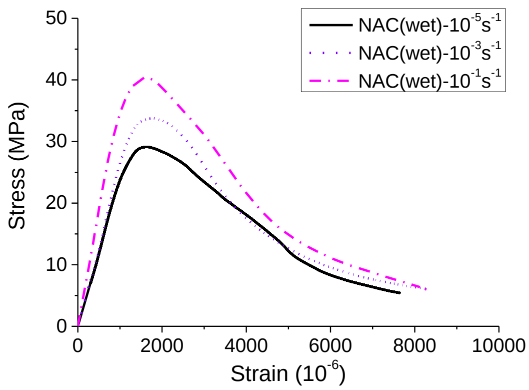

Fig. 3-24 Stress-strain curves of NAC(wet) at different strain rates

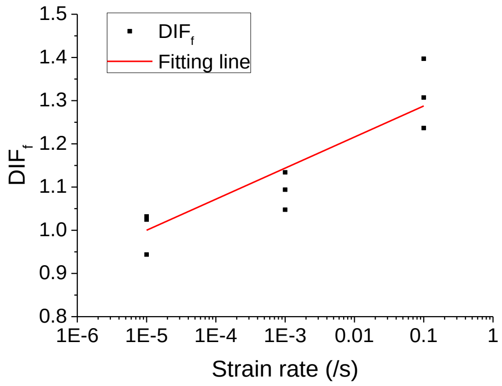

Fig. 3-25 Relationship between the DIF_f of NAC(wet) and strain rate

3.3.6.2 Effect of strain rate on peak stress of NAC(wet)

According to Table 3-9, the average peak stress of the NAC(wet) specimens were 30.88MPa, 33.72MPa and 40.57MPa respectively when the strain rate were 10^{-5} /s, 10^{-3} /s and 10^{-1} /s. The corresponding DIF_f were 1, 1.092 and 1.314, respectively. It indicates that the peak stress of NAC(wet) increased with the increase in strain rate. The relationship between the DIF_f of NAC(wet) and strain rate is shown in Fig. 3-25. The fitting line could be expressed as

$$DIF_f = 1 + 0.0719 \cdot \lg(\dot{\varepsilon} / \dot{\varepsilon}_s) \tag{3-17}$$

3.3.6.3 Effect of strain rate on peak strain of NAC(wet)

According to Table 3-9, the average peak strain of the NAC(wet) specimens were 1576με, 1700με and 1609με respectively when the strain rate were 10^{-5} /s, 10^{-3} /s and 10^{-1} /s. The corresponding DIF_ε were 1, 1.079 and 1.021, respectively. It shows that the peak strain of NAC(wet) increased first and thus decreased with the increase in strain rate. The relationship between DIF_ε of NAC(wet) and strain rate is shown in Fig. 3-26, the fitting curve could be expressed as

$$DIF_\varepsilon = 1 + 0.0121 \cdot \lg(\dot{\varepsilon} / \dot{\varepsilon}_s) \tag{3-18}$$

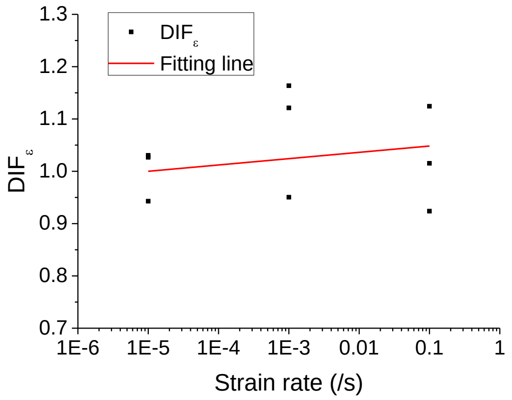

Fig. 3-26 Relationship between the DIF_ε of NAC(wet) and strain rate

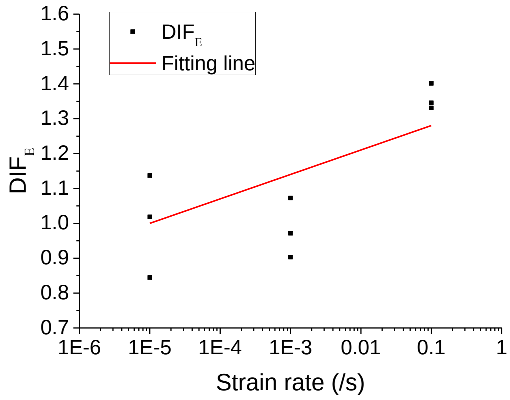

Fig. 3-27 Relationship between the DIF_E of NAC(wet) and strain rate

3.3.6.4 Effect of strain rate on elastic modulus of NAC(wet)

According to Table 3.9, the average elastic modulus of the NAC(wet) specimens were 27.80GPa, 27.31GPa and 37.79GPa respectively when the strain rate were 10^{-5} /s, 10^{-3} /s and 10^{-1} /s. The corresponding DIF_E are 1, 0.982 and 1.359, respectively. It shows that the elastic modulus of NAC(wet) increased with the increase in strain rate. The relationship between the DIF_E of

NAC(wet) and strain rate is shown in Fig. 3-27. The fitting line could be expressed as

$$DIF_{\mathrm{E}} = 1 + 0.0701 \cdot \lg(\dot{\varepsilon} / \dot{\varepsilon}_{\mathrm{s}}) \tag{3-19}$$

3.3.7 RAC100(wet) Specimen

3.3.7.1 Stress-strain curves of RAC100(wet) at different strain rates

The stress-strain curves of RAC100(wet) at all the strain rates studied are shown in Fig. 3-28. The results show that the stress-strain curves were similar in all the strain rates studied, and the nonlinearity of the stress-strain curves became obvious when the stress sas close to the peak stress. As the strain rate was increased, the peak stress and the elastic modulus increased, the peak strain also showed an increasing tendency. The peak stress, peak strain and elastic modulus of RAC100(wet) specimens are shown in Table 3-10.

Table 3-10 The peak stress, peak strain and elastic modulus of RAC100(wet) specimens

Strain rate (/s)	No.	Peak stress (MPa)	DIF_f	Peak strain (10^{-6})	DIF_ε	Elastic modulus (GPa)	DIF_E
10^{-5}	1	22.8	0.902	2034	1.068	14.3	0.782
	2	25.1	0.990	1922	1.009	18.1	0.989
	3	28.0	1.107	1758	0.923	22.5	1.230
	AVG	25.3	1.000	1905	1.000	18.3	1.000
10^{-3}	1	25.2	0.996	2463	1.293	12.2	0.666
	2	35.5	1.405	1802	0.946	24.1	1.321
	3	29.0	1.146	1977	1.038	20.7	1.135
	AVG	29.9	1.182	2081	1.092	19.0	1.040
10^{-1}	1	33.2	1.313	2101	1.103	24.9	1.361
	2	38.4	1.518	2227	1.169	26.7	1.458
	3	29.4	1.160	2825	1.483	14.8	0.809
	AVG	33.7	1.330	2384	1.251	22.1	1.209

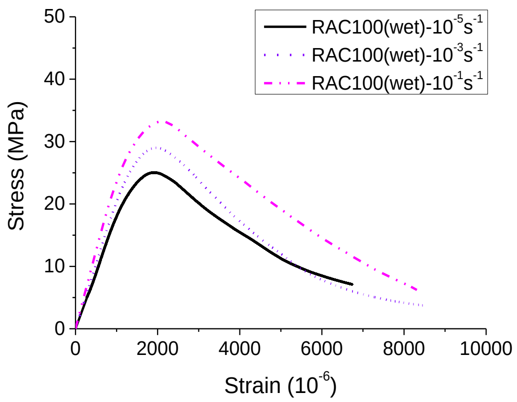

Fig. 3-28 Stress-strain curves of RAC100(wet) at different strain rates

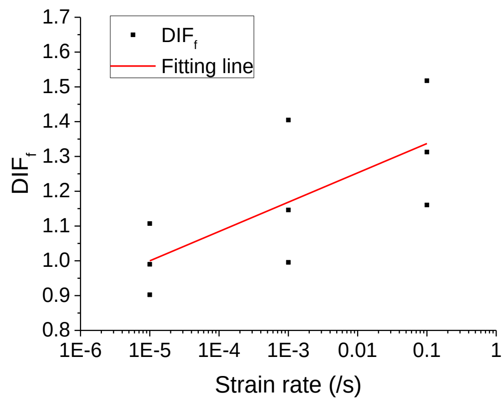

Fig. 3-29 Relationship between the DIF_f of RAC100(wet) and strain rate

3.3.7.2 Effect of strain rate on peak stress of RAC100(wet)

According to Table 3-10, the average peak stress of the RAC100(wet) were 25.30MPa, 29.91MPa and 33.66MPa respectively when the strain rate were 10^{-5} /s, 10^{-3} /s and 10^{-1} /s. The corresponding DIF_f were 1, 1.182 and 1.330, respectively. It indicates that the peak stress of RAC100(wet) increased with the increase in strain rate. The relationship between the DIF_f of RAC100(wet) and strain rate is shown in Fig. 3-29. The fitting line could be expressed as

$$DIF_f = 1 + 0.0843 \cdot \lg(\dot{\varepsilon} / \dot{\varepsilon}_s) \tag{3-20}$$

3.3.7.3 Effect of strain rate on peak strain of RAC100(wet)

According to Table 3-10, the average peak strain of the RAC100(wet) specimens were 1905με, 2081με and 2384μεrespectively when the strain rate were 10^{-5} /s, 10^{-3} /s and 10^{-1} /s. The corresponding DIF_ε were 1, 1.092 and 1.251, respectively. It shows that the peak strain of RAC100(wet) showed an increasing tendency with the increase in strain rate. The relationship between the DIF_ε of RAC100(wet) and strain rate is shown in Fig. 3-30. The fitting line could be expressed as

$$DIF_\varepsilon = 1{+}0.0596 \cdot \lg(\dot{\varepsilon} / \dot{\varepsilon}_s) \tag{3-21}$$

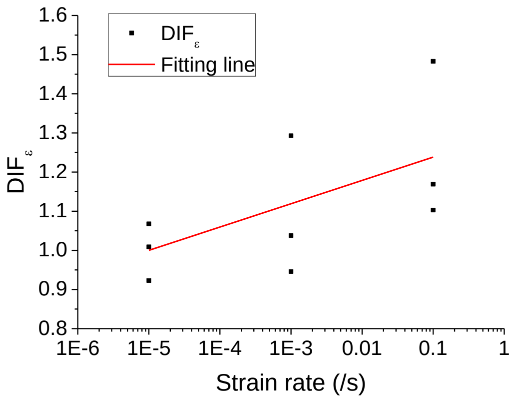

Fig. 3-30 Relationship between the DIF_ε of RAC100(wet) and strain rate

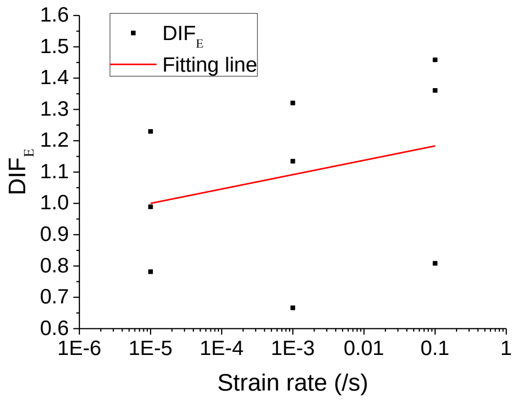

Fig. 3-31 Relationship between the DIF_E of RAC100(wet) and strain rate

3.3.7.4 Effect of strain rate on elastic modulus of RAC100(wet)

According to Table 3.10, the average elastic modulus of the RAC100(wet) specimens were 18.28GPa, 19.02GPa and 22.10GPa respectively when the strain rate were 10^{-5} /s, 10^{-3} /s and 10^{-1} /s. The corresponding DIF_E were 1, 1.040 and 1.209, respectively. It shows that the elastic modulus of RAC100(wet) increased with the increase in strain rate. The relationship between DIF_E of RAC100(wet) and strain rate is shown in Fig. 3-31. The fitting curve could be expressed as

$$DIF_{\mathrm{E}} = 1 + 0.0459 \cdot \lg(\dot{\varepsilon} / \dot{\varepsilon}_{\mathrm{s}}) \tag{3-22}$$

3.4 Analysis and Discussion

According to the above test results, the strain-rate sensitivity of RAC will be analysed in the following section by evaluating the strain rate effect on the peak stress, peak strain, elastic modulus and failure pattern. At the same time, the effect of moisture condition and RCA replacement ratio will be studied to explore the main factors influencing the strain-rate sensitivity of RAC, which is important in understanding the mechanism of strain-rate sensitivity of RAC.

3.4.1 Strain-rate sensitivity of RAC at low strain rates

3.4.1.1 Influence of strain rate on peak stress

The relationships between the average peak stress of RAC with different RCA replacement percentages and strain rate are shown in Fig. 3-32. The results show that the peak stress of all types of RACs increased linearly with the increase in strain rate, the rates of the increase in peak stress of RACs with different RCA replacement percentages were different. The variation in the average DIF_f of RAC with the strain rate is shown in Fig. 3-33. The results show that the DIF_f of the RAC100 specimen was slightly larger than that of the CEB model, while the DIF_f of the RAC30, RAC50 and RAC70 specimens was slightly smaller than the CEB model. In general, the DIF_f of RACs in this study was close to the result of CEB model when the static strength was similar.

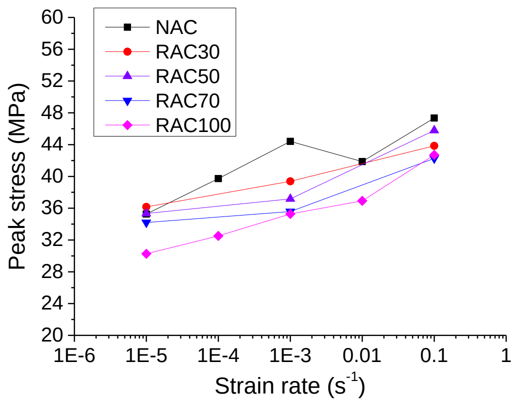

Fig. 3-32 Effect of strain rate on the peak stress of RAC

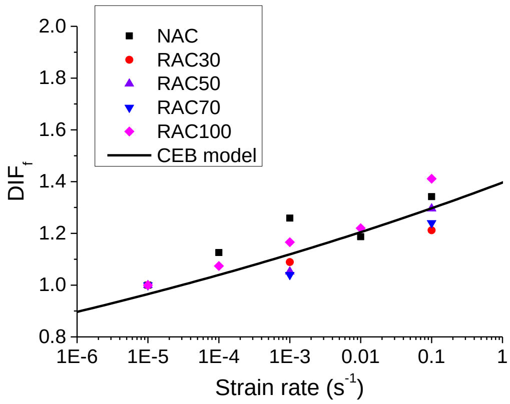

Fig. 3-33 Effect of strain rate on the DIF_f of RAC

3.4.1.2 Influence of strain rate on peak strain

The variations of the average peak strain of RAC with different RCA replacement percentages and the strain rate are shown in Fig. 3-34. The results show that there was no consistent trend between the peak strain and the strain rate for different RACs. With the increase in strain rate, some of them showed a decreasing trend, some of them decreased first and then increased, and some of them increase first and then decrease. Generally, the change in the peak strain with the strain rate was not significant. Therefore, it can be concluded that the peak strain of RAC does not change significantly with the change in strain rate, and the phenomenon of fluctuation is caused by the discretization of the experiment. The results are different from those of the CEB model, which suggests that the peak strain increases with the increase in strain rate, as shown in Fig. 3-35.

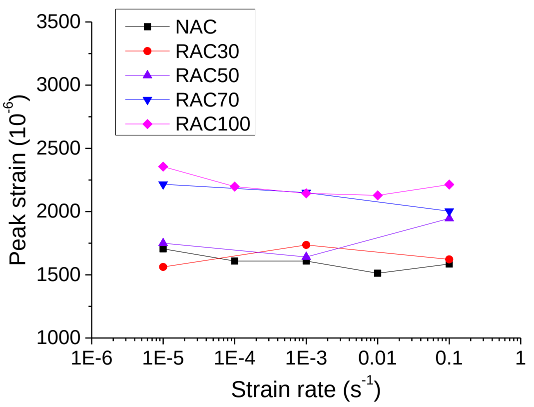

Fig. 3-34 Effect of strain rate on the peak strain of RAC

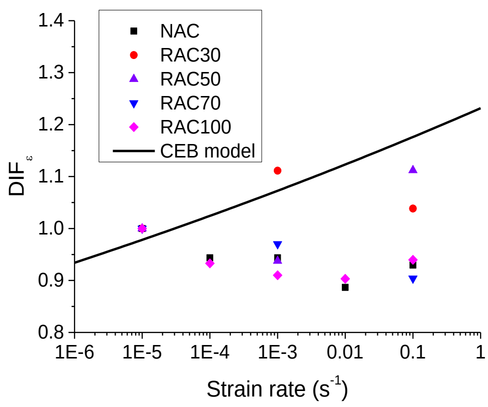

Fig. 3-35 Effect of strain rate on the DIF_{ε} of RAC

3.4.1.3 Influence of strain rate on elastic modulus

The relationships between the average elastic modulus of RAC with different RCA replacement percentages and strain rate are shown in Fig. 3-36. The results show that the elastic modulus of RAC increased approximately linearly with the increase in strain rate, the rates of the increase in elastic modulus of RACs with different RCA replacement percentages were different. The variation in the average DIF_E of RAC with the strain rate is shown in Fig. 3-37. It shows that the average DIF_E of RAC in this experiment is larger that of the CEB model, indicating that the effect of strain rate on the elastic modulus of RAC is more significant than that of conventional concrete. Moreover, compared with the DIF_f of RAC, the DIF_E of RAC is larger, which indicates that the elastic modulus of RAC is more sensitive to strain rate than the peak stress.

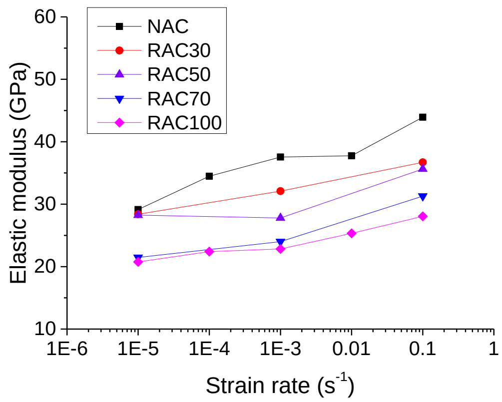

Fig. 3-36 Effect of strain rate on the elastic modulus of RAC

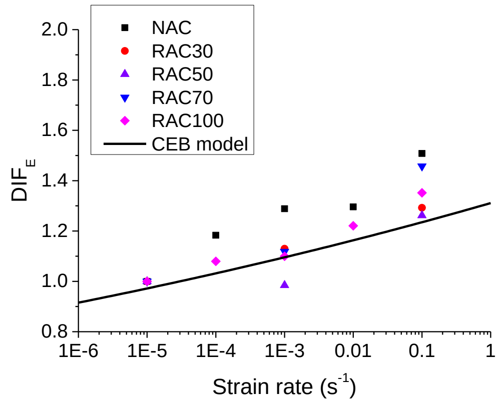

Fig. 3-37 Effect of strain rate on the DIF_E of RAC

3.4.1.4 Influence of strain rate on energy absorption capacity

Toughness which is defined as the area under the stress-strain curve represents the energy absorption capacity of the materials. Different definitions for the toughness using the area under the stress-strain curve have been proposed by different researchers. Mansur et al. (1999) defined the toughness as the area under the stress-strain curve before the strain was 3 times the peak strain. Nataraja et al. (1999) used the area under the stress-strain curve before 0.015 strain to define the toughness value. In this study, the toughness is defined as the area under the stress-strain curve up to a strain of 0.0075, which was considered sufficient to represent the trend of the post-peak behavior. The effect of the strain rate on the toughness of the RACs is demonstrated in Fig. 3-38. It is observed that the toughness of all types of RACs show an increasing trend as the strain rate increased. This feature is consistent with the results of SHPB tests as reported by Wang *et al*. (2011) and Chen *et al*. (2013).

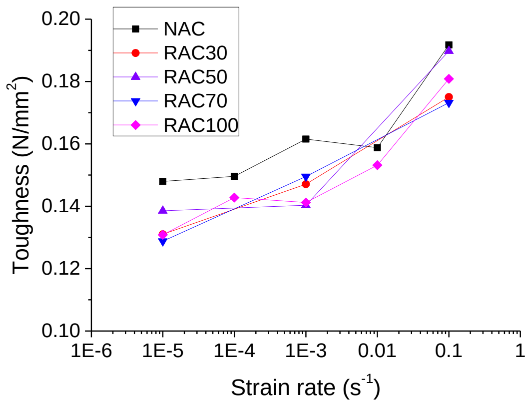

Fig. 3-38 Effect of strain rate on the energy absorption capacity of RAC

Fig. 3-39 Failure patterns of RAC100 at different strain rates

3.4.1.5 Influence of strain rate on failure pattern

To understand the mechanism of strain-rate sensitivity of RAC, it is important to understand the failure patterns of RAC. The failure patterns of RAC100 specimens as shown in Fig. 3-39 are taken as an example to illustrate the failure patterns of the RAC under different strain rates. From the end surface of the specimens, it can be seen that most of the cracks passed through the interfaces between the aggregate and the cement paste while few cracks propagated from the aggregate. This is a common feature in this study under all the strain rates studied. From the side surface of the specimens, it can be seen that the most of the cracks were almost parallel to the specimen at all the strain rates. Moreover, there is no clear trend to show whether the number of the cracks increased or decreased with the increase in strain rate. To sum up, the failure patterns of the RACs showed no significant change as the strain rate was increased. This phenomenon can be explained as follows. The loading rates in this test, which are in the range of 1.4×10^{-3} mm/s to 14mm/s, are much smaller than the velocity of the stress wave transmitted in the specimens which is about 3000m/s. Therefore, the stress at the loading end can be considered to reach to another end of the specimens immediately. That is to say, the stress transmission and the cracking mode should be similar in the same specimen under the loading rates studied. As a result, the failure patterns show no significant difference as the strain rate is changed. However, when the loading rate is much higher such as during impact or explosion loading, the stress at the loading end cannot reach to another end of the specimens immediately. As a result, the crack has insufficient time to propagate along the weakest locations like ITZ, it may pass through the mortar or aggregate directly. Therefore, the cracking mode may be changed and more cracks will pass through the aggregate.

3.4.2 Effect of RCA replacement percentage on strain-rate sensitivity of RAC

3.4.2.1 Effect of RCA replacement percentage on peak stress, peak strain, elastic modulus

The variation in peak stress, peak strain and elastic modulus of RACs with RCA replacement percentages are illustrated in Fig. 3-40, Fig. 3-41 and Fig. 3-42, respectively. It shows that the peak stress of RAC decreased with the increase in RCA replacement percentage in general at all the strain rates studied, but there was an abnormal point, i.e., the peak stress of the NAC specimen was smaller than that of RAC30 and RAC50 at a strain rate of 10^{-5} /s. The elastic modulus also decreased with the increase in RCA replacement percentage. The peak strain of RAC exhibited an increasing trend as the RCA replacement percentage increased. This feature is consistent with the results in static loading tests which have been reported by many investigators (Xiao et al. 2005; Kou et al 2012). In other words, the effect of RCA replacement percentage on the dynamic mechanical properties of RAC is similar to its effect on static mechanical properties of RAC.

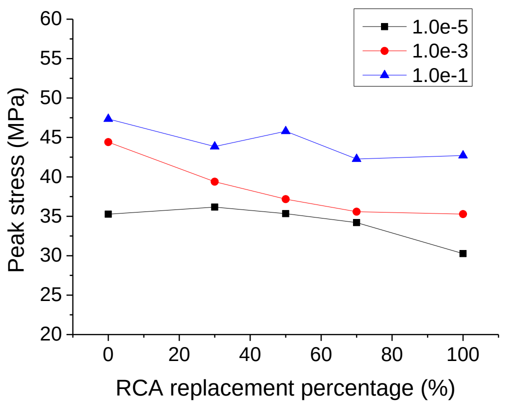

Fig. 3-40 Effect of RCA replacement percentage on dynamic peak stress of RAC

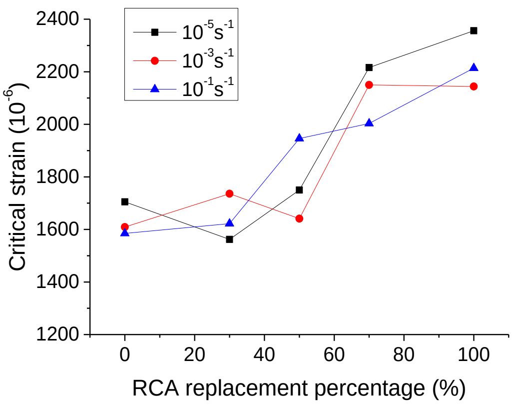

Fig. 3-41 Effect of RCA replacement percentage on dynamic peak strain of RAC

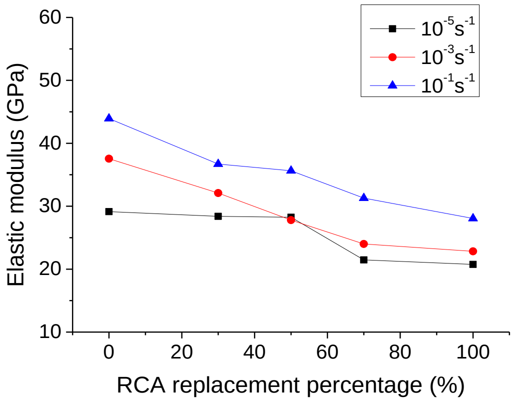

Fig. 3-42 Effect of RCA replacement percentage on dynamic elastic modulus of RAC

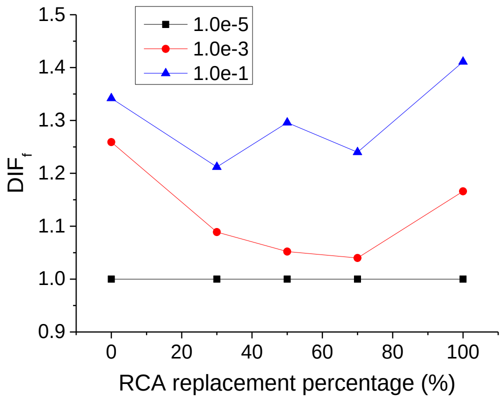

Fig. 3-43 Effect of RCA replacement percentage on DIF_f of RAC

3.4.2.2 Effect of RCA replacement percentage on strain-rate sensitivity of RAC

Fig. 3-43 shows the variation in the DIF_f of RAC with the RAC replacement percentage to study its effect on the strain-rate sensitivity of RAC. It indicates that the DIF_f of RAC100 was the largest, which reached 41.1% at $10^{-1}s^{-1}$. It is shown that the DIF_f of NAC was larger than that of RAC30, RAC50 and RAC70. However, this point may be abnormal because the static strength of NAC was smaller than that of RAC30 and RAC50, but this is not consistent with the normal case that the strength of RAC decreases with the increase in RCA replacement percentage. Thus, the value of DIF_f of NAC may be larger than its real value. Moreover, It can be seen from Fig. 3-43 that the relationship between the DIF_f of RAC and the RCA replacement percentage is not clear even if NAC is not taken into account, and the difference in the strain-rate sensitivity of the RAC with different RCA replacement percentages may not be determined usinf the single factor of RCA replacement percentage, it may also be influenced by the mortar content and the micro-structure of RAC. Overall, the strain-rate sensitivity of RAC with 100% RCA is greater than that of NAC, but there is no clear relationship between the RCA replacement percentage and the strain-rate sensitivity of RAC.

3.4.3 Effect of moisture condition on strain-rate sensitivity of RAC

3.4.3.1 Influence of moisture condition on the peak stress

The peak stress of RAC100 and NAC tested in an air-dry condition and wet conditions versus strain rate are compared in Fig. 3-44. It shows that the peak stress of the specimens under wet condition increased with the increase in strain rate, which is the same with the feature under air-dry condition. Under the same strain rate, the peak stress of the specimens in a wet condition were lower than those tested in an air-dry conditions, as shown in Fig. 3-44. The phenomenon that the water content tends to decrease the static and dynamic compressive strength of concrete has been reported by some other studies (Barlett & MacGregor 1993; Yurtdas et al. 2004; Wu et al. 2012; Harris et al. 2000). This phenomenon can be explained by means of surface energy variations (Wittmann 1973), i.e. the presence of water reduced the Van der Walls forces between the gel particles which are proportional to the specific surface energy and consequently facilitated the propagations of bond cracks. However, under dynamic loading, there is no consistent conclusion on the effect of moisture condition on the dynamic strength of concrete. The results of most studies (such as Yan 2006; Zhou et al. 2014; Wu et al. 2012; Chen et al. 2012) showed that the strength of concrete decreases with increasing water content under dynamic loading, this is consistent with that in static loading. However, some of the results (e.g., Ross et al. 1996; Wang et al. 2007) reported that the strength of saturated concrete under dynamic loading is higher than that of dry concrete.

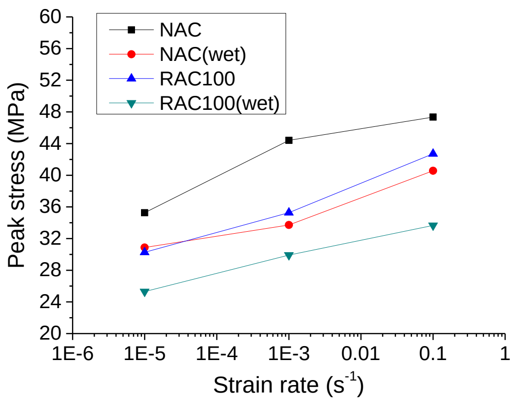

Fig. 3-44 Effect of moisture condition on dynamic peak stress of RAC

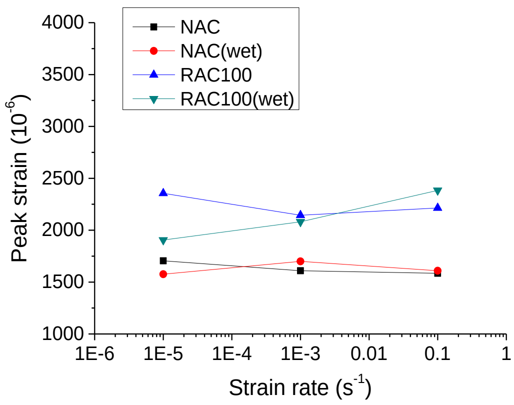

Fig. 3-45 Effect of moisture condition on dynamic peak strain of RAC

3.4.3.2 Effect of moisture condition on peak strain

The variation in the dynamic peak strain of the NAC and RAC100 specimens under an air-dry or wet condition with the strain rate is shown in Fig. 3-45. The results show that under the quasi-static state, the peak strain of RAC in the wet state was smaller than that of the air-dry state. At higher strain rates, the peak strain of RAC in the wet state was below or above that in an air-dry state. That is to say, the effect of the moisture condition on the dynamic peak strain is not clear.

3.4.3.3 Effect of moisture condition on elastic modulus

The variation in the dynamic elastic modulus of the NAC specimens and the RAC100 specimens in an air-dry or wet condition with the strain rate is shown in Fig. 3-46. The results show that the elastic modulus of the NAC and the RAC100 in the wet state was smaller than that in the air-dry state, both under quasi-static and dynamic loadings. This is consistent with the results of some other researchers. For example, Zhou et al. (2011) found that the elastic modulus of mortar decreases with the increase in water content under impact loading. However, some researchers have obtained the opposite conclusion. For example, Li (2009) reported that the elastic modulus of concrete under static loading increases with the increase in water content; the results by Wu et al. (2012) show that the elastic modulus of concrete increases with the increase in water content no matter under the static loading or dynamic loading.

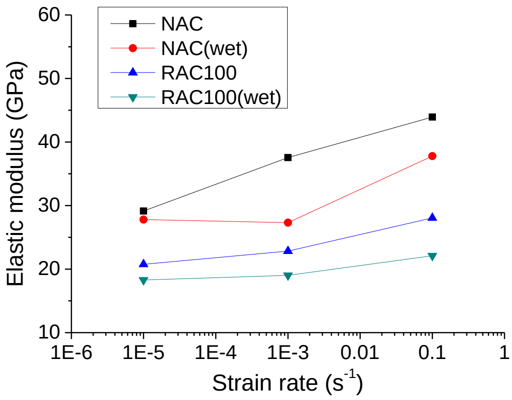

Fig. 3-46 Effect of moisture condition on dynamic elastic modulus of RAC

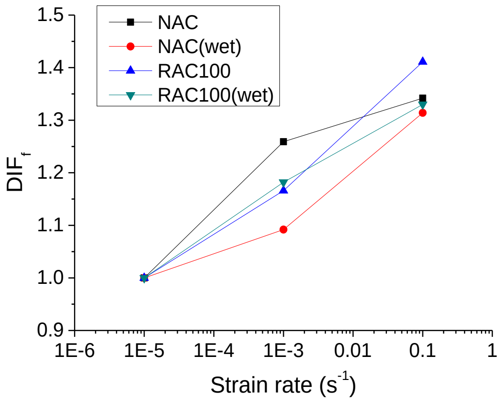

Fig. 3-47 Effect of moisture condition on DIF_f of RAC

3.4.3.4 Effect of moisture condition on strain-rate sensitivity of RAC

There have been a lot of studies on the effect of moisture condition on the dynamic mechanical properties of concrete in the past. Most of the results (such as Ross et al. 1996; Rossi 1992, 1994; Bischoff et al. 1995; Harris et al. 2000) reported that the strain-rate sensitivity of wet concrete is higher than that of dry concrete. They believe that this phenomenon is due to the viscous effect of free water in concrete. Reinhardt et al. (1990) even argued that the tensile strength of dry concrete almost exhibit no strain-rate sensitivity under moderate strain rate, while the strain-rate sensitivity of wet concrete is very significant. However, there are different conclusions. For example, Zielinski et al. (1981) show that the humidity conditions have little effect on the dynamic tensile strength of concrete.

The relationship between the DIF_f of NAC and RAC100 specimen in an air-dry and wet state and the strain rate is shown in Fig. 3-47. The results show that NAC and RAC100 in the wet state also showed strain-rate sensitivity, but the wet specimens did not show greater strain-rate sensitivity. On the other hand, if the water content is a decisive factor for the strain-rate sensitivity of concrete, then the concrete in a dry state should not be sensitive to strain rate. But, rare studies showed that dry concrete has no strain-rate sensitivity. Therefore, it is considered that the free water content in the concrete at low strain rates is not the main factor for strain-rate sensitivity of RAC. It is believed that the viscous effect caused by the free water is not significant at low strain rates, which does not cause obvious improvement on the strength of RAC.

3.5 Summary

In this chapter, the stress-strain curves of recycled aggregate concrete (RAC) are experimentally studied at low strain rates (i.e., 10^{-5} /s ~ 10^{-1} /s). The strain-rate sensitivity of RAC was studied. At the same time, the effects of the recycled coarse aggregate (RCA) replacement percentage and the moisture condition on the strain-rate sensitivity of RAC were discussed. In summary, the main conclusions are displayed as follows:

(1) With the increase in the strain rate, the peak stress, elastic modulus and energy absorption capacity of RAC showed an increasing trend, and the peak strain fluctuated around a constant value, the failure pattern showed no significant change.

(2) The peak stress of RAC under the same strain rate decreased with the increase in the RCA replacement percentage, and the peak strain increased with the increase in the RCA replacement percentage. The strain-rate sensitivity of RAC with 100% RCA was higher than that of conventional concrete, but the strain-rate sensitivity of RAC did not increase monotonically with the increase in RCA replacement percentage.

(3) The peak stress and the elastic modulus of wet RAC under the same strain rate were lower than those of the air-dry RAC at low strain rates studied, and the effect of moisture condition on the peak strain was not obvious. In contrast, this thesis argues that the effect of moisture condition on the strain-rate sensitivity of RAC is not obvious and it may not be the main factor affecting the strain-rate sensitivity of RAC at low strain rates.

Chapter 4 Dynamic mechanical behavior of RAC at high strain rates

Concrete has now become the most widely used material in engineering construction. Among them, some structures such as airport runways, dams, offshore platforms and military engineering, are required to bear impact or explosive load. Moreover, in recent years, terrorist attacks continue to increase around the world. Therefore, people paid more and more attention on the safety of engineering structures under impact or explosive loadings, and many researchers have studied the dynamic mechanical properties of concrete under impact or explosive loadings. Compared with earthquake loading, the corresponding strain rate under the impact or explosive loading is higher, which is above 10^1 /s. Because the strain rate in the concrete component under impact or explosive loading is very large, and the loading speed provided by the conventional hydraulic test equipment cannot reach such high loading speed, scholars tried various test methods to obtain the dynamic mechanical properties of the concrete under the impact or explosion loading. At present, the dynamic mechanical properties of concrete under high strain rates are mainly studied using the Hopkins pressure bar (SHPB) test device. And because the size of aggregate in concrete specimen is large, a large diameter SHPB testing system which is often greater than 50mm is commonly used to study the dynamic mechanical properties of concrete.

In this chapter, a varied cross section SHPB testing system with a diameter of 74mm was used to study the dynamic mechanical properties of RAC at high strain rates of 10^1 /s ~ 10^2 /s. The stress-strain curves and failure modes of RAC at these high strain rates were studied. The strain-rate sensitivity of RAC was studied by analyzing the effect of strain rate on peak stress, peak strain, elastic modulus and failure mode. The effects of RCA replacement percentage and moisture condition on the strain-rate sensitivity of RAC at these high strain rates were also investigated.

4.1 Test design

4.1.1 Materials and specimen

The material used in this test is the same as that in Chapter 3, the difference is the height of the specimen and the curing age. In this test, cylindrical specimens of sizes Φ70mm × 35mm and

Φ70mm × 140mm were used for impact testing and quasi-static test respectively. The preparation of the specimens has been described in Chapter 3. The curing age of the specimen was 90 days.

In this test, the number and distribution of RAC specimens with five RCA replacement percentages of size Φ70mm×35mm are shown in Table 4-1. There were 20 specimens for each type of RAC specimen in an air-dry state for testing at four different strain rates to study the strain-rate sensitivity of RAC. Five RCA replacement percentages were considered to study the effect of RCA replacement percentage on the strain-rate sensitivity of RAC. In order to explore the influence of the moisture condition on the strain-rate sensitivity of RAC, some NAC specimens and RAC100 specimens in a wet state (immersing specimens in water for 2 days) were prepared for the testing in first and fourth groups of strain rates. In addition, five specimens for each type of RAC specimens were prepared to measure their static strength.

Table 4-1 Number of RAC specimens

Speed of striker bar	Number of specimens				
	NAC	RAC30	RAC50	RAC70	RAC100
10 m/s	5+5	5	5	5	5+5
12 m/s	5	5	5	5	5
16 m/s	5	5	5	5	5
20 m/s	5+5	5	5	5	5+5

4.1.2 Experimental setup and experimental principle

Impact tests under strain rates ranging from 10^1/s to 10^2/s were conducted using a 74 mm-diameter conic variable cross-sectional SHPB as shown in Fig. 4-1. The SHPB apparatus consists of four basic parts: a striker bar (37 mm in diameter, 400 mm in length); a conic variable cross-sectional incident bar (the striking end is 37 mm in diameter, the other end is 74 mm in diameter, 3060 mm in length), a transmitter bar (74 mm in diameter, 1800 mm in length) and the testing specimen. The material used for fabricating these bars was high-strength alloy steel, the elastic modulus of the bars were 210GPa, of density 7850kg/m^3, and yield strength 400MPa. The specimens were sandwiched between the incident and the transmitted bars. Vaseline was applied uniformly on to the two contact surfaces between the bar and the specimen to reduce friction.

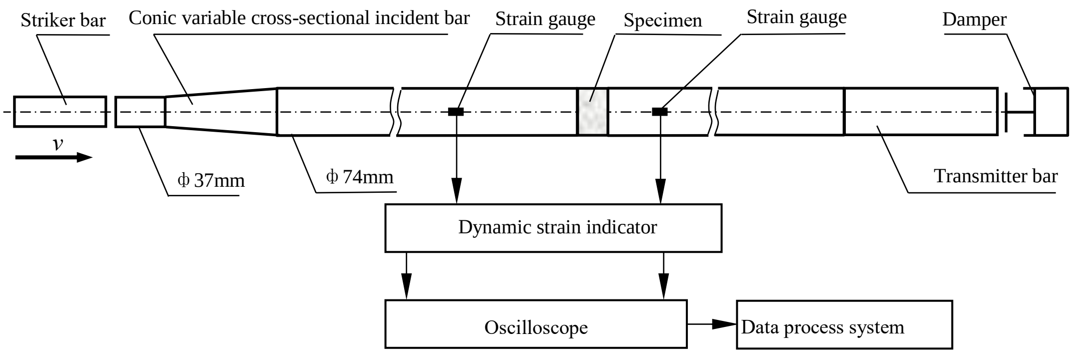

Fig. 4-1 74 mm-diameter conic variable cross-sectional SHPB

The experimental principle is described as follows. The striker bar, propelled by pressurized gas, impacts against the incident bar with a known velocity, which generates a stress pulse in the incident bar. Then, the stress pulse of the incident bar impinges on the specimen. Because of the impedance mismatch between the specimen and the incident bar, part of the stress pulse is reflected from the specimen as a tensile pulse, and part of the pulse is transmitted through the specimen as a compressive pulse into the transmitted bar. The incident, reflected and transmitted pulses are recorded by the strain gauges on the incident and the transmitter bars. Based on the data from these strain gauges, the time histories of the stress $\sigma_S(t)$, strain $\varepsilon_S(t)$ and strain rate $\dot{\varepsilon}_S(t)$ in the specimen during deformation measurements could be determined using the following fomuleas:

$$\begin{cases} \sigma_S(t) = \dfrac{E_0 A_0}{A_S}\varepsilon_t(t) \\ \varepsilon_S(t) = \dfrac{2C_0}{l_S}\displaystyle\int_0^t [\varepsilon_i(t) - \varepsilon_t(t)]\,\mathrm{d}t \\ \dot{\varepsilon}_S(t) = \dfrac{2C_0}{l_S}[\varepsilon_i(t) - \varepsilon_t(t)] \end{cases} \tag{4-1}$$

where $\varepsilon_i(t)$ and $\varepsilon_t(t)$ are the amplitudes of the incident and transmited strain pulses respectively; E_0, A_0 and C_0 are the Young's modulus, cross-sectional area and longitudinal wave speed of the bars respectively; A_S and l_S are respectively the initial cross-sectional area and the length of the specimen.

In this study, the distance of the strain gauge on the incident bar from the incident bar/specimen interface was 1282 mm.The distance of the strain gauge on the transmitter bar from the transmitted bar/specimen interface was 404 mm. The strain gauge signals were recorded by a digital oscilloscope. Fig. 4-2 shows the typical signals recorded from the strain gauges mounted on the incident and the transmitter bars during an experiment.

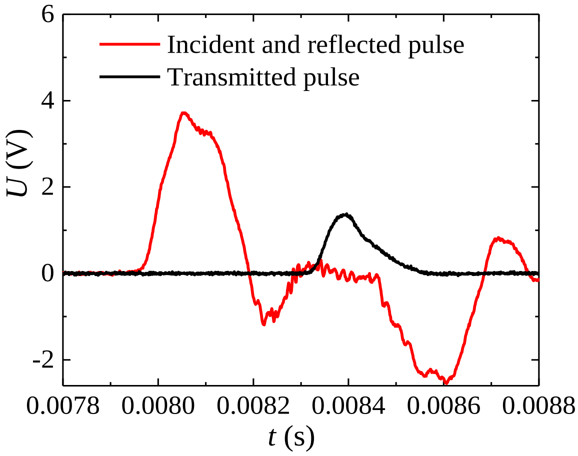

Fig. 4-2 Typical signals recorded from strain gauges

4.1.3 Experimental program

In this test, all types of RAC specimens were loaded with four different strain rates which was controlled by the impact speed of striker bar. There were four impact speeds of striker bar, i.e., 10m /s, 12m /s, 16m /s and 20m /s. The corresponding strain rates were about 40 /s, 50 /s, 75 /s and 100 /s, respectively.

In order to improve the accuracy of the test, the following measures were taken. First, to reduce the adverse effect of diffusion of the incident wave on the test, all tests were carried out with a Φ12mm × 1mm brass plate as a waveform shaper at the end of the incident rod. Second, a universal pad was added to the test in order to reduce the adverse effect of parallelism of the specimen. In addtion, axial strain gauges were mounted on the part of the sample for the direct measurement of strain to improve the accuracy of data processing.

4.2 Data processing method

4.2.1 Strain data acquisition

In the test, all the collected signals are voltage signals. So it is necessary to convert the voltage signal into a strain signal. For the strain gauge on the bars, in order to eliminate the bending effect, two axial strain gauges were attached on opposite sides at the same section, and they were accessed to the bridge according to Fig. 4-3, where ε_1 represents the strain gauge on the bar, ε_T represents the temperature compensator. All strain gauges on the specimens were accessed to the 1/4 bridge shown in Fig. 4-4. The frequency of measurement was 1 MHz.

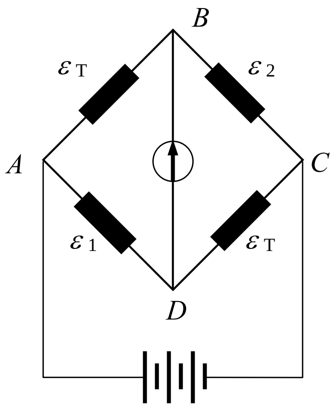

Fig. 4-3 Bridge joint of two strain gauge at the same cross-section in pressure bar

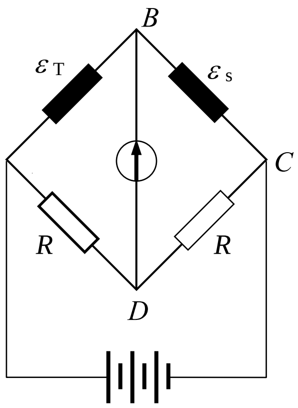

Fig. 4-4 Bridge joint of the strain gauge on the specimen

For the pressure bar and the specimen, the Eq. (4-2) and Eq. (4-3) were used to convert the strain gauge voltage signal into strain values:

$$\varepsilon_{bar} = \frac{\{U_{cn}\}_{\mathrm{V}}}{3.99} \times \frac{2000\mu\varepsilon}{2} \times \frac{2}{2.08} \tag{4-2}$$

$$\varepsilon_{specimen} = \frac{\{U_{cm}\}_{\mathrm{V}}}{3.99} \times 2000\mu\varepsilon \times \frac{2}{2.08} \tag{4-3}$$

Where, U_{cn} and U_{cm} are the voltage signals of the strain gauges on the pressure bar and the specimen.

4.2.2 Determination of strain rate

In general, the strain rates achieved in the SHPB test were not constant throughout the test. The representative strain rate in SHPB tests is defined in different ways. Chen *et al*. (2013) used the strain rate at the failure point as the representative strain rate. But this strain rate may not represent the strain rate of the entire experimental process. Grote *et al*. (2001) used a mean strain rate defined as the total strain during loading divided by the total time duration. Tang and Saadatmanesh (2003) indicated that the mean strain rate is significantly lower than the instantaneous failure strain rate in an SHPB test, and may not represent the actual strain rate. In this paper, the slope of the main straight line before the point corresponding to the peak stress in the strain-time curve is defined as the representative strain rate. An example is shown in Fig. 4-5, in which the strain rate is 37.9 /s.

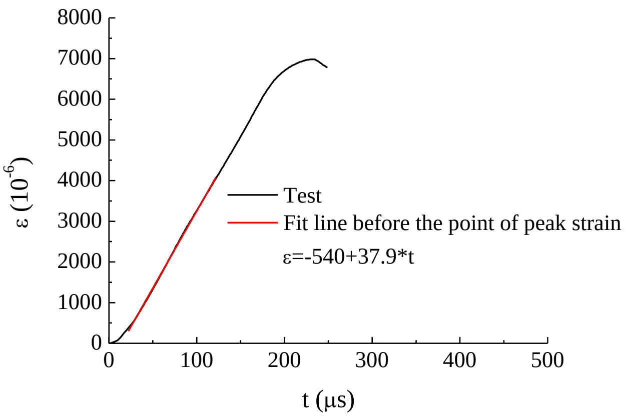

Fig. 4-5 A example of the representative strain rate

4.3 Test results

In this experiment, the stress-strain curves and failure modes of the specimens were obtained. The quasi-static compressive strength of each type of specimen was the peak stress at a strain rate of 10^{-5} /s. The dynamic peak stress of each specimen was the peak point of the stress in the stress-strain curve, the peak strain was the strain corresponding to the peak stress, and the modulus of elasticity was the slope of the secant line between 5% and 25% of peak stress. When comparing the stress-strain curves at different strain rates, the average stress-strain curve was used.

4.3.1 Quasi-static test results

The failure patterns of the RAC specimens with different RCA replacement percentages were similar to each other under the quasi-static testing. It was observed that most cracks propagated in directions parallel to the compressive loading. There were always several main cracks running through the specimens. The edges at the top were crushed in some specimens. Most of the cracks passed through the interfaces including the matrix-NCA interfaces, the matrix-RCA interfaces and the old mortar-original NCA interfaces in RCA. A few fractured NCA particles including the new NCA and the original NCA in RAC were found at the failure surface. The typical failure pattern of RAC specimens under the quasi-static state is presented in Fig. 4-6.

The measured compressive strength as a function of RCA replacement percentage is shown in Fig. 4-7. It indicates that the quasi-static compressive strength of RAC decreased with increasing RCA replacement percentage in general. However, the quasi-static compressive strength of RAC50 was the highest among the tested specimens. This phenomenon is similar to what was found in other studies (Xiao et al. 2004; Cai et al. 2012; Xiao et al. 2016. The possible reason for this observation is that the coarse aggregate prepared with 50% NCA and 50% RCA had a better grading. Although a detailed sieve analysis of the RCA was not conducted, by simple observation, the size of RCA was larger than that of NCA. According to a previous study Xiao et al. 2016), when 50% NCA were replaced by RCA in which the proportion of the larger size aggregate was higher, the mixed coarse aggregate should have a better grading, so the space in the concrete would be filled more densely, resulting in higher strength.

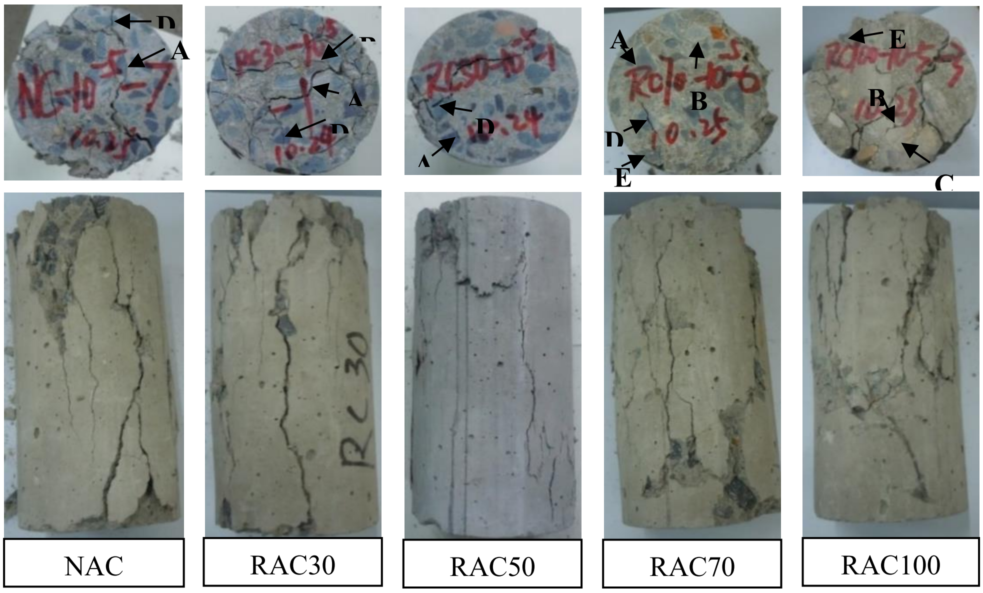

Fig. 4-6 Failure patterns of RAC under static loading

(**A**—cracks passed through the matrix-NCA interfaces, **B**—cracks passed through the matrix-RCA interfaces, **C**—cracks passed through the old mortar-original NCA interfaces, **D**—cracks passed through the new NCA, E—cracks passed through the original NCA in RAC)

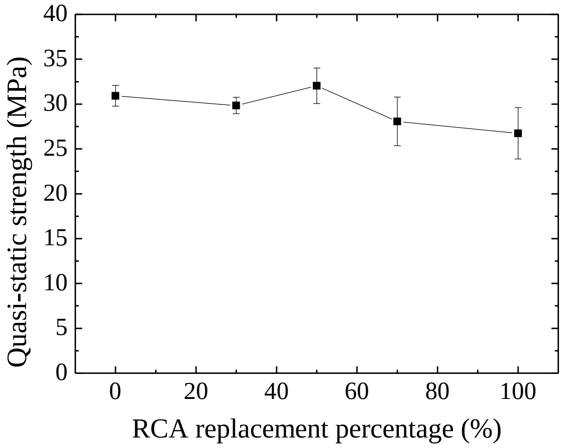

Fig. 4-7 Relation between compressive strength of RAC and RCA replacement percentage

Table 4-2 Peak stress, peak strain and elastic modulus of NAC specimens

Velocity of Striker bar	No.	Peak stress (MPa)	DIF_f	Peak strain (10^{-6})	Elastic modulus (GPa)	Strain rate (1/s)
10m/s	NAC-1-1	46.4	1.500	3780	16.2	30.4
	NAC-1-2	42.4	1.371	4960	16.9	35.9
	NAC-1-3	45.1	1.458	4130	13.6	37.7
	NAC-1-4	44.6	1.442	4490	24.9	42.1
	AVG	**44.6**	**1.443**	**4340**	**17.9**	**36.5**
	SD	**1.67**	**0.054**	**505**	**4.88**	**4.84**
12m/s	NAC-2-1	50.7	1.639	4800	29.4	44.4
	NAC-2-2	55.1	1.782	3490	34.2	37.6
	NAC-2-3	47.6	1.539	5130	15.3	49.2
	NAC-2-4	46.1	1.491	5210	14.4	49.7
	NAC-2-5	53.5	1.730	5560	26.3	52
	AVG	**50.6**	**1.636**	**4838**	**23.9**	**46.6**
	SD	**3.81**	**0.123**	**801**	**8.75**	**5.73**
16m/s	NAC-3-1	63.9	2.066	5410	32.9	85.6
	NAC-3-2	57.5	1.859	4600	31.7	71.5
	NAC-3-3	59.6	1.927	5200	28.4	72.5
	NAC-3-4	60.1	1.943	5790	32.1	80
	NAC-3-5	56.4	1.824	3990	18.0	73.7
	NAC-3-6	59.0	1.908	3660	25.5	62.3
	AVG	**59.4**	**1.921**	**4775**	**28.1**	**71.1**
	SD	**2.59**	**0.084**	**837**	**5.67**	**11.17**
20m/s	NAC-4-1	66.9	2.163	3440	39.2	91.9
	NAC-4-2	78.5	2.538	3100	35.7	90.2
	NAC-4-3	75.6	2.445	3450	36.7	83.5
	NAC-4-4	71.1	2.299	4680	32.2	85.7
	NAC-4-5	73.6	2.380	4790	32.6	94.5
	NAC-4-6	70.1	2.267	3830	36.4	83.6
	AVG	**72.6**	**2.349**	**3882**	**35.5**	**80.5**
	SD	**4.14**	**0.134**	**701**	**2.66**	**8.97**

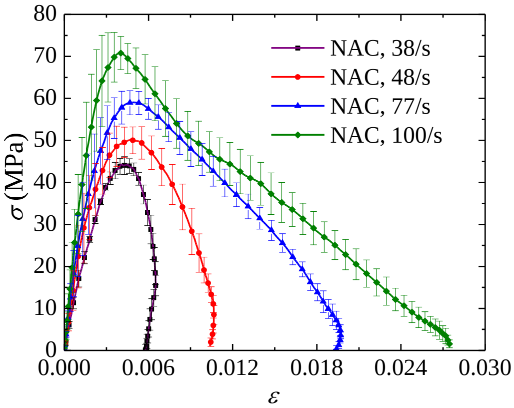

Fig. 4-8 Stress-strain curve of NAC under different impact loading

4.3.2 NAC Specimen

4.3.2.1 Stress-strain curves of NAC at different strain rates

The average stress-strain curves of NAC specimens at different strain rates are shown in Fig. 4-8. The results show that the stress-strain curves were similar in all the strain rates studied. With the increase in the strain rate, the peak stress and elastic modulus increased, the peak strain did not show any obvious trend, the decreasing rate of stress after peak stress was slower. The peak stress, peak strain and elastic modulus of NAC are shown in Table 4-2.

4.3.2.2 Effect of strain rate on peak stress and DIF_f of NAC

According to Table 4-2, the average peak stress of NAC were 44.6MPa, 50.6MPa, 59.4MPa and 72.6MPa respectively when the impact velocities were 10m/s, 12m/s, 16m/s and 20m/s. It indicates that the peak stress of NAC increased with the increase in strain rate. The relationship between the peak stress and the DIF_f of NAC and strain rate are shown in Fig. 4-9 and Fig. 4-10， respectively. It can be seen that the peak stress of NAC increased almost linearly with the increase in strain rate. In this strain rate range, the DIF_f of NAC increased linearly with the increase in logarithm of strain rate. The fitting line is shown as follows:

$$DIF_f = -1.787 + 0.893 \cdot \lg(\dot{\varepsilon}) \tag{4-4}$$

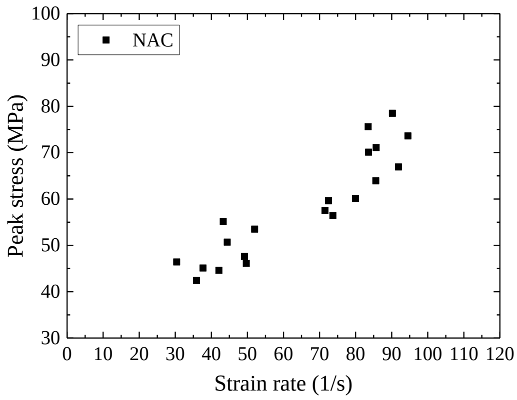

Fig. 4-9 Relationship between the peak stress of NAC and strain rate

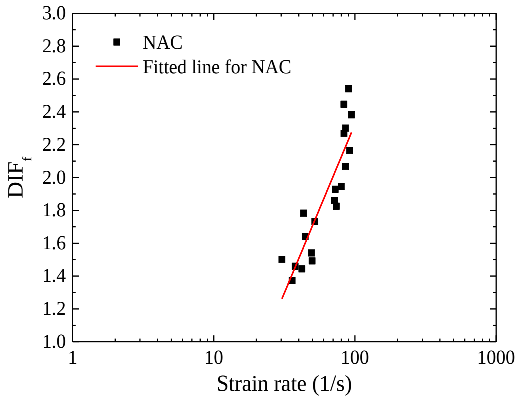

Fig. 4-10 Relationship between the DIF_f of NAC and strain rate

4.3.2.3 Effect of strain rate on peak strain of NAC

The relationship between peak strain of NAC and strain rate are shown in Fig. 4-11. It can be seen that the peak strain did not show a significant increase or decrease with the increase in the strain rate, it fluctuated generally around a constant value. Therefore, it can be concluded that the peak strain of NAC does not increase with the strain rate.

4.3.2.4 Effect of strain rate on elastic modulus of NAC

The relationship between elastic modulus of NAC and strain rate are shown in Fig. 4-12. It can be seen that the elastic modulus of NAC showed an increasing trend with the increase in the strain rate. According to Table 4-2, the average elastic modulus of NAC were 17.9GPa, 23.9GPa, 28.1GPa and 35.5GPa respectively when the impact velocities were 10m/s, 12m/s, 16m/s and 20m/s. It also indicates that the elastic modulus of NAC increased with the increase in strain rate.

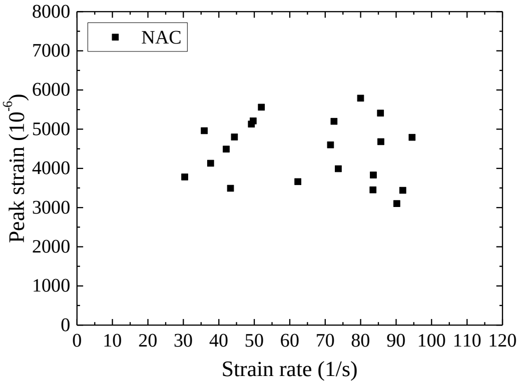

Fig. 4-11 Relationship between the peak strain of NAC and strain rate

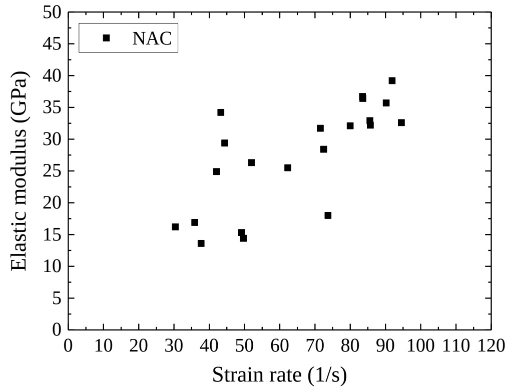

Fig. 4-12 Relationship between the elastic modulus of NAC and strain rate

4.3.3 RAC30 Specimen

4.3.3.1 Stress-strain curves of RAC30 at different strain rates

The average stress-strain curves of RAC30 specimens at different strain rates are shown in Fig. 4-13. The results show that the stress-strain curves were similar for all the strain rates studied. With the increase in the strain rate, the peak stress increased, the elastic modulus showed an increasing trend in general, the peak strain did not show an obvious trend, the decreasing rate of stress after peak stress became slower. The peak stress, peak strain and elastic modulus of RAC30 are shown in Table 4-3.

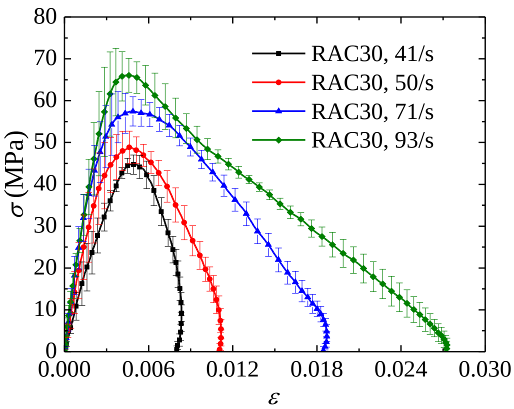

Fig. 4-13 Stress-strain curve of RAC30 under different impact loading

Table 4-3 Peak stress, peak strain and elastic modulus of RAC30 specimens

Velocity of Striker bar	No.	Peak stress (MPa)	DIF_f	Peak strain (10^{-6})	Elastic modulus (GPa)	Strain rate (1/s)
10m/s	RAC30-1-1	48.5	1.628	4780	11.5	37.2
	RAC30-1-2	46.2	1.550	4810	11.3	37.3
	RAC30-1-3	43.4	1.456	4270	25.2	39.8
	RAC30-1-4	44.2	1.483	4620	10.5	40.9
	RAC30-1-5	42.8	1.436	5610	10.1	47.1
	AVG	45.0	1.511	4818	13.7	40.5
	SD	2.33	0.078	492	6.44	4.04
12m/s	RAC30-2-1	53.6	1.799	4750	19.1	45.6
	RAC30-2-2	49.8	1.671	4970	20.6	49.1
	RAC30-2-3	45.6	1.530	5260	21.6	52.2
	RAC30-2-4	46.0	1.544	4240	14.0	46.5
	RAC30-2-5	51.4	1.725	4170	21.4	46.2
	AVG	49.3	1.654	4678	19.3	47.9
	SD	3.45	0.116	469	3.14	2.74
16m/s	RAC30-3-1	52.4	1.758	5190	24.4	66.7
	RAC30-3-2	58.5	1.963	5300	25.5	73.7
	RAC30-3-3	57.4	1.926	5570	25.6	68.5
	RAC30-3-4	61.9	2.077	3870	22.6	64.4
	RAC30-3-5	63.5	2.131	3640	28.9	69.3
	AVG	58.7	1.971	4714	25.4	68.5
	SD	4.32	0.145	890	2.30	3.45
20m/s	RAC30-4-1	65.0	2.181	3220	30.4	88.9
	RAC30-4-2	67.7	2.272	5480	26.7	95.8
	RAC30-4-3	78.4	2.631	2530	37.0	70.8
	RAC30-4-4	68.7	2.305	5940	18.9	100.6
	RAC30-4-5	64.1	2.151	6390	26.1	106.8
	AVG	68.8	2.308	4712	27.8	92.6
	SD	5.70	0.19	1725	6.61	13.83

4.3.3.2 Effect of strain rate on peak stress and DIF_f of RAC30

According to Table 4-3, the average peak stress of RAC30 were 45.0MPa, 49.3MPa, 58.7MPa and 68.7MPa respectively when the impact velocities were 10m/s, 12m/s, 16m/s and 20m/s. The corresponding DIF_f were 1.511, 1.654, 1.971 and 2.308, respectively. It indicates that the peak stress of RAC30 increased with the increase in strain rate. The relationship between the peak stress of RAC30 and its DIF_f and strain rate are shown in Fig. 4-14 and Fig. 4-15. It can be seen that the peak stress of RAC30 increased almost linearly with the increase in strain rate except for an abnormal data. In this strain rate range, the DIF_f of RAC30 also increased linearly with the increase in logarithm of strain rate. The fitting line is shown as follows:

$$DIF_f = -1.504 + 0.825 \cdot \lg(\dot{\varepsilon}) \tag{4-5}$$

4.3.3.3 Effect of strain rate on peak strain of RAC30

The relationship between the peak strain of RAC30 and strain rate are shown in Fig. 4-16. It can be seen that the peak strain did not show a significant increase or decrease with the increase in the strain rate, it fluctuated generally around a constant value. According to Table 4-3, the average peak stress of RAC30 were 4818με, 4678με, 4714με and 4712με respectively when the impact velocities were 10m/s, 12m/s, 16m/s and 20m/s. It also indicates that the peak strain of RAC30 did not show a significant change with the increase in strain rate.

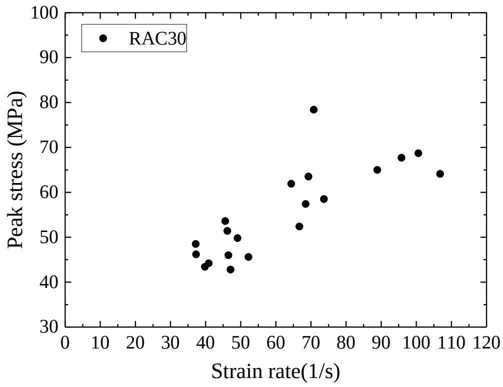

Fig. 4-14 Relationship between the peak stress of RAC30 and strain rate

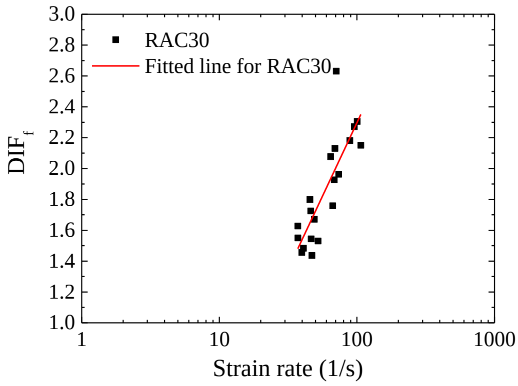

Fig. 4-15 Relationship between the DIF_f of RAC30 and strain rate

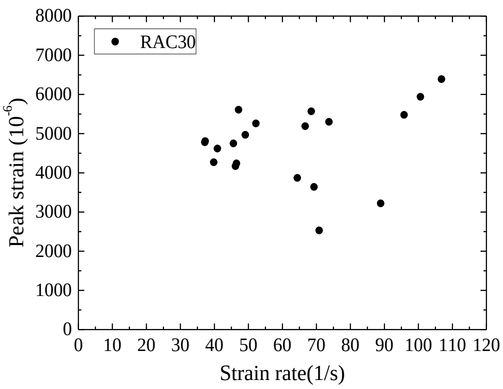

Fig. 4-16 Relationship between the peak strain of RAC30 and strain rate

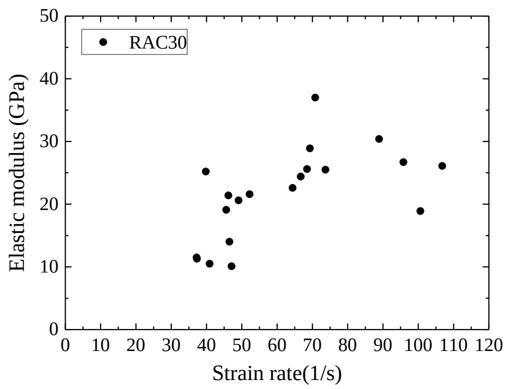

Fig. 4-17 Relationship between the elastic modulus of RAC30 and strain rate

4.3.3.4 Effect of strain rate on elastic modulus of RAC30

The relationship between the elastic modulus of RAC30 and strain rate is shown in Fig. 4-17. It can be seen that the elastic modulus of RAC30 showed an increasing trend with the increase in the strain rate, but the dispersion was large. According to Table 4-3, the average elastic modulus of RAC30 were 13.7GPa, 19.3GPa, 25.4GPa and 27.8GPa respectively when the impact velocities were 10m/s, 12m/s, 16m/s and 20m/s. It also indicates that the elastic modulus of RAC30 increased with the increase in strain rate.

Table 4-4 Peak stress, peak strain and elastic modulus of RAC50 specimens

Velocity of Striker bar	No.	Peak stress (MPa)	DIF_f	Peak strain (10^{-6})	Elastic modulus (GPa)	Strain rate (1/s)
10m/s	RAC50-1-1	41.6	1.298	3910	13.6	35.3
	RAC50-1-2	41.6	1.298	4570	11.3	41.8
	RAC50-1-3	44.3	1.383	3990	15.3	34
	RAC50-1-4	48.0	1.498	4540	13.3	35.6
	RAC50-1-5	43.6	1.361	4370	11.4	32.6
	AVG	43.8	1.368	4276	13.0	35.9
	SD	2.63	0.082	309	1.67	3.53
12m/s	RAC50-2-1	51.6	1.610	5060	12.3	48.7
	RAC50-2-2	52.7	1.645	5550	11.7	47.4
	RAC50-2-3	48.7	1.520	3430	35.3	42.8
	RAC50-2-4	48.8	1.523	5950	24.7	54.1
	RAC50-2-5	44.7	1.395	5220	20.0	53.2
	AVG	49.3	1.539	5042	20.8	49.2
	SD	3.11	0.097	963	9.76	4.59
16m/s	RAC50-3-1	59.5	1.857	4980	30.0	70.0
	RAC50-3-2	59.5	1.857	4400	24.2	67.9
	RAC50-3-3	61.9	1.932	4170	18.1	73.8
	RAC50-3-4	60.1	1.876	5060	19.2	74.6
	RAC50-3-5	58.9	1.838	3230	28.7	67.8
	AVG	60.0	1.872	4368	24.0	70.8
	SD	1.15	0.036	740	5.38	3.22
20m/s	RAC50-4-1	80.3	2.506	2220	40.9	71.6
	RAC50-4-2	69.5	2.169	4470	32.8	88.3
	RAC50-4-3	74.7	2.331	4750	23.3	114.3
	RAC50-4-4	73.1	2.282	4800	32.6	92.2
	RAC50-4-5	73.1	2.282	4800	33.0	86.8
	AVG	74.1	2.314	4208	32.5	90.6
	SD	3.94	0.123	1120	6.24	15.37

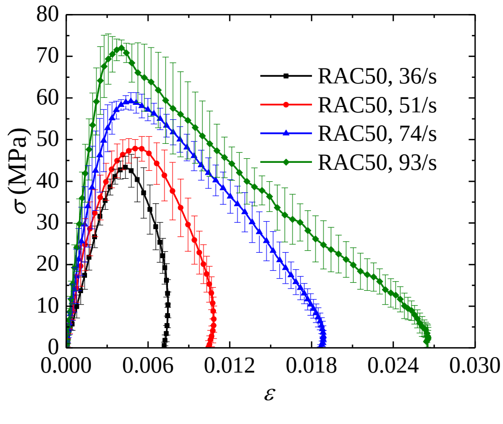

Fig. 4-18 Stress-strain curve of RAC50 under different impact loading

4.3.4 RAC50 Specimen

4.3.4.1 Stress-strain curves of RAC50 at different strain rates

The average stress-strain curves of RAC50 specimens at different strain rates are shown in Fig. 4-18. The results show that the stress-strain curves were similar for all the strain rates studied. With the increase in the strain rate, the peak stress and elastic modulus of RAC50 increased, the peak strain did not show any obvious trend, the rate of decrease in the stress after peak stress beacme slower. The peak stress, peak strain and elastic modulus of RAC50 are shown in Table 4-4.

4.3.4.2 Effect of strain rate on peak stress and DIF_f of RAC50

According to Table 4-4, the average peak stress of RAC50 are 43.8MPa, 49.3MPa, 60.0MPa and 74.1MPa respectively when the impact velocities were 10m/s, 12m/s, 16m/s and 20m/s. The corresponding DIF_f were 1.368, 1.539, 1.872 and 2.314 respectively. It indicated that the peak stress of RAC50 increased with the increase in strain rate. The relationship between peak stress and its DIF_f of RAC50 and strain rate are shown in Fig. 4-19 and Fig. 4-20. It can be seen that the peak stress of RAC50 increased almost linearly with the increase in strain rate. In this strain rate range, the DIF_f of RAC50 also increased linearly with the increase in logarithm of strain rate. The fitting curve is shown as follows:

$$DIF_f = -1.898 + 0.906 \cdot \lg(\dot{\varepsilon}) \tag{4-6}$$

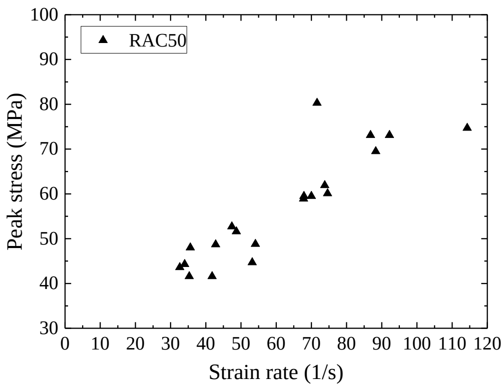

Fig. 4-19 Relationship between the peak stress of RAC50 and strain rate

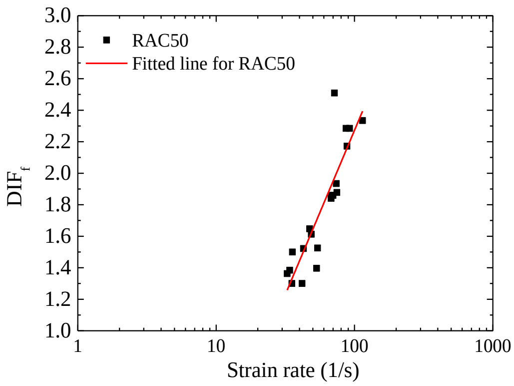

Fig. 4-20 Relationship between the DIF_f of RAC50 and strain rate

4.3.4.3 Effect of strain rate on peak strain of RAC50

The relationship between the peak strain of RAC50 and strain rate is shown in Fig. 4-21. It indicates that the peak strain did not show a clear trend with the increase in strain rate, it fluctuated around a constant value. According to Table 4-4, the average peak stress of RAC50 were 4276με, 5042με, 4368με and 4208με respectively when the impact velocities were 10m/s, 12m/s, 16m/s and 20m/s. It indicates that the peak strain of RAC50 did not show any significant change with the increase in strain rate in general.

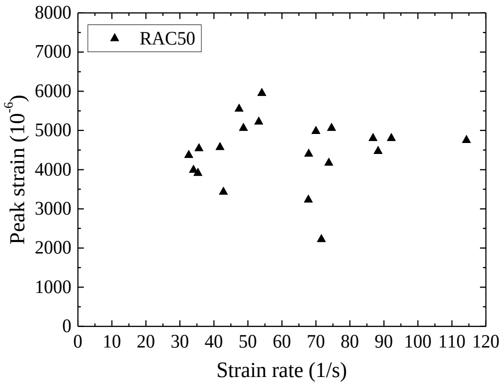

Fig. 4-21 Relationship between the peak strain of RAC50 and strain rate

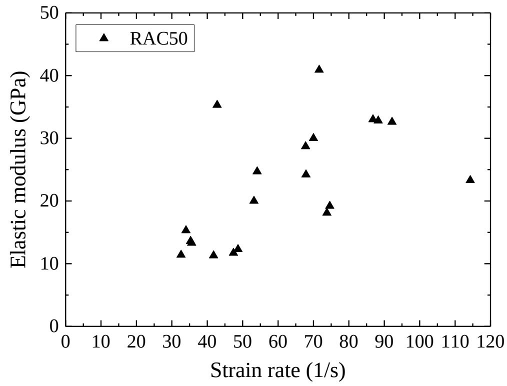

Fig. 4-22 Relationship between the elastic modulus of RAC50 and strain rate

4.3.4.4 Effect of strain rate on elastic modulus of RAC50

The relationship between the elastic modulus of RAC50 and strain rate are shown in Fig. 4-22. It can be seen that the elastic modulus of RAC50 showed an increasing trend with the increase in the strain rate, but the dispersion was large. According to Table 4-4, the average elastic modulus of RAC50 were 13.0GPa, 20.8GPa, 24.0GPa and 32.5GPa respectively when the impact velocities were 10m/s, 12m/s, 16m/s and 20m/s. It also indicates that the elastic modulus of RAC50 increased with the increase in strain rate.

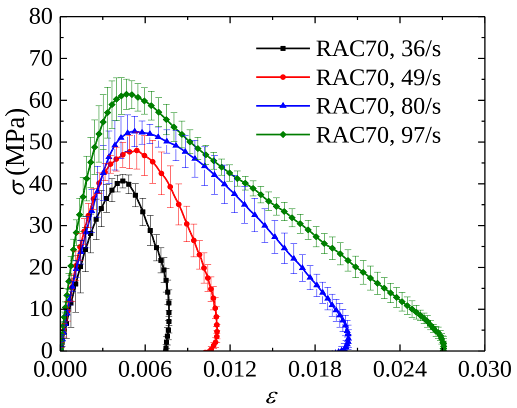

Fig. 4-23 Stress-strain curve of RAC70 under different impact loading

4.3.5 RAC70 Specimen

4.3.5.1 Stress-strain curves of RAC70 at different strain rates

The average stress-strain curves of RAC70 specimens at different strain rates are shown in Fig. 4-23. The results show that the stress-strain curves were similar for all the strain rates studied. With the increase in the strain rate, the peak stress increased, the elastic modulus showed an increasing trend, the peak strain did not show an obvious trend, the decreasing rate of stress after peak stress became slower. The peak stress, peak strain and elastic modulus of RAC70 are shown in Table 4-5.

Table 4-5 Peak stress, peak strain and elastic modulus of RAC70 specimens

Velocity of Striker bar	No.	Peak stress (MPa)	DIF_f	Peak strain (10^{-6})	Elastic modulus (GPa)	Strain rate (1/s)
10m/s	RAC70-1-1	40.9	1.457	3090	14.2	23.1
	RAC70-1-2	40.3	1.436	3830	15.9	35.3
	RAC70-1-3	43.0	1.532	5380	10.8	46.1
	RAC70-1-4	41.7	1.486	4140	23.8	36.1
	RAC70-1-5	39.2	1.397	4800	11.4	39.6
	AVG	41.0	1.461	4248	15.2	36.0
	SD	1.43	0.051	882	5.23	8.39
12m/s	RAC70-2-1	47.0	1.675	5500	19.2	47.8
	RAC70-2-2	47.0	1.675	3850	19.0	43.0
	RAC70-2-3	50.7	1.806	4380	20.7	44.9
	RAC70-2-4	54.2	1.931	4870	14.6	44.8
	RAC70-2-5	43.3	1.543	5380	19.4	57.3
	AVG	48.4	1.726	4796	18.6	47.6
	SD	4.15	0.148	691	2.32	5.71
16m/s	RAC70-3-1	49.1	1.749	5600	15.6	74.7
	RAC70-3-2	54.8	1.952	7270	17.6	78.6
	RAC70-3-3	57.9	2.063	4760	23.2	73.5
	RAC70-3-4	53.9	1.920	4240	23.3	72.6
	RAC70-3-5	54.6	1.945	4760	16.6	71.4
	AVG	54.1	1.926	5326	19.3	74.2
	SD	3.17	0.113	1191	3.71	2.76
20m/s	RAC70-4-1	67.6	2.408	3740	31.7	89.4
	RAC70-4-2	61.0	2.173	5490	20.2	91.1
	RAC70-4-3	61.8	2.202	3690	30.3	86.8
	RAC70-4-4	64.0	2.280	5680	32.6	101.7
	RAC70-4-5	57.0	2.031	5530	26.5	100.6
	AVG	62.3	2.219	4826	28.3	93.9
	SD	3.91	0.139	1017	5.07	6.79

4.3.5.2 Effect of strain rate on peak stress and DIF_f of RAC70

According to Table 4-5, the average peak stress of RAC70 were 41.0MPa, 48.4MPa, 54.1MPa and 62.3MPa respectively when the impact velocities were 10m/s, 12m/s, 16m/s and 20m/s. The corresponding DIF_f were 1.461, 1.726, 1.926 and 2.219 respectively. It indicates that the peak stress of RAC70 increased with the increase in strain rate. The relationship between the peak stress and its DIF_f of RAC70 and strain rate are shown in Fig. 4-24 and Fig. 4-25. It can be seen that the peak stress of RAC70 increased almost linearly with the increase in strain rate. In this strain rate range, the DIF_f of RAC70 also increased linearly with the increase in logarithm of strain rate. The fitting line is shown as follows:

$$DIF_f = -0.703 + 0.623 \cdot \lg(\dot{\varepsilon}) \tag{4-7}$$

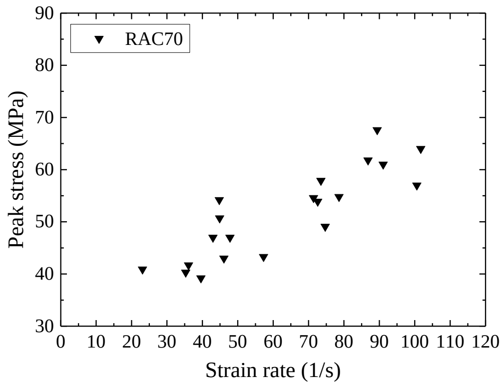

Fig. 4-24 Relationship between the peak stress of RAC70 and strain rate

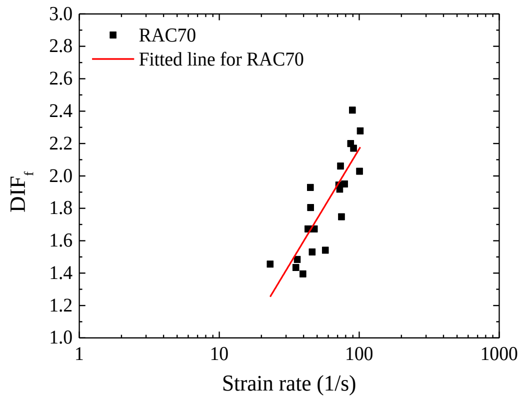

Fig. 4-25 Relationship between the DIF_f of RAC70 and strain rate

4.3.5.3 Effect of strain rate on peak strain of RAC70

The relationship between the peak strain of RAC70 and strain rate is shown in Fig. 4-26. It can be seen that the peak strain did not show a significant increase or decrease with the increase in the strain rate. According to Table 4-5, the average peak stress of RAC70 were 4248με, 4796με, 5326με and 4826με respectively when the impact velocities were 10m/s, 12m/s, 16m/s and 20m/s. It also indicates that the peak strain of RAC70 did not show any significant change with the increase in strain rate.

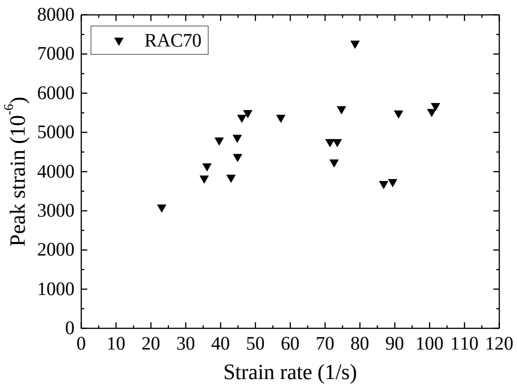

Fig. 4-26 Relationship between the peak strain of RAC70 and strain rate

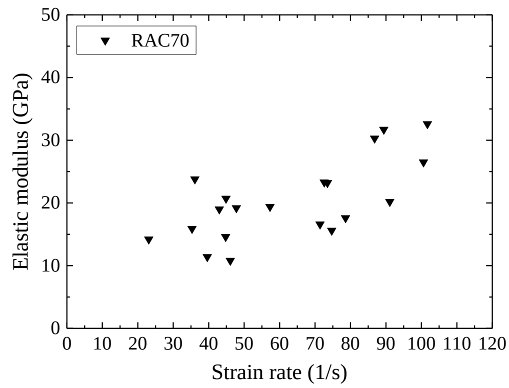

Fig. 4-27 Relationship between the elastic modulus of RAC70 and strain rate

4.3.5.4 Effect of strain rate on elastic modulus of RAC70

The relationship between the elastic modulus of RAC70 and strain rate is shown in Fig. 4-27. It can be seen that the elastic modulus of RAC70 showed an increasing trend with the increase in the strain rate. According to Table 4-5, the average elastic modulus of RAC70 were 15.2GPa, 18.6GPa, 19.3GPa and 28.3GPa respectively when the impact velocities were 10m/s, 12m/s, 16m/s and 20m/s. It also indicates that the elastic modulus of RAC70 increased with the increase in strain rate.

4.3.6 RAC100 Specimen

4.3.6.1 Stress-strain curves of RAC100 at different strain rates

The average stress-strain curves of RAC100 specimens at different strain rates are shown in Fig. 4-28. The results show that the stress-strain curves were similar for all studied strain rates. With the increase in the strain rate, the peak stress and elastic modulus of RAC100 increased, the peak strain did not show an obvious trend, the decreasing rate of stress after the peak stress became slower. The peak stress, peak strain and elastic modulus of RAC100 are shown in Table 4-6.

Table 4-6 Peak stress, peak strain and elastic modulus of RAC100 specimens

Velocity of Striker bar	No.	Peak stress (MPa)	DIF_f	Peak strain (10^{-6})	Elastic modulus (GPa)	Strain rate (1/s)
10m/s	RAC100-1-1	43.9	1.642	4580	11.2	37.6
	RAC100-1-2	35.8	1.339	5110	11.1	47.1
	RAC100-1-3	43.3	1.619	4080	20.9	33.7
	RAC100-1-4	40.7	1.522	4250	10.9	36.1
	RAC100-1-5	43.3	1.619	4450	10.9	38.3
	AVG	41.4	1.548	4494	13.0	38.6
	SD	3.37	0.126	394	4.42	5.09
12m/s	RAC100-2-1	37	1.384	5300	11.7	58.0
	RAC100-2-2	50.9	1.904	3410	35.4	42.5
	RAC100-2-3	48.3	1.806	5110	19.3	54.5
	RAC100-2-4	45.1	1.687	5440	18.1	57.9
	RAC100-2-5	46.6	1.743	4770	20.3	48.5
	AVG	45.6	1.705	4806	21.0	52.3
	SD	5.26	0.197	820	8.74	6.69
16m/s	RAC100-3-1	50.3	1.881	5320	16.8	71.2
	RAC100-3-2	53.1	1.986	5110	20.2	77.2
	RAC100-3-3	49.9	1.866	5910	19.5	81.8
	RAC100-3-4	50.7	1.896	2660	38.4	64.6
	RAC100-3-5	53.7	2.008	2340	38.3	59.7
	AVG	51.5	1.927	4268	26.6	70.9
	SD	1.73	0.065	1644	10.76	9.00
20m/s	RAC100-4-1	58.8	2.199	3940	29.8	89.3
	RAC100-4-2	60.8	2.274	4550	28.8	86.2
	RAC100-4-3	69.3	2.592	6130	27.6	103.9
	RAC100-4-4	70.0	2.618	6810	25.3	100.2
	RAC100-4-5	68.5	2.562	4870	30.3	97.0
	AVG	65.5	2.449	5260	28.4	95.3
	SD	5.26	0.197	1179	2.00	7.41

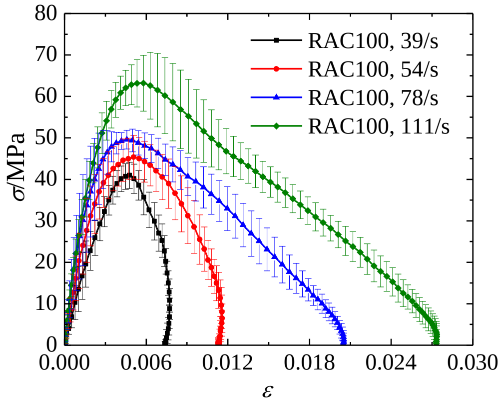

Fig. 4-28 Stress-strain curve of RAC100 under different impact loading

4.3.6.2 Effect of strain rate on peak stress and DIF_f of RAC100

According to Table 4-6, the average peak stress of RAC100 are 41.4MPa, 45.6MPa, 51.5MPa and 65.5MPa respectively when the impact velocities were 10m/s, 12m/s, 16m/s and 20m/s. The corresponding DIF_f were 1.548, 1.705, 1.927 and 2.449 respectively. It indicates that the peak stress of RAC100 increased with the increase in strain rate. The relationship between the peak stress and its DIF_f of RAC100 and strain rate are shown in Fig. 4-29 and Fig. 4-30. It can be seen that the peak stress of RAC100 increased almost linearly with the increase in strain rate. In this strain rate range, the DIF_f of RAC100 also increased linearly with the increase in logarithm of strain rate. The fitting line is shown as follows:

$$DIF_f = -1.555 + 0.845 \cdot \lg(\dot{\varepsilon}) \tag{4-8}$$

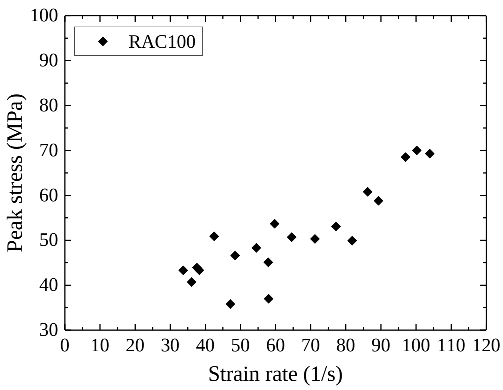

Fig. 4-29 Relationship between the peak stress of RAC100 and strain rate

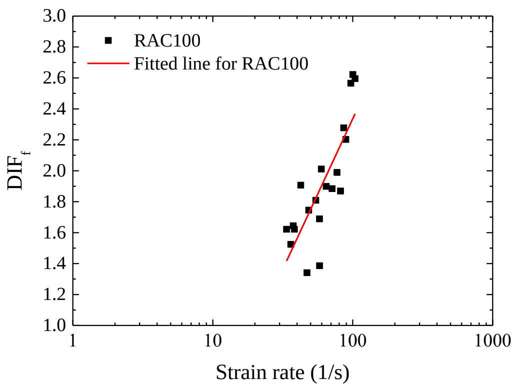

Fig. 4-30 Relationship between the DIF_f of RAC100 and strain rate

4.3.6.3 Effect of strain rate on peak strain of RAC100

The relationship between the peak strain of RAC100 and strain rate is shown in Fig. 4-31. It can be seen that the peak strain showed an increasing trend with the increase in the strain rate. However, because the dispersion was large, it is uncertain whether it is true. According to Table 4-6, the average peak stress of RAC100 were 4494με, 4806με, 4268με and 5260με respectively when the impact velocities were 10m/s, 12m/s, 16m/s and 20m/s. It indicates that the peak strain of RAC100 fluctuated with the increase in strain rate.

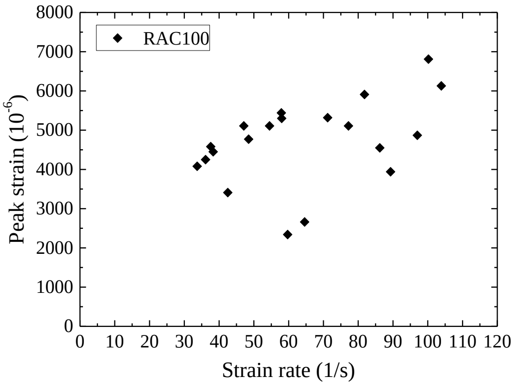

Fig. 4-31 Relationship between the peak strain of RAC100 and strain rate

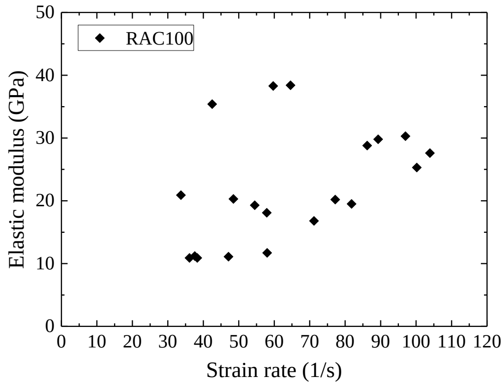

Fig. 4-32 Relationship between the elastic modulus of RAC100 and strain rate

4.3.6.4 Effect of strain rate on elastic modulus of RAC100

The relationship between the elastic modulus of RAC100 and the strain rate is shown in Fig. 4-32. It can be seen that the elastic modulus of RAC100 showed an increasing trend with the increase in the strain rate, but the dispersion was large, and there were several abnormal data points. According to Table 4-6, the average elastic modulus of RAC100 were 13.0GPa, 1.0GPa, 26.6GPa and 28.4GPa respectively when the impact velocities were 10m/s, 12m/s, 16m/s and 20m/s. In general, it indicates that the elastic modulus of RAC100 increased with the increase in strain rate.

4.3.7 NAC(wet) Specimen

4.3.7.1 Stress-strain curves of NAC(wet) at different strain rates

The average stress-strain curves of NAC(wet) specimens at different strain rates are shown in Fig. 4-33. The results show that the stress-strain curves are similar for all the strain rates studied. At a higher strain rate, the peak stress and elastic modulus were larger, the peak strain was also larger, the decreasing rate of stress after peak stress was slower. The peak stress, peak strain and elastic modulus of NAC(wet) are shown in Table 4-7.

Table 4-7 Peak stress, peak strain and elastic modulus of NAC(wet) specimens

Velocity of Striker bar	No.	Peak stress (MPa)	DIF_f	Peak strain (10^{-6})	Elastic modulus (GPa)	Strain rate (1/s)
10m/s	NAC(wet)-1-1	39.5	1.496	4470	19.6	40.2
	NAC(wet)-1-2	39.0	1.477	4900	16.9	44.6
	NAC(wet)-1-3	39.1	1.481	4190	17.6	38.9
	NAC(wet)-1-4	44.0	1.667	4070	14.3	39.7
	NAC(wet)-1-5	46.4	1.758	3720	25.0	37.8
	AVG	41.6	1.576	4270	18.7	40.24
	SD	3.40	0.129	443	4.01	2.60
20m/s	NAC(wet)-4-1	56.3	2.133	6180	19.0	111.4
	NAC(wet)-4-2	60.4	2.288	6590	31.7	111.9
	NAC(wet)-4-3	65.7	2.489	2960	22.8	85.8
	NAC(wet)-4-4	63.7	2.413	4290	26.4	92.0
	NAC(wet)-4-5	49.9	1.890	4150	33.8	93.5
	AVG	59.2	2.242	4834	26.7	98.92
	SD	6.30	0.239	1514	6.12	11.98

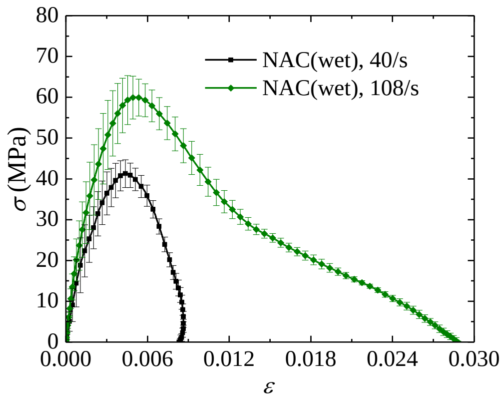

Fig. 4- 33 Stress-strain curve of NAC(wet) under different impact loading

4.3.7.2 Effect of strain rate on peak stress and DIF_f of NAC(wet)

According to Table 4-7, the average peak stress of NAC(wet) are 41.6MPa and 59.2MPa respectively when the impact velocities are 10m/s and 20m/s. The corresponding DIF_f are 1.576 and 2.242respectively. The relationship between the peak stress and its DIF_f of NAC(wet) and strain rate are shown in Fig. 4-34 and Fig. 4-35. It can be seen that the peak stress of NAC(wet) was higher at a higher strain rate.

4.3.7.3 Effect of strain rate on peak strain of NAC(wet)

The relationship between the peak strain of NAC(wet) and strain rate are shown in Fig. 4-36. It can be seen that the peak strain was larger at a higher strain rate. At the higher strain rate, the dispersion is large. According to Table 4-7, the average peak stress of NAC(wet) were 4270με and 4834με respectively when the impact velocities were 10m/s and 20m/s. It indicated that the peak strain was larger at a higher strain rate.

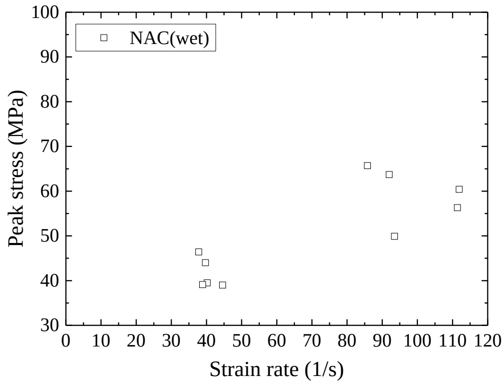

Fig. 4-34 Relationship between the peak stress of NAC(wet) and strain rate

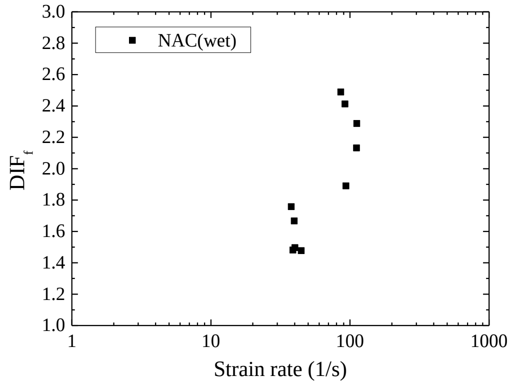

Fig. 4-35 Relationship between the DIF_f of NAC(wet)and strain rate

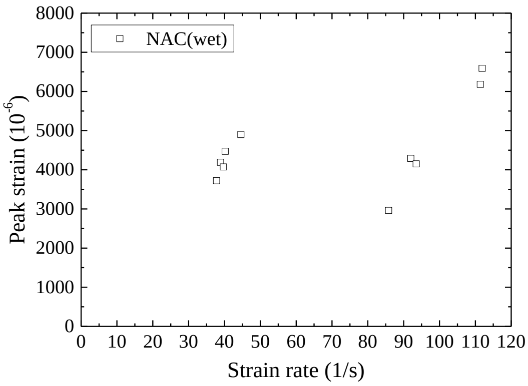

Fig. 4-36 Relationship between the peak strain of NAC(wet) and strain rate

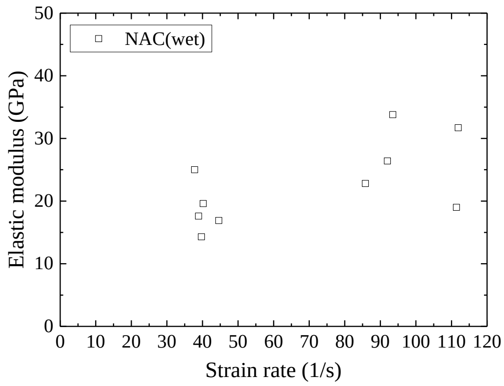

Fig. 4-37 Relationship between the elastic modulus of NAC(wet) and strain rate

4.3.7.4 Effect of strain rate on elastic modulus of NAC(wet)

The relationship between elastic modulus of NAC(wet) and strain rate are is shown in Fig. 4-37. It can be seen that the elastic modulus of NAC(wet) was larger at a higher strain rate. According to Table 4-7, the average elastic modulus of NAC(wet) were 18.7GPa and 26.7GPa respectively when the impact velocities were 10m/s and 20m/s. It also indicates that the elastic modulus of NAC(wet) was larger at a higher strain rate.

4.3.8 RAC100(wet) Specimen

4.3.8.1 Stress-strain curves of RAC100 (wet) at different strain rates

The average stress-strain curves of RAC100 (wet) specimens at different strain rates are shown in Fig. 4-38. The results show that the stress-strain curves are similar for all the strain rates studied.

At a higher strain rate, the peak stress and elastic modulus were larger, the peak strain was also larger, the decreasing rate of stress after peak stress was slower. The peak stress, peak strain and elastic modulus of RAC100 (wet) are shown in Table 4-8.

Table 4-8 Peak stress, peak strain and elastic modulus of RAC100(wet) specimens

Velocity of Striker bar	No.	Peak stress (MPa)	DIF_f	Peak strain (10^{-6})	Elastic modulus (GPa)	Strain rate (1/s)
10m/s	RAC100(wet)-1-1	37.5	1.402	5170	9.8	45.8
	RAC100(wet)-1-2	38.6	1.444	3360	26.5	36.4
	RAC100(wet)-1-3	41.5	1.552	4620	18.7	40.4
	RAC100(wet)-1-4	39.2	1.466	4830	11.5	45.6
	RAC100(wet)-1-5	38.8	1.451	5260	12.3	43.3
	AVG	39.12	1.463	4648	15.8	42.3
	SD	1.47	0.055	765	6.89	3.95
20m/s	RAC100(wet)-4-1	56.2	2.102	6300	18.3	118.9
	RAC100(wet)-4-2	65.0	2.431	4330	19.2	81.2
	RAC100(wet)-4-3	57.9	2.165	4930	33.0	104.8
	RAC100(wet)-4-4	57.3	2.143	6140	30.0	103.0
	RAC100(wet)-4-5	66.6	2.491	4410	27.0	93.8
	AVG	60.60	2.266	5222	25.5	100.3
	SD	4.82	0.180	941	6.52	13.97

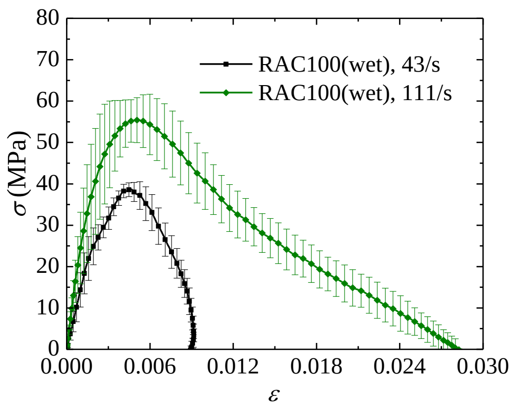

Fig. 4-38 Stress-strain curve of RAC100(wet) under different impact loading

4.3.8.2 Effect of strain rate on peak stress and DIF_f of RAC100 (wet)

According to Table 4-8, the average peak stress of RAC100(wet) are 39.12MPa and 60.60MPa respectively when the impact velocities are 10m/s and 20m/s. The corresponding DIF_f are 1.463 and 2.266 respectively. It indicates that the peak stress of RAC100 was larger at a higher strain rate The relationship between the peak stress and its DIF_f of RAC100(wet) and strain rate are shown in Fig. 4-39 and Fig. 4-40. It can be also seen that the peak stress of RAC100(wet) was larger at a higher strain rate.

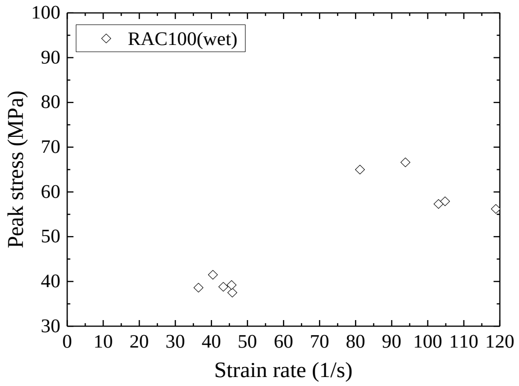

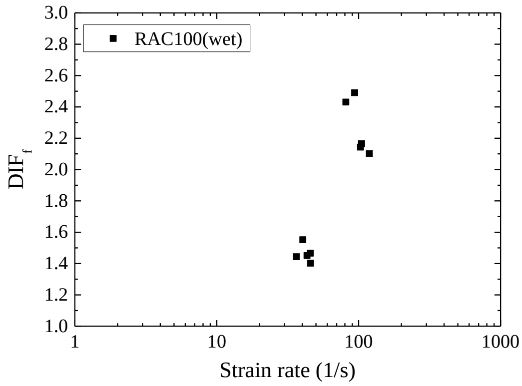

Fig. 4-39 Relationship between the peak stress of RAC100(wet) and strain rate

Fig. 4-40 Relationship between the DIF_f of RAC100(wet) and strain rate

4.3.8.3 Effect of strain rate on peak strain of RAC100 (wet)

The relationship between the peak strain of RAC100(wet) and strain rate is shown in Fig. 4-41. It can be seen that the peak strain was larger at a higher strain rate. According to Table 4-8, the average peak stress of RAC100 (wet) were 4648με and 5222με respectively when the impact velocities were 10m/s and 20m/s. It also indicates that the peak strain of RAC100(wet) was larger at a higher strain rate.

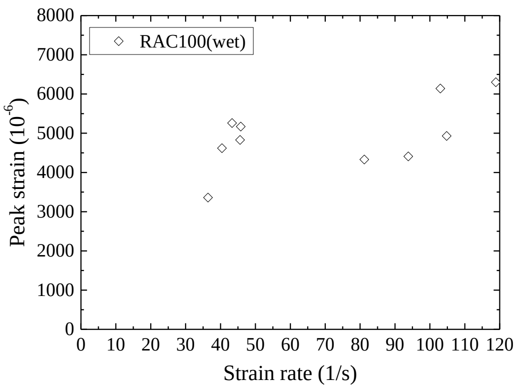

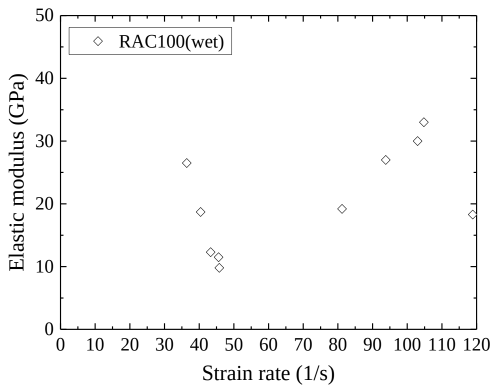

Fig. 4-41 Relationship between the peak strain of RAC100(wet) and strain rate

Fig. 4-42 Relationship between the elastic modulus of RAC100(wet) and strain rate

4.3.8.4 Effect of strain rate on elastic modulus of RAC100 (wet)

The relationship between the elastic modulus of RAC100 (wet) and strain rate are shown in Fig. 4-42. It can be seen that the elastic modulus of RAC100 (wet) was larger at a higher strain rate. At the first strain rate, the dispersion was large. According to Table 4-8, the average elastic modulus of RAC100 (wet) were 15.8GPa and 25.5GPa respectively when the impact velocities were 10m/s and 20m/s. It also indicated that the elastic modulus of RAC100 (wet) was larger at a higher strain rate.

4.4 Analysis and Discussion

According to the above test results, the strain-rate sensitivity of RAC at high strain rates will be analysed by evaluating the effect of strain rate on the peak stress, peak strain, elastic modulus and failure mode. At the same time, in order to better understand the strain-rate sensitivity mechanism of RAC, the effects of the RCA replacement percentage and moisture condition on the strain-rate sensitivity of RAC will also be analyzed.

4.4.1 Strain-rate sensitivity of RAC at high strain rates

4.4.1.1 Effect of strain rate on peak stress

The relationships between the average peak stress of RAC with different RCA replacement percentages and strain rate are shown in Fig. 4-43. The results show that the peak stress of RAC increased approximately linearly with the increase in strain rate. The variation inin the average DIF_f of RACs with the logarithm of the strain rate is shown in Fig. 4-44. The results show that the DIF_f of RACs increased approximately linearly with the increase in the logarithm of the strain rate. The test results of the average DIF_f were close to those of the CEB model. Under the first three impact rates, the average DIF_f of all kinds of RAC in this experiment was slightly smaller than that of CEB model. For the fourth impact rate, the average DIF_f of most RACs in this experiment was slightly larger than that of CEB model.

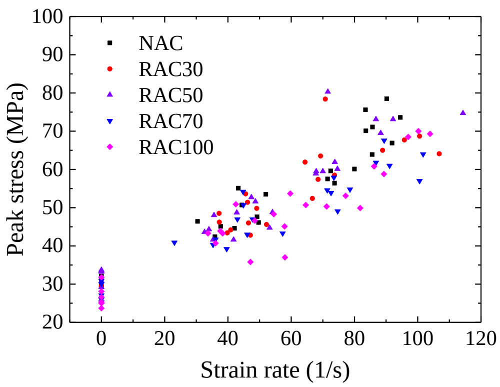

Fig. 4-43 Relationship between the peak stress of all RAC specimens and strain rate

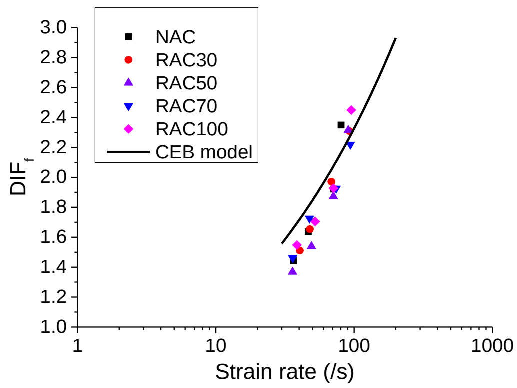

Fig. 4-44 Relationship between the DIF_f of all RAC specimens and strain rate

4.4.1.2 Effect of strain rate on peak strain

The relationship between the average peak strain of RAC with different RCA replacement percentages and the strain rate are shown in Fig. 4-45. The results show that there was no consistent trend between the peak strain and the strain rate for different RACs. According to Fig. 4-45, generally the peak strain of RAC fluctuated around a constant value with the increase in strain rate, but the dispersion was large. Therefore, it is argued that the peak strain of RAC does not change significantly with the change in strain rate, and the phenomenon of fluctuation is caused by the discretization of the experiment.

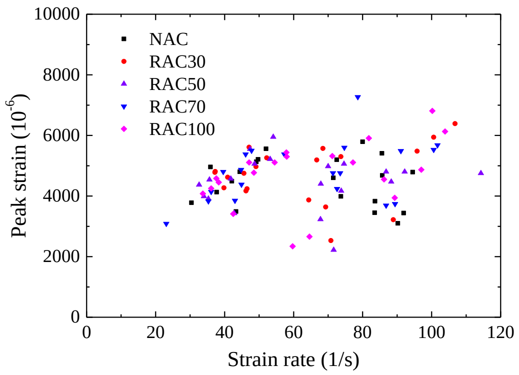

Fig. 4-45 Relationship between the peak strain of all RAC specimens and strain rate

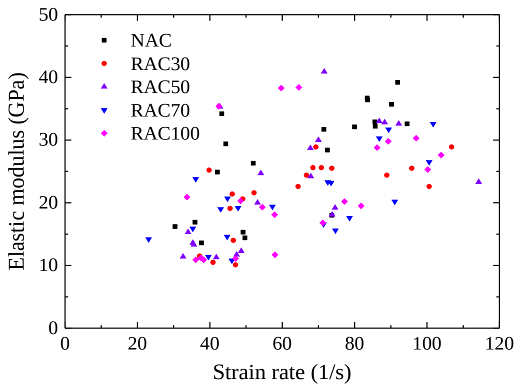

Fig. 4-46 Relationship between the elastic modulus of all RAC specimens and strain rate

4.4.1.3 Effect of strain rate on elastic modulus

The relationships between the average elastic modulus of RAC with different RCA replacement percentages and strain rate are shown in Fig. 4-46. The results show that the elastic modulus of RAC increased approximately linearly with the increase in strain rate in general. Moreover, compared with peak stress, the dispersion of elastic modulus was larger.

4.4.1.4 Effect of strain rate on failure mode

The failure patterns of RAC specimens at the four velocities are presented in Fig. 4-47. It is observed that the failure patterns of the RAC specimens with different RCA replacement percentages were similar. The failure pattern was more and more severe with increasing impact velocity which is summarized as follows: the specimens failed with a few visible cracks under the first impact velocity; at the second impact velocity, the specimens cracked into several large pieces; the specimens were crushed into fine fragments under the third and fourth impact velocity and the crushing was more serious under the fourth impact velocity. However, it is not certain whether the extent of damage was related to the strain rate because the total strains of the specimens were not constant under the different strain rates. Another interesting observation is that there were more fractured NCA particles under impacting loading than that under static loading. As the strength of NCA is higher than mortar matrix and ITZ, more fractured NCA particles indicated that it requires larger stress for the propagation of cracks. This may be a factor for the increase in compressive strength at a high strain rate. However, the fractured NCA particles still made up only a small proportion of the whole aggregate particles at the fractured surface. Moreover, most of the fractured NCA particles were elongated aggregates rather than rounded aggregates. To sum up, most of the cracks still passed through the interfaces, which is similar to that under static loading reported by Xiao *et al*. [**Error! Bookmark not defined.**]. Therefore, it is suggested that the more fractured NCA particles generated under impact loading may be a factor but not the main factor for the increase in dynamic strength.

10m/s 12m/s 16m/s 20m/s

(a) NAC

10m/s 12m/s 16m/s 20m/s

(b) RAC30

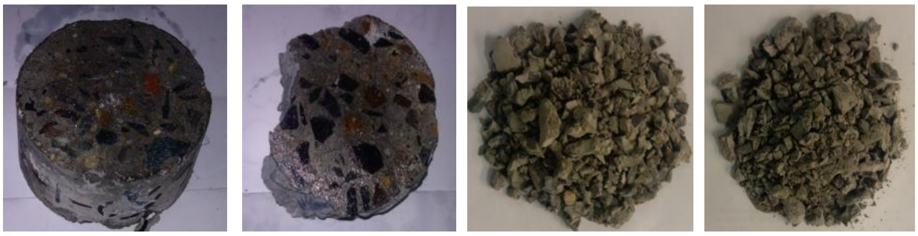

10m/s 12m/s 16m/s 20m/s

(c) RAC50

10m/s 12m/s 16m/s 20m/s

(d) RAC70

10m/s 12m/s 16m/s 20m/s

(e) RAC100

Fig. 4-47 Failure patterns of RAC specimens under different impact loadings

4.4.2 Effect of RCA replacement percentage

4.4.2.1 Effect of RCA replacement percentage on peak stress, peak strain and elastic modulus

The variation in peak stress, peak strain and elastic modulus of RACs with RCA replacement percentages are illustrated in Fig. 4-48, Fig. 4-49 and Fig. 4-50. It shows that the peak stress of RAC decreased with the increase in RCA replacement percentage in general at all the strain rates studied. The elastic modulus also decreased with the increase in RCA replacement percentage. The peak strain of RAC did not exhibit a clear trend as the RCA replacement percentage increased. This feature is consistent with the results in static loading tests which have been reported by many investigators. The reason why the peak stress and elastic modulus of RAC decreased with the increase in RCA replacement percentage under static load is that there are many microcracks and weak ITZ in the RCA. It indicates that the microcracks and ITZ in the RCA are still the main factors affecting the strength of RAC in the impact load. It can be seen from Fig. 4-49 that the peak strain of RAC did not show increasing or decreasing as RCA replacement percentage increases at the same impact velocity, it fluctuated around a constant value. This phenomenon is different from the static result. Xiao et al. (2005) have shown that the static peak strain of RAC increases with the increase in the RCA replacement percentage.

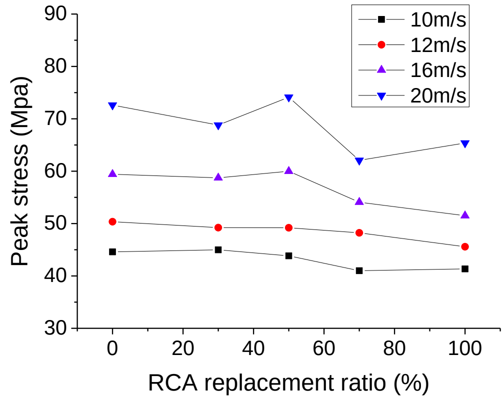

Fig. 4-48 Effect of RCA replacement percentage on the dynamic peak stress of RAC

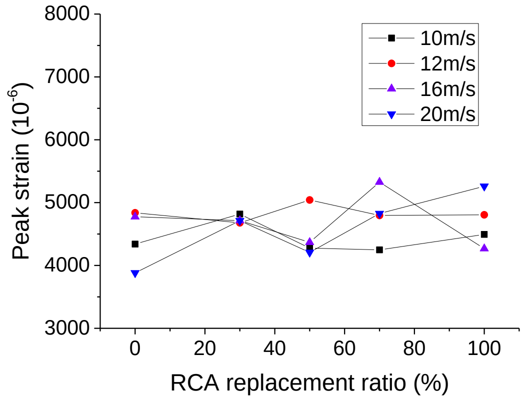

Fig. 4-49 Effect of RCA replacement percentage on the dynamic peak strain of RAC

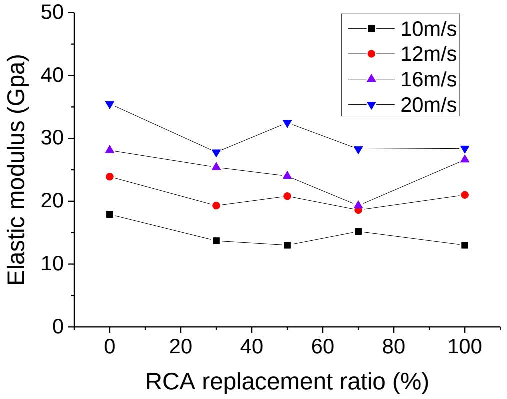

Fig. 4-50 Effect of RCA replacement percentage on the dynamic elastic modulus of RAC

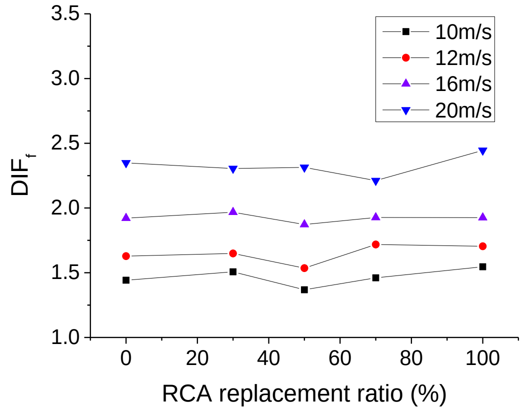

Fig. 4-51 Effect of RCA replacement percentage on the DIF_f of RAC

4.4.2.2 Effect of RCA replacement percentage on strain-rate sensitivity of RAC

Fig. 4.56 shows the variation in DIF_f with the RAC replacement percentage to study its effect on the strain-rate sensitivity of RAC. The results show that the DIF_f of RAC did not show a strict increasing with the increase in the RCA replacement percentage at each impact rate. For example, the DIF_f of RAC50 was lower than that of NAC and RAC30 at the first three impact rates, and the

DIF_f of of the NAC was even greater than that of the RAC30, RAC50 and RAC70 at the fourth impact rate. However, in general the DIF_f of RAC tended to increase slightly with the increase in the RCA replacement percentage. That's because with the increase in RCA replacement percentage, the content of mortar which is more strain-rate sensitive than aggregate in the RAC was higher, thus DIF_f of RAC increased. However, it can be seen from the test results that the effect of RCA replacement percentage on the DIF_f of RAC was not significant. At each impact velocity, the differences between the DIF_f values of the RAC with different RCA replacement percentages were not significant. Therefore, it may be argued that the difference in the strian-rate sensitivity of RACs with different RCA replacement percentages is not determined separately from the mortar content, and the difference in microstructure may also affect the strain-rate sensitivity of RAC

4.4.3 Effect of moisture condition

4.4.3.1 Effect of moisture condition on the peak stress

The peak stress of RAC100 and NAC tested under air-dry condition and wet condition versus strain rate are compared in Fig. 4-52. The results show that the peak stress of the NAC and the RAC100 in a wet state was lower than that in the air-dry state under the same strain rate. This is consistent with the result under static load, and also consistent with the phenomenon under low strain rates. In other words, the presence of free water at the impact load still causes a decrease in the strength of the concrete, and the viscous effect caused by free water has not yet played a leading role.

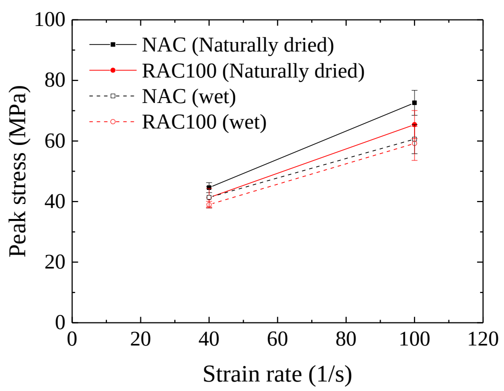

Fig. 4-52 Effect of moisture condition on the dynamic peak stress of RAC

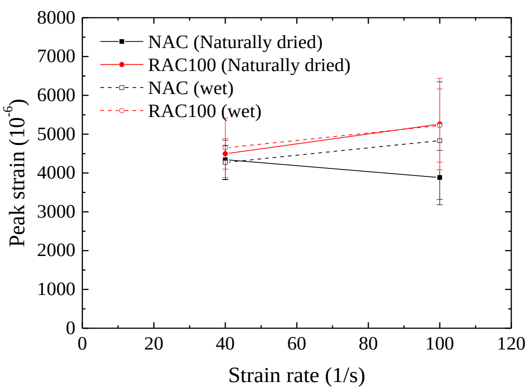

Fig. 4-53 Effect of moisture condition on the dynamic peak strain of RAC

4.4.3.2 Effect of moisture condition on peak strain

The variation in the dynamic peak strain of the NAC specimen and the RAC100 specimen in an air-dry and wet condition with the strain rate is shown in Fig. 4-53. The results show that some of the peak strain of RAC in a wet state was lower than that in an air-dry state, while some of the peak strain of RAC in a wet state was higher. In other words, the effect of moisture condition on the dynamic peak strain is not clear under impact loading.

4.4.3.3 Effect of moisture condition on elastic modulus

The variation in the dynamic elastic modulus of the NAC specimen and the RAC100 specimen in an air-dry and wet condition with the strain rate is shown in Fig. 4-54. The results show that the elastic modulus of NAC(wet) specimen and RAC100 (wet) specimen was larger than that in an air-dry state at the first strain rate. At the fourth strain rate, the elastic modulus of the NAC(wet) specimen and the RAC100 (wet) specimen were smaller than those at an air-dry state. Therefore, it is difficult to determine the Effect of the moisture condition on the elastic modulus during impact loading. Previous studies also showed that there is no consistent conclusion on the effect of moisture condition on the dynamic elastic modulus. For example, Zhou et al. (2011) reported that the dynamic elastic modulus decreases with the increase in water content, but Wu et al. (2012) reported that the dynamic elastic modulus increases with the increase in water content. Therefore, the effect of moisture condition on the dynamic elastic modulus of RAC needs further study.

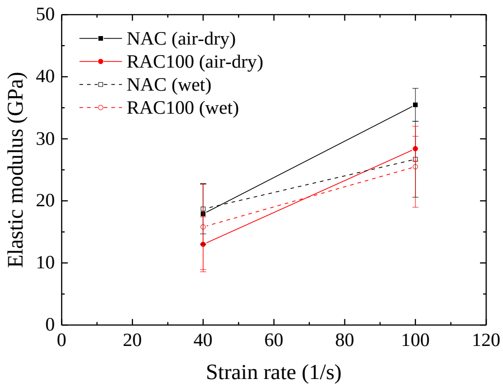

Fig. 4-54 Effect of moisture condition on the dynamic elastic modulus of RAC

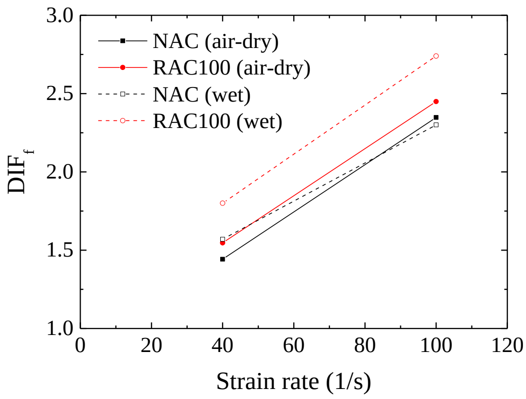

Fig. 4-55 Effect of moisture condition on the DIF_f of RAC

4.4.3.4 Effect of moisture condition on strain-rate sensitivity of RAC

In this test, the relationship between the DIF_f of NAC and RAC100 specimen in an air-dry and wet state and the strain rate is shown in Fig. 4-55. The results show that NAC and RAC100 in a wet state also showed strain-rate sensitivity. For NAC, some of the DIF_f of NAC specimens in a wet state were greater than that in an air-dry state while some were lower. For RAC, the DIF_f of RAC100 specimens in a wet state were significantly greater than that in an air-dry state. However, the increasing rate of DIF_f of RAC100 specimens in a wet state was not significantly different fromfrom that in an air-dry state. In general, the strain-rate sensitivity of RAC in a wet state has no significant difference from that in an air-dry state. Therefore, it is believed that the viscous effect caused by the free water is not significant under the strain rate range studied. Brara et al. (2006) also showed that the moisture condition in concrete is not a major contributor to the increase in dynamic strength of concrete. This phenomenon is consistent with the phenomenon at low strain rates. However, it is reported in many researches that free water in concrete is a major contributor to the strain-rate sensitivity of concrete, which is different fromfrom the results obtained in this study. Therefore, it is needs further study on whether the water content is a dominant factor for the strain-rate sensitivity of concrete.

4.5 Summary

In this chapter, the stress-strain curves of recycled aggregate concrete (RAC) were experimentally studied under high strain rates (i.e., 10^1 /s ~ 10^2 /s) using a Split Hopkins pressure bar (SHPB). By analyzing the effect of strain rate on peak stress, peak strain, elastic modulus and failure pattern, the strain-rate sensitivity of RAC was studied. At the same time, the effects of recycled coarse aggregate (RCA) repalcement percentage and moisture condition on the strain-rate sensitivity of RAC were discussed. In summary, the main conclusions are displayed as follows:

(1) Under impact loading, with an increase in the strain rate, the peak stress and elastic modulus of RAC showed an approximately linearly increasing trend, and the peak strain fluctuated around a constant value.

(2) Compared to the failure mode under quasi-static load, more aggregates fractured under impact loading. The phenomenon of cracks passing through the aggregate is considered as one of the factors that contribute to the strain-rate sensitivity of the RAC, but may not be the main influencing factor.

(3) Under impact loading, the peak stress and elastic modulus of RAC decreased with the increase

in RCA replacement percentage, while the peak strain did not change significantly with the increase in RCA replacement percentage.

(4) The strain-rate sensitivity of RAC increased slightly with the increase in RCA replacement percentage, but it is not significant.

(5) Under impact loading, the peak stress of RAC in a wet sate was still lower than that in an air-dry RAC specimen; there was no clear conclusion on the effect of moisture condition on the dynamic elastic modulus and peak strain of RAC.

(6) The strain-rate sensitivity of the wet RAC specimen and air-dry RAC specimen did not show significant differences. It is believed that the water content of the specimen may not be the main factor contributing to the strain-rate sensitivity of RAC under the strain rate range studied.

Chapter 5 Dynamic mechanical behavior of RAC with carbonated RCA at low strain rates

Carbonation technique is one of the ways to improve the properties of RCA, thus improve the properties of RAC. As described in the previous chapters, RAC is a strain-rate sensitive material. To apply the RAC with modified RCA, it is essential to study its strain-rate sensitivity. However, there is still no study on the dynamic properties of RAC using carbonated RCA (CRCA).

In this chapter, the effects of carconation on the mesoscopic properties of RCA and the static mechanical behavior of RAC were studied based on MRAC. The effect of RCA modification by carbonation on the dynamic compressive behavior of RAC prepared with CRCA (CRAC) was experimentally studied using cylindrical specimens at low strain rates (10^{-5}/s ~ 10^{-1}/s). Based on the results of microhardness test, the mechanical behaviors of ITZ and old mortar in RCA after carbonation were determined, and then numerical study on the effect of carbonation on static mechanical behaviors of MRAC were conducted.

5.1 Test design

5.1.1 Materials

5.1.1.1 For MRAC specimen

An ASTM Type I Portland cement 52.5, with a density of 3.15 g/cm^3, was used in this study. The fine aggregate used was a natural river sand. The water was tap water. The modeled natural coarse aggregate (MNCA) was cylindrical granite aggregates, 30 mm in diameter and 30 mm in height, cored from a 30 mm thickness granite slab, as shown in Fig. 5-1 (a). The MRCA used was prepared in the laboratory by casting a layer of mortar (namely the old mortar) on the above cylindrical MNCA, i.e. the MRCA was a cylinder, 40 mm in diameter and 30 mm in height, with a mortar layer, 5 mm in thickness, as shown in Fig. 5-1 (b). Two types of old mortars, named M1 and M2, were used in the test. The w/c of M1 and M2 were 0.5 and 0.6 respectively. The cement-to-sand ratios (w/c) of M1 and M2 were both 1/3. The average 28 days compressive strengths of M1 and M2 were 55.6 MPa and 37.5 MPa respectively. The MRCAs with the old mortar M1, the old mortar M2, the carbonated old mortar M1 and the carbonated old mortar M2 were named

MRCA-M1, MRCA-M2, MRCA-CM1 and MRCA-CM2, respectively. Only one type of new mortar, of which the mix proportion was the same as M1, was used in the test.

(a) MNCA

(b) MRCA

Fig. 5-1 Modeled coarse aggregate

One half of the prepared MRCAs were treated with a CO_2 curing process. The laboratory CO_2 curing setup is illustrated in Fig. 5-2. An air-tight cylindrical vessel with a volume of about 33 L was used as the curing chamber, which was vacuumed to -0.5bar before the pure CO_2 gas injection. The CO_2 pressure in chamber was controlled by a regulator and kept at 0.1bar. Considering the adverse effect of high humidity on carbonation, anhydrous silica gel was put inside the chamber to remove the evaporated water from the specimens during the carbonation process. The CO_2 curing chamber was placed in a laboratory condition at about 25℃. After three weeks of carbonation, phenolphthalein solution was sprayed on the surface of samples, it could be seen that the attached mortar in MRCA-CM2 was all carbonated while only part of the old mortar in MRCA-CM1 was carbonated, as shown in Fig. 5-3.

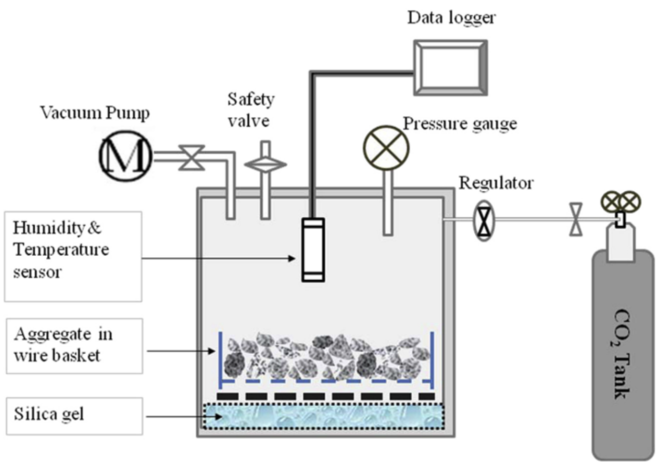

Fig. 5-2 Schematic of CO_2 curing setup

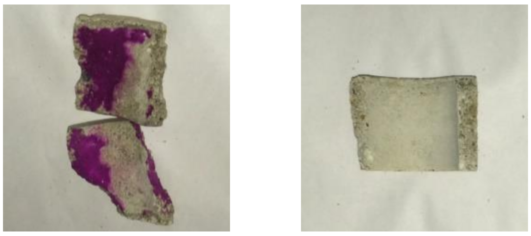

(a) MRCA-CM1 (b) MRCA-CM2

Fig. 5-3 Carbonation degree of the old adhered mortar in MRCA

The water absorptions values of the four types of MRCAs were measured according to the method for natural coarse aggregate specified in the ASTM C127. The results are shown in Table 5-1. It is obvious that the water absorptions of MRCAs modified by carbonation were lower than that of uncarbonated MRCAs. The water absorption of the material is related to the porosity of the material. Therefore, it is verified that carbonation could reduce the porosity of MRCA.

Table 5-1 Water absorption values of MRCA before and after carbonation

No.	MRCA-M1	MRCA-CM1	MRCA-M2	MRCA-CM2
Water absorption	3.86%	3.16%	4.12%	3.67%

5.1.1.2 For RAC specimen

The cement used was a type of ASTM Type I Portland cement. River sand was used as the fine aggregate. The RCA was obtained by crushing a batch of concrete which was produced by a concrete supplier. The mixture proportion of the original concrete for producing RCA is given in Table 5-2. After 6 months of on-site curing, the original concrete was crushed in a construction waste recycling plant. The 28 days compressive strength of the original concrete was designed with 45 MPa. The crushed concrete was sieved into several fractions with different sizes. In this study, the crushed fractions with sizes of 5-10 mm and 10-20 mm were selected as RCA to produce the RAC.

Table 5-2 Mix proportion of the original concrete for producing RCA

	w/c	Water	Cement	Natural aggregate		Sand	Super-plasticiser
				5-10mm	10-20mm		
Original concrete	0.45	205	460	430	530	700	3.47

To investigate the effect of the CRCA on the mechanical properties of RAC, a proportion of RCA was carbonated with an accelerated carbonation procedure. The carbonation device, which is given in Fig. 5-4 (Xuan et al. 2016), includes an airtight steel-cylindrical chamber with a volume of about 100 L, a CO_2 storage tank and an air pump. Before carbonation, the RCA was put into a drying chamber, in which the temperature was 25 ± 3°C and the relative humidity was 50 ± 5%. The relative humidity was in the optimum range of 40% to 70% (Morandeau et al. 2014). The accelerated carbonation procedure of RCA is displayed as follows. First, the chamber was vacuumed to -0.6 bar by the air pump after the RCA was put into the chamber. Then, CO_2 was injected into the chamber and the pressure of the chamber was kept at a constant level which was controlled by a gas regulator. In this study, RCA was carbonated for 7 days in the chamber with a CO_2 concentration about 100% at a pressure level of 1 bar.

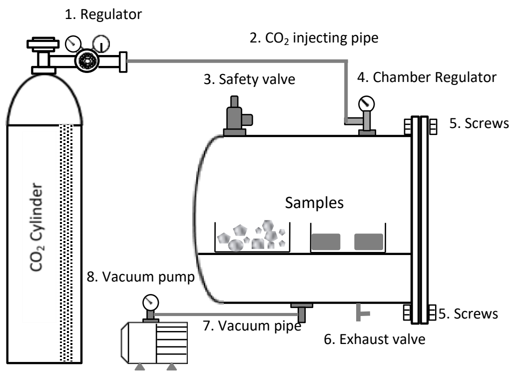

Fig. 5-4 Schematic of carbonation chamber (Xuan et al. 2016)

The physical properties of RCA and CRCA are given in Table 5-3. The results show that the physical properties of RCA were improved by carbonation, which is consistent with the results in some previous studies (Kou et al. 2014; Zhan et al. 2014). The apparent density of CRCA was slightly higher than that of RCA. The reduction of water absorption of CRCA was about 14.6% ~ 22.3% when compared with RCA. The crushing index of CRCA was lower than that of RCA.

Table 5-3 Physical properties of RCA and CRCA

Type	Size (mm)	Apparent density (kg/m^3)	Water absorption (%)	Crushing value (%)
Sand	< 5	2676	1.1	-
RCA	5-10	2611	6.22	-
	10-20	2583	6.19	27.8
CRCA	5-10	2621	5.31	-
	10-20	2604	4.81	21.9

The mix proportions of RAC and CRAC specimens are listed in Table 5-4. In this study, the air-dry RCA and CRCA were used when casting RAC and CRAC specimens. Hence, according to the water absorption of RCA and CRCA, additional amounts of water were added to assure the same effective w/c.

Table 5-4 Mix proportions of RAC and CRAC

Specimen	Effective w/c	Water (kg/m^3)	Cement (kg/m^3)	Sand (kg/m^3)	Coarse aggregate (kg/m^3)	
					5-10 mm	10-20 mm
RAC	0.55	225	409	751	306	712
CRAC	0.55	225	409	754	307	714

5.1.2 Specimen design

5.1.2.1 For MRAC specimen

The MRAC specimens were prepared with four types of MRCAs. The corresponding MRAC specimens were named MRAC-M1, MRAC-M2, MRAC-CM1 and MRAC-CM2 respectively. The purpose is to study the effect of MRCA carbonation on the properties of MRAC with two different old mortars. There were 3 specimens for each type of MRAC. The geometric dimensions of these MRAC specimens are given in Fig. 5-5.

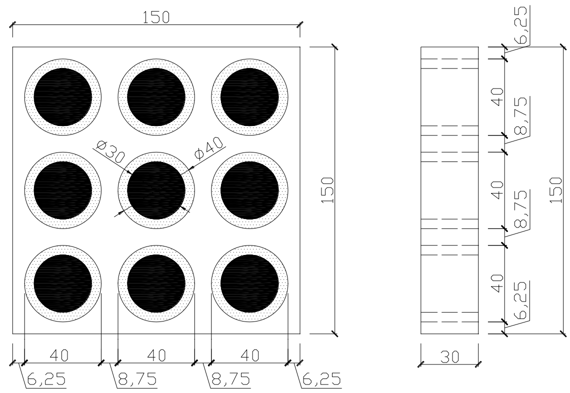

Fig. 5-5 Geometric dimensions of MRAC specimens

The MRCAs were soaked in water to a saturation condition, and then placed in air for approximately 1 hour before the casting of MRAC specimens. To prevent change inin positions during vibrating, the MRCAs were stuck on the bottom of the steel mold with a quick-dry glue. After casting the new mortar, the specimens were covered with plastic films. They were then removed from the steel molds after one day in the laboratory. Then the specimens were kept in a water tank (Temp at about 25℃) for 2 months before testing.

5.1.2.2 For RAC specimen

For both RAC and CRAC, a series of 100 mm cubic specimens and cylindrical specimens with the dimension of Φ100mm × 200mm were cast in steel moulds. After curing in the laboratory for 24 hours, all the specimens were demolded and further cured in a water tank with the temperature at 25±3°C. After curing in the water tank for 7, 28 and 90 days, the compressive strength of the cubic specimens was tested. At the same time, the cylindrical specimens were taken out from the water tank and kept under indoor conditions for 1 year. Before testing their dynamic mechanical properties, high-strength gypsum paste was capped on both sides.

5.1.3 Experimental setup and testing

5.1.3.1 For MRAC specimen

Microhardness testing was conducted on the MRCAs to study the properties of old ITZ and old mortar. It is now generally accepted that the microstructure of cement pastes in the vicinity of the surface of an aggregate which is called ITZ is quite different from that of the bulk cement matrix. The ITZ can extend to distances of about 50 um from the aggregates surface. When compared with the bulk, the ITZ has a higher porosity and a more heterogeneous microstructure. Microhardness testing has been reported as a means of characterizing the properties of this zone relative to the bulk and as a means of estimating its width (Igarashi et al. 1996; Asbridge et al. 2002; Lee & Choi 2013). Considering the typical width of the ITZ, the size of indentation should not be too large. Therefore, the applying load in the microhardness test should be controlled to ensure the size of the indentation. In this test, the load applied was set at 0.98 N. The sizes of the indentation diagonal in MRCA-M1 and MRCA-M2 were around 10 um and 25 um respectively. The method for selecting the indentation points are presented in Fig. 5-6. This method ensured dense mapping and sufficient large spaces between individual measuring points.

The MRAC specimens were loaded under quasi-static uni-axial compression using a servo-hydraulic testing machine. Displacement-controlled loading with a constant loading rate 0.1mm/min was selected in this study. The loadings applied to the specimen were recorded by the internal force transducer in the system. Two strain gauges were fixed at mid-height on opposite faces of the specimens to measure the average axial longitudinal strain. In order to reduce the frictional constraints, two Teflon sheets of thickness 0.1mm were used at the top and bottom of the specimens. Preloading which was about 10% of peak load was applied to prevent eccentric loading on the loading surface by comparing the strains at the two sides of specimens. The loading history and longitudinal strain history were measured. At the same time, the cracking processes and failure patterns were recorded with a digital video camera.

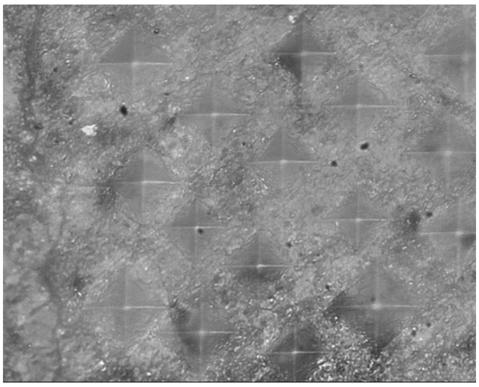

Fig. 5-6 Strategy for selecting the indentation points

5.1.3.2 For RAC specimen

The servo-hydraulic testing machine (MTS815.02) as described in the chapter 2 and chapter 3 was used to apply the dynamic uni-axial compressive loadings at different strain rates. In this test, five loading speeds ranging from 2×10^{-3} mm/s to 20mm/s were applied on the RAC and CRAC specimens, which correspondsto the five different strain rates ranging from 10^{-5}/s to 10^{-1}/s. The loadings were terminated when the displacements reached 2 mm. It was sufficient to obtain the complete stress-strain curves, including both the ascending and descending phases. When the strain rate was 10^{-5}/s, the loading was considered as quasi-static loading. The applied loadings on the specimens were measured using an internal force transducer in the system. The displacements of the loading platen, which consists of the displacement of specimens and testing machine, were recorded via the internal linear variable differential transformer (LVDT). The average axial longitudinal strain was measured by two extensometers which were fixed on opposite faces of the specimens by strings.

5.2 Test results

5.2.1 Effect of carbonation on the Microhardness of MRCA

The microhardness of the cement paste, measured along the distance from the interface of

MNCA used, are shown in Fig. 5-7. It is shown that the microhardness of the cement paste in the vicinity of the surface of MRCA was lower than that in the bulk paste in the case of MRCA-M1 and MRCA-M2. This phenomenon the ITZ being weaker than the bulk paste has been widely accepted. The test results showed that this ITZ zone could extend for distance of about 60 um from the interface of MNCA. The microhardness of ITZ was about 80%~85% of that in the bulk paste. Xiao et al. (2013) also reported that the average elastic modulus of ITZ was approximately 80%~85% of those of the bulk mortar matrix.

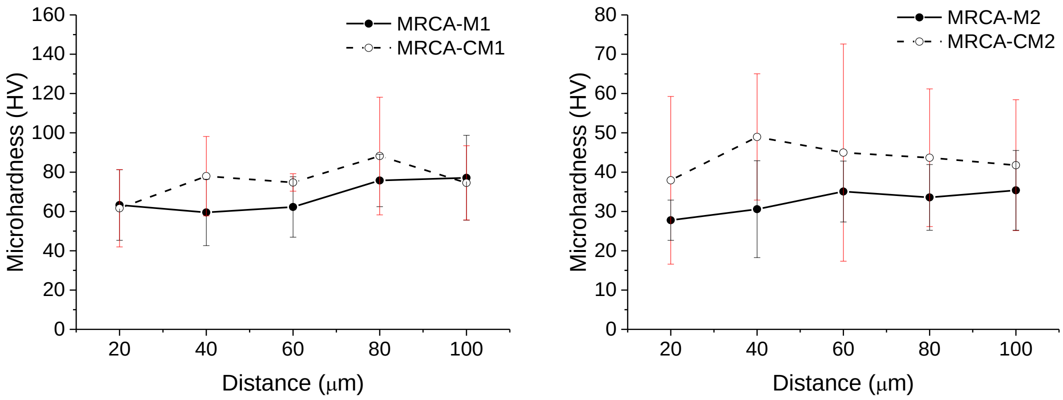

(a) MRCA-M1 and MRCA-CM1 (b) MRCA-M2 and MRCA-CM2

Fig. 5-7 Microhardness of cement pastes adjacent to MNCA in MRCA samples

It is interesting that the microhardness of the ITZ was not obviously weaker than that in bulk paste when the MRCA was carbonated. The reason may be due to the improvement of ITZ by carbonation was higher than the bulk paste because the higher porosity of the cement paste would facilitate better carbonation. Comparing the microhardness results of MRCA-M2 with that of MRCA-CM2, the average increase in the ITZ was about 40% while the average increase in the bulk paste was about 24%, as shown in Fig. 5-7 (b).

As shown in Fig. 5-7, it is also found that the increase in microhardness of the cement paste by carbonation in MRCA-M1 was smaller than that in MRCA-M2. The average microhardness of the cement paste within the 100um distance from the MNCA surface in MRCA-CM1 and MRCA-CM2 were about 34% and 12% higher than that of MRCA-M1 and MRCA-M2, respectively. That may be because the microstructure of the cement paste prepared with a higher w/c could be improved more obviously by carbonation.

5.2.2 Effect of carbonation on static mechanical behaviors of MRAC

5.2.2.1 Failure pattern

The failure patterns of the four types of MRAC specimens are displayed in Fig. 5-8. During the loading process, most cracks first initiated in the old interfaces between MNCA and the old mortar or the new interfaces between old and new mortar. These cracks continued to propagate vertically and met together before the specimen failed. These features were basically consistent with the results reported by Li et al. (2012). In addition, when comparing with the failure pattern of MRAC with the uncarbonated MRCAs, the number of cracks in the new interfaces in MRAC prepared with the carbonated MRCAs was more. Specifically, the amount of visible cracks passing through new interfaces for MRAC-M1, MRAC-CM1, MRAC-M2 and MRAC-CM2 accounted for about 55%, 80%, 60% and 75% of total amount of cracks passing through new and old interfaces respectively. That was because the old ITZs in MRAC were enhanced by carbonation treatment as mentioned above. It means that the failure pattern of RAC would be influenced by the carbonation treatment of RCA.

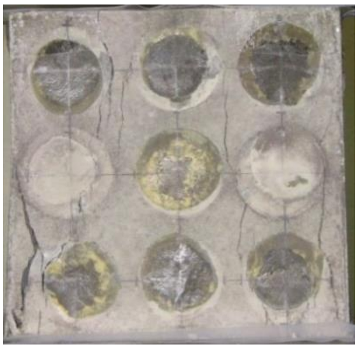

(a) MRAC-M1

(b) MRAC-CM1

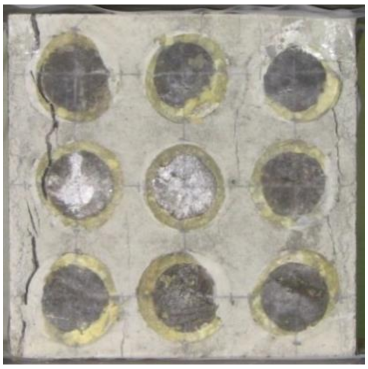

(c) MRAC-M2

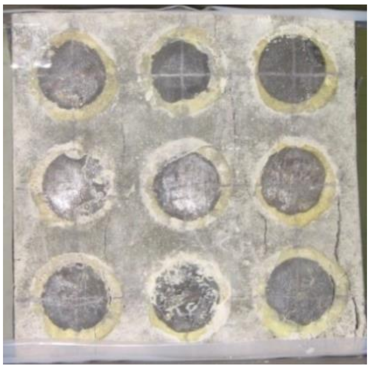

(d) MRAC-CM2

Fig. 5-8 Failure patterns of MRAC specimens

5.2.2.2 Stress-strain curve

Fig. 5-9 displays the typical stress-strain curves of the MRAC specimens. It is observed that the compressive strength (peak stress) and elastic modulus of MRAC with the carbonated MRCAs were higher while the peak strain was lower when compared with MRAC with the uncarbonated MRCAs. In addition, it can be seen that the nonlinearity of the ascending part of the stress-strain curves decreased.

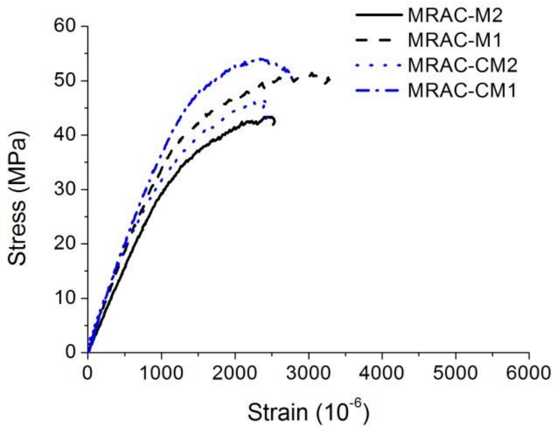

Fig. 5-9 Stress-strain curves of MRAC specimens

5.2.2.3 Peak stress

Fig. 5-10 shows the peak stress of the MRAC specimens. It shows that the compressive strength of MRAC with the carbonated MRCAs were larger than that of MRAC prepared with uncarbonated MRCAs. That is because the carbonation treatment can reduce the porosity of MRCAs which led to the increase in the strength of the old ITZ and old mortar, and thus increasing the compressive strength of MRAC. The peak stress of MRAC-CM1 and MRAC-CM2 were 6.07% and 7.69% higher than that of MRAC-M1 and MRAC-M2 respectively. The range of increase by MRCA carbonation is similar to the results reported by Xuan et al. (2016), which showed that the increase in RAC strength by RCA carbonation was about 6.6% to 22.6%. In addition, the test results showed that the increase in peak stress by carbonation treatment was more significant when the w/c of the old mortar in MRCA was higher. This may be because the strength of the old ITZ and old mortar were enhanced more significantly by the carbonation when the w/c of old mortar was higher.

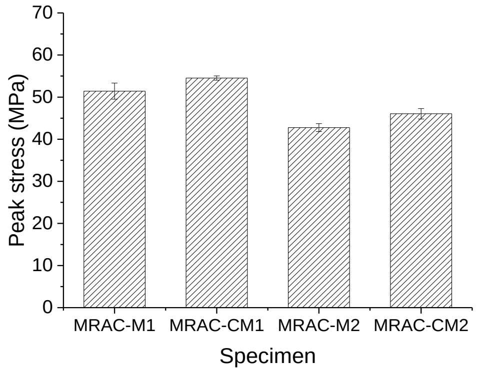

Fig. 5-10 Peak stress of MRAC

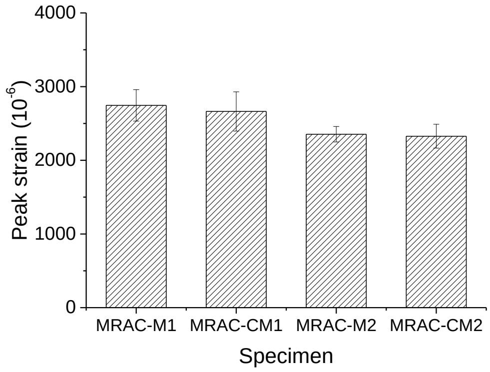

Fig. 5-11 Peak strain of MRAC

5.2.2.4 Peak strain

Fig. 5-11 illustrates the peak strain of each type of MRAC specimens. The results indicated that there was a slight decrease in the peak strain of MRAC with the carbonated MRCAs when compared with MRAC with the uncarbonated MRCAs. The peak strain of MRAC-CM1 was 2.97% lower than that of MRAC-M1 while the peak strain of MRAC-CM2 was 1.13% lower than that of MRAC-M2. At the same time, the variations in the peak strain of the MRAC with the carbonated MRCAs were larger than that of the MRAC with the uncarbonated MRCAs. The decrease in the peak strain of MRAC maybe because the old mortar and old ITZ become more brittle after the carbonation treatment. In addition, it is shown that the peak strain of MRAC prepared with the lower w/c MRCAs was higher.

5.2.2.5 Elastic modulus and secant modulus

In this study, the elastic modulus is defined as the secant slope of the stress-strain curve when the stress is between 20 and 40 percent of the compressive strength. The test results showed that the elastic modulus of MRAC with the carbonated MRCAs were larger than that of MRAC with the uncarbonated MRCAs, as shown in Fig. 5-12. However, the increments of elastic modulus due to MRCA carbonation for the two types of MRAC specimens were significantly different, which were about 17.7% and 1.9% respectively for MRAC-CM1 and MRAC-CM2. It is not clear whether this feature is a true trend or just because of experimental error. Therefore, the secant modulus of MRAC specimens at the maximum stress are compared, as shown in Fig. 5-13. It is found that the secant modulus of MRAC-CM1 and MRAC-CM2 increased by about 9.75% and 6.67% respectively when compared with that of MRAC-M1 and MRAC-M2. To sum up, the results showed that the modulus of MRAC can be increased by MRCA carbonation.

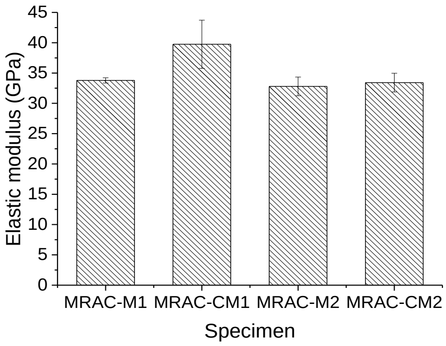

Fig. 5-12 Elastic modulus of MRAC

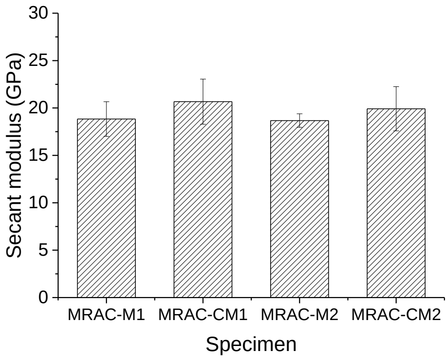

Fig. 5-13 Secant modulus of MRAC

5.2.3 Effect of carbonation on dynamic mechanical behaviors of RAC

5.2.3.1 Cube compressive strength of RAC and CRAC specimens

The 7 days, 28 days and 90 days cube compressive strength of RAC and CRAC specimens are given in Table 5-5. It is shown that the compressive strengths of CRAC were higher in comparison with RAC. The increasess were by 8.2%, 17.5% and 12.2% respectively for the 7 days, 28 days and 90 days compressive strength. This indicates that the compressive strength of RAC can be improved by using CRCA.

Table 5-5 Cubic compressive strength of RAC and CRAC specimens

	Number	Compressive strength (MPa)		
		7 days	28 days	90 days
RAC specimens	1	32.8	40.2	44.5
	2	34.7	38.4	45.6
	3	34.1	38.4	43.6
	AVG	33.9	39.0	44.6
	SD	1.0	1.0	1.0
CRAC specimens	1	35.9	46.0	50.5
	2	37.0	45.8	47.1
	3	37.0	45.6	52.4
	AVG	36.6	45.8	50.0
	SD	0.7	0.2	2.7

5.2.3.2 Stress-strain curves of RAC and CRAC specimens

The typical stress-strain curves of RAC and CRAC specimens are illustrated in Fig. 5-14. It is observed that the stress-strain curves of the RAC and CRAC specimens exhibited some common features. Overall, the shapes of all the stress-strain curves were similar at the different strain rates. The compressive strength increased with the increase in the strain rate. The initial slope of the stress-strain curves was steeper when the strain rate was higher.

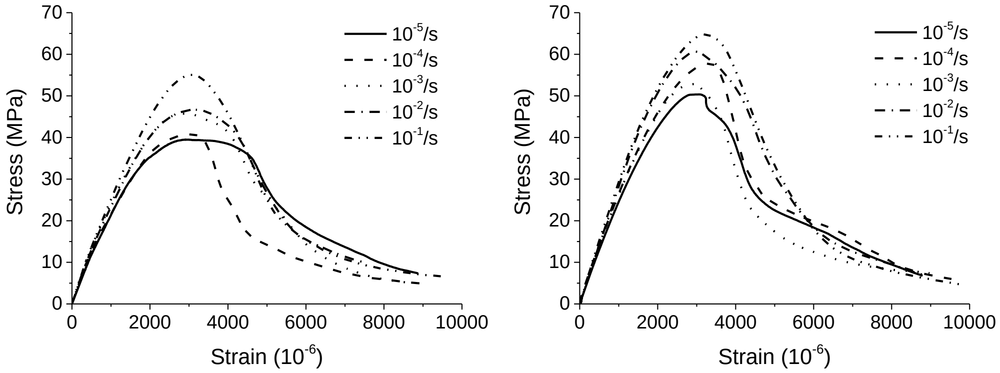

(a) RAC (b) CRAC

Fig. 5-14 Typical stress-strain curves of RAC and CRAC at different strain rates

Based on the Chinese *Code for Design of Concrete Structures* (GB50010-2010) (2010), the uni-axial compressive stress-strain curve can be calculated according to the following equations:

$$\sigma = (1 - d_c) E_c \varepsilon \tag{1}$$

$$d_c = \begin{cases} 1 - \dfrac{\rho_c n}{n - 1 + x^n} & x \le 1 \\ 1 - \dfrac{\rho_c}{\alpha_c (x-1)^2 + x} & x > 1 \end{cases} \tag{2}$$

$$n = \frac{E_c \varepsilon_{c,r}}{E_c \varepsilon_{c,r} - f_{c,r}} \tag{3}$$

$$\rho_c = \frac{f_{c,r}}{E_c \varepsilon_{c,r}} \tag{4}$$

$$x = \frac{\varepsilon}{\varepsilon_{c,r}} \tag{5}$$

Where, d_c is a parameter for damage evolution; α_c is a parameter for the descending part of stress-strain curve, it is related to the compressive strength of concrete and could be determined from the code; $f_{c,r}$ is the representative value of compressive strength of concrete; $\varepsilon_{c,r}$ is peak strain of concrete; and E_c is elastic modulus of concrete.

The experimental stress-strain curves of RAC and CRAC at all the strain rates studied were compared with the stress-strain curves calculated which were determined by substituting the relevant test data (i.e., $f_{c,r}$, E_c and $\varepsilon_{c,r}$ in dynamic loadings) into the above equation, as shown in Fig. 5-15. It is noticed that the experimental stress-strain curves of RAC and CRAC at all the strain rates studied were matched the calculated stress-strain curves well. It is thus suggested that the static uni-axial compressive stress-strain curve of the conventional concrete given in the Chinese code are also suitable for the RAC and CRAC when the strain rate is at the range of 10^{-5}/s to 10^{-1}/s, while the value of $f_{c,r}$, E_c and $\varepsilon_{c,r}$ are determined according to the relevant test results. The differences in the stress-strain curves of RAC or CRAC at different strain rates may be represented by the differences in compressive strength, elastic modulus and peak strain of the RAC or CRAC respectively.

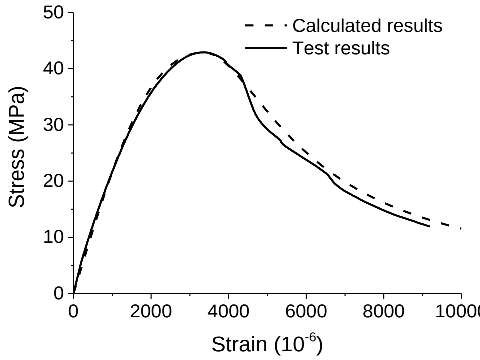

(a) RAC_10^{-5}/s

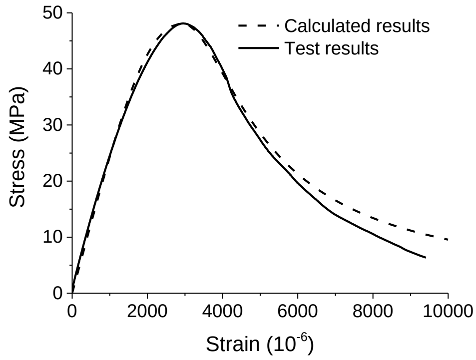

(b) RAC_10^{-4} /s

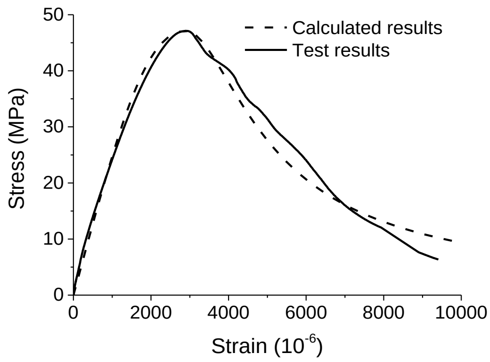

(c) RAC_10^{-3} /s

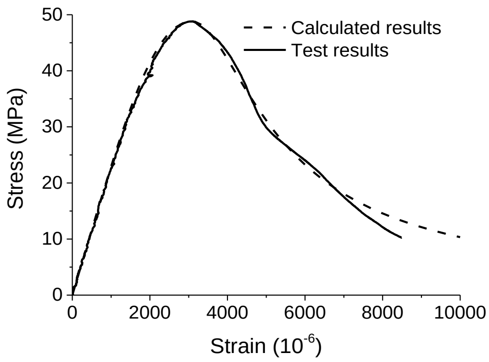

(d) RAC_10^{-2} /s

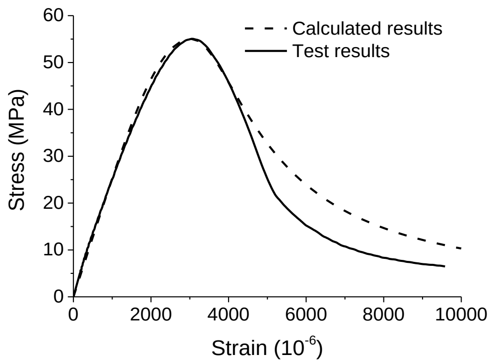

(e) RAC_10^{-1} /s

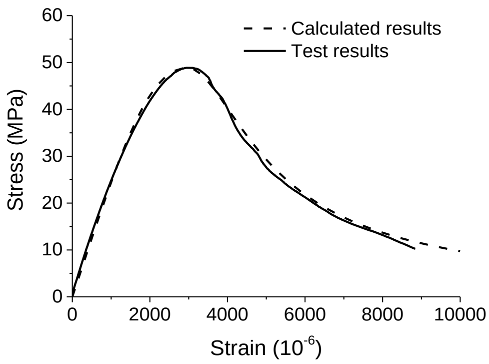

(f) CRAC_10^{-5} /s

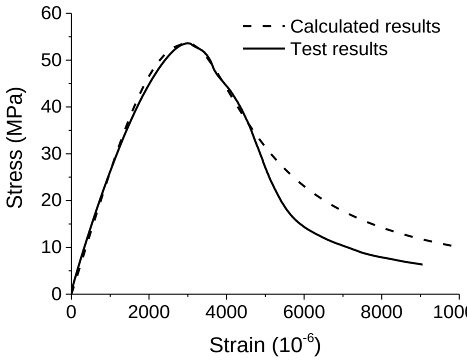

(g) CRAC_10^{-4} /s

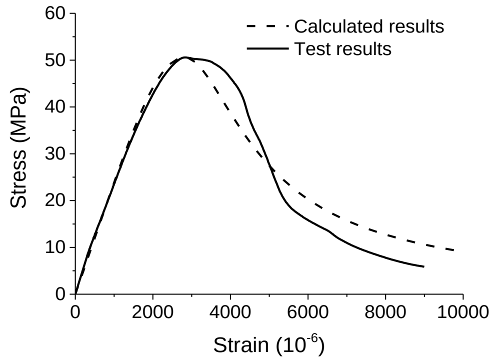

(h) CRAC_10^{-3} /s

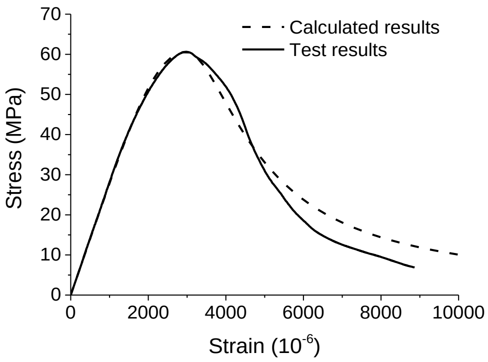

(i) CRAC_10^{-2} /s

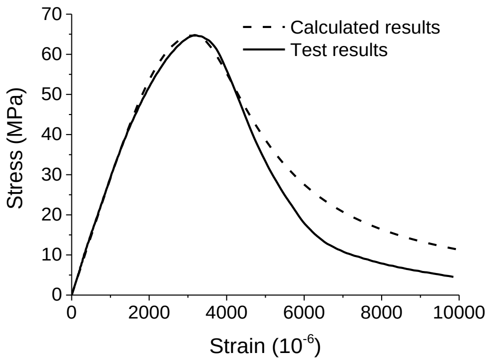

(j) CRAC_10^{-1} /s

Fig. 5-15 Stress-strain curves of RAC and CRAC at different strain rates

Table 5-6 Peak stress of RAC and CRAC specimens

	number	Peak stress at different strain rates (MPa)				
		0.00001/s	0.0001/s	0.001/s	0.01/s	0.01/s
RAC specimens	1	41.3	48.1	45.7	46.7	53.7
	2	39.5	37.5	47.1	48.8	55.1
	3	42.9	40.8	44.3	52.7	57.2
	AVG	41.2	42.1	45.7	49.4	55.3
	SD	2.4	5.4	1.4	3.0	1.7
CRAC specimens	1	48.9	53.6	52.8	60.6	55.7
	2	50.4	57.8	50.6	58.0	64.8
	AVG	49.6	55.7	51.7	59.3	60.3
	SD	1.1	3.0	1.6	1.9	6.4

5.2.3.3 Peak stress of RAC and CRAC specimens

The peak stress ($f_{c,r}$) of RAC and CRAC specimens at different strain rates are displayed in Table 5-6. The results show that the average peak stress of both RAC and CRAC specimens increased with the increase in strain rate. At each strain rate, the average peak stress of CRAC was larger than that of RAC. The increases were by 15.6%, 36.5%, 16.6%, 12.6% and 5.4% for strain rates of 10^{-5}/s, 10^{-4}/s, 10^{-3}/s, 10^{-2}/s and 10^{-1}/s, respectively. In general, the difference between the peak stress of CRAC and CRAC reduced as the strain rate increased.

Fig. 5-16 shows the relation of dynamic increase factor of peak stress (DIF_f) versus strain rate for RAC specimens and CRAC specimens, respectively. Here, DIF_f represents the ratio of peak stress at a higher strain rate to its corresponding quasi-static peak stress. The fitting line of DIF_f and strain-rate relation for the RAC specimens and CRAC specimens are displayed in the following two equations:

$$DIF_{f,RAC} = 1 + 0.0858 \cdot \lg(\dot{\varepsilon} / \dot{\varepsilon}_s) \tag{6}$$

$$DIF_{f,CRAC} = 1 + 0.0550 \cdot \lg(\dot{\varepsilon} / \dot{\varepsilon}_s) \tag{7}$$

Where, $\dot{\varepsilon}_0$ is the quasi-static peak strain, which is 10^{-5}/s in this study; $\dot{\varepsilon}$ is the strain rate. The results show that if the strain rate increased by a factor of 10, the DIF_f of the RAC and CRAC specimens increased by 8.58% and 5.50%, respectively. It indicates that the strain-rate sensitivity of peak stress of CRAC specimens was less significant than that of the RAC specimens.

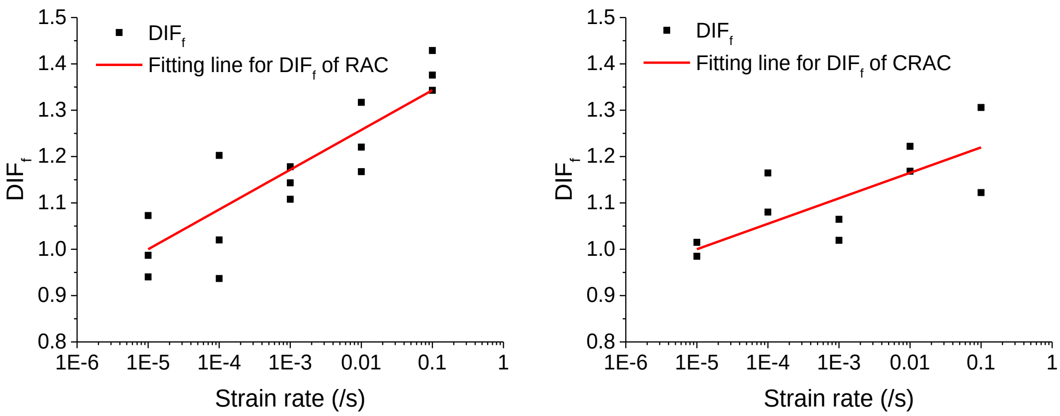

(a) RAC specimens (b) CRAC specimens

Fig. 5-16 Relation of DIF_f versus strain rate for RAC and CRAC specimens

5.2.3.4 Elastic modulus of RAC and CRAC specimens

In this study, the elastic modulus (E_c) was determined from the stress-strain curve using the following equations:

$$E_c = \frac{\sigma_{0.4} - \sigma_0}{\varepsilon_{0.4} - \varepsilon_0} \tag{8}$$

Where $\sigma_{0.4}$ is 40% of the peak stress; $\varepsilon_{0.4}$ is the corresponding strain; σ_0 and ε_0 are the stress and the strain respectively at the first data point of stress-strain curve.

The elastic modulus of RAC and CRAC specimens at different strain rates are listed in Table 5-7. The results show that the average elastic modulus of both RAC and CRAC specimens increased with an increase in strain rate in general. At each strain rate, the average elastic modulus of CRAC specimens was larger than that of RAC specimens. The increases were by 8.8%, 12.2%, 2.6%, 10.9% and 2.2% for strain rates of 10^{-5}/s, 10^{-4}/s, 10^{-3}/s, 10^{-2}/s and 10^{-1}/s, respectively. It indicates that the increase in peak stress of RAC by incorporating CRCA was more obvious than that in elastic modulus.

Table 5-7 Elastic modulus of RAC and CRAC specimens

	number	Elastic modulus at different strain rates (GPa)				
		0.00001/s	0.0001/s	0.001/s	0.01/s	0.01/s
RAC specimens	1	23.5	24.9	25.5	23.2	30.1
	2	22.4	22.4	25.5	24.4	25.5
	3	22.8	23.6	23.2	27.7	26.8
	AVG	22.9	23.6	24.7	25.1	27.4
	SD	0.3	1.2	1.3	2.3	2.4
CRAC specimens	1	24.9	26.6	26.8	28.0	26.7
	2	24.9	26.3	23.9	27.6	29.4
	AVG	24.9	26.5	25.4	27.8	28.0
	SD	0.0	0.2	2.0	0.3	1.9

Fig. 5-17 shows the relation between the dynamic increase factor of elastic modulus (DIF_E) of RAC specimens and CRAC specimens and strain rate. Here, DIF_E represents the ratio of elastic modulus at a higher strain rate compared to its corresponding quasi-static elastic modulus. The fitting line of DIF_E and strain-rate relation for the RAC specimens and CRAC specimens are expressed in the following two equations:

$$DIF_{E,\,RAC} = 1 + 0.0426 \cdot \lg(\dot{\varepsilon} / \dot{\varepsilon}_s) \tag{9}$$

$$DIF_{E,\,CRAC} = 1 + 0.0318 \cdot \lg(\dot{\varepsilon} / \dot{\varepsilon}_s) \tag{10}$$

The results show that if the strain rate was increased by a factor of 10s, the DIF_E of RAC and CRAC specimens increase by 4.26% and 3.18%, respectively. It indicates that the strain-rate sensitivity of elastic modulus of CRAC specimens was less significant than that of RAC specimens. In addition, for both RAC and CRAC specimens, the strain-rate sensitivity of elastic modulus was less significant than the strain-rate sensitivity of peak stress. This feature is consistent with the previous study by Bischoff and Perry (1991).

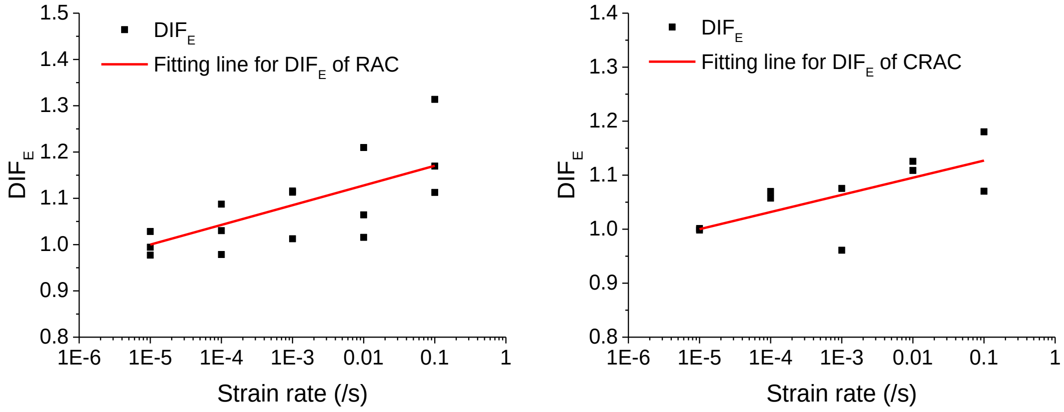

(a) RAC specimens (b) CRAC specimens

Fig. 5-17 Relation of DIF_E versus strain rate for RAC specimens and CRAC specimens

5.2.3.5 Peak strain of RAC and CRAC specimens

The peak strains ($\varepsilon_{c,r}$) of RAC and CRAC specimens at different strain rates are listed in Table 5-8. The average peak strain of both RAC and CRAC specimens remained approximately constant irrespective of the strain rates although there was a big variation. Additionally, the average peak strain of CRAC specimens was slightly lower than that of RAC specimens for the same strain rate.

Table 5-8 Peak strain of RAC and CRAC specimens

	number	Peak strain at different strain rates (10^{-6})				
		0.00001/s	0.0001/s	0.001/s	0.01/s	0.01/s
RAC specimens	1	2605	2941	2872	3094	3090
	2	2914	3660	2900	3086	3051
	3	3380	2920	3590	—	3288
	AVG	3147	3174	3121	3090	3143
	SD	330	421	407	6	127
CRAC specimens	1	2974	3007	2895	2977	2844
	2	3047	3296	2824	3216	3179
	AVG	3011	3152	2860	3097	3012
	SD	52	204	50	169	237

Fig. 5-18 shows the relation of dynamic increase factor of peak strain (DIF_ε) versus strain rate for the RAC and CRAC specimens, respectively. Herein, DIF_ε represents the ratio of peak strain at a higher strain rate compared to its corresponding quasi-static peak strain. The fitting line of DIF_ε and the strain-rate relation for the RAC specimens and CRAC specimens are given by the following two equations:

$$DIF_{\varepsilon,RAC} = 1 - 0.0018 \cdot \lg(\dot{\varepsilon} / \dot{\varepsilon}_s) \tag{11}$$

$$DIF_{\varepsilon,CRAC} = 1 + 0.0011 \cdot \lg(\dot{\varepsilon} / \dot{\varepsilon}_s) \tag{12}$$

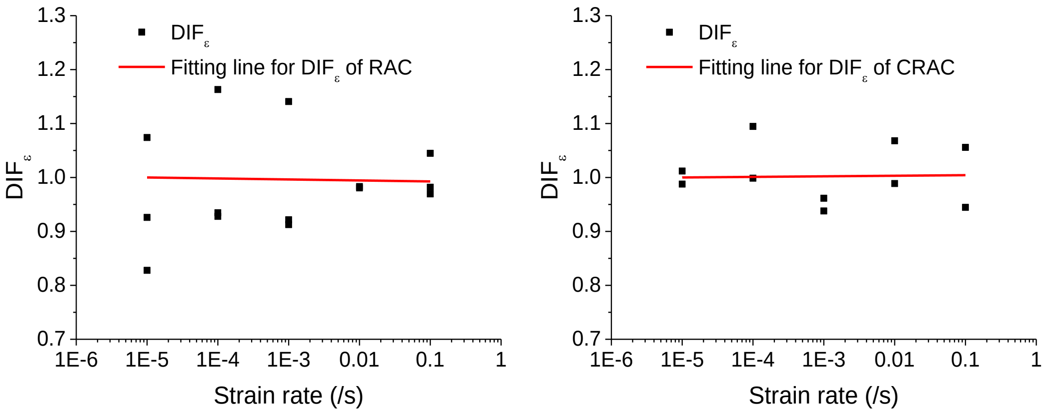

(a) RAC specimens (b) CRAC specimens

Fig. 5-18 Relation of DIF_ε versus strain rate for RAC and CRAC specimens

The results show that as the strain rate was increased by a factor of 10, the DIF_ε of RAC specimens decreased by 0.18% while the DIF_ε of CRAC specimens increased by 0.11%. As the decrease or increase in the DIF_ε for both RAC specimens and CRAC specimens were very small, this study considered that the peak strain remained unchanged with the increase in strain rate.

5.2.3.6 Ultimate strain of RAC and CRAC specimens

In this study, the ultimate strain (ε_{cu}) is taken as the strain corresponding to a stress which is 50% of the peak stress in the descending part of the stress-strain curve. The ultimate strains of RAC and CRAC specimens at different strain rates are displayed in Table 5-9. The results show that the average ultimate strain of RAC specimens indicated a decreasing trend with the increase in strain rate, while the ultimate strain of CRAC specimens decreased first and then increased with the increase in strain rate. Therefore, the relation between ultimate strain and strain rate did not exhibit any trend.

The ratio of ultimate strain to peak strain ($\varepsilon_{cu}/\varepsilon_{c,r}$) can describe the trend of the descending part of stress-strain curve. The $\varepsilon_{cu}/\varepsilon_{c,r}$ of RAC and CRAC specimens at different strain rates are displayed in Table 5-10. In general, $\varepsilon_{cu}/\varepsilon_{c,r}$ of both RAC and CRAC specimens showed a decreasing trend with the increase in strain rate. It indicated that the specimens were more brittle after peak stress was reached as the strain rate increased. On the other hand, the $\varepsilon_{cu}/\varepsilon_{c,r}$ value of CRAC specimens was lower than that of RAC specimens for the same strain rate. This indicated the CRAC specimens were more brittle than RAC specimens. As the mechanical properties of RCA can be enhanced by carbonation, generally it is more difficult to deform than for the un-carbonated RCA.

Therefore, the RCA would be more brittle after carbonation, leading to more brittle behavior of CRAC.

Table 5-9 Ultimate strains of RAC and CRAC specimens

	number	Ultimate strain at different strain rates (10^{-6})				
		0.00001/s	0.0001/s	0.001/s	0.01/s	0.01/s
RAC specimens	1	6130	5384	5244	5924	5632
	2	5764	6390	6052	5219	4895
	3	6480	—	6053	—	—
	AVG	6125	5887	5783	5219	5264
	SD	358	711	467	499	521
CRAC specimens	1	5456	5012	4200	5040	—
	2	4626	4503	5100	4933	5050
	AVG	5041	4758	4650	4987	5050
	SD	587	360	636	76	—

Table 5-10 $\varepsilon_{cu}/\varepsilon_{c,r}$ of RAC and CRAC specimens

	number	$\varepsilon_{cu}/\varepsilon_{c,r}$ at different strain rates				
		0.00001/s	0.0001/s	0.001/s	0.01/s	0.01/s
RAC specimens	1	2.353	1.831	1.826	1.915	1.823
	2	1.978	1.746	2.087	1.691	1.604
	3	1.917	—	1.686	—	—
	AVG	2.083	1.788	1.866	1.803	1.714
	SD	0.236	0.0599	0.203	0.158	0.154
CRAC specimens	1	1.835	1.667	1.451	1.693	—
	2	1.518	1.366	1.806	1.534	1.589
	AVG	1.676	1.516	1.628	1.613	1.589
	SD	0.158	0.150	0.178	0.080	—

5.2.3.7 Energy absorption capacity

Toughness is often defined as the area under the stress-strain curve, which is used to represent the energy absorption capacity of a material. Different definitions for the toughness using the area under the stress-strain curve have been proposed by different researchers (Mansur et al. 1999; Nataraja et al. 1999). In this study, the toughness is defined as the area under the stress-strain curve up to a stress corresponding to 50% of peak stress at the descending part, which is considered sufficient to represent the trend of the post-peak behavior. The toughness of RAC and CRAC specimens at different strain rates are listed in Table 5-11. The results confirm that the average toughness of both RAC and CRAC specimens showed an increasing trend with the increase in strain rate in general, this feature is consistent with results in Chapter 3. However, there was no clear trend to account for the differences between the toughness of RAC specimens and CRAC specimens.

Table 5-11 Toughness of RAC and CRAC specimens

	number	Toughness at different strain rates (N/m^2)				
		0.00001/s	0.0001/s	0.001/s	0.01/s	0.01/s
RAC specimens	1	182274	180224	172605	197291	219063
	2	171120	181335	198878	175980	184817
	3	195436	—	190938	—	—
	AVG	183278	180780	187474	186635	201940
	SD	17194	786	13475	15069	24215
CRAC specimens	1	184552	188145	152306	211803	—
	2	158897	174153	184177	198472	222580
	AVG	171725	181149	168241	205138	222580
	SD	18141	9893	22536	9426	—

Fig. 5-19 shows the relation of dynamic increase factor of toughness (DIF_t) versus strain rate for RAC and CRAC specimens, respectively. Herein, DIF_t represents the ratio of toughness at a higher strain rate compared to its corresponding quasi-static toughness. The fitting line of DIF_t and strain-rate relation for the RAC specimens and CRAC specimens are given by the following two equations:

$$DIF_{t,RAC} = 1 + 0.0162 \cdot \lg(\dot{\varepsilon} / \dot{\varepsilon}_s) \tag{13}$$

$$DIF_{t,CRAC} = 1 + 0.0541 \cdot \lg(\dot{\varepsilon} / \dot{\varepsilon}_s) \tag{14}$$

The results show that as the strain rate was increased by a factor of 10, the DIF_t of RAC specimens increased by 1.62% while the DIF_t of CRAC specimens increased by 5.41%. It indicated that the strain-rate sensitivity of toughness of CRAC was more significant than that of RAC.

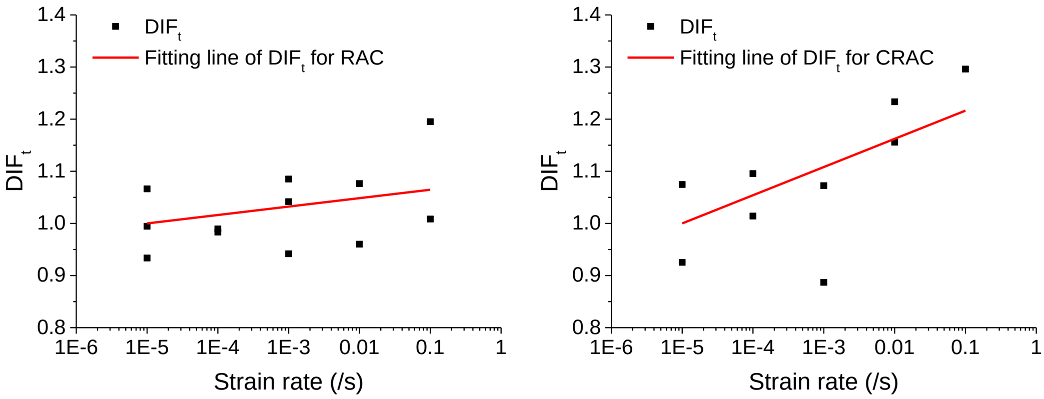

(a) RAC specimens (b) CRAC specimens

Fig. 5-19 Relation of DIF_t versus strain rate for RAC specimens and CRAC specimens

5.2.3.8 Failure pattern

In general, there was no significant difference between the failure patterns of the RAC and

CRAC specimens at the strain rate studied. The failure modes of RAC specimens which are shown in Fig. 5-20 are taken as an example to illustrate the effect of strain rate on the failure modes of the RAC and CRAC specimens. The results indicate that at all the strain rates studied there were some common features of the failure modes. There were several main cracks passing through the RAC specimens, part of the cracks were parallel to the loading direction while there were also some diagonal cracks. Most of the cracks passed through the interfaces between the aggregate and the cement paste while a few cracks propagated through the weaker aggregates. As the strain rate increased, the number of the cracks did not show an increasing or decreasing trend. In general, the test results show that there was no significant difference among the failure modes of RAC specimens at the different strain rates. That may be because the stress wave effect was not significant when the strain rate was in the range of 10^{-5}/s to 10^{-1}/s. More specifically, the velocity of the stress wave transmitted in the concrete is about 3000m/s, which is much higher than the loading rates in this study which were in the range of 2×10^{-3} mm/s to 20mm/s. Therefore, it can be concluded that the stress wave which was produced in the loading end could reach to another end of the specimens immediately. In other words, the path of stress transmission did not show any significant difference when the strain rate was changed under the studied strain rate range. As a result, the failure modes did not show any significant change. However, as the loading rate was increased to a level which cannot be neglected when compared with the stress wave velocity of concrete, it will exert considerable effect on the failure mode of concrete. As reported in the previous study (Xiao et al. 2015), there were more fractured aggregates in RAC under impact loading than that under static loading.

(a) 10^{-5}/s (b) 10^{-4}/s (c) 10^{-3}/s (d) 10^{-2}/s (e) 10^{-1}/s

Fig. 5-20 Failure patterns of RAC under different strain rates

5.3 Simulaton of effect of carbonation on mechanical behaviors of MRAC

5.3.1 Finite element model

A commercial software ABAQUS was used. The geometry model of MRAC, the constitutive model of each meso-phase material, and the loading method will be described in detail in Chapter 7. The material parameters of the meso-phase materials are given as follows.

In the experiment, it was found that there was no cracking in the MNCA. Therefore, the MNCA was considered to be a linear-isotropic material. Xiao *et al*. (2013) pointed out that the elastic modulus and strength of ITZs can be set to be 80%~85% of the mortars, and the constitutive model of ITZs can be set to be the same as the mortars. Therefore， the same tensile and compressive constitutive models, namely the concrete damaged plasticity model in ABAQUS which will be introduced in Chapter 7, were used for the mortars and ITZs in this study. The elastic modulus, tensile strength and compressive strength of the ITZs were all set to be 80% of those values of the corresponding mortar.

For the uncarbonated old mortar, the compressive strength was obtained based on the test results. For the carbonated old mortar and ITZ, the compressive strength, elastic modulus and tensile strength increased according to the trend of the microhardness test results. It was reported that there is a linear relationship between hardness and strength of cement paste (Morandeau et al. 2014). Therefore, the hardness values obtained from microhardness test were assumed to adopt a linear relationship between the hardness and compressive strength in this study. According to the test results, the average increase in the microhardness including the old ITZ and old mortar for MRAC-CM1 and MRAC-CM2 were 12% and 34% respectively as compared with MRAC-M1 and MRAC-M2. Therefore, in this simulation the average increase in compressive strength, tensile strength and elastic modulus of the old ITZ and old mortar for MRAC-CM1 were set as 12%, while that for MRAC-CM2 was set as 34%. Considering the age of the test specimens, the compressive strength of the old mortar and the new mortar were set to be 20% higher than the 28 day compressive strength. The tensile strength of ITZ or mortar was set as 10% of the corresponding compressive strength. The Poisson’s ratio and elastic modulus of each meso-phase materials were determined according to the results by Xiao et al. (2015). The mechanical properties of the meso-phase materials of MRAC specimens are given in Table 5-12.

Table 5-12 Mechanical properties of constitutes of MRAC specimens

	Elastic modulus (GPa)	Poisson's ratio	Compressive strength (MPa)	Tensile strength (MPa)
NCA	70.0	0.15	-	-
Old mortar in MRAC-M1	25.0	0.22	65.0	6.5
Old mortar in MRAC-M2	17.3	0.22	45.0	4.5
Old mortar in MRAC-CM1	28.0	0.22	72.8	7.3
Old mortar in MRAC-CM2	23.2	0.22	60.3	6.0
New mortar	25.0	0.22	65.0	6.5
Old ITZ in MRAC-M1	20.0	0.20	52.0	5.2
Old ITZ in MRAC-M2	13.9	0.20	36.0	3.6
Old ITZ in MRAC-CM1	22.4	0.20	58.2	5.8
Old ITZ in MRAC-CM2	18.6	0.20	48.2	4.8
New ITZ	20.0	0.20	52.0	5.2

5.3.2 Simulation results

According to the above descriptions, the complete compressive stress-strain curves and failure patterns of MRAC specimens under uniaxial compression loadings were simulated. In order to calibrate and validate the finite element model, the simulated stress-strain curves of the MRAC specimens are compared with that of the test results, as shown in Fig. 5-21. It can be seen that the simulation results before the peak stress are in good agreement with the experimental data.

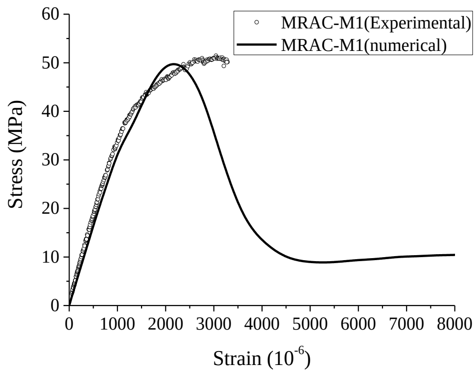

(a)MRAC-M1

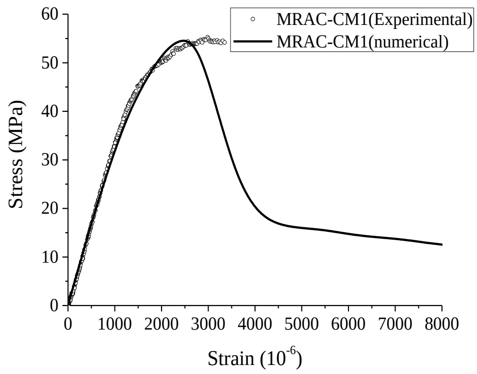

(b) MRAC-CM1

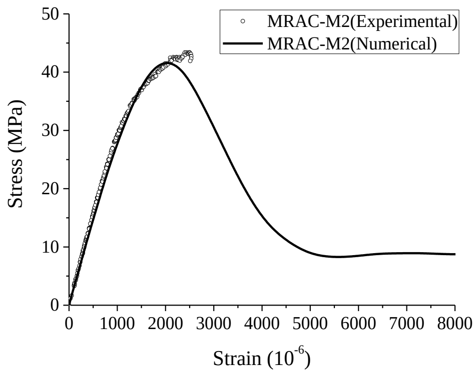

(c) MRAC-M2

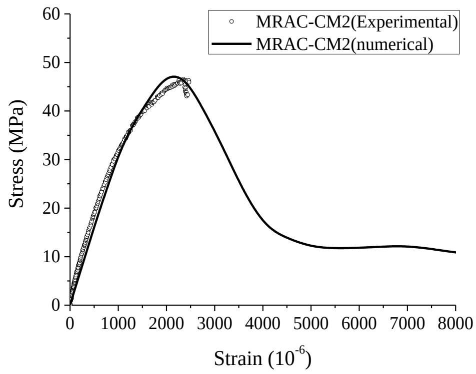

(d) MRAC-CM2

Fig. 5-21 Comparison of stress-strain curves between experimental and simulation results

Table 5-13 Comparison of experimental results and simulation results

Specimen	Compressive strength			Elastic modulus		
	Test results（MPa）	Simulation results（MPa）	Variation	Test results（GPa）	Simulation results（GPa）	Variation
MRAC-M1	51.4	50.0	2.72%	33.8	33.0	2.4%
MRAC-CM1	54.5	54.9	0.73%	39.7	34.0	14.3%
MRAC-M2	42.8	42.2	1.40%	32.8	29.9	8.8%
MRAC-CM2	46.1	47.3	2.60%	33.4	32.4	3.0%

The simulated compressive strength and elastic modulus of the MRAC specimens were compared with the test results, as displayed in Table 5-13. As shown in Table 5-13, the compressive strength of MRAC-CM1 based on the simulation is 9.8% higher than that of MRAC-M1. The compressive strength of MRAC-CM2 in simulation is 12.1% higher than that of MRAC-M2. It is shown that the increase in compressive strength as a result of carbonation treatment is more significant when the w/c of the old mortar in MRCA was higher. These features are consistent with the actual test results. The elastic modulus of MRAC-CM1 and MRAC-CM2 were increased by about 3.0% and 8.4% respectively when compared with that of MRAC-M1 and MRAC-M2. That means the increase in elastic modulus as a result of carbonation treatment is also more obvious as the w/c of the old mortar is increased.

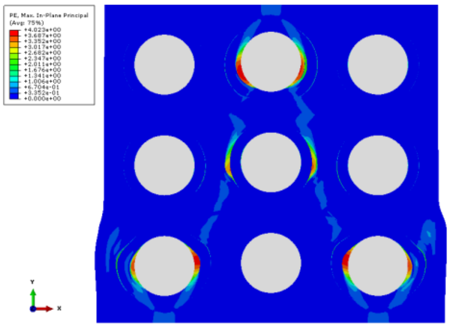

(a) MRAC-M1

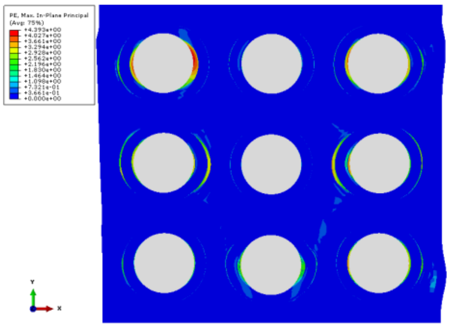

(b) MRAC-CM1

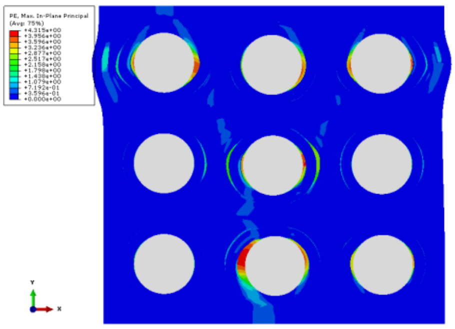

(c) MRAC-M2

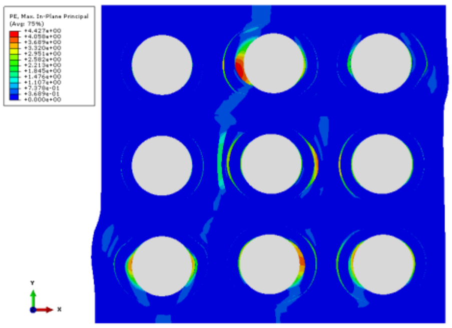

(d) MRAC-CM2

Fig. 5-22 Simulated failure patterns of MRAC specimens

In this simulation, the maximum principal plastic strain was utilized as a damage parameter to analyze the crack development and failure patterns. The simulated failure patterns of MRAC specimens are illustrated in Fig. 5-22. It is shown that the majority of the cracks appeared in the ITZs. Moreover, the proportion of visible cracks passing through the new ITZs tends to be higher in the MRAC with carbonated MRCAs than that of the MRAC with uncarbonated MRCAs. Here, it is considered as visible cracks passing through ITZs where the plastic strain of ITZs is large and also when plastic strains begin to develop in the adjacent mortar. Specifically, the proportion of visible cracks by number passing through new ITZs for MRAC-M1, MRAC-CM1, MRAC-M2 and MRAC-CM2 accounts for about 25%, 50%, 33% and 42% respectively. These features are similar to the results of the actual test. Generally, more cracks appeared at the new ITZs because of the enhancement of the old ITZs through carbonation.

In a word, the simulation results are in good agreement with the actual test results. It indicates that it is reasonable to use this model to simulate the macroscopic compressive mechanical behavior of RAC when the meso-phase materials parameters are known. It is a useful method to study the relationship between the meso-scopic and macro-scopic mechanical behavior of RAC. Moreover, because the microhardness of the meso-phase materials has relationship with their strength and elastic modulus, testing the microhardness of meso-phase materials is a good method to determine the mechanical behaviors of ITZ and old mortar in RCA after modifications such as the carbonation treatment which is not easy to be measured directly. Therefore, the microhardness test is useful in the carrying out of numerical study on the the relationship between the meso-scopic and macro-scopic mechanical behavior of RAC. In addition, when the relastionship between the strain-rate sensitivity and strength of mortar is established, this simulation can also be extended to study the effect of carbonation on the dynamic mechanical behaviors of RAC

5.4 Summary

In this chapter, the modeled recycled aggregate concrete (MRAC) was used to experimentally and numerically stduy the effect of RCA carbonation on the static mechanical properties of recycled aggregate concrete (RAC). The dynamic compressive behavior of RAC with carbonated RCA (CRAC) was experimentally studied using cylindrical specimens at low strain rates of 10^{-5}/s to 10^{-1}/s, and it was compared with that of RAC. The main conclusions are as follows:

(1) The microhardness of the old interfacial transition zone (ITZ) and the old mortar in MRCA could be enhanced through the carbonation treatment and the enhancement of the old ITZ was more significant than that of the old mortar. Besides, the microhardness of MRCA with a higher w/c exhibited larger enhancement effects through the carbonation treatment.

(2) MRCA carbonation treatment could increase the compressive strength and modulus of MRAC while reducing the peak strain slightly. The level of increase in the compressive strength for MRAC prepared with the higher w/c MRCAs was larger than that for MRAC with the lower w/c MRCAs, and the increase were 7.69% and 6.07% respectively.

(3) For both RAC and CRAC, as the strain rate increased, the peak stress, elastic modulus and energy absorption capacity showed an increasing tendency, while the peak strain remained approximately constant. For the failure pattern, there was no difference between RAC and CRAC, and it showed no obvious change with the increase in strain rate.

(4) The uni-axial compressive stress-strain curve of conventional concrete given in the Chinese code was suitable for the RAC and CRAC as well when the strain rate was in the range of 10-5/s to 10-1/s. The difference in the stress-strain curves of RAC or CRAC at the different strain rates can be accounted for using different the compressive strength, elastic modulus and peak strain.

(5) Testing the microhardness of meso-phase materials is a good method to determine the mechanical behaviors of ITZ and the old mortar in RCA especially after carbonation, and it is useful when incorporated into numerical studies on the relationship between the meso-scopic and the macro-scopic mechanical behavior of RAC.

Chapter 6 Discussion on the mechanism of the strain-rate sensitivity of RAC

In the previous chapters, some understanding of the strain-rate sensitivity of RAC under different strain rates and the factors that affect the strain-rate sensitivity of RAC have been gained through the experimental studies conducted. In this chapter, theoretically studies on the mechanism of the strain-rate sensitivity of RAC, which is important to establish a reasonable dynamic constitutive model of RAC that is an indispensable element in the dynamic analysis of RAC structure, will be carried out.

Many researchers have discussed the mechanism of the strain-rate sensitivity of conventional concrete from several aspects, i.e., Stefan effect caused by free water in the concrete, effect of inertial force, effect of crack development and so on. According to the experimental results mentioned in the previous chapters, this chapter discusses the mechanism of strain-rate sensitivity of RAC from the above aspects. The difference in the strain-rate sensitivity between RAC and NAC will also be explained based on a simplified model of RAC and NAC.

6.1 Discussion on the mechanism of strain-rate sensitivity of RAC

According to the previous studies on the dynamic mechanical properties of RAC at different strain rates ranging from 10^{-5} /s to 10^{2} /s, The relationship between the DIF_f of RAC and the strain rate is shown in Fig. 6-1, and it is also compared with the results calculated using the CEB model.

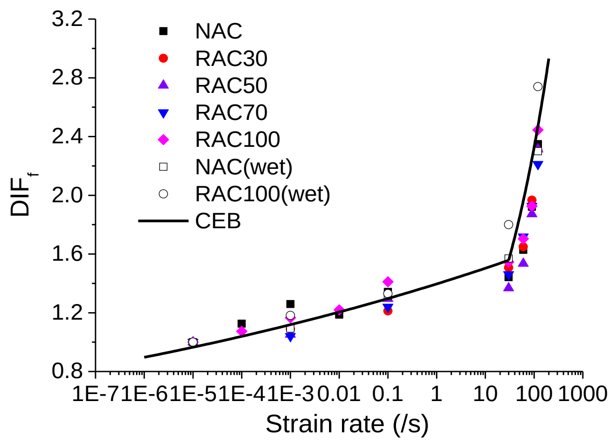

Fig. 6-1 Variation in DIF_f of RAC with strain rate at the low and high strain rates

According to Fig. 6-1, we can observe the following characteristics, based on which the mechanism of strain-rate sensitivity of RAC will be explored from the perspective of Stefan effect, inertia force effect and crack development.

(1) The DIF_f of RAC increases as the strain rate increased. The rate of increase in DIF_f of RAC is slower at low strain rates. At high strain rates, the rate of increase in DIF_f of RAC is obviously accelerated. This feature is similar to the CEB model. Moreover, the critical strain rate of RAC is similar to that of CEB model. Therefore, it may be concluded that the critical strain rate of RAC is the same as that in CEB model, namely 30 /s.

(2) The DIF_f of RAC in a wet statein a wet state is not much different from that in an air-dry state.

(3) The strain-rate sensitivity of RAC with 100% RCA is higher than that of conventional concrete, but the strain-rate sensitivity of RAC did not show an obvious increase with the increase in RCA replacement percentage.

However, in the only existing literature (Lu et al. 2014) which studied the effect of RCA replacement percentage on the strain rate sensitivity of RAC, it showed that the DIF_f of RAC is generally reduced with the increase of RCA replacement percentage, which is contrary to the findings in this study. That is because in the literature, the w/c of RAC with different RCA replacement percentages were constant, which means that the effective w/c of RAC with different RCA replacement percentages were different, which led to the phenomenon that the quasi-static strength of RAC with a higher RCA replacement percentage were even higher than that with 0% RCA. In other words, the strain rate sensitivity of RAC reported in the published literature was also partly resulted from the effect of RCA replacement percentage on the quasi-static strength instead of truly based on the strain rete sensitivity.

6.1.1 Stefan effect

The Stefan effect, which is also known as the Stefan-Reynolds equation, was first deduced by Stefan in 1874. The Stefan effect describes a physical phenomenon as shown in Fig. 6-2. When two discs with a small pitch in the viscous fluid are separated or are closing at a certain speed, the viscous fluid produces a viscous resistance (F_v) that hinders the movement of the discs, which is expressed as

$$F_v = \frac{3\pi\eta R^4}{2h^3} \cdot \frac{\mathrm{d}h}{\mathrm{d}t} \tag{6-1}$$

Here, R is the radius of the disc; h is the distance between the two discs; η is the viscosity coefficient of the fluid.

When the volume $V = \pi R^2 h$, the viscous resistance could be expressed as

$$F_v = \frac{3\eta V^2}{2\pi h^5} \cdot \frac{\mathrm{d}h}{\mathrm{d}t} \tag{6-2}$$

It can be seen that the equation is not limited to the separation of two discs, and it is applicable for any shape of the two plates. The viscous resistance is related to the volume of the fluid and the distance between the two plates.

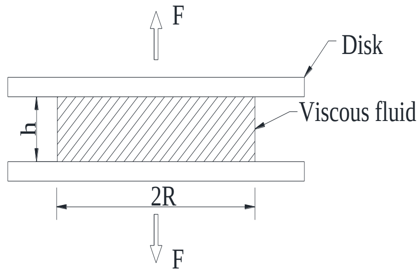

Fig. 6-2 Stefan effect

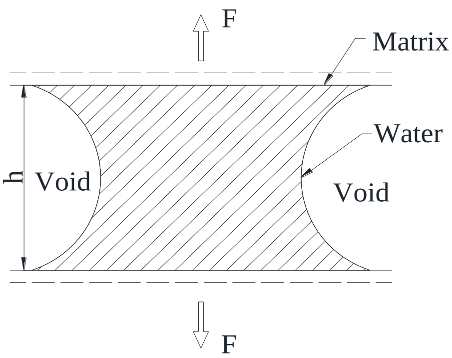

Fig. 6-3 Stefan effect in concrete micro-unit

The internal structures of concrete could be considered as a series of micro-disc systems. When a concrete specimen is under dynamic loading, due to the existence of free water within the micro-pores, when the pores are deformed such as cracking, the free water will produce resistance force to resist deformation such as crack expansion, resulting in the Stefan effect.

A micro-unit composed of micro-pores with free water inside the concrete, may be assumed as a tiny disc system, as shown in Fig. 6-3. For the unit, the relationship between the stress produced by the Stefan effect and the strain rate can be expressed as:

$$\sigma = \frac{F}{A} = \frac{3\pi\eta R^4}{2h^3 \pi R^2} \cdot \frac{\mathrm{d}h}{\mathrm{d}t} = \frac{3\eta}{2}\left(\frac{R}{h}\right)^2 \dot{\varepsilon} \tag{6-3}$$

Here, the dimensionless R/h reflects the ratio of the length of pores to the width, that is to say, the pores structures will have an important effect on the Stefan effect; η is the viscosity coefficient of the water, which is 1.005×10^{-3}Pa • s.

Generally, the tensile strength of concrete is in the order of 10^0MPa. Therefore, when the stress generated by the Stefan effect reaches magnitude of 10^{-1} MPa, the effect of Stefan effect could be considered to be significant.

Fig. 6-4 compares the changes in stress produced by the Stefan effect at different R/h as the strain rate increases. It is shown that the Stefan effect is significant when the strain rate is greater than 10^3 /s as R/h is 100; As R/h is 1000, the Stefan effect is significant when the strain rate is greater than 10^1 /s; As R/h is 10000, the Stefan effect begins to be significant when the strain rate is greater than 10^{-1} /s. It can be seen that the Stefan effect begins to be significant only when the strain rate is large enough. When the R/h is different, the critical values of the strain rate of the Stefan effect shows large differences.

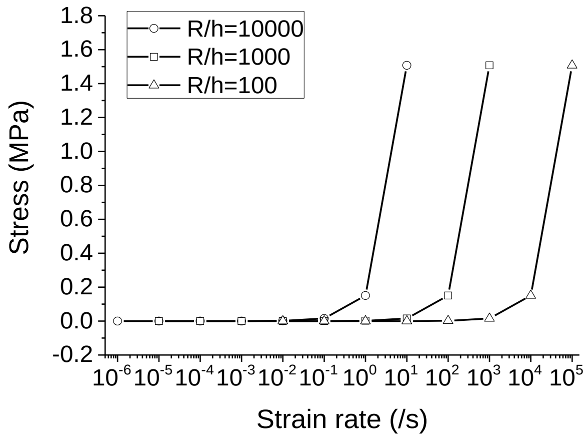

Fig. 6-4 The stress produced by Stefan effect

It can be seen from the conclusion of the previous chapters that when the strain rate is between 10^{-5} /s and 10^2 /s, the free water content does not contribute to increasing the strain-rate sensitivity of RAC. It indicates that in this strain rate range, the stress produced by the Stefan effect is still small. In other words, the Stefan effect may not be the main factor contributing to strain-rate sensitivity of RAC in this strain rate range. When the strain rate is higher, the Stefan effect may become significant.

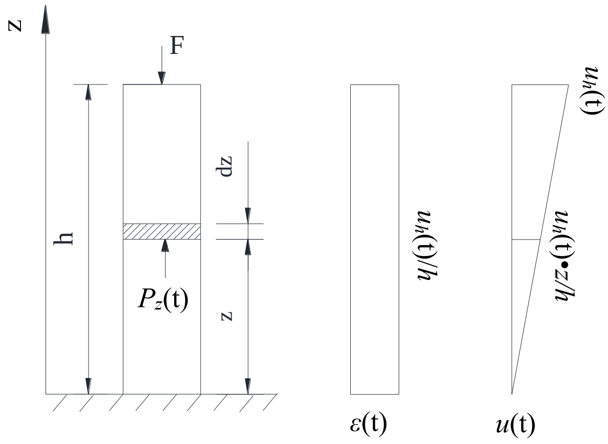

Fig. 6-5 The force analysis of a specimen subjected to a dynamic loading

6.1.2 Inertial effect

6.1.2.1 Longitudinal inertial effect

Fig. 6-5 shows the force analysis of a specimen subjected to a dynamic loading. It is assumed that the strain is uniform across the specimen. At any time, the strain $\varepsilon(t)$ could be displayed as

$$\varepsilon(t)=u_h(t)/h \tag{6-4}$$

Where $u_h(t)$ is the displacement at height h which is the height of the specimen. Then, the displacement at height z at time t is expressed as

$$u_z(t)=u_h(t)\frac{z}{h} \tag{6-5}$$

Thus, the acceleration at height z at time t is expressed as

$$\ddot{u}_z(t)=\ddot{u}_h(t)\frac{z}{h} \tag{6-6}$$

The inertial force of the mass unit dm at the height z is

$$P_z(t)=\ddot{u}_z(t)\mathrm{d}m==\ddot{u}_z(t)\rho A\mathrm{d}z=\ddot{u}_h(t)\frac{z}{h}\rho A\mathrm{d}z \tag{6-7}$$

The inertia force of the whole specimen could be displayed as

$$P(t)=\int_0^h P_z(t)\mathrm{d}z=\int_0^h \ddot{u}_h(t)\frac{z}{h}\rho A\mathrm{d}z=\frac{h}{2}\rho A\ddot{u}_h(t) \tag{6-8}$$

Because $\varepsilon(t)$ is equal to $u_h(t)/h$, the inertia force of the whole specimen can be expressed as

$$P(t)=\frac{h}{2}\rho A\ddot{u}_h(t)=\frac{h^2}{2}\rho A\ddot{\varepsilon}_h(t) \tag{6-9}$$

In the tests on dynamic mechanical behavior of concrete using hydraulic testing system, a constant strain rate can be guaranteed, that is to say $\ddot{\varepsilon}_h(t)$ is zero, so the inertial force is zero. It indicates that the dynamic effect of concrete measured by hydraulic testing systems need not take into account the influence of the longitudinal inertia effect.

However, in SHPB tests, it is difficult to ensure a constant strain rate. The strain rate could be expressed as

$$\dot{\varepsilon}_{\mathrm{S}}(t)=\frac{2C_0}{l_{\mathrm{S}}}\left[\varepsilon_{\mathrm{i}}(t)-\varepsilon_{\mathrm{t}}(t)\right] \tag{6-10}$$

The derivative of the strain rate is

$$\ddot{\varepsilon}_{\mathrm{S}}(t)=\frac{2C_0}{l_{\mathrm{S}}}\left[\dot{\varepsilon}_{\mathrm{i}}(t)-\dot{\varepsilon}_{\mathrm{t}}(t)\right] \tag{6-11}$$

The longitudinal force is

$$P(t)=\rho A l_{\mathrm{S}} C_0\left[\dot{\varepsilon}_{\mathrm{i}}(t)-\dot{\varepsilon}_{\mathrm{t}}(t)\right] \tag{6-12}$$

It indicates that the longitudinal inertial force is related to the difference between the value of $\dot{\varepsilon}_i(t)$ and $\dot{\varepsilon}_t(t)$.

The relationship between the strain-rate and time and the relationship between the stress and time corresponding to the mean stress-strain curves of the NAC specimens as described in Chapter 4 are shown in Fig. 6-6 and Fig. 6-7, respectively. AVNC-1, AVNC-2, AVNC-3 and AVNC-4 represent the average stress-strain curves of NAC specimens at four different impact rates, respectively.

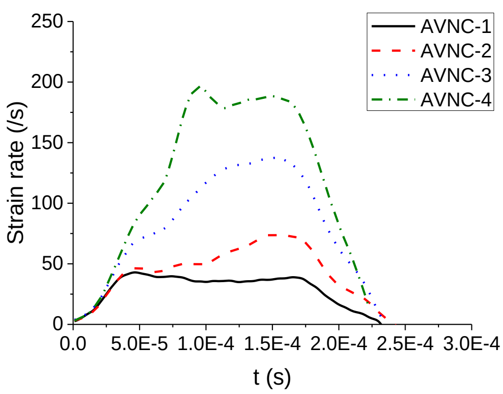

Fig. 6-6 Strain rate-time curve of AVNC

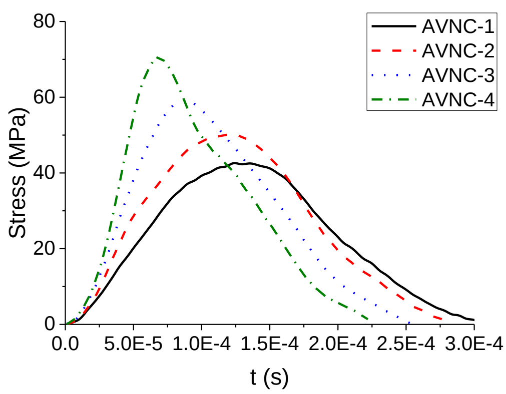

Fig. 6-7 Stress-time curve of AVNC

According to the two graphs, the strain rate changes with time over the stress, especially before the stress reaches the peak stress. Especially for the AVNC-4 specimen, the strain rate increases with a large slope over time before the peak stress is reached. That is to say, the $\ddot{\varepsilon}_h(t)$ of the specimen is larger before the peak stress. At the same time, the slope of the strain rate has been changing over time, indicating that the $\ddot{\varepsilon}_h(t)$ has changed over time. In other words, the inertial force has changed over time. The slope of the secant line, which corresponds to a portion of rising part of strain rate-time curve where the slope had no significant change, is defined as the representative value of $\ddot{\varepsilon}_h(t)$. The representative values of $\ddot{\varepsilon}_h(t)$ of AVNC-1, AVNC-2, AVNC-3 and AVNC-4 are 1.23×10^6 s^{-2}, 1.44×10^6 s^{-2}, 1.92×10^6 s^{-2} and 2.48×10^6 s^{-2}, respectively. According to Eq. (6-9), the inertial forces of AVNC-1, AVNC-2, AVNC-3 and AVNC-4 specimens are 7.24 KN, 8.48 KN, 11.31 KN and 14.60 KN respectively, and the corresponding increase in strength are 1.88 MPa, 2.20 MPa, 2.94 MPa and 3.79MPa respectively, accounting for 6.1%, 7.1%, 9.5% and 12.2% of the quasi-static strength, respectively. It indicates that when the SHPB testing system is used for impact testing, the longitudinal inertia effect will cause an increase in the strength of RAC. But in general, the longitudinal inertial effect is not the most important factor accounting for the increase in the dynamic strength of RAC. In fact, the strength caused by the longitudinal inertia effect is not an inherent property of the material itself, but it is caused by the experimental conditions, which could be considered as a structural effect. This feature should be noted when considering the strain-rate sensitivity of concrete.

In general, it is argued in this study that the longitudinal inertial effect is not the main factor causing the strain-rate sensitivity of RAC at low strain rates (10^{-5} /s ~ 10^{-1} /s). At high strain rates (10^{1} /s ~ 10^{2} /s), the longitudinal inertial effect has some influence on the strain-rate sensitivity of RAC, but it is not a dominant factor.

6.1.2.2 Transverse inertial effect

Many experimental results showed that there is a critical strain rate after which the growth rate of concrete strength becomes larger with the increase in strain rate. Rossi et al. (1996） reported that the reason for this phenomenon is a transition of the dominant mechanism, i.e., when the strain rate is less than the critical strain rate, the viscous effect of free water in the concrete plays a leading role; when the strain rate is greater than the critical strain rate, the inertial effect plays a leading role. Eibl et al. (1999) and Bischoff et al. (1991) argued that the strain-rate sensitivity of concrete at high strain rates is caused mainly by the transverse inertial effect, i.e., a cylinder under rapid loading in the axial direction will not be able to expand instantaneously in the lateral direction because of inertial restraint, causing it to be initially in a state of uniaxial strain with corresponding lateral stresses that will act as a confinement. However, there are contradictions when explaining the strain rate effect of concrete by this view. If the concrete at high strain rates is equivalent to a change from a state of uni-axial stress into a state of uni-axial strain, the same will be the case under dynamic tensile loading, and the dynamic tensile strength should also reduce. But in fact, the dynamic tension strength of concrete increases more obviously at high strain rates than the dynamic compressive strength.

Wang et al. (2005) deduced the effect of transverse inertial effect on the axial stress in the range of the elastic wave: the work done by a pair of static equilibrium forces is converted into the internal energy of the micro-element or strain energy. When considering the role of transverse movement, it is consisted of two parts, i.e. the strain energy and the lateral kinetic energy generated by the work of the lateral stress in the lateral movement. It can be expressed as

$$\sigma = E\varepsilon + \rho_0 v^2 r_g^2 \frac{\partial^2 \varepsilon}{\partial t^2} \tag{6-13}$$

Where, E is the elastic modulus, ε is the axial strain, ρ_0 is the density of the specimen, v is the Poisson's ratio for the specimen, r_g is the radius of gyration of the cross section of the specimen, $\partial\varepsilon / \partial t$ is the strain rate.

In Eq. (6-13), the second term is the effect of the transverse inertial effect on the axial stress. When this term is neglected, the equation is transformed into Hooke's law in one-dimensional state. Since this inertial effect correction is proportional to the second derivative of the strain over time, this correction is necessary only if the change in strain rate is significant.

Likewise, the value of lateral inertial force can be estimated based on the representative values of $\ddot{\varepsilon}_h(t)$. According to Eq. (6-13), the increase in the strength of AVNC-1, AVNC-2, AVNC-3 and AVNC-4 specimens is 0.150 MPa, 0.176 MPa, 0.235 MPa and 0.304 MPa, respectively, which are corresponding to 0.48%, 0.57%, 0.76% and 0.98% of the static strength. It can be seen that the contribution of the transverse inertial effect to the increase in the dynamic strength is very small and much less than the contribution of the longitudinal inertia effect when the SHPB testing system is used for the impact test.

In general, it is argued that the transverse inertial effect has little effect on the strain-rate sensitivity of RAC at low strain rates. At high strain rates, the effect of transverse inertial effect on the strain-rate sensitivity of RAC is also small.

6.1.3 Crack effect

6.1.3.1 Effect of crack passing through aggregates

Many researchers have found that under the dynamic loading, the number of cracks passing through the aggregates increases with an increase in strain rate. Because these cracks have not enough time to pass through the weak ITZs within the concrete but directly through the aggregates of which the strength is higher, so that the strength of concrete increases. It can be seen from the experimental results reported in the previous chapters that the number of cracks in the RAC at low strain rates is almost unrelated to the strain rate. At high strain rates, the number of cracks passing through the aggregate is more than when subjected to quasi-static loading. The phenomenon will be analysed below.

As shown in Fig. 6-8, the shaded part is the aggregate and the rest is the mortar matrix. Under tensile loading, it is assumed that there is a crack AB coming across the aggregate. With the increase in the tensile load, the crack will continue to develop, and the crack may propagate along the interface between the aggregate and the mortar (ABCDEF), or it may pass through the aggregate (ABEF).

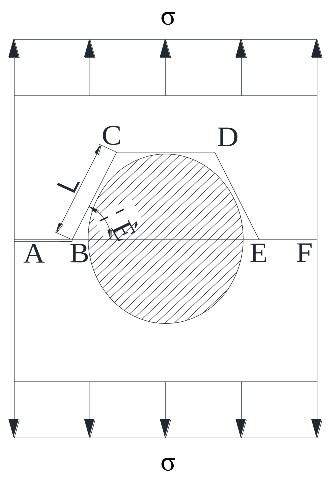

Fig. 6-8 Illustration of different cracking modes around an aggregate

The question is when will the crack pass through the aggregate? It is generally recognized that the crack will pass through the interface because the tensile stress at the interface is greater than the tensile strength or the shear stress at the interface is larger than its shear strength. Therefore, it is assumed that the crack around the aggregate may develop as the following types, that is, interfacial cracking (mode I) caused by the interface tensile stress, interfacial shear slippage (mode II) caused by the interface shear stress, and the aggregate cracking (mode III) caused by the tensile stress acting on the aggregate. Here, in order to investigate whether the crack will pass through the aggregate, only the competition between mode I and mode III, and the competition between mode II and mode III are considered.

First, consider the competition between Mode I and Mode III. As shown in Fig. 6-8, assuming that the concentrated stress in the direction perpendicular to the AB direction is σ_0, the angle between BC and AB is θ, the tensile stress σ_t perpendicular to the BC direction and the shear stress τ parallel to the BC direction can be expressed as

$$\sigma_t = \sigma_0 \cos\theta \tag{6-14}$$

$$\tau = \sigma_0 \sin\theta \tag{6-15}$$

When the shear failure caused by the shear stress is not taken into account, the conditions under which the crack is to pass through the aggregate are

$$\frac{\sigma_0}{f_{t,g}} > \frac{\sigma_t}{f_{t,ITZ}} \tag{6-16}$$

Where, $f_{t,g}$ is the tensile strength of aggregate, $f_{t,ITZ}$ is the tensile strength of ITZ. This equation can also be expressed as

$$\cos\theta < \frac{f_{t,ITZ}}{f_{t,g}} \tag{6-17}$$

Therefore, only when $\theta > acr\cos(f_{t,ITZ} / f_{t,g})$, the crack may pass through the aggregate.

Secondly, considering the competition between Mode II and Mode III, as shown in Fig. 6-8, unlike the crack BC caused by tensile stress, the crack caused by shear stress entails the slippage of the entire length of BC, therefore, only when the concentrated stress at point B (σ_B) spread to point C and when the shear stress at the point C is greater than the shear strength, can the crack form. So, when not considering the cracks caused by the tensile stress, the condition under which the crack is to pass through the aggregate is

$$\frac{\sigma_B}{f_{t,g}} > \frac{\tau_C}{f_{\tau,ITZ}} \tag{6-18}$$

Where, $f_{\tau,ITZ}$ is the shear strength of ITZ.

Under a static loading, the concentrated stress at B can be considered as instantaneously propagating to C, that is $\sigma_C \approx \sigma_B$. At this time,

$$\tau_C = \sigma_C \sin\theta = \sigma_B \sin\theta \tag{6-19}$$

Then, Eq. (6-18) can be expressed as

$$\sin\theta < \frac{f_{t,ITZ}}{f_{t,g}} \tag{6-20}$$

Therefore, under static loading, only when $\theta < acr\sin(f_{\tau,ITZ} / f_{t,g})$, will the crack pass through the aggregate.

However, at high strain rates, the propagation of stress waves should be considered. Assume that the development of concentrated stress at point B is shown in Fig. 6-9.

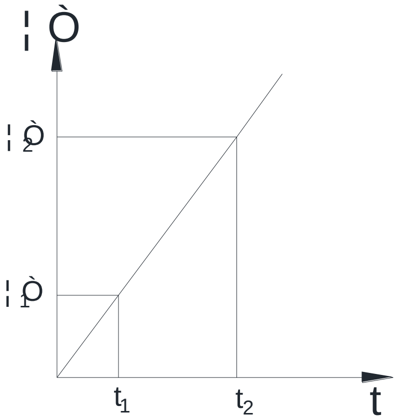

Fig. 6-9 The development of stress with time

At time t_1, the vertical stress at point B perpendicular to the AB direction is σ_1, the angle between BC and AB is *θ*. The period when the stress wave pass from point B to point C is Δt. At time t_2, the stress wave propagates to the point C. However, the tensile stress at point B at time t_2 has been changed as σ_2. The condition under which the crack is to pass through the aggregate is displayed as

$$\frac{\sigma_2}{f_{t,g}} > \frac{\sigma_1 \sin\theta}{f_{\tau,ITZ}} \tag{6-21}$$

That is,

$$\sin\theta < \frac{\sigma_2 f_{\tau,ITZ}}{\sigma_1 f_{t,g}} \tag{6-22}$$

Therefore, under high strain rates, only when $\theta < arc\sin(\sigma_2 f_{\tau,ITZ} / \sigma_1 f_{t,g})$, will the crack pass through the aggregate.

In summary, the crack is expected to pass through the aggregate under static loading on the condition that

$$\begin{cases} \theta < arc\sin(f_{\tau,ITZ} / f_{t,g}) \\ \theta > arc\cos(f_{t,ITZ} / f_{t,g}) \end{cases} \tag{6-23}$$

Assuming $f_{\tau,ITZ} = f_{\mathrm{t},ITZ} = 2\mathrm{MPa}$ and $f_{\mathrm{t},g} = 10\mathrm{MPa}$, there is arccos(0.2) < θ < arcsin(0.2). Since it has no solution, this explain why there is almost no crack through the aggregate under static loading.

Under high strain rates, the conditions under which the crack is to pass through the aggregate isexpressed as

$$\begin{cases} \theta < arc\sin(\sigma_2 f_{\tau,ITZ} / \sigma_1 f_{t,g}) \\ \theta > arc\cos(f_{t,ITZ} / f_{t,g}) \end{cases} \tag{6-24}$$

When the strain rate is large enough to make the value of σ_2 / σ_1 large enough, so that Eq. (6-25) is established, there is a solution for θ. At this time, the crack will pass through the aggregate.

$$arc\cos(f_{t,ITZ} / f_{t,g}) < arc\sin(\sigma_2 f_{\tau,ITZ} / \sigma_1 f_{t,g}) \tag{6-25}$$

Assuming the length of BC (l_{BC}) is 0.01m, the velocity of stress wave (c) is 3000m/s, we can obtain a Δt (Δt = l_{BC} / c) of 3.3×10^{-6}s. When the strain rate reaches 100/s, the time required to produce a strain of 1000με is 1×10^{-5}s. In other words, when the strain rate reaches this order of magnitude, the value of σ_2 / σ_1 during the period Δt is large enough. When the strain rate reaches 1000/s, Δt is even greater than the hold time of the stress pulse. That is to say, before the stress at point B reached the point C, the aggregate has already cracked.

In general, it is considered that under low strain rates, the crack development is not the main factor causing strain-rate sensitivity of RAC. At high strain rates, a small part of the cracks will pass through the aggregate, so the crack development may contributes to the strain-rate sensitivity of RAC, but this contribution is small.

6.1.3.2 Rate-dependence of crack propagation resistance of mesoscopic materials

There are some defects in the interior of almost all materials. Some of the materials are sensitive to the defect, and some are not sensitive. In fracture mechanics, in order to make the mathematical processing simple, the defects are often simplified as cracks. For concrete materials, a large number of studies have shown that in the process of solidification after pouring, due to evaporation of water, shrinkage of cement mortar, etc s, some micro-cracks may be pre-existing inside the concrete before external loading. The micro-cracks are mainly distributed at the interfacs between the aggregate and the mortar and inside the mortar. The mechanical properties of concrete are closely related to the development of pre-existing internal micro-cracks. Guo (2004) summarized the relationship between the development of microcracks in concrete and the mechanical properties of concrete. First, the microcracks are formed at the interface between coarse aggregate and cement mortar and inside the mortar. As stress increases, these cracks gradually propagate, connecting up with each other thus forming macroscopic cracks. Finally, due to the damage accumulation of mortar, its bonding with the aggregate was disrupted, the integrity of the concrete destroyed, gradually losing load bearing capacity. Therefore, the ability to resist the development and extension of microcracks is directly related to the strength and the elastic modulus of the concrete.

In fracture mechanics, the stress intensity factor (K_I) is the physical quantity that describes the intensity of the stress in the vicinity of the crack tip., For an ideal brittle material, when the K_I reaches a certain critical value with the increase in the external force, the crack will continue to propagate sharply even if the external force is no longer increased, which is called instability expansion. The critical value of the stress intensity factor (K_{IC}) is called the fracture toughness of the material, which is an important physical quantity in the fracture mechanics and is an index to measure the material's resistance to crack’s instability expansion. The crack is less likely to expand as the fracture toughness is larger. It is generally believed that fracture toughness is an inherent property of the material, which is related to the property of the material, heat treatment and temperature, regardless of the geometric properties of the crack and the magnitude of the applied load. Fracture toughness is usually determined by experiment. Therefore, the critical condition for crack's instability propagation is $K_I = K_{IC}$.

Under the dynamic loading, the dynamic stress intensity factor in the crack tip is related to the rate of crack propagation, and it can be expressed as:

$$K_{Id}(t) = k(v)K_I \tag{6-26}$$

Where, K_{Id}(t) is the dynamic stress intensity factor of the crack tip, K_I is the static stress intensity factor, v is the crack propagation velocity, k (v) is the function of the crack propagation velocity. At present, there are no exact deterministic expressions for $k(v)$, only some approximate expressions. In general, it decreases with the increase in the crack propagation velocity. When v is 0, $k(v)$ is 1; $k(v)$ is 0 when v is the Rayleigh wave velocity of the material.

Under the dynamic loading, the criterion for crack instability expansion is:

$$K_{Id}(t) = k(v)K_I = K_{Id} \tag{6-27}$$

Where, K_{Id} is the dynamic fracture toughness of the material.

Some studies (e.g., Zhang et al. (1999); Paliwal & Ramesh 2008; Li & Wang 2006; Li et al. 2001) showed that the dynamic fracture toughness of the rock is strain-rate dependent. In experiments of Li et al. (2001), when the strain rate is in the range of 10^{-4} /s ~ 10^{0} /s, the dynamic fracture toughness of rock increases linearly with the logarithm of strain rate. Li and Wang (2006) reported that the dynamic fracture toughness of marble increases with the loading rate when the loading rate is below 18.85×10^4 $MPa\cdot m^{1/2}s^{-1}$. Zhang et al. (1999) showed that the static fracture toughness of rocks is almost constant, but when the loading rate is more than 10^4 $MPa\cdot m^{1/2}s^{-1}$, the dynamic fracture toughness increases with the loading rate, which is dislayed as

$$\log(K_{Id}) = a\log(\dot{k}) + b \tag{6-28}$$

As mentioned earlier, fracture toughness reflects the ability of a material to resist crack propagation. That is to say, the ability of the rock material to resist crack propagation increases with the increase in loading rate.

Consider a micro-unit in a rock-like material that contains the initial microcracks as shown in Fig. 6-10. Under the dynamic loading, the crack propagation resistance increases with the increase in the loading rate, so the strength and elastic modulus of the micro-unit will increase with the loading rate, and thus the brittle rock materials exhibite a strain-rate sensitivity at the macroscopic level. At the meso level, the concrete material consistes of three materials, i.e., aggregate, mortar and ITZ, and each of them is rock-like brittle material. Therefore, under dynamic loading, the strength and elastic modulus of the micro-unit of aggregate, mortar and ITZ will increase with the increase in loading rate. That is to say, each material at the meso-level has strain-rate sensitivity characteristics, which results in the overall strain-rate sensitivity of the concrete as a whole.

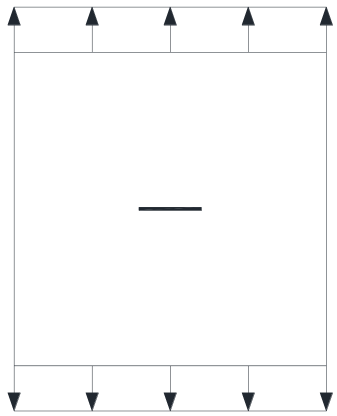

Fig. 6-10 Illustration of rock micro-unit

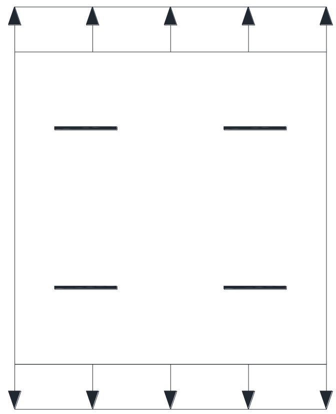

Fig. 6-11 Illustration of mortar micro-unit

Here, the rock, mortar and ITZ can be seen as the same kind of brittle material with different porosity. As we know, the greater the porosity, the more the number of microcracks. Therefore, when compared with rock, the porosity of mortar is larger, and the number of micro-cracks in the mortar micro-unit is larger than in the rock micro-unit of the same size. This is also the reason why the strength of the mortar is much less than that of rock. The micro-unit of mortar could be simplified and shown in Fig. 6-11.

However, under dynamic loading, the number of micro-cracks in a mortar micro-unit is larger than that in the rock micro-unit of the same size. As each micro-crack will contributes to the dynamic strength of the micro-unit, so a higher number of micro-cracks will result in greater increase in the dynamic strength of the micro-unit. That is, the strain-rate sensitivity of the mortar is greater than that of the rock. Likewise, the strain-rate sensitivity of the ITZ is greater than that of the rock and mortar.

In general, the crack propagation resistance of the meso-phase material of RAC (i.e., rock, mortar and ITZ) increases with the increase in strrain rate. This phenomenon can qualitatively explain the strain-rate sensitivity of RAC.The strain-rate dependent of the crack propagation resistance of the meso-phase material may be a dominant factor of the strain-rate sensitivity of RAC in the strain rate range (10^{-5} /s ~ 10^{2} /s). However, there is no definite conclusion on the relationship between the dynamic fracture toughness of the meso-phase materials and the loading rate, and the reason for this phenomenon is not conclusive. Moreover, the applicability of the strain-rate sensitivity of the crack propagation resistance of a material obtained via macroscopic testing to the micro-unit needs further study.

6.2 Discussion on the difference between the strain-rate sensitivity of RAC and NAC

Due to the difference between RCA and NCA, the mechanical properties of RAC are different from those of NAC. The results of the previous studies show that RAC with 100% RCA was more sensitive to strain rate than NAC, but the strain-rate sensitivity of RAC did not show a strictly increasing trend with the increase in RCA replacement percentage. In the following, the difference between the strain-rate sensitivity of RAC and NAC will be analyzed based on simplified static and dynamic models of RAC and NAC.

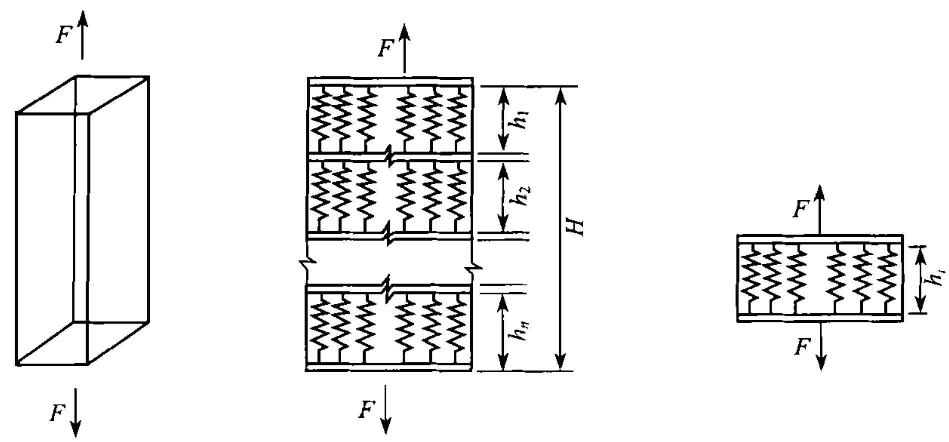

(a) Concrete Specimen (b) Simplified spring system (c) Typical unit

Fig. 6-12 Mesoscopic stochastic fracture model of conventional concrete (Li & Zhang 2001)

6.2.1 Mesoscopic stochastic fracture model of NAC

In the following, a brief overview of the mesoscopic stochastic fracture model of conventional concrete proposed by Li and Zhang (2001) is presented. In general, damage in concrete is caused mainly by two physical mechanisms, i.e., tension mechanism and shear mechanism. Here, only the mesoscopic stochastic fracture model of conventional concrete under uniaxial tension is discussed. In this model, a concrete specimen (Fig. 6-12 (a)) under a tensile load can be simplified as a series parallel spring system, as shown in Fig. 6-12 (b), where the typical unit is assumed to be consisted of a series of series-parallel springs whose ends are fixed rigid plates, as shown in Fig. 6-12 (c). The entire specimen is assumed to be consisted of a series of parallel springs which are connected by rigid plate.

In this model, the macroscopic properties of the material are represented by a series-parallel spring system. The micro-element of the material is represented by a spring, and the breakage of the spring indicates the generation of damage. The proposed simplified model contains two basic assumptions:

(1) Concrete specimen in tension can be made by a series of damaged body. Each damaged body is composed of a series of parallel and equidistant distributed elastic-brittle springs. There is only one failure surface in each damage body.

(2) Before the occurrence of macroscopic cracks, all damage bodies are damaged, the location of damage is random, and the internal forces between the damage bodies are in a balanced state. As the macroscopic cracks appear, damage is concentrated at a main failure surface.

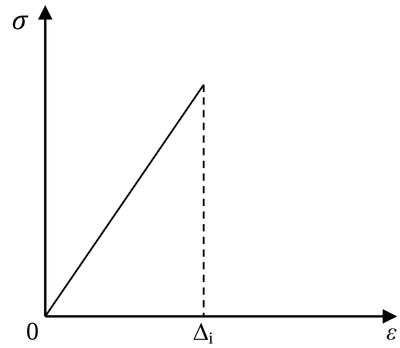

Fig. 6-13 Ideal elastic-fracture stress-strain relationship

Assume that the springs have an ideal elastic-fracture property, as shown in Fig. 6-13. In the typical unit, E_i is used to denote the stiffness of the spring i, A_i is the area of each spring, and the spring stiffness and area in each unit are the same; Δ_i is used to denote the ultimate strain of spring i. The ultimate strains at different springs are considered as random variables with the same distribution, which takes into account the discrete properties of the concrete due to non-uniformity, initial micro-defections and other factors. The differrences in the tensile strength of different micro-elements are represented by the different ultimate strains. Since it is assumed that the rigid plates are fixed at both ends of the spring, the stress produced because of the break of a spring is uniformly taken by the unbroken springs.

For the above typical unit, the area of the material out of work due to the break of the spring can be expressed as:

$$A(\varepsilon)=\sum_{i=1}^{n}H(\varepsilon-\Delta_i)\mathrm{d}A_i \tag{6-29}$$

Where, H () is Heaviside function, which is shown as:

$$H(\varepsilon-\Delta_i)=\begin{cases}0 & \varepsilon\le\Delta_i\\ 1 & \varepsilon>\Delta_i\end{cases} \tag{6-30}$$

Where ε is the tensile strain of spring in the typical unit, n is the number of springs in the typical unit, and Δ_i is the ultimate strain of the spring i.

When the typical unit is in a quasi-static state during the whole loading process, the macroscopic external force is balanced by the sum of the internal forces of the micro-elements. According to the assumption $E_1 = E_2 = \cdots = E_i = E$, the following equation is established.

$$\begin{aligned}F(\varepsilon)=\sigma(\varepsilon)A&=\sum_{i=1}^{n}E_i[1\text{-}H(\varepsilon-\Delta_i)]\varepsilon\mathrm{d}A_i\\&=E\varepsilon\sum_{i=1}^{n}[1\text{-}H(\varepsilon-\Delta_i)]\mathrm{d}A_i\\&=E\varepsilon[A-A(\varepsilon)]\end{aligned} \tag{6-31}$$

Where, E is the stiffness of typical unit, $F(\varepsilon)$ is the external force of the specimen. Therefore, the nominal stress of the typical unit can be expressed as:

$$\sigma(\varepsilon)=E\varepsilon[A-A(\varepsilon)]/A=E\varepsilon[1-D(\varepsilon)] \tag{6-32}$$

Where $D(\varepsilon) = A(\varepsilon) / A$, it is the damage variable of the failure surface

The definition is the same as that of classical damage mechanics. According to area-based damage definition by Robotnov (1938), damage in concrete materials can be described in the following form:

$$D=A_D/A \tag{6-33}$$

Where, A_D is the area of the material out of work due to the destruction of the micro-elements, A is the cross-sectional area of the specimen.

When $n \to \infty$, the typical unit is a continuum, the damage variable is

$$\begin{aligned} D = A(\varepsilon) / A &= \frac{1}{A}\int_0^A H[\varepsilon - \Delta(x)]dx \\ &= \frac{1}{A}\int_0^A H[\varepsilon - \Delta(x / A)]d(x / A) \\ &= \int_0^1 H[\varepsilon - \Delta(y)]dy \end{aligned} \tag{6-34}$$

Where y is the index of the location of the micro-spring in the typical unit; $\Delta(y)$ is the strain at the position y, which is a random variable.

Li and Zhang (2001) also pointed out that the damage evolution of the tensile specimen before the critical strain is exactly the same as that of the typical unit, and thus the damage of the tensile specimen can be represented by the damage of a typical unit.

6.2.2 A simplified static model of RAC

In the above mesoscopic stochastic fracture model of concrete, it is assumed that the elastic modulus of each micro-element represented by the spring is equal, and the difference in the properties of the micro-elements is described by the difference in ultimate strain. But in fact, the elastic modulus of different micro-elements in real concrete is not equal. When considering this factor, the nominal stress of a typical unit can be expressed as:

$$\sigma = \sum_{i=1}^{n} \frac{E_i A_i}{A}[1 - H(\varepsilon - \Delta_i)]\varepsilon = E\varepsilon[1 - D(\varepsilon)] \tag{6-35}$$

In this equation,

$$E = \sum_{i=1}^{n} E_i A_i / A \tag{6-36}$$

$$D = \sum_{i=1}^{n} \frac{E_i A_i}{EA} H(\varepsilon - \Delta_i) \tag{6-37}$$

Where ε is the tensile strain of the spring in a typical unit, n is the number of springs in the typical unit, Δ_i is the ultimate strain of the spring i, E_i and A_i represent the elasticity modulus and area of the spring i in the typical unit. A is the area of the specimen, E represents the elasticity modulus of the specimen, and D is the overall damage.

At the meso level, the concrete material is made up of three-phase materials, i.e., cement mortar, ITZ and aggregate. The three-phase materials are all brittle materials, which is uneven and has internal initial defects. Strictly speaking, the elastic modulus of the different micro-elements is not the same. However, the material in the samephase can be regarded as a homogeneous material when compared to the performance of the materials in other phases. It is therefore assumed that the same-phase material have the same property. Assuming that the elastic modulus of the ITZ is E_1, the elastic modulus of the cement mortar is E_2, the elastic modulus of the aggregate is E_3, and $E_1 < E_2 < E_3$ is generally satisfied. In each phase material, the fracture strain is still a random variable. At this time, the nominal stress of a typical unit can be expressed as:

$$\sigma_c = \sum_{i=1}^{N_1} \frac{E_1 A_i}{A} H'(\varepsilon - \Delta_i)\varepsilon + \sum_{j=1}^{N_2} \frac{E_2 A_j}{A} H'(\varepsilon - \Delta_j)\varepsilon + \sum_{k=1}^{N_3} \frac{E_3 A_k}{A} H'(\varepsilon - \Delta_k)\varepsilon \quad (6\text{-}38)$$

Where, $H'(\varepsilon - \Delta_i) = 1 - H(\varepsilon - \Delta_i)$; N_1, N_2 and N_3 represent the number of micro-elements in the ITZ, cement mortar and aggregate, respectively; A_i, A_j , A_k represent the area of the ITZ micro-element i, the mortar micro-element j, and the aggregate micro-element k, respectively; Δ_i, Δ_j and Δ_k represent the ultimate strain of the ITZ micro-element i, the mortar micro-element j, and the aggregate micro-element k, respectively;

Therefore, the elastic modulus of the typical unit of concrete can be expressed as

$$E_c = \sum_{i=1}^{N_1} \frac{E_1 A_i}{A} + \sum_{j=1}^{N_2} \frac{E_2 A_j}{A} + \sum_{k=1}^{N_3} \frac{E_3 A_k}{A} \quad (6\text{-}39)$$

When the strain is peak strain (ε_0) the corresponding stress is peak stress, which is expressed as

$$f_c = \sum_{i=1}^{N_1} \frac{E_1 A_i}{A} H'(\varepsilon_0 - \Delta_i)\varepsilon_0 + \sum_{j=1}^{N_2} \frac{E_2 A_j}{A} H'(\varepsilon_0 - \Delta_j)\varepsilon_0 + \sum_{k=1}^{N_3} \frac{E_3 A_k}{A} H'(\varepsilon_0 - \Delta_k)\varepsilon_0 \quad (6\text{-}40)$$

Assuming that

$$A_1 = \sum_{i=1}^{N_1} A_i \, , \quad A_2 = \sum_{j=1}^{N_2} A_j \quad , \quad A_3 = \sum_{k=1}^{N_3} A_k \, ,$$

$$f_1 = \sum_{i=1}^{N_1} \frac{A_i}{A} H'(\varepsilon_0 - \Delta_i)\varepsilon_0 , \quad f_2 = \sum_{j=1}^{N_2} \frac{A_j}{A} H'(\varepsilon_0 - \Delta_j)\varepsilon_0 , \quad f_3 = \sum_{k=1}^{N_3} \frac{A_k}{A} H'(\varepsilon_0 - \Delta_k)\varepsilon_0$$

Then, E_c and f_c can be simplified as:

$$E_c = (E_1 A_1 + E_2 A_2 + E_3 A_3) / A \quad (6\text{-}41)$$

$$f_c = E_1 f_1 + E_2 f_2 + E_3 f_3 \tag{6-42}$$

It is well known that the difference between RAC and NAC lies in the aggregate. RCA is mainly composed of old NCA and attached old mortar. Therefore, compared to NAC, the proportion of mortar and ITZ in RAC is more than in NAC. At the meso level, the number of mortar and ITZ micro-element in RAC is more than in NAC. Therefore, the nominal stress of a typical unit of RAC can be expressed as:

$$\begin{aligned}\sigma_{rc} = &\sum_{i=1}^{N_1} \frac{E_1 A_i}{A} H^{'}(\varepsilon - \Delta_i)\varepsilon + \sum_{j=1}^{N_2} \frac{E_2 A_j}{A} H^{'}(\varepsilon - \Delta_j)\varepsilon + \sum_{k1=1}^{N_{31}} \frac{E_1 A_{k1}}{A} H^{'}(\varepsilon - \Delta_{k1})\varepsilon \\ &+ \sum_{k2=1}^{N_{32}} \frac{E_2 A_{k2}}{A} H^{'}(\varepsilon - \Delta_{k2})\varepsilon + \sum_{k3=1}^{N_{33}} \frac{E_3 A_{k3}}{A} H^{'}(\varepsilon - \Delta_{k3})\varepsilon\end{aligned} \tag{6-43}$$

Where, N_1, N_2, N_{31}, N_{32} and N_{33} represent the number of micro-elements of the new ITZ, new mortar, old ITZ, old mortar and aggregate, respectively; A_i, A_j, A_{k1}, A_{k2} and A_{k3} represent the area of micro-element i of the new ITZ, micro-element j of the new mortar, the area of micro-element k_1 of the old ITZ, micro-element k_2 of the new mortar, and the aggregate micro-element k_3, respectively; Δ_i, Δ_j, Δ_{k1}, Δ_{k2} and Δ_{k3} represent the ultimate strain of the new ITZ, the new mortar, the old ITZ, the old mortar, and the aggregate, respectively; ε is strain.

Replacing the micro-elements of the aggregate in NAC with the micro-element of the old mortar, the old ITZ and natural aggregate, the NAC become RAC. That is to say, the aggregate springs with area A_3 are replaced by the old ITZ springs with the area of A_{31}, the old mortar springs with the area of A_{32} and the natural aggregate springs with area of A_{33}, that is, $A_3 = A_{31} + A_{32} + A_{33}$. And assume that the elastic modulus of the old ITZ and the old mortar is equal to the elastic modulus of the new ITZ and the new mortar. At this time, the elastic modulus and peak stress in the equation of nominal stress of the typical unit of RAC can be expressed as

$$E_{rc} = (E_1 A_1 + E_2 A_2 + E_1 A_{31} + E_2 A_{32} + E_3 A_{33}) / A \tag{6-44}$$

$$f_{rc} = E_1 f_1 + E_2 f_2 + E_1 f_{31} + E_2 f_{32} + E_3 f_{33} \tag{6-45}$$

Where,

$$A_1 = \sum_{i=1}^{N_1} A_i, \quad A_2 = \sum_{j=1}^{N_2} A_j, \quad \mathrm{A}_{31} = \sum_{\mathrm{k1}=1}^{\mathrm{N}_{31}} \mathrm{A}_{\mathrm{k1}}, \quad A_{32} = \sum_{k2=1}^{N_{32}} A_{k2}, \quad A_{33} = \sum_{k3=1}^{N_{33}} A_{k3},$$

$$f_1 = \sum_{i=1}^{N_1} \frac{A_i}{A} H^{'}(\varepsilon_0 - \Delta_i)\varepsilon_0, \quad f_2 = \sum_{j=1}^{N_2} \frac{A_j}{A} H^{'}(\varepsilon_0 - \Delta_j)\varepsilon_0, \quad f_{31} = \sum_{k1=1}^{N_{31}} \frac{A_{k1}}{A} H^{'}(\varepsilon_0 - \Delta_{k1})\varepsilon_0,$$

$$f_{32}=\sum_{k2=1}^{N_{32}}\frac{A_{k2}}{A}H^{'}(\varepsilon_0-\Delta_{k2})\varepsilon_0,\quad f_{33}=\sum_{k3=1}^{N_{33}}\frac{A_{k3}}{A}H^{'}(\varepsilon_0-\Delta_{k3})\varepsilon_0$$

Because $E_1 < E_2 < E_3$, when comparing the elastic modulus and peak stress of RAC and NAC, we can obtain

$$\begin{cases} E_{rc} < E_c \\ f_{rc} < f_c \end{cases} \tag{6-46}$$

It can be seen that the elastic modulus and peak stress of RAC under static load are less than that of NAC with the same w/c. From the expression of elastic modulus and peak stress, it is shown that the higher the RCA replacement percentage, the smaller the elastic modulus and peak stress.

6.2.3 A simplified dynamic model of RAC

As mentioned above, the crack propagation resistance of the micro-element of meso-phase materials increases with the increase in loading rate, which increases the strength and elastic modulus of the micro-element. In the meso-stochastic fracture model, this feature is characterized by an increase in the elastic modulus of the spring. Under the dynamic loading, the fracture strain of the micro-element does not change, the dynamic elastic modulus becomes kE (k >1), and it increases with the increase in strain rate, as shown in Fig. 6-14.

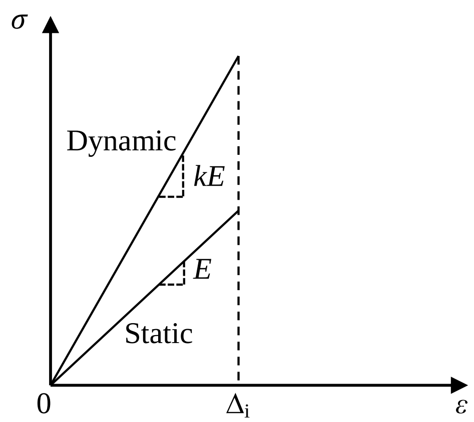

Fig. 6-14 Dynamic ideal fracture model

It is assumed that the dynamic elastic modulus of the ITZ is k_1E_1, the dynamic elastic modulus of the cement mortar is k_2E_2, and the dynamic elastic modulus of the aggregate is k_3E_3. As mentioned earlier, the strain-rate sensitivity of rocks, mortars and ITZ increases in turn. That is, at the same strain rate, $k_1 > k_2 > k_3$. In this case, the dynamic nominal stress of the typical units of

NAC and RAC can be expressed by the following two equations.

$$\sigma_c = \sum_{i=1}^{N_1} \frac{k_1 E_1 A_i}{A} H^{'}(\varepsilon - \Delta_i)\varepsilon + \sum_{j=1}^{N_2} \frac{k_2 E_2 A_j}{A} H^{'}(\varepsilon - \Delta_j)\varepsilon + \sum_{k=1}^{N_3} \frac{k_3 E_3 A_k}{A} H^{'}(\varepsilon - \Delta_k)\varepsilon \quad (6\text{-}47)$$

$$\begin{aligned}\sigma_{rc} = &\sum_{i=1}^{N_1} \frac{k_1 A_i}{A} H^{'}(\varepsilon - \Delta_i)\varepsilon + \sum_{j=1}^{N_2} \frac{k_2 A_j}{A} H^{'}(\varepsilon - \Delta_j)\varepsilon + \sum_{k1=1}^{N_{31}} \frac{k_1 A_{k1}}{A} H^{'}(\varepsilon - \Delta_{k1})\varepsilon \\ &+ \sum_{k2=1}^{N_{32}} \frac{k_2 A_{k2}}{A} H^{'}(\varepsilon - \Delta_{k2})\varepsilon + \sum_{k3=1}^{N_{33}} \frac{k_3 A_{k3}}{A} H^{'}(\varepsilon - \Delta_{k3})\varepsilon\end{aligned} \quad (6\text{-}48)$$

At this time, the dynamic elastic modulus and peak stress of the typical unit of NAC can be expressed as:

$$E_c^d = (k_1 E_1 A_1 + k_2 E_2 A_2 + k_3 E_3 A_3) / A \quad (6\text{-}49)$$

$$f_c^d = k_1 E_1 f_1 + k_2 E_2 f_2 + k_3 E_3 f_3 \quad (6\text{-}50)$$

The dynamic elastic modulus and peak stress of the typical unit of RAC can be expressed as:

$$E_{rc}^d = (k_1 E_1 A_1 + k_2 E_2 A_2 + k_1 E_1 A_{31} + k_2 E_2 A_{32} + k_3 E_3 A_{33}) / A \quad (6\text{-}51)$$

$$f_{rc}^d = k_1 E_1 f_1 + k_2 E_2 f_2 + k_1 E_1 f_{31} + k_2 E_2 f_{32} + k_3 E_3 f_{33} \quad (6\text{-}52)$$

Therefore, the DIF_f of RAC ($DIF_{f,rc}$) and the DIF_f of NAC ($DIF_{f,c}$) can be expressed as

$$DIF_{f,c} = \frac{k_1 E_1 f_1 + k_2 E_2 f_2 + k_3 E_3 f_3}{E_1 f_1 + E_2 f_2 + E_3 f_3} \quad (6\text{-}53)$$

$$DIF_{f,rc} = \frac{k_1 E_1 f_1 + k_2 E_2 f_2 + k_1 E_1 f_{31} + k_2 E_2 f_{32} + k_3 E_3 f_{33}}{E_1 f_1 + E_2 f_2 + E_1 f_{31} + E_2 f_{32} + E_3 f_{33}} \quad (6\text{-}54)$$

The DIF_E of RAC ($DIF_{E,rc}$) and The DIF_E of NAC ($DIF_{E,c}$) can be expressed as

$$DIF_{E,c} = \frac{k_1 E_1 A_1 + k_2 E_2 A_2 + k_3 E_3 A_3}{E_1 A_1 + E_2 A_2 + E_3 A_3} \quad (6\text{-}55)$$

$$DIF_{E,rc} = \frac{k_1 E_1 A_1 + k_2 E_2 A_2 + k_1 E_1 A_{31} + k_2 E_2 A_{32} + k_3 E_3 A_{33}}{E_1 A_1 + E_2 A_2 + E_1 A_{31} + E_2 A_{32} + E_3 A_{33}} \quad (6\text{-}56)$$

In order to facilitate the derivation when comparing the strain-rate sensitivity between RAC and NAC, the expression of DIF_f and DIF_E are simplified, namely, the effect of the ITZ is not taken into account. In other words, the area of the ITZ is set as zero. At this time,

$$DIF_{E,c} = \frac{k_2 E_2 A_2 + k_3 E_3 A_3}{E_2 A_2 + E_3 A_3} = k_2 - \frac{(k_2 - k_3) E_3 A_3}{E_2 A_2 + E_3 A_3} \quad (6\text{-}57)$$

$$DIF_{E,rc}=\frac{k_2E_2A_2+k_2E_2A_{32}+k_3E_3A_{33}}{E_2A_2+E_2A_{32}+E_3A_{33}}=k_2-\frac{(k_2-k_3)E_3A_{33}}{E_2A_2+E_2A_{32}+E_3A_{33}} \tag{6-58}$$

$$DIF_{f,c}=\frac{k_2E_2f_2+k_3E_3f_3}{E_2f_2+E_3f_3}=k_2-\frac{(k_2-k_3)E_3f_3}{E_2f_2+E_3f_3} \tag{6-59}$$

$$DIF_{f,rc}=\frac{k_2E_2f_2+k_2E_2f_{32}+k_3E_3f_{33}}{E_2f_2+E_2f_{32}+E_3f_{33}}=k_2-\frac{(k_2-k_3)E_3f_{33}}{E_2f_2+E_2f_{32}+E_3f_{33}} \tag{6-60}$$

Because $\frac{b}{a}<\frac{b+c}{a+c}$ (a > b > 0， c > 0), we can obtain that

$$\frac{E_3A_{33}}{E_2A_2+E_2A_{32}+E_3A_{33}}<\frac{(E_2A_{32}+E_3A_{33})}{E_2A_2+(E_2A_{32}+E_3A_{33})}<\frac{E_3A_3}{E_2A_2+E_3A_3} \tag{6-61}$$

$$\frac{E_3f_{33}}{E_2f_2+E_2f_{32}+E_3f_{33}}<\frac{(E_2f_{32}+E_3f_{33})}{E_2f_2+(E_2f_{32}+E_3f_{33})}<\frac{E_3f_3}{E_2f_2+E_3f_3} \tag{6-62}$$

Then, we can obtain that

$$DIF_{E,c}<DIF_{E,rc} \tag{6-63}$$

$$DIF_{f,c}<DIF_{f,rc} \tag{6-64}$$

Therefore, the strain-rate sensitivity of RAC with 100% RCA is higher than that of NAC. This feature is consistent with the experimental results. According to these equations, with the increase in RCA replacement percentage, the mortar content increases, so that the DIF_f and DIF_E increase. However, in the test results, the relationship between the RCA replacement percentage and the strain-rate sensitivity of RAC shows no obvious trend. On the one hand, this may be caused by the discretization of the test results. On the other hand, there are differences in the micro-structure of RACS with different RCA replacement percentages, for example, there is more ITZ when the RCA replacement percentage is larger. In the above simplified model, the impact of the microstructure was not taken into account, which may lead to the difference between the test results and the theoretical analysis. If it is not because the discretization of the test results, it indicates that the difference in the micro-structure of RAC with different RCA replacement percentage can also affect the strain-rate sensitivity of RAC.

6.3 Discussion on the difference in the strain-rate sensitivity between RAC and CRAC

Regarding the improvement in the compressive strength and the elastic modulus of CRAC, the reason is that the quality of RCA is improved by carbonation, which is based on the reactions between CO_2 and hydration products of cement in concrete, i.e., $Ca(OH)_2$, C-S-H, etc (Xiao et al. 2016; Kashef-Haghighi et al. 2015). The reaction product $CaCO_3$ will precipitate in the pore space and thus densify the microstructure of RCA (Xuan et al. 2016). As a result, the density of the RCA is increased, while the porosity and water absorption of RCA are decreased. Moreover, some micro-cracks in the RCA would be closed again because of the reaction. Consequently, the strength and elastic modulus of CRAC can be improved when compared with RAC. In other words, the features that the porosity of CRAC is smaller and the number of micro-cracks in CRAC is less are the reason for the improvement in the static strength and elastic modulus of CRAC than RAC. In this study, the test results show that the strain-rate sensitivity of CRAC was less significant than that of RAC. The following will discuss the reason for the lower strain-rate sensitivity of CRAC than RAC from these two aspects.

On one hand, because the porosity of CRAC specimens is lower than that of RAC, which means less micro units are present to produce viscous resistances based on Stefan effect which will be described in the next chapter, thus the increase in the strength and elastic modulus of CRAC specimens will be smaller than that of RAC. In other words, the strain-rate sensitivity of CRAC is less significant than that of RAC.

On the other hand, some studies indicated that the fracture toughness of rock-like materials was strain-rate dependent (Li et al. 2000), i.e., the fracture toughness of rock-like materials increase with the increase in strain rate. From the sketch of fracture toughness test which is drawn in Fig. 6-15, it indicates that the fracture toughness reflects the crack propagation resistance of rock-like materials, which will be discussed further in the next chapter. In other words, the crack propagation resistance increases as the strain rate increases. Therefore, for the micro-unit in concrete, each crack will produce an additional resistant force (F_d) under dynamic loadings when compared with that under static loading, as shown in Fig. 6-16. Because the number of micro-cracks in CRAC is less than that in RAC, the total additional resistant force in CRAC produced by micro-cracks under dynamic loading is lower than that in RAC, which means again that the strain-rate sensitivity of

CRAC is less significant than RAC.

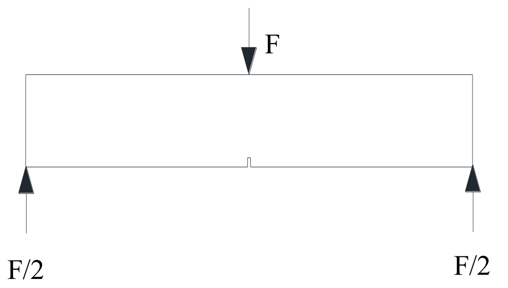

Fig. 6-15 Sketch of fracture toughness test

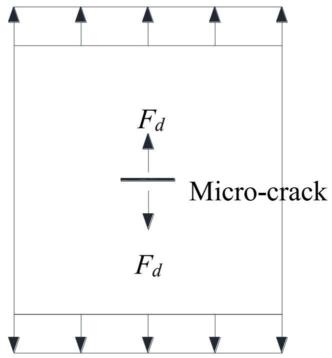

Fig. 6-16 Additional resistant force produced by micro-crack in concrete

6.4 Summary

Based on the experimental results in previous chapters, this chapter discussed the mechanism of the strain-rate sensitivity of RAC from the perspective of Stefan effect, inertial force effect and crack propagation effect. A simplified static and dynamic model of concrete for NAC and RAC was established. Based on this, the reason why the strain-rate sensitivity of RAC with 100% RCA was higher than that of NAC was explained. The main conclusions are shown as follows:

(1) At low strain rates (10^{-5} /s ~ 10^{-1} /s), Stefan effect, inertial force effect and the effect of crack passing through aggregate may not be the main factors that cause the strain-rate sensitivity of RAC. The dominant factor may be the strain-rate sensitivity of crack propagation resistance of the meso-phase materials.

(2) The influence of Stefan effect on the strain-rate sensitivity of RAC is small at high strain rates (10^{1} /s ~ 10^{2} /s), and the effect of transverse inertial effect is also small, while the longitudinal inertial effect has some impact, but it is not the dominant factor. The dominant factor in the strain-rate sensitivity of RAC at high strain rates may also be the strain-rate sensitivity of crack propagation resistance of the meso-phase materials. The contribution of multiple factors is the reason why the dynamic increase factor of peak stress (DIF_f) of RAC at high strain rates increases faster than that at low strain rates.

(3) The simplified static and dynamic model canaccount for why the strain-rate sensitivity of RAC with 100% RCA is greater than that of NAC. Differences between the test results and theoretical analysis indicate that difference in the micro-structure of RAC with different RCA

replacement percentages can also affect the strain-rate sensitivity of RAC.

(4) The strain-rate sensitivity of CRAC was less significant than that of RAC. The reason was due to its lower porosity and less micro-cracking, which could result in less Stefan effect and smaller crack propagation resistance, respectively.

Chapter 7 Numerical simulation on the strain-rate sensitivity of RAC

Concrete is a kind of non-homogeneous material mainly composed of mortar, aggregate and ITZ, and its meso-structure is complicated. The irregularity in the shape of the aggregate and the distribution of the mortar leads to a heterogeneous structure. In the RAC, the presence of the old mortar and old ITZ leads to a more complex meso-structure. Moreover, in conventional concrete or RAC, not only the meso-structure is heterogeneous, but also the meso-phase materials themselves are heterogeneous. There is a difference in the physical and mechanical properties of different aggregate, hardened mortar matrix in different areas, and the ITZ in different areas. The combination of macro and meso/micro methods can be used to explain the mechanism of macroscopic mechanical behavior of concrete. However, at the current mathematical and mechanical level it is difficult to solve the failure process of heterogeneous concrete materials using analytical methods, and there are also many limitations on testing at meso and micro scopic levels. Therefore, the use of numerical simulation at the meso-scopic level has become one of the important directions in this field of research.

In this chapter, ABAQUS software is used to establish the finite element model of RAC to study the strain-rate sensitivity of RAC at low strain rates (10^{-5} /s ~ 10^{-1} /s). On the one hand, we can more accurately understand the dynamic mechanical properties and strain-rate sensitivity of RAC, because many uncontrollable factors may cause some uncertainty in the test results. On the other hand, because of the limitation of economic, human and other resources, we can only choose a limited number of parameters for experimental analyses, so the use of numerical simulation to conduct variable parameter analysis is helpful to obtain a more comprehensive understanding of the dynamic mechanical properties of RAC and the accompanying mechanisms.

7.1 Finite element model

7.1.1 Geometric model

The geometric model of the RAC specimens in this simulation was the same as the plane size of the MRAC in chapter 2. It consists of five meso-phase materials, namely natural aggregate, old mortar, new mortar, the old ITZ and the new ITZ, as shown in Fig. 7-1.

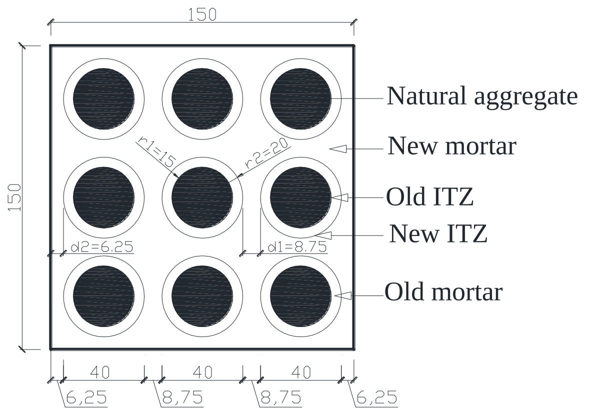

Fig. 7-1 Five meso-phase materials of MRAC

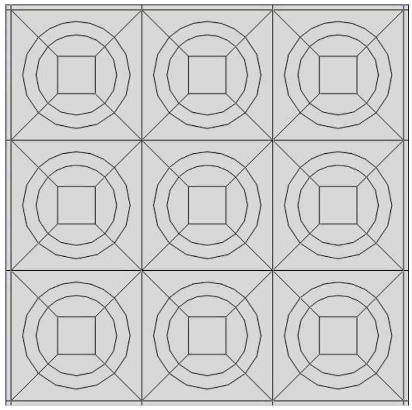

Fig. 7-2 Finite element model of MRAC

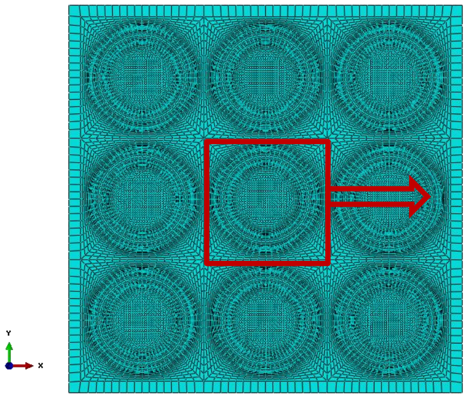

Fig. 7-3 Meshing of MRAC

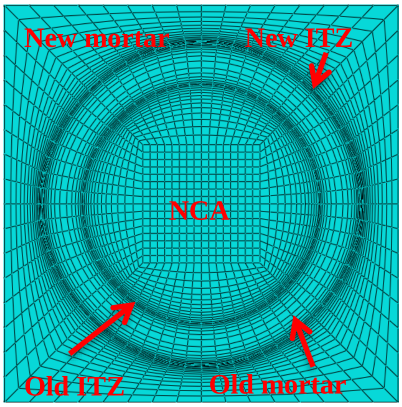

Fig. 7-4 Meso-phase materials after mesh

Many studies have shown that the size of ITZ is very small. With the emergence of nano-indentation technology, it is possible to measure the microscopic mechanical properties of ITZ (Xiao et al. 2013). It showed that the thickness of the old ITZ and the new ITZ is about 50μm and 60μm, respectively. Therefore, in this numerical simulation, the thicknesses of the old ITZ and the new ITZ were set as 50μm and 60μm, respectively. The geometric model of RAC in the simulation is shown in Fig. 7-2. A 4-node plane stress reduction integral unit (CPS4R) was used in this simulation. Dividing the grid by sweeping, the grid is shown in Fig. 7-3, the mesophase materials are shown in Fig. 7-4.

7.1.2 Materials

7.1.2.1 Natural aggregate

From the experimental study of the dynamic mechanical properties of RAC in the chapter 2, it is found that there was no cracking or destruction of NCA at all the strain rates studied, which was consistent with the static results in reference (Xiao et al. 2013). At the same time, the strength of the granite aggregates was above 150MPa, which was much higher than the stresses presented in the element of NCA in the simulation. Therefore, it was assumed that the NCA was always in the elastic phase during the loading process, and it was defined as an isotropic linear elastic material in this simulation.

Granite is also a strain-rate sensitive material, but it is less sensitive to strain rate than that of mortar and concrete. A large number of studies (Zhai et al. 2007, 2009) have reported this phenomenon. Therefore, the strain-rate sensitivity should be considered when setting the material parameters of the granite aggregate at higher strain rates. In this simulation, the strain-rate sensitivity of the aggregate was considered by increasing its elastic modulus. When the strain rates were 10^{-5} /s, 10^{-4} /s, 10^{-3} /s, 10^{-2} /s, 10^{-1} /s, the elastic modulus of aggregate were set as 70GPa, 71.75 GPa, 73.5 GPa, 75.25 GPa and 77 Gpa, respectively. The Poisson's ratio was 0.16.

7.1.2.2 Mortar

In the simulation, the constitutive relationship of mortar was based on the Concrete Damage Plasticity Model in ABAQUS software. The stress-strain relationship required in the model was based on the stress-strain relationship in the “Chinese Design Code for Concrete Structures” (GB50010-2010). The parameters in the constitutive model were determined according to the test results. These are described in detail below.

(1) Concrete Damage Plasticity Model

The Concrete Damage Plasticity Model in ABAQUS is a continuous, plastic-based concrete damage model, using isotropic elastic damage and isotropic tension and compression plasticity theory to characterize the nonlinear behavior of concrete. It can simulate the mechanical behavior of concrete under monotonous, cyclic and dynamic loadings at low water pressure (Liu et al. 2014) . The model assumes that the concrete material is mainly damaged by cracking in tension or by crushing in compression, and the evolution of the yield or failure surface is controlled by the equivalent tensile plastic strain ($\tilde{\varepsilon}_t^{pl}$) and the equivalent compressive plastic strain ($\tilde{\varepsilon}_c^{pl}$).

The Concrete Damage Plasticity Model introduces damage index into the concrete model. The elastic stiffness matrix of concrete is reduced to simulate the decrease in the unloading stiffness of concrete with the increase in damage (Jiang et al. 2005). In this model, it uses different damage factors to describe this stiffness degradation in compression and in tension. The uniaxial compressive and tensile stress-strain relationships of concrete are shown in Fig. 7-5 and Fig. 7-6, respectively.

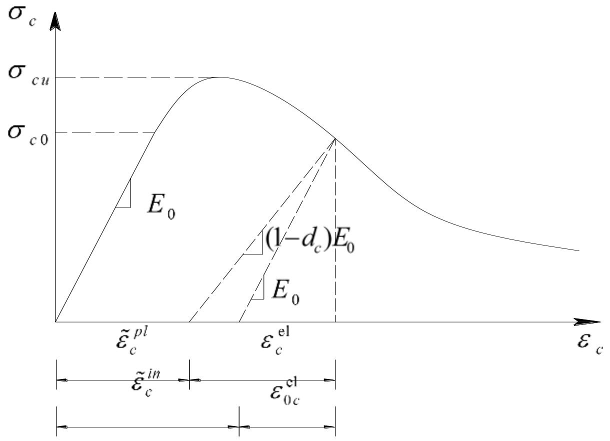

Fig. 7-5 The uniaxial compression stress-strain relationship of concrete

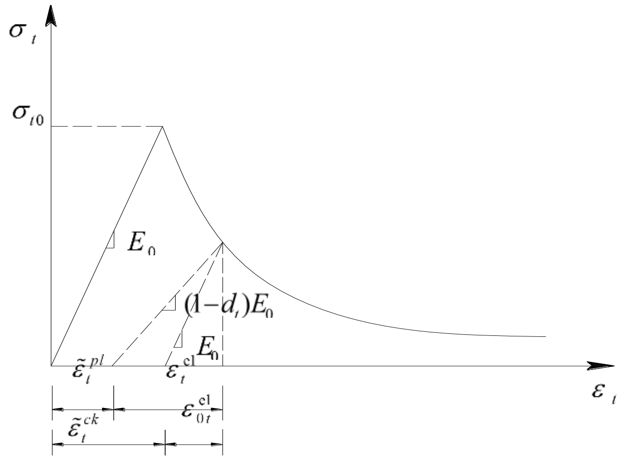

Fig. 7-6 The uniaxial tensile stress-strain relationship of concrete

For uniaxial tension, the concrete shows a linearly elastic characteristics before reaching the tensile peak stress (σ_{t0}). When the stress exceeds σ_{t0}, the stress decreases rapidly, which is due to the appearance of the microcracks. For uniaxial compression, the concrete material shows a linearly elastic characteristic before reaching the yield point (σ_{c0}). After the yield point, it comes into the hardening stage. After the peak stress (σ_{cu}), it comes into the softening stage. The decrease in the material stiffness can be expressed by the parameters of tensile damage (d_t) and the compression damage (d_c). The simplified uniaxial stress-strain relationship captures the main deformation characteristics of the concrete material, and the tensile and compressive stress-strain relationships can be expressed as

$$\sigma_t = (1-d_t)E_0(\varepsilon_t - \tilde{\varepsilon}_t^{pl}) \tag{7-1}$$

$$\sigma_c = (1-d_c)E_0(\varepsilon_c - \tilde{\varepsilon}_c^{pl}) \tag{7-2}$$

Where, σ_t and σ_c represent the tensile stress and compressive stress respectively, ε_t and ε_c represent the tensile strain and compressive strain respectively, E_0 is elastic modulus.

In defining compression hardening, the harden data is defined according to the compressive inelastic strain ($\tilde{\varepsilon}_c^{in}$), and the compressive inelastic strain can be expressed as the difference between the compressive total strain (ε_c) and the compressive elastic strain (ε_{0c}^{el}) of the non-destructive material:

$$\tilde{\varepsilon}_c^{in} = \varepsilon_c - \varepsilon_{0c}^{el} \tag{7-3}$$

Where, $\varepsilon_{0c}^{el} = \sigma_c / E_0$.

The unloaded data is supplied to ABAQUS according to the $d_c - \tilde{\varepsilon}_c^{in}$ relationship. The compressive plastic strain ($\tilde{\varepsilon}_c^{pl}$) can be expressed as:

$$\tilde{\varepsilon}_c^{pl} = \tilde{\varepsilon}_c^{in} - \frac{d_c}{(1-d_c)}\frac{\sigma_c}{E_0} \tag{7-4}$$

In tension, the softening properties and subsequent failure behavior of the concrete can be characterized by tensile hardening. The tensile hardening data are defined according to the cracking strain ($\tilde{\varepsilon}_t^{ck}$). The tensile cracking strain can be expressed as the difference between the tensile total strain (ε_t) and the tensile elastic strain (ε_{0t}^{el}) of the non-destructive material:

$$\tilde{\varepsilon}_t^{ck} = \varepsilon_t - \varepsilon_{0t}^{el} \tag{7-5}$$

Where, $\varepsilon_{0t}^{el} = \sigma_t / E_0$.

The unloaded data is supplied to ABAQUS according to the $d_t - \tilde{\varepsilon}_t^{ck}$ relationship, the tensile plastic strain ($\tilde{\varepsilon}_t^{pl}$) can be expressed as:

$$\tilde{\varepsilon}_t^{pl} = \tilde{\varepsilon}_t^{ck} - \frac{d_t}{(1-d_t)}\frac{\sigma_t}{E_0} \tag{7-6}$$

(2) Stress-strain relationship in the model

When using the Concrete Dmage Plasticity Model, the tensile stress-cracking strain curve and compressive stress-inelastic strain curve of the material are required for input by the user. The tensile damage factor-cracking strain curve and compressive damage factor-inelastic strain curve of the material are also required for input into the ABAQUS. Therefore, in the simulation, because of the lack of test data, some parameters were determined according to the stress-strain relationship given in Chinese "concrete structure design specifications" (GB50010 -2010).

For the uniaxial tensile stress-strain relationship, it was assumed that the stress-strain curve of the concrete showed a linearly elastic characteristic before the peak stress, and the secant modulus at the peak point was taken as the initial elastic modulus. The non-elastic phase of the stress-strain relationship used the equation in the above specification. Therefore, the uniaxial tensile stress-strain relationship was determined as follows:

$$y=\begin{cases} x & 0<x\leq 1 \\ \dfrac{x}{\alpha_t(x-1)^{1.7}+x} & x\geq 1 \end{cases} \tag{7-7}$$

$$x=\frac{\varepsilon}{\varepsilon_{tr}} \tag{7-8}$$

$$y=\frac{\sigma}{f_{tr}} \tag{7-9}$$

Where, α_t is a parameter of the descending part of the stress-strain curve in uniaxial tension; f_{tr} is the representative value of concrete tensile strength; ε_{tr} is tensile peak strain of concrete.

For the uniaxial compression stres -strain relationship, the stress-strain curve showed a linearly elastic characteristic when the stress was less than 1/2 of the peak stress, and the initial tangentialelastic modulus of the concrete was E_c. The stress-strain relationship at the strengthening section and the softening section used the equation in the specification. Therefore, the uniaxial compressive stress-strain relationship was determined as follows:

$$y=\begin{cases} \dfrac{1}{2x_0}x & 0\leq x\leq x_0 \\ \dfrac{nx}{n-1+x^n} & x_0<x\leq 1 \\ \dfrac{x}{\alpha_c(x-1)^2+x} & x>1 \end{cases} \tag{7-10}$$

$$x = \frac{\varepsilon}{\varepsilon_{cr}} \tag{7-11}$$

$$y = \frac{\sigma}{f_{cr}} \tag{7-12}$$

$$x_0 = \frac{f_{cr}}{2E_c\varepsilon_{cr}} \tag{7-13}$$

$$n = \frac{E_c\varepsilon_{cr}}{E_c\varepsilon_{cr} - f_{cr}} \tag{7-14}$$

Where, α_c is a parameter of the descending section of the stress-strain curve in uniaxial compression; f_{cr} is the representative value of concrete compressive strength; ε_{cr} is the compressive peak strain of concrete.

(3) Determination of damage index

In the Concrete Damage Plasticity Model, the $d_t - \tilde{\varepsilon}_t^{ck}$ and $d_c - \tilde{\varepsilon}_c^{in}$ relationships are required to be specified. Assuming that the ratio of the $\tilde{\varepsilon}_c^{pl}$ to the $\tilde{\varepsilon}_c^{in}$ is η_c, and the ratio of the $\tilde{\varepsilon}_t^{pl}$ to the $\tilde{\varepsilon}_t^{ck}$ is η_t, In this study, η_c was set as 0.8, η_t was set as 0.95. Then, the $d_t - \tilde{\varepsilon}_t^{ck}$ and $d_c - \tilde{\varepsilon}_c^{in}$ relationships can be calculated according to following two equations.

$$d_t = \frac{(1-\eta_t)\tilde{\varepsilon}_t^{ck}E_t}{\sigma_t + (1-\eta_t)\tilde{\varepsilon}_t^{ck}E_t} \tag{7-15}$$

$$d_c = \frac{(1-\eta_c)\tilde{\varepsilon}_c^{in}E_c}{\sigma_c + (1-\eta_c)\tilde{\varepsilon}_c^{in}E_c} \tag{7-16}$$

(4) Determination of material parameters of mortar

In this simulation, the strength of mortar M30 was determined based on the results of the MM30 specimens in Chapter 2. However, because the strength of MM30 in the test was not shown to uniformly increase with the increase in the strain rate, the mortar strength at each strain rate was determined according to the fitting line. As a result, the value of DIF_f increased by 10.2% as strain rate increased 10 times. In the test, the elastic modulus of MM30 increased with the increase in strain rate, but the dispersion was large. Therefore, the DIF_E in the test was not used in this simulation. It is assumed that the strain-rate sensitivity of elastic modulus was consistent with that of peak stress. Therefore, the DIF_E was chosen to be the same as the DIF_f. According to the test results, the quasi-static elastic modulus of M30 was set to 20GPa, and the elastic modulus at other strain rates are calculated according to the DIF_E. It was assumed that the peak strain of RAC did not change with the change in strain rate, so the same peak strain was applied at all the strain rates studied. Due to the lack of tensile strength data, the tensile strength of mortar in the simulation was taken as 1/10 of the corresponding compressive strength. The parameters of the descending section of the compression constitutive curve α_c were obtained according to the different strength values in the Code for Design of Concrete Structures (GB50010-2010). The Poisson's ratio was 0.22. The material parameters of M30 are shown in Table 7-1. The uniaxial stress-strain curves of the M30 at each strain rate are shown in Fig. 7-7 and Fig. 7-8, respectively.

In this simulation, the strength and elastic modulus of M20 and M40 were empirically assumed, and their DIF_f and DIF_E were also based on empirical assumptions. Considering that the lower the strength of the mortar, the more sensitive to strain rate, as the strain rate increase 10 times, the value of DIF_f (or DIF_E) of M20 mortar and M40 mortar increased by 15% and 5%. The other parameters were considered in the same way as M30 mortar. The material parameters of M20 and M40 are shown in Table 7-2 and Table 7-3, respectively.

Table 7-1 Material parameters of M30

Strain rate/s^{-1}	f_c /MPa	E_c /GPa	$\varepsilon_{cp}/10^{-6}$	α_c	η_c	f_t /MPa	E_t/GPa	ε_{tp} /10^{-6}	α_t	η_t
10^{-5}	48.0	20.0	4000	2.372	0.8	4.8	20.0	240	2	0.95
10^{-4}	52.9	22.0	4000	2.631	0.8	5.3	22.0	240	2	0.95
10^{-3}	57.8	24.1	4000	2.885	0.8	5.8	24.1	240	2	0.95
10^{-2}	62.7	26.1	4000	3.134	0.8	6.3	26.1	240	2	0.95
10^{-1}	67.6	28.2	4000	3.379	0.8	6.8	28.2	240	2	0.95

Table 7-2 Material parameters of M20

Strain rate/s^{-1}	f_c /MPa	E_c /GPa	$\varepsilon_{cp}/10^{-6}$	α_c	η_c	f_t /MPa	E_t/GPa	ε_{tp} /10^{-6}	α_t	η_t
10^{-5}	36.0	15.0	4000	1.708	0.8	3.6	15.0	240	2	0.95
10^{-4}	41.4	17.3	4000	2.016	0.8	4.1	17.3	240	2	0.95
10^{-3}	46.8	19.5	4000	2.307	0.8	4.7	19.5	240	2	0.95
10^{-2}	52.2	21.8	4000	2.594	0.8	5.2	21.8	240	2	0.95
10^{-1}	57.6	24.0	4000	2.875	0.8	5.8	24.0	240	2	0.95

Table 7-3 Material parameters of M40

Strain rate/s^{-1}	f_c /MPa	E_c /GPa	$\varepsilon_{cp}/10^{-6}$	α_c	η_c	f_t /MPa	E_t/GPa	ε_{tp} /10^{-6}	α_t	η_t
10^{-5}	60.0	25.0	4000	3	0.8	6.0	25.0	240	2	0.95
10^{-4}	63.0	26.3	4000	3.15	0.8	6.3	26.3	240	2	0.95
10^{-3}	66.0	27.5	4000	3.3	0.8	6.6	27.5	240	2	0.95
10^{-2}	69.0	28.8	4000	3.45	0.8	6.9	28.8	240	2	0.95
10^{-1}	72.0	30.0	4000	3.6	0.8	7.2	30.0	240	2	0.95

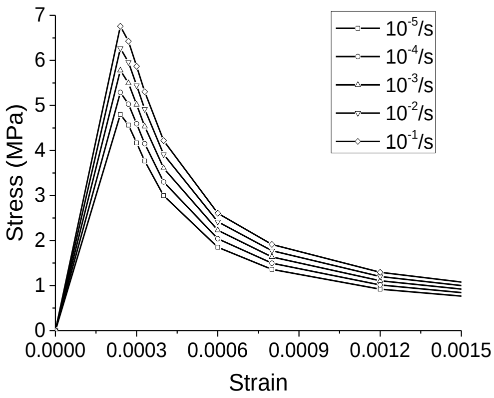

Fig. 7-7 Tensile constitutive curve of mortar at different strain rates

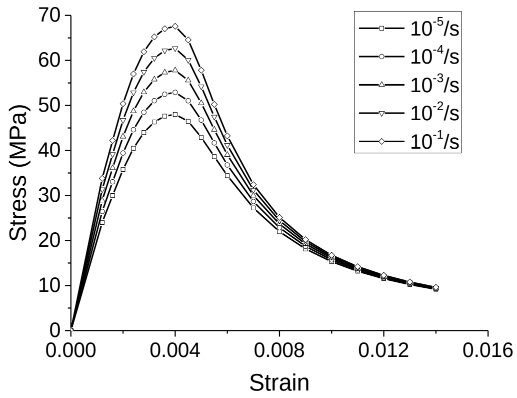

Fig. 7-8 Compressive constitutive curve of mortar at different strain rates

7.1.2.3 ITZ

Xiao et al. (2013) showed that the elastic modulus and strength of the ITZ have a relationship with the corresponding elastic modulus and strength of the mortar, namely the elastic modulus and strength of the ITZ were about 80% ~ 85% of the corresponding mortar. Moreover, the constitutive model of the ITZ can adopt a constitutive model similar to that of mortar. Therefore, the constitutive model of the ITZ also adopted the Concrete Damage Plasticity Model. The compressive strength, tensile strength and elastic modulus of the ITZ were set at 80% of the corresponding mortar. The other parameters were considered in the same way as mortar. The material parameters of the ITZ corresponding to M20, M30 and M40 are shown in Table 7-4, Table 7-5 and Table 7-6, respectively.

Table 7-4 Material parameters of ITZ corresponding to M20

Strain rate/s^{-1}	f_c /MPa	E_c /GPa	ε_{cp}/10^{-6}	α_c	η_c	f_t /MPa	E_t/GPa	ε_{tp} /10^{-6}	α_t	η_t
10^{-5}	28.8	12.0	4000	1.288	0.8	2.9	12.0	240	2	0.95
10^{-4}	33.1	13.8	4000	1.541	0.8	3.3	13.8	240	2	0.95
10^{-3}	37.4	15.6	4000	1.792	0.8	3.7	15.6	240	2	0.95
10^{-2}	41.8	17.4	4000	2.035	0.8	4.2	17.4	240	2	0.95
10^{-1}	46.1	19.2	4000	2.268	0.8	4.6	19.2	240	2	0.95

Table 7-5 Material parameters of ITZ corresponding to M30

Strain rate/s^{-1}	f_c /MPa	E_c /GPa	ε_{cp}/10^{-6}	α_c	η_c	f_t /MPa	E_t/GPa	ε_{tp} /10^{-6}	α_t	η_t
10^{-5}	38.4	16.0	4000	1.847	0.8	3.8	16.0	240	2	0.95
10^{-4}	42.3	17.6	4000	2.064	0.8	4.2	17.6	240	2	0.95
10^{-3}	46.2	19.3	4000	2.275	0.8	4.6	19.3	240	2	0.95
10^{-2}	50.2	20.9	4000	2.488	0.8	5.0	20.9	240	2	0.95
10^{-1}	54.1	22.5	4000	2.691	0.8	5.4	22.5	240	2	0.95

Table 7-6 Material parameters of ITZ corresponding to M40

Strain rate/s^{-1}	f_c /MPa	E_c /GPa	ε_{cp}/10^{-6}	α_c	η_c	f_t /MPa	E_t/GPa	ε_{tp} /10^{-6}	α_t	η_t
10^{-5}	48.0	20	4000	2.372	0.8	4.8	20.0	240	2	0.95
10^{-4}	50.4	21	4000	2.501	0.8	5.0	21.0	240	2	0.95
10^{-3}	52.8	22	4000	2.626	0.8	5.3	22.0	240	2	0.95
10^{-2}	55.2	23	4000	2.75	0.8	5.5	23.0	240	2	0.95
10^{-1}	57.6	24	4000	2.875	0.8	5.8	24.0	240	2	0.95

7.1.3 Specimen design

In this simulation, the MRAC30-30 specimen represents the MRAC specimen of which the new and old mortar are M30, and it s used for comparison with the MRAC30 specimen in the test. At the same time, based on MRAC30-30 specimen, the strain-rate sensitivity of RAC and the influence of the constituent meso-phase materials were studied.

In order to study the effect of RCA replacement percentage on the strain-rate sensitivity of RAC, five RCA replacement percentages, namely 0%, 33%, 55%, 66% and 100%, were considered. The corresponding specimen were named with MRAC30-0%, MRAC30-33%, MRAC30-55%, MRAC30-66% and MRAC30-100% (i.e., MRAC30-30), respectively. In this simulation, all the material parameters were not changed, only the material parameters of some MRCAs in MRAC30-30 which include the old mortar and the old ITZ were set as material parameters of the aggregate, which were equivalent to replacing NCA by RCA.

In order to study the effect of new mortar strength on the dynamic mechanical properties of RAC, the MRAC30-20, MRAC30-30 and MRAC30-40 specimens were selected to represent the RAC specimen of which the old mortar was M30, while the new mortar was M20, M30 and M40, respectively. To study the effect of the strength of the old mortar on the dynamic mechanical properties of RAC, the MRAC20-30, MRAC30-30 and MRAC40-30 specimens were designed to represent the RAC specimen of which the new mortar was M30 while the old mortar was M20, M30 and M40, respectively.

7.1.4 Loading and solution

ABAQUS/Explicit solver was used in this simulation. At the top of the specimen, a uniform distributed displacement was defined, and the load was control by displacement. The same loading rate was used in all cases, and the strain-rate sensitivity of RAC was reflected by the strain-rate sensitivity of the meso-phase materials. In order to obtain a complete stress-strain curve, the loading was stopped when the Y-direction displacement reached 0.9 mm. The corresponding strain was 6000×10^{-6}. The Y direction of all nodes at the bottom was constrained, and the X direction and rotation were not limited. The sum of the reaction forces of all the nodes at the bottom face was the force of the whole specimen, which divided by the area of the bottom face is the stress of the specimen; the displacement of the node at the top was the displacement of the whole specimen, which divided by the height of the specimen is the strain of the specimen. Then, the stress-strain curve of the whole specimen can be obtained.

7.2 Calibration of the model

7.2.1 Stress-strain curve

The stress-strain curves of MRAC30-30 at all the strain rates studied obtained in this simulation are compared with the stress-strain curve of the MRAC30 specimen at the same strain rate, as shown in Fig. 7-9. The results show that the ascending part of the stress-strain curve obtained in this simulation was in good agreement with the experimental results. This feature is explained in the following by comparing the variations in the peak stress, elastic modulus and peak strain with the strain rate obtained in the simulation with the test results. The difference was that the decreasing trend of the simulated stress-strain curve at descending section was steeper than that of the test results. The possible reasons are shown as follows. The parameter of descending section of the stress-strain curve of the mortar and the ITZ in the constitutive model in this simulation was taken as the same parameter for concrete with same strength, but in fact, the aggregate behaves like a linear elastic material and the aggregate will rebound after the peak load, thus the overall deformation of the MRAC specimen including ITZ, mortar and aggregate is likely to be smaller than that of concrete, namely the decreasing trend of stress-strain curve of the MRAC at descending part is steeper than that of concrete material which represent the result of MRAC specimen in the test. Therefore, the parameters of the descending section of stress-strain curve of the mortar and the ITZ should be higher than the parameters of the descending section for concrete of the same strength when using this finite element model. However, the method is still to be further studied.

Although there are some differences between the descending part of the stress-strain curves of the simulation results and the test results, it does not affect the analysis on the strain-rate sensitivity of RAC because the main mechanical properties can be obtained from the ascending part of the stress-strain curve. The reliability of using the finite element model to study the strain-rate sensitivity of RAC is explained by comparing the change in the peak stress, elastic modulus and peak strain with strain rate obtained in the simulation with the corresponding test results.

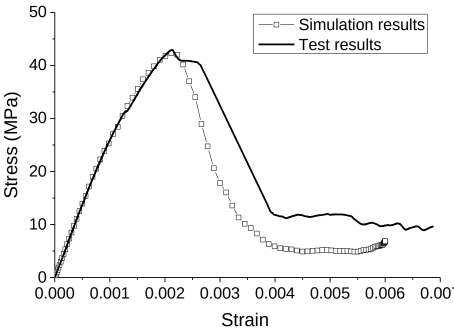

(a) 10^{-5}/s

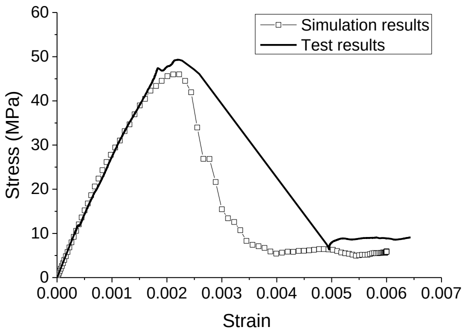

(b) 10^{-4}/s

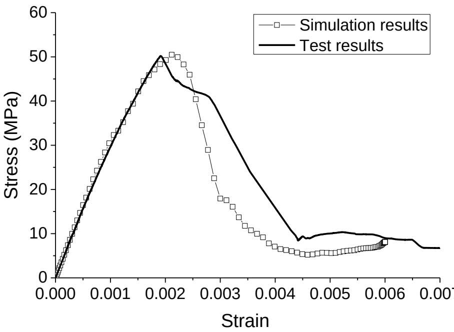

(c) 10^{-3}/s

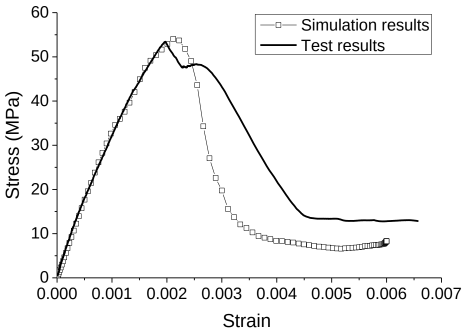

(d) 10^{-2}/s

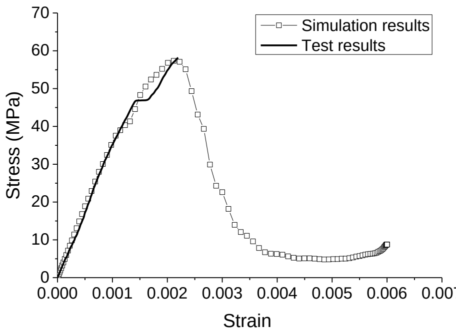

(e) 10^{-1}/s

Fig. 7-9 Experimental and numerical stress-strain curve of MRAC at different strain rate

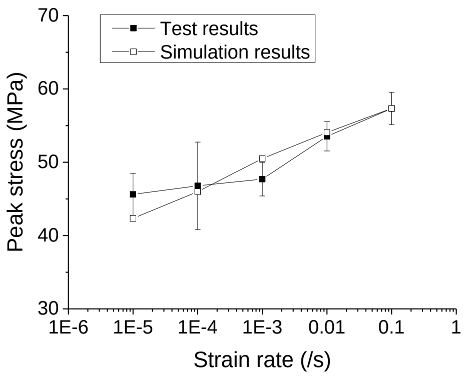

Fig. 7-10 Relationship between the peak stress of MRAC30-30 and strain rate

Fig. 7-10, Fig. 7-11 and Fig. 7-12 compare the change in the peak stress, elastic modulus and peak strain with the strain rate obtained in the test and in the simulation. The results show that the peak stress, elastic modulus and peak strain were close to that in the test results. Moreover, the peak stress, elastic modulus and peak strain in the simulation and test results show a consistent tendency with the increase in the strain rate, i.e., the peak stress and elastic modulus increase with the increase in strain rate, and the peak strain tends to fluctuate with the increase in strain rate.

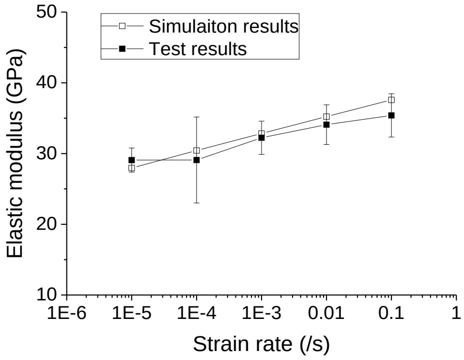

Fig. 7-11 Relationship between the elastic modulus of MRAC30-30 and strain rate

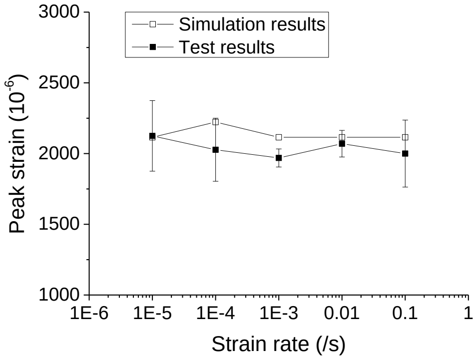

Fig. 7-12 Relationship between the peak strain of MRAC30-30 and strain rate

7.2.2 Failure pattern

In this simulation, the plastic strain was used to reflect the crack distribution, the lateral displacement was used to illustrate the failure pattern. At each strain rate, the plastic strain and lateral displacement of MRAC30-30 are shown in Fig. 7-13. The results show that the microcracks had no obvious difference at different strain rates, and the microcracks were evenly distributed in the new and old ITZ. Microcracks also developed in the mortar until the microcracks propagated through the whole specimen. The plastic strain of the old ITZ was larger than that of the new ITZ, indicating a higher degree of cracking. The failure modes at different strain rates were not significantly different, i.e., there were oblique damage surfaces which mainly passed through the old and new ITZ, and passed through more old ITZs. In general, the simulation results show that the effect of strain rate on the failure mode of RAC was not obvious, and it was consistent with the test results.

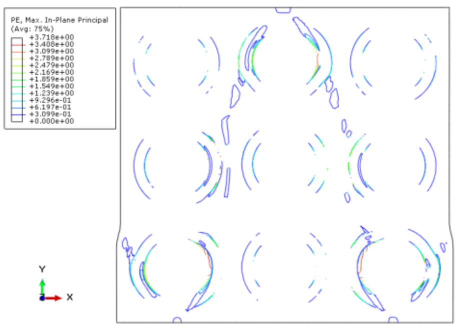

(a) Crack distribution at 10^{-5}/s

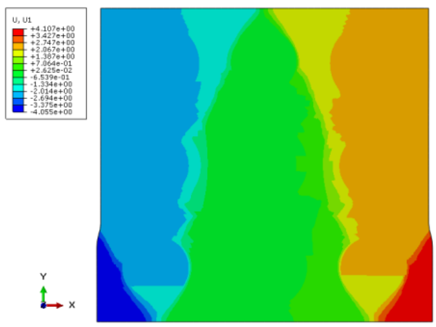

(b) Failure mode at 10^{-5}/s

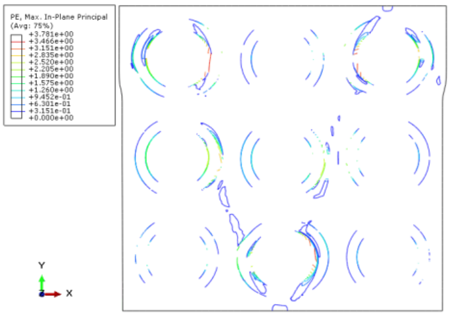

(c) Crack distribution at 10^{-4}/s

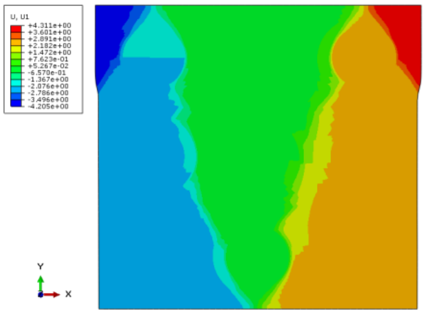

(d) Failure mode at 10^{-4}/s

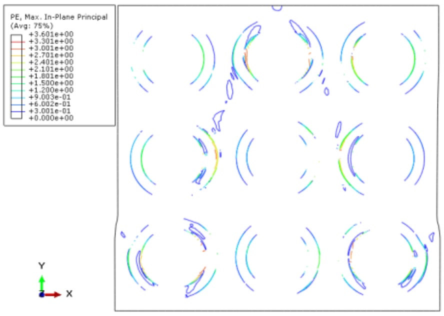

(e) Crack distribution at 10^{-3}/s

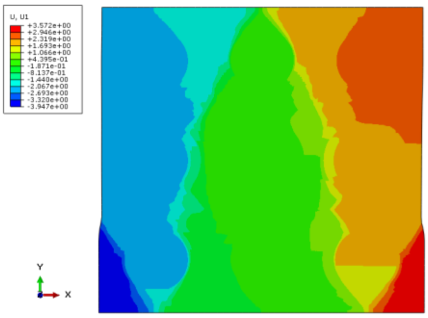

(f) Failure mode at 10^{-3}/s

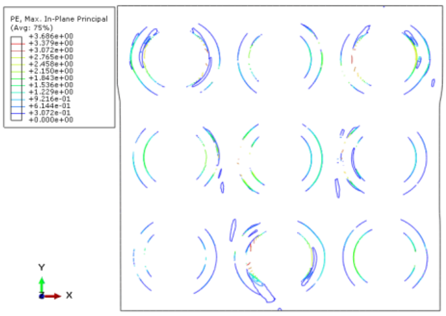

(g) Crack distribution at 10^{-2}/s

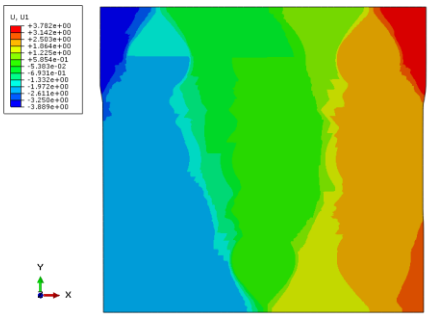

(h) Failure mode at 10^{-2}/s

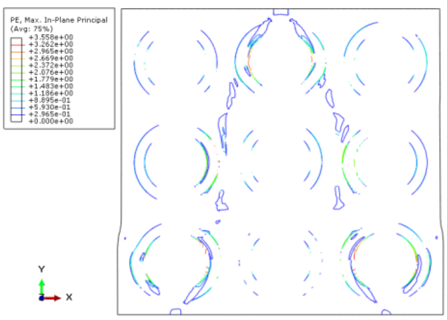

(i) Crack distribution at 10^{-1}/s

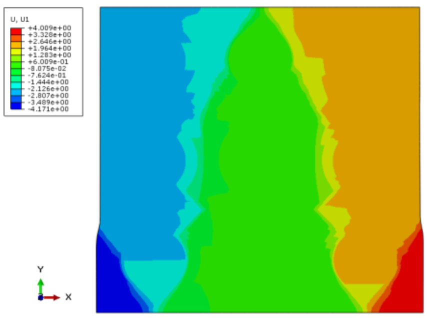

(j) Failure mode at 10^{-1}/s

Fig. 7-13 Crack distribution and failure mode of MRAC30-30 at different strain rates

7.3 Effect of meso-phase materials on the strain-rate sensitivity of RAC

Fig. 7-14 compares the strain-rate sensitivity of peak stress of MRAC30-30 with its constituent meso-materials. It can be noted that the strain-rate sensitivity of MRAC30-30 was higher than that of aggregate and lower than that of mortar and ITZ. In fact, the strain-rate sensitivity of MRAC30-30 can be regarded as the weighted average of the strain-rate sensitivity of its constituent mesoscopic materials, and the weights of each mesoscopic material are different. In order to investigate the effect of mesoscopic materials on the strain-rate sensitivity of RAC, the influences of the strain-rate sensitivity of the aggregate, the mortar and the ITZ on the strain-rate sensitivity of the RAC were studied.

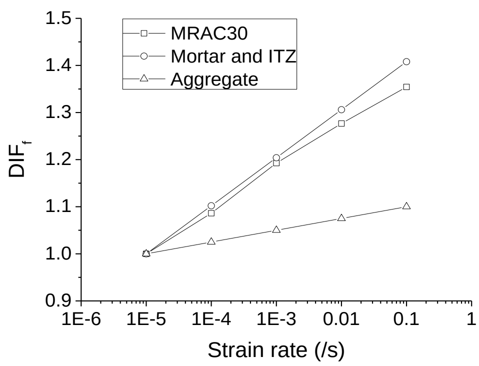

Fig. 7-14 Comparison of the DIF_f of MRAC30-30 with its meso-material

7.3.1 Effect of meso-phase materials on the strain-rate sensitivity of peak stress

The relationship between the DIF_f of RAC and strain rate is shown in Fig. 7-15 when only considering the strain-rate sensitivity of aggregate, mortar and ITZ, respectively. The results show that the DIF_f of RAC had almost no change with the increase in strain rate when only the strain-rate sensitivity of the aggregate was considered. It indicates that the strain-rate sensitivity of the aggregate has little effect on the strain-rate sensitivity of the peak stress of the whole specimen. It is because the aggregate at each strain rate is in an elastic stage which has little effect on the overall peak stress of RAC. When only the strain-rate sensitivity of the ITZ was considered, the DIF_f of RAC increases with the increase in the strain rate, which indicates that it has some effect on the strain-rate sensitivity of the overall peak stress. When only the strain-rate sensitivity of the mortar is considered, the DIF_f of RAC increased significantly with the increase in strain rate, and its growth rate was close to that when considering the strain-rate sensitivity of all the constituent mesophase materials. In general, the strain-rate sensitivity of the mortar in RAC plays a dominant role in the strain-rate sensitivity of the peak stress of RAC.

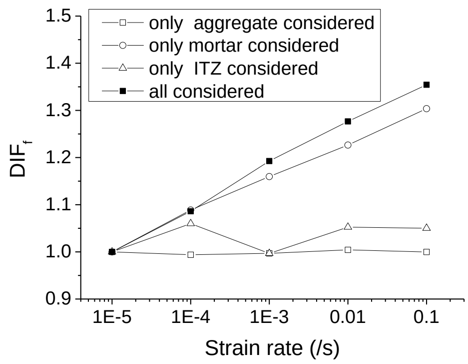

Fig. 7-15 Effect of the strain-rate sensitivity of meso-phase materials on DIF_f of RAC

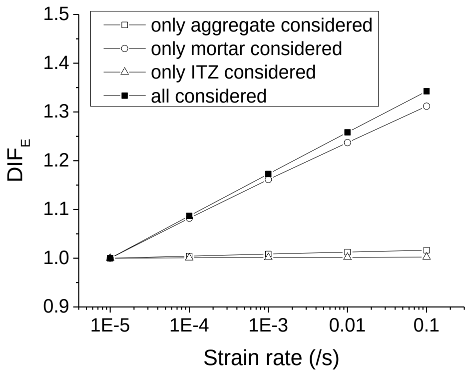

Fig. 7-16 Effect of the strain-rate sensitivity of meso-phase materials on DIF_E of RAC

7.3.2 Effect of meso-phase materials on strain-rate sensitivity of elastic modulus

The relationship between the DIF_E of RAC and strain rate is shown in Fig. 7-16 when only considering the strain-rate sensitivity of aggregate, mortar and ITZ, respectively. The results show that the DIF_E of RAC increased slightly with the increase in strain rate when only the strain-rate sensitivity of aggregate was considered, which indicates that the strain-rate sensitivity of aggregate had some influence on the strain-rate sensitivity of elastic modulus, but the effect was small. When only the strain-rate sensitivity of the iITZ was considered, the DIF_E of RAC slightly increased with the increase in the strain rate, and its growth rate was even smaller than that when considering only the strain-rate sensitivity of aggregate. It indicates that the strain-rate sensitivity of the ITZ has little effect on the strain-rate sensitivity of the overall elastic modulus, and it is much less than its effect on to the strain-rate sensitivity of the overall peak stress. When only the strain-rate sensitivity of mortar was considered, the DIF_E of RAC increased with the increase in strain rate, and its growth rate was close to the condition considering the strain-rate sensitivity of all the constituent meso-phase materials. It indicates that the strain-rate sensitivity of elastic modulus of RAC is mainly affected by the strain-rate sensitivity of the mortar in RAC.

7.3.3 Effect of meso-phase materials on the strain-rate sensitivity of peak strain

The simulation results show that the peak strain was almost unchanged regardless of whether the strain-rate sensitivity of only one meso-material was considered or the strain-rate sensitivity of all the constituent meso-phase materials was considered. This may be due to the fact that the peak strain does not change with the increase in strain rate in the material parameters of the mortar and the ITZ, so that the overall peak strain does not change with the increase in strain rate. It indicates that if the meso-structure of RAC is unchanged, the change in the elastic modulus and peak stress of each phase material will not result in a change in the peak strain of the RAC specimen. However, the peak strain may vary when the meso-structure is different, such as in the RAC specimens with different RCA replacement percentages. This phenomenon will be explained in the following section.

7.4 Effect of RCA replacement percentage on strain-rate sensitivity of RAC

The simulation results of different types of MRACs show that the effect of strain rate on stress-strain curve, peak stress, peak strain, elastic modulus and failure mode was similar to that of MRAC30-30. So it will not be described here. Only the effect of RCA replacement percentage on the dynamic mechanical properties of RAC is given.

7.4.1 Effect of RCA replacement percentage on peak stress and DIF_f

The change in the peak stress of RAC with different RCA replacement percentages with strain rate is shown in Fig. 7-17. The results show that the peak stress of RAC increased linearly with the increase in the strain rate. At the same strain rate, the peak stress of RAC decreased with the increase in the RCA replacement percentage, which is consistent with the static result. That is because with the increase in the RCA replacement percentage, there are more ITZ, Which means that the weak areas of the specimen are more, thus leading to the smaller peak stress.

The change in the DIF_f of RAC with different RCA replacement percentage with the strain rate is shown in Fig. 7-18. It can be noted that the increasing rate of the DIF_f of RAC with 0% RCA was smaller than the DIF_f of RAC with other RCA replacement percentages. When the RCA replacement percentage were 33%, 55%, 66% and 100%, the increasing rate of the DIF_f of RACs at a strain rate of 10^{-1} /s had no obvious difference. It means that the increasing rate of the DIF_f of the RAC does not increase with the increase in the RCA replacement percentage. It can be concluded that the RCA replacement percentage may not be the main factor leading to the strain-rate sensitivity of the peak stress of RAC. At the same time, it indicates that the effect of the RCA replacement percentage on the strain-rate sensitivity of the peak stress of RAC is not determined by the mortar content alone, and the different meso structures may also result in the differences in the strain-rate sensitivity of concrete.

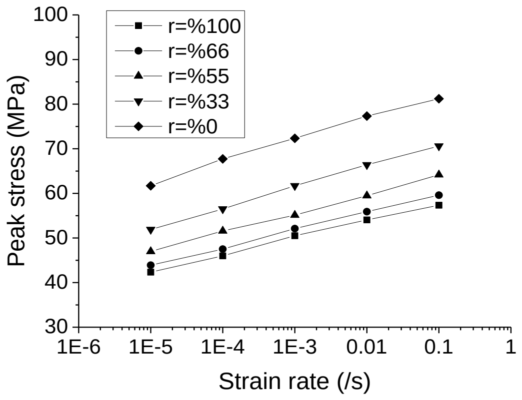

Fig. 7-17 Effect of RCA replacement percentage on the peak stress of RAC

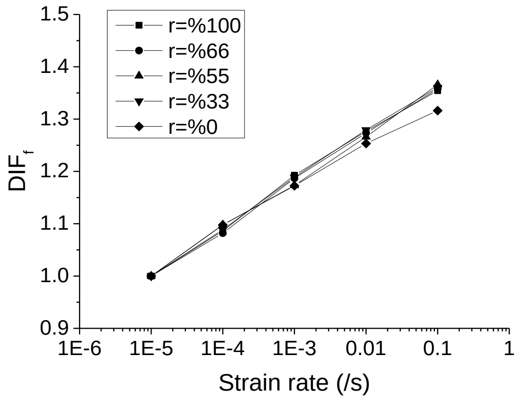

Fig. 7-18 Effect of RCA replacement percentage on the DIF_f of RAC

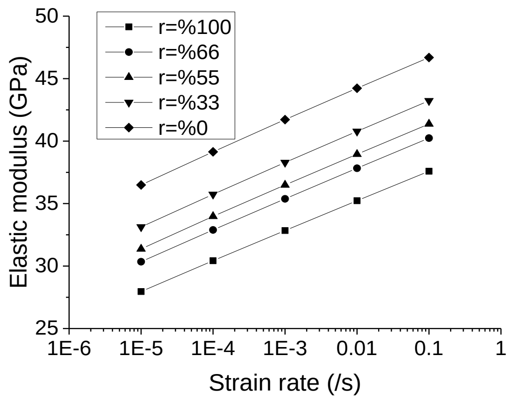

Fig. 7-19 Effect of RCA replacement percentage on the elastic modulus of RAC

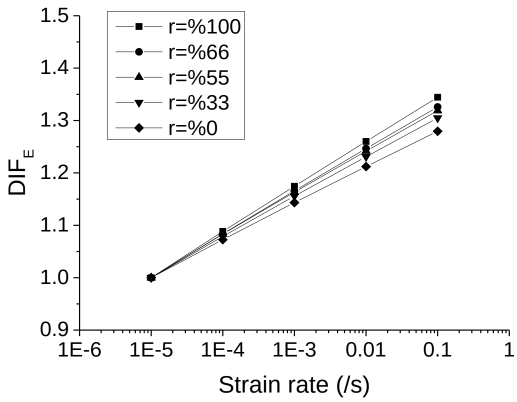

Fig. 7-20 Effect of RCA replacement percentage on the DIF_E of RAC

7.4.2 Effect of RCA replacement percentage on elastic modulus and DIF_E

The relationships between the elastic modulus of RACs with different RCA replacement percentages and the strain rate are shown in Fig. 7-19. The results show that the elastic modulus of all types of RACs increased almost linearly with the increase in strain rate. At the same strain rate, the elastic modulus of RAC decreased with the increase in the RCA replacement percentage, which was consistent with the static result, because the higher the RCA replacement percentage, the higher the content of the mortar and ITZ which has much smallwer elastic modulus compared to the aggregate, so that the overall elastic modulus of the specimen is smaller. The change in the DIF_E of RACs with different RCA replacement percentages with strain rate is shown in Fig. 7-20. It can be noted that with the increase in the RCA replacement percentage, the DIF_E of RAC increased faster. This phenomenon was different from the law of the DIF_f of RAC, which indicates that the effect of RCA replacement percentage on the DIF_E of RAC is mainly determined by the mortar content, and the influence of the constituent mesoscopic structure is not obvious.

7.4.3 Effect of RCA replacement percentage on peak strain

The change in the peak strain of RACs with different RCA replacement percentage with strain rate is shown in Fig. 7-21. The results show that the peak strains of RACs were almost constant with the increase in strain rate. At the same strain rate, the peak strains of RACs with different RCA replacement percentages were different, indicating that the difference in constituent meso-structures will affect the peak strain of RAC. In general, the peak strain of RAC was the largest when the RCA replacement percentage was 0%, but the peak strain of RAC did not show an increasing or decreasing trend with the increase in the RCA replacement percentage. It indicates that other factors may also influence the peak strain of RAC and not the RCA replacement percentage.

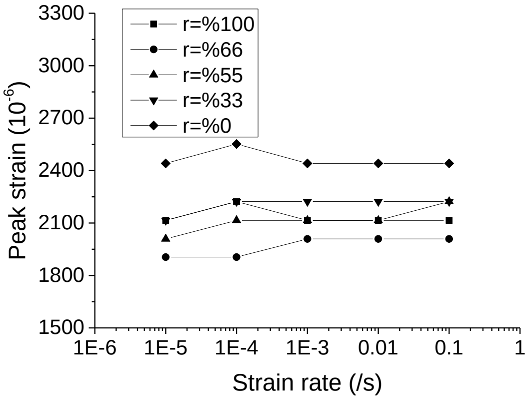

Fig. 7-21 Effect of RCA replacement percentage on the peak strain of RAC

7.5 Effect of new mortar strength on the strain-rate sensitivity of RAC

7.5.1 Effect of new mortar strength on the peak stress and DIF_f of RAC

The relationships between the peak stress of RAsC with three types of new mortars and the strain rate are shown in Fig. 7-22. The results show that the peak stress of the RACs increased with the increase in strain rate, and the peak stress of RAC with higher strength of new mortar was higher under the same strain rate. The relationships between the DIF_f of RACs with three different new mortars and the strain rate and the fitting curves are shown in Fig. 7-23. It can be noted that with the increase in the strength of the new mortar, the increasing rate of the DIF_f of RAC reduced. That is to say, the strain-rate sensitivity of peak stress was smaller. This is because the higher strength of new mortar has lower strain-rate sensitivity, making the overall strain-rate sensitivity lower. The fitting curves of the relationship between the DIF_f of the RACs (i.e., MRAC30-20, MRAC30-30 and MRAC30-40) and the strain rate can be expressed as:

$$DIF_f = 1 + 0.113 \cdot \lg(\dot{\varepsilon} / \dot{\varepsilon}_s) \tag{7-19}$$

$$DIF_f = 1 + 0.0906 \cdot \lg(\dot{\varepsilon} / \dot{\varepsilon}_s) \tag{7-20}$$

$$DIF_f = 1 + 0.0806 \cdot \lg(\dot{\varepsilon} / \dot{\varepsilon}_s) \tag{7-21}$$

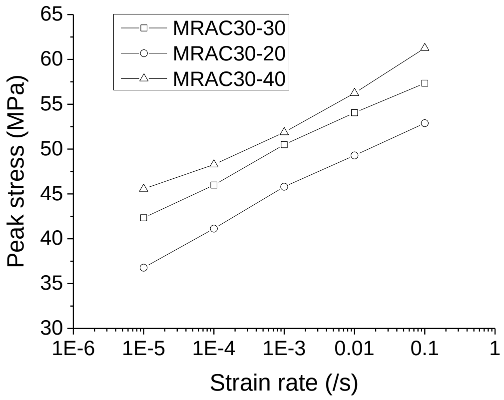

Fig. 7-22 Effect of new mortar strength on the peak stress of RAC

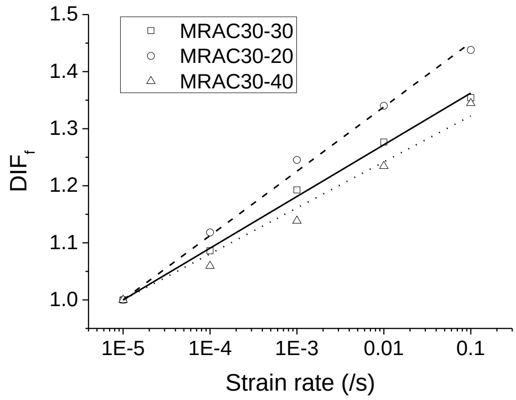

Fig. 7-23 Effect of new mortar strength on the DIF_f of RAC

7.5.2 Effect of new mortar strength on the elastic modulus and *DIF_E* of RAC

The relationships between the elastic modulus of RACs with different new mortars and the strain rate are shown in Fig. 7-24. The results show that the elastic modulus of the RACs increased with the increase in strain rate, and the elastic modulus of RAC with higher strength of new mortar was higher under the same strain rate. The relationship between the DIF_E of the RACs and the strain rate and the fitting curves are shown in Fig. 7-25. The fitting curves of the relationship between the DIF_E of the RACs (i.e., MRAC30-20, MRAC30-30 and MRAC30-40) and the strain rate can be expressed as the following equations.

$$DIF_E = 1 + 0.113 \cdot \lg(\dot{\varepsilon} / \dot{\varepsilon}_s) \tag{7-22}$$

$$DIF_E = 1 + 0.859 \cdot \lg(\dot{\varepsilon} / \dot{\varepsilon}_s) \tag{7-23}$$

$$DIF_E = 1 + 0.594 \cdot \lg(\dot{\varepsilon} / \dot{\varepsilon}_s) \tag{7-24}$$

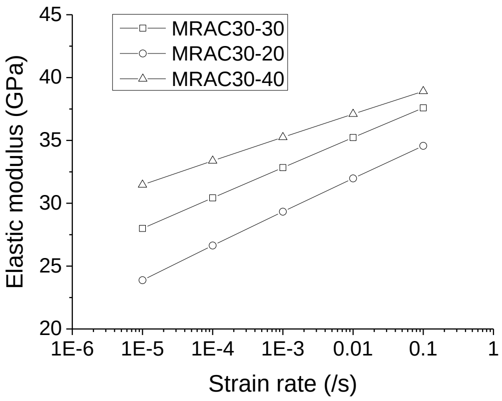

Fig. 7-24 Effect of new mortar strength on the elastic modulus of RAC

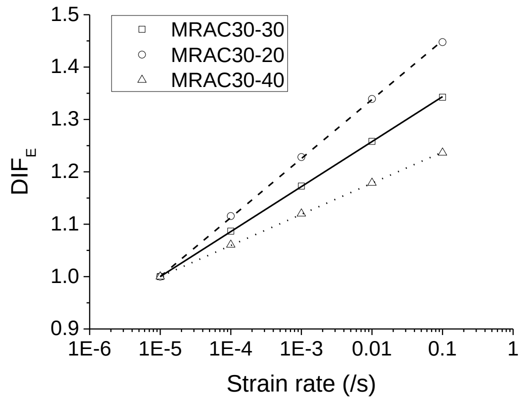

Fig. 7-25 Effect of new mortar strength on the DIF_E of RAC

It can be noted that with the increase in the strength of new mortar, the increasing rate of the DIF_E of RAC was smaller. That is because the higher the strength of the new mortar, the smaller the growth rate of elastic modulus as the strain rate increased, leading to a smaller increasing rate of overall elastic modulus of the RAC specimen. This feature is consistent with the effect of new mortar strength on the peak stress of RAC. However, it can be noted that as the strain rate increased, the elastic modulus showed an almost uniform increasing trend which was different from that of the peak stress. Moreover, the difference in the growth rate of the DIF_E of the RACs with different new mortars was also uniform. This is because the elastic modulus of the specimen as a whole is mainly determined by the elastic modulus of the constituent mesoscopic materials, but the overall peak stress of the specimen is determined by a variety of factors, which is much more complicated.

7.5.3 Effect of new mortar strength on peak strain of RAC

The relationships between the peak strain of RACs with three different new mortars and the strain rate are shown in Fig. 7-26. The results show that the peak strain of the RACs did not increase or decrease with the increase in the strain rate, and it fluctuated almost around a constant value. Therefore, the peak strain of the RAC may be considered to remain the same as the strain rate increases. At the same strain rate, the RAC with lower strength of new mortar had a slightly higher peak strain. This phenomenon shows that the relative difference in strength of the new mortar to the old mortar may be an important factor affecting the peak strain of RAC.

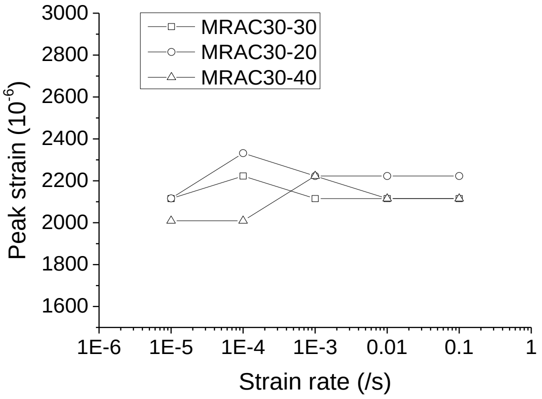

Fig. 7-26 Effect of new mortar strength on the peak strain of RAC

7.6 Effect of old mortar strength on the strain-rate sensitivity of RAC

7.6.1 Effect of old mortar strength on the peak stress and DIF_f of RAC

The relationships between the peak stress of RACs with three different old mortars and the strain rate are shown in Fig. 7-27. The results show that the peak stress of the RACs increased with the increase in the strain rate, and the peak stress of RAC with higher strength of old mortar was higher under the same strain rate. The relationships between the DIF_f of RACs and the strain rate and the fitting curves are shown in Fig. 7-28. The fitting curves of the relationship between the DIF_f of the three RACs (i.e., MRAC20-30, MRAC30-30 and MRAC40-30) and the strain rate can be expressed as follows:

$$DIF_f = 1 + 0.0864 \cdot \lg(\dot{\varepsilon} / \dot{\varepsilon}_s) \tag{7-25}$$

$$DIF_f = 1 + 0.0906 \cdot \lg(\dot{\varepsilon} / \dot{\varepsilon}_s) \tag{7-26}$$

$$DIF_f = 1 + 0.0672 \cdot \lg(\dot{\varepsilon} / \dot{\varepsilon}_s) \tag{7-27}$$

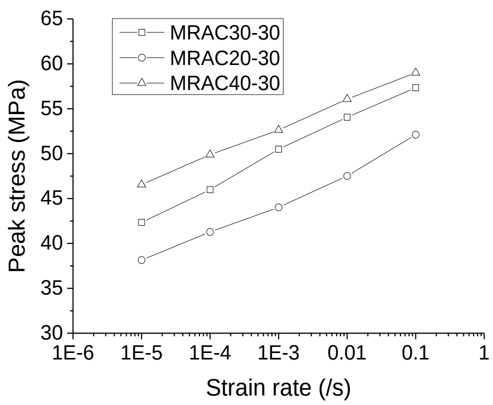

Fig. 7-27 Effect of old mortar strength on the peak stress of RAC

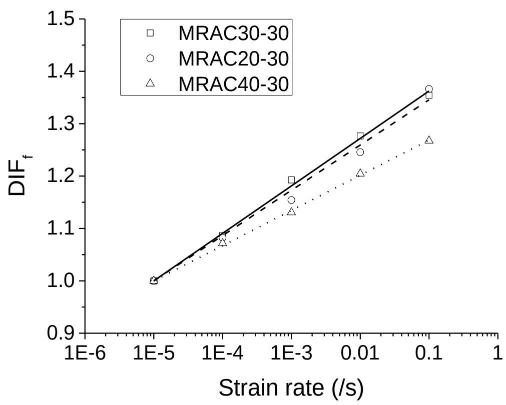

Fig. 7-28 Effect of old mortar strength on the DIF_f of RAC

It can be noted that the DIF_f of MRAC30-30 was the largest. Although the strain-rate sensitivity of the old mortar in MRAC20-30 is greater than that in MRAC30-30, the strain-rate sensitivity of the MRAC20-30 specimen was slightly smaller than that of MRAC30-30. It indicates that the overall strain-rate sensitivity of the RAC specimen does not increase with the increase in the strain-rate sensitivity of old mortar, and the relative strength of the new mortar to the old mortar may also affect the overall strain-rate sensitivity.

7.6.2 Effect of old mortar strength on the elastic modulus and DIF_E of RAC

The relationships between the elastic modulus of RACs with three different old mortars and the strain rate are shown in Fig. 7-29. The results show that the elastic modulus of the RACs increased with the increase in strain rate, and the elastic modulus of RAC with old mortar of higher strength was higher under the same strain rate. The relationships between the DIF_E of RACs and the strain rate and the fitting curves are shown in Fig. 7-30. The fitting curves of the relationships between the DIF_E of the three types of RACs (i.e., MRAC20-30, MRAC30-30 and MRAC40-30) and the strain rate can be expressed as Eq. (7-28), Eq. (7-29) and Eq. (7-30).

$$DIF_E = 1 + 0.1020 \cdot \lg(\dot{\varepsilon} / \dot{\varepsilon}_s) \tag{7-28}$$

$$DIF_E = 1 + 0.0859 \cdot \lg(\dot{\varepsilon} / \dot{\varepsilon}_s) \tag{7-29}$$

$$DIF_E = 1 + 0.0720 \cdot \lg(\dot{\varepsilon} / \dot{\varepsilon}_s) \tag{7-30}$$

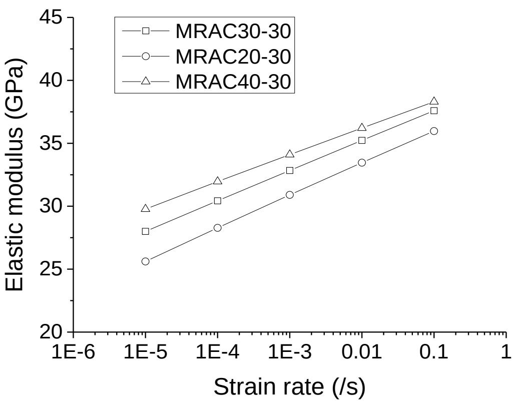

Fig. 7-29 Effect of old mortar strength on the elastic modulus of RAC

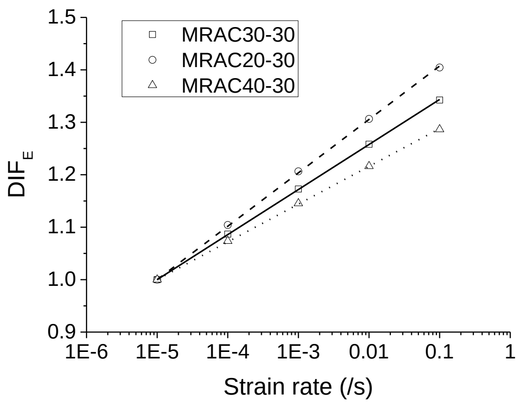

Fig. 7-30 Effect of old mortar strength on the DIF_E of RAC

It can be noted that the effect of the old mortar strength on the DIF_E of RAC was different from that of the DIF_f of RAC. With the increase in the strength of the old mortar, the DIF_E of RAC increased at a slower pace. With the increase in strain rate, the DIF_E of RAC was almost uniformly linearly increasing. In conclusion, the higher the strain-rate sensitivity of the old mortar, the greater the strain-rate sensitivity of the RAC. This is because the overall elastic modulus of the specimen is determined by the elastic modulus of the constituent meso-phase materials, but the factors that determine the overall peak stress of the specimen are more complex.

7.6.3 Effect of old mortar strength on peak strain of RAC

The relationships between the peak strains of RACs with three different old mortars and the strain rate are shown in Fig. 7-31. The results show that the peak strain of the RACs fluctuated almost around a constant value. Therefore, the peak strain of the RACs may be considered to ramain the same as the strain rate increases. At the same strain rate, the peak strain of MRAC40-30 was slightly larger than other two types of RACs. According to this phenomenon, combined with the effect of the new mortar strength on the peak strain, it can be speculated that when the strength of the old mortar is greater than that of the new mortar, the overall peak strain may be improved.

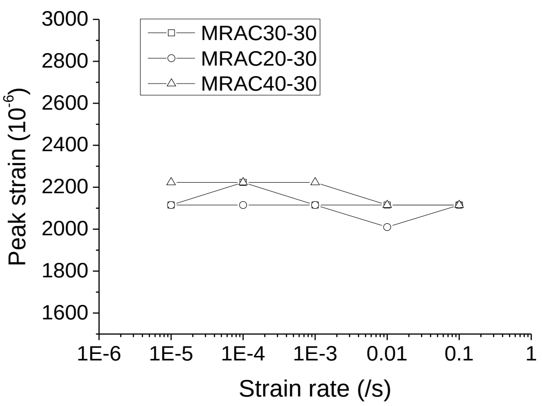

Fig. 7-31 Effect of old mortar strength on the peak strain of RAC

7.6.4 The difference between the effect of new and old mortar strength

Fig. 7-32 and Fig. 7-33 compare the effects of the new and old mortar strength on the DIF_f and DIF_E of the RAC specimen. It can be seen from Fig. 7-33 that the DIF_E of MRAC30-20 was larger than that of MRAC20-30, which indicates that the elastic modulus of RAC with lower strength of new mortar increased faster than that of RAC with lower strength of old mortar. The DIF_E of

MRAC30-40 was smaller than that of MRAC40-30, indicating that the growth rate of the elastic modulus of the RAC with higher strength of new mortar increased slower than that of RAC with higher strength old mortar. In other words, the effect of the strain-rate sensitivity of the new mortar on the DIF_E of the RAC specimen is more significant than that of the old mortar. That is because the content of the new mortar in the RAC is greater than that of the old mortar, which will have a greater effect on the overall elastic modulus. However, it can be seen from Fig. 7-32, the effects of the new and old mortar strength on the DIF_f of the specimen did not show a clear trend which is more significant. In general, because the new mortar content in the RAC specimen is higher than that of the old mortar, the effect of the new mortar on the DIF_E of the RAC is greater, but the influence on the DIF_f is not clear, because the factors affecting the overall peak stress are more complex than the factors that affect the elasticity modulus.

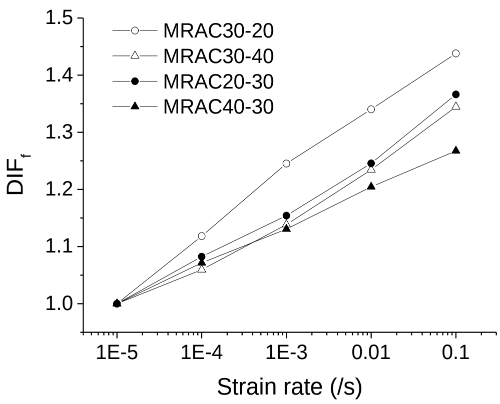

Fig. 7-32 Contrast between the effect of new and old mortar strength on the DIF_f of RAC

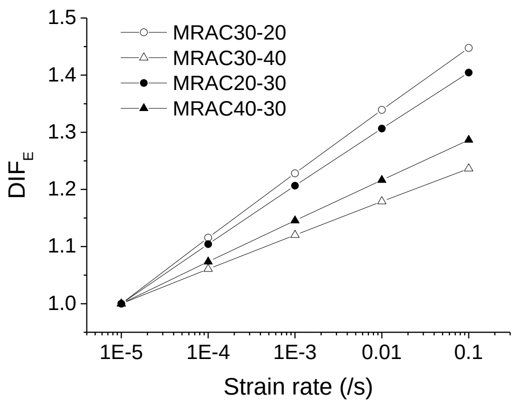

Fig. 7-33 Contrast between the effect of new and old mortar strength on the DIF_E of RAC

7.7 Discussion

In this chapter, we discussed the influence of strain-rate sensitivity of the constituent meso-phase materials, the RCA replacement percentage and the strain-rate sensitivity of new and old mortar strength on the strain-rate sensitivity of RAC. It is found that the influence of these factors on the strain-rate sensitivity of elastic modulus and peak stress are different. This phenomenon will be discussed below in conjunction with the mesoscopic model in Chapter 6.

The elastic modulus of RAC reflects the deformation characteristics in the elastic stage, which can be regarded as the weighted average of the elastic modulus of each constituent mesophase material. The weight is determined by the volume fraction of each mesophase. Therefore, the mortar which has a larger volume fraction plays a more dominant role in the strain-rate sensitivity of the elastic modulus of RAC, and the effect of the ITZ of which the volume fraction is small is not significant; When the RCA replacement percentage is larger, the mortar content in the RAC is higher, which makes strain-rate sensitivity of elastic modulus of RAC larger because the strain-rate sensitivity of the mortar is higher than that of the aggregate; when higher strain-rate sensitivity of the new and old mortar is used, the strain-rate sensitivity of the elastic modulus of RAC is larger.

According to the concrete stochastic constitutive model proposed by Li and Zhang (2001) in Chapter 6, the strength of the concrete specimen is controlled by the strength of the weakest typical unit as shown in Eq. (6-40), by which the following features are explained. First, although the volume fraction of the ITZs is small, they are the weaker parts of the whole RAC specimen, which determines strength based on the weakest constituent unit. Therefore, the strain-rate sensitivity of peak stress of the ITZ will have a certain impact on the strain-rate sensitivity of the peak stress of the RAC specimen, and the effect is more significant than that the strain-rate sensitivity of the elastic modulus. However, although the volume fraction of the aggregate in RAC is large, it has little influence on the strain-rate sensitivity of the peak stress of RAC because the amount of aggregate in the weakest typical constituent unit is very small. Moreover, when the constituent meso-structure of the RAC specimen or the relative strength of constituent meso-phase materials changes, the strength of the weakest constituent unit will also change, indicating that they will affect the overall strength of the RAC specimen. Therefore, although the mortar content is increased when the RCA replacement percentage increased, the strain-rate sensitivity of peak stress did not show an increasing trend as the RCA replacement percentage increased because the constituent meso-structure was also changed. At the same time, when the greater strain-rate sensitivity of the new or old mortar was adopted, the strain-rate sensitivity of the peak stress of RAC did not show a strictly increasing trend because the relative strength of the constituent meso-phase materials was also changed.

7.8 Summary

In this chapter, the strain-rate sensitivity of RAC was simulated by assuming the mechanical properties of the constituent mesophase materials (i.e., mortar, aggregate and ITZ) at each strain rate. First, the simulation results and the experimental results were compared. Then, the influences of the strain-rate sensitivity of the constituent mesophase materials on the strain-rate sensitivity of the RAC specimen were investigated. In addition, the effects of the RCA replacement percentage, the strength of the new or old mortar on the strain-rate sensitivity of RAC were studied. The main conclusions are as follows:

(1) The finite element model can simulate the strain-rate sensitivity of RAC well, and the relationship between the mechanical properties and the strain rate obtained in the simulation was consistent with the experimental results, i.e., the peak stress and elastic modulus increased with the strain rate. The peak strain did not change significantly with the increase in strain rate. There was no obvious difference in the failure patterns of RAC under different strain rates.

(2) The strain-rate sensitivity of the mortar in RAC played a major role in influencing of the strain-rate sensitivity of peak stress and the strain-rate sensitivity of elastic modulus of RAC specimen, while the influence on the strain-rate sensitivity of the ITZ and the aggregate were less obvious.

(3) The greater the RCA replacement percentage, the greater the strain-rate sensitivity of the elastic modulus of RAC; there was no significant difference in the strain-rate sensitivity of RACs when the RCA replacement percentage were 33%, 55%, 66% and 100%, and they were all higher than that of RAC with 0% RCA (namely NAC).

(4) The influences of the strength of the new or old mortar on the strain-rate sensitivity of the peak stress and elastic modulus were different, i.e., the lower the strength of the old or new mortar, the greater the strain-rate sensitivity of elastic modulus of RAC; The strain-rate sensitivity of peak stress of RAC increased with the decrease in the new mortar strength, but it did not show an increasing trend with a decrease in the old mortar strength.

Chapter 8 Conclusion and suggestions for further research

8.1 Conclusions

In this thesis, experimental and theoretical studies on the dynamic mechanical properties of RAC from the low strain rates (10^{-5} /s ~ 10^{-1} /s) to the high strain rates (10^{1} /s ~ 10^{2} /s) were carried out. The model recycled aggregate concrete (MRAC) specimens and cylindrical RAC specimens were used to study the dynamic mechanical properties of RAC at low strain rates. The dynamic mechanical properties RAC with carbonated RCA were also studied. The cylindrical RAC specimens were used to study the dynamic mechanical properties of RAC at high strain rates. The strain-rate sensitivity mechanism of RAC was discussed based on the experimental results. The dynamic mechanical properties of RAC at low strain rates were further studied by numerical simulation. The main conclusions are as follows:

(1) At low strain rates, the stress-strain curves of RACs with different RCA replacement percentages are similar. With the increase in strain rate, the peak stress, elastic modulus and energy absorption capacity increases, the peak strain fluctuates, and the failure modes show no significant differences. The lower the static strength, the larger the strain-rate sensitivity of RAC. The strain-rate sensitivity of RAC with 100% RCA is more significant than that of conventional concrete, but the strain-rate sensitivity of RAC does not show a clear increasing or decreasing tendency with RCA replacement percentages. The peak stress and elastic modulus of RAC in a wet state are smaller than those in an air-dry state. The strain-rate sensitivity of RAC in a wet state has no significant difference with that in an air-dry state. The strain-rate sensitivity of the mortar in the RAC is more significant than that of RAC.

(2) At high strain rates, the peak stress and elastic modulus of RAC increase approximately linearly with the increase in the strain rate while the peak strain fluctuates around a constant value. With the increase in strain rate, the increasing rate of the DIF_f at high strain rates is larger than that at low strain rates. There are more fractured aggregates under impact loading than that under static loading, but the amount is still small. The RCA replacement percentage is not the main factor affecting strain-rate sensitivity of RAC at high strain rates. The strain-rate sensitivity of RAC in a wet state has no significant difference with that in an air-dry state.

(3) The microhardness of the old ITZ and old mortar in RCA can be enhanced through

carbonation, and the enhancement of the old ITZ are more significant. Carbonation of RCA can increase the peak stress and elastic modulus of RAC, and the increase is larger when the w/c is larger. The strain-rate sensitivity of RAC with carbonated RCA at low strain rates is less significant than that of RAC.

(4) At low strain rates, the influence of Stefan effect, inertial effect and crack pattern on the strain-rate sensitivity of RAC is small. It is believed that the strain-rate sensitivity of the crack propagation resistance of the constituent meso-phase materials is the dominant factor affecting the strain-rate sensitivity of RAC. At high strain rates, the effects of Stefan effect and transverse inertial effect on the strain-rate sensitivity of RAC are also small, while the longitudinal inertial effect has some impact, but it is not the dominant factor. The dominant factor for the strain-rate sensitivity of RAC at high strain rates may also be the strain-rate sensitivity of the crack propagation resistance of the constituent meso-phase materials. The contribution of multiple factors is the reason why the DIF_f at high strain rates increase faster than that at low strain rates. The simplified static and dynamic model presented in this thesis can account for why the strain-rate sensitivity of RAC with 100% RCA is greater than that of NAC.

(5) The finite element model developed based on the MRAC can be used to simulate the strain-rate sensitivity of RAC well. The results show that the peak stress and elastic modulus increase with the increase in strain rate, and the elastic modulus increases more uniformly. The strain-rate sensitivity of the mortar plays a major role in the strain-rate sensitivity of the peak stress and elastic modulus of RAC, while the strain-rate sensitivity of the ITZ and the aggregate have less influences. As the RCA replacement percentage increased, the strain-rate sensitivity of the elastic modulus of RAC increases, while the strain-rate sensitivity of the peak stress of RAC specimens does not show a clear tendency. As the strength of the old or new mortar increases, the strain-rate sensitivity of the elastic modulus of RAC decreases, but the strain-rate sensitivity of the peak stress of RAC specimen does not show a clear tendency.

8.2 Suggestions for further research

This thesis makes a prelimilary exploration on the dynamic mechanical behavior of RAC, further researches are needed. The following are some suggestions for the further research.

(1) In this study, both the experimental and numerical results showed that the strain-rate sensitivity of RAC with 100% RCA was more significant than that of conventional concrete, but the strain-rate sensitivity of RAC did not show an increasing tendency with the increase in RCA replacement percentage. The reasons for this need further study.

(2) The experimental result shows that moisture condition has little effect on the strain-rate sensitivity of RAC when the strain rate was varied from 10^{-5} /s to 10^{2} /s, which was consistent with the conclusions of some other researchers. But other scholars reported that the free water in concrete was one of the main factors affecting the strain-rate sensitivity of concrete. Therefore, it is necessary to carry out further experimental study for a more comprehensive understanding on the effect of free water content on the strain-rate sensitivity of RAC.

(3) It is found that when the strain rate is in the range of 10^{-5} /s ~ 10^{2} /s, the Stefan effect and inertia effect which were considered as the important factors for the strain-rate sensitivity of concrete in the past may be not the main factors. In this study, the strain-rate sensitivity of the crack propagation resistance of the constituent meso-phase materials is considered as the main factor, but this has yet to be confirmed. That is to say, the mechanism of the strain-rate sensitivity of RAC is not clear at present, which still needs further study.

(4) The aggregates used in the geometric model of RAC in the simulation were of the same size and uniformly distributed. A change in the size, shape and distribution of the aggregates, a model which more closely resembles the actual constituent meso-structure of RAC needs to be established.

(5) In this study, the numerical simulation on the strain-rate sensitivity of RAC under the low strain rates was carried out. In the future, there is a need to carry out further numerical simulation of the strain-rate sensitivity of RAC under the high strain rates.

(6) The dynamic mechanical properties of RAC under uniaxial compression were explored in this study. In the future, it is necessary to study the dynamic mechanical properties under uni-axial tension, multi-axial compression and tension, etc.

(7) The quality of RCA such as the mortar content in RCA may influence the strain rate sensitivity of RAC, but this factor was not considered in this study. Therefore, the effect of the quality of RCA on the strain rate sensitivity of RAC will be further investigated in the future.

References

Abrams D.A. (1917). Effect of rate of application of load on the compressive strength of concrete. Proceedings, ASTM, 17(part II): 366-374.

ACI Committee 555 (2002). Removal and reuse of hardened concrete [J]. ACI Materials Journal, 99(3): 300-325.

Ahmad S.H., Shah S.E. (1985). Behavior of hoop confined concrete under high strain rates [J]. ACI Journal, 82(5): 634-647.

Asbridge A.H., Page C.L., Page M.M. (2002) Effects of metakaolin, water/binder ratio and interfacial transition zones on the microhardness of cement mortars [J]. Cement and Concrete Research, 32(9): 1365-1369.

Asprone D., Cadoni E., Prota A. (2009). Experimental Analysis on Tensile Dynamic Behavior of Existing Concrete under High Strain Rates [J]. ACI Structural Journal, 106(1): 106-113.

ASTM C33/C33M-13 (2013). Standard Specification for Concrete Aggregates [S]. American Society for Testing and Materials (ASTM), USA.

Atchley B.L., Furr H.L. (1967). Strength and energy absorption capabilities of plain concrete under dynamic and static loadings [J]. ACI Journal, 64: 745-756.

B.C.S.J. (1978). Study on recycled aggregate and recycled aggregate concrete, Building Contractors Society of Japan. Committee on disposal and reuse of concrete construction waste. Summary in Concrete Journal, Japan, 16(7):18-31 (in Japanese).

Barlett F.M., MacGregor J.G. (1993). Effect of moisture condition on concrete core strength [J]. ACI Materials Journal, 91(3): 227-236.

Basnayake B.F.A., Chiemchaisri C., Visvanathan C. (2006). Wastelands: clearing up after the tsunami in Sri Lanka and Thailand [J]. Waste Management World: 31-38.

Bischoff P.H., Perry S.H. (1991). Compressive behavior of concrete at high strain rates [J]. Materials and Structures. 24(6): 425-450.

Bischoff P.H., Perry S.H. (1995). Impact behavior of plain concrete loaded in uniaxial compression. Journal of Engineering Mechanics, 121(6): 685-693.

Brara A., Camborde F., Klepaczko J.R, Mariotti C. (2001). Experimental and numerical study of concrete at high strain rates in tension [J]. Mechanics of Materials, 33(1): 33-45.

Brara A., Klepaczko J.R. (2004). Dynamic tensile behavior of concrete: Experiment and numerical analysis [J]. ACI Materials Journal, 101(2): 162-167.

Brara A., Klepaczko J.R. (2006). Experimental characterization of concrete in dynamic tension [J]. Mechanics of Materials, 38(3): 253-267.

Buyukozturk O., Nilson A.H., Slate F.O. (1971). Stress-strain response and fracture of a concrete model in biaxial loading [J]. ACI Journal, 68(8):590-599.

Cadoni E., Labibes K., Albertini C., et al. (2001). Strain-rate effect on the tensile behaviour of concrete at different relative humidity levels [J]. Materials and Structures, 34(235): 21-26.

Cadoni E., Labibes K., Berra M., et al. (2000). High-strain-rate tensile behaviour of concrete [J]. Magazine of Concrete Research, 52(5): 365-370.

Cadoni E., Solomos G., Albertin C. (2009). Mechanical characterisation of concrete in tension and compression at high strain rate using a modified Hopkinson bar [J]. Magazine of Concrete Research, 61(3): 221-230.

Cai H.Y., Zhang M., Dang L.B. (2012). Experimental study on compressive strength of recycled aggregate concrete with different replacement ratios [J]. Applied Mechanics and Materials, 174-177: 1277-1280.

Chen X., Huang W., Zhou J. (2012). Effect of moisture content on compressive and split tensile strength of concrete[J]. Indian Journal of Engineering & Materials Sciences, 19: 427-435.

Chen X., Wu S., Zhou J. (2013). Experimental and modeling study of dynamic mechanical properties of cement paste, mortar and concrete [J]. Construction and Building Materials, 47: 419-430.

Chen X., Wu S., Zhou J. (2014). Quantification of dynamic tensile behavior of cement-based materials [J]. Construction and Building Materials, 51: 15-23.

Cheng G. (2005). Experimental study on the basic performance of recycled aggregate concrete with different displacement ratio [J]. Concrete, 11: 67-70. (in Chinese)

Code for design of concrete structures (GB50010-2010) [S]. Beijing: China Architecture and Building Press, 2010. (in Chinese)

Comité Eurointernational du Béton (CEB). CEB-FIP Model Code 1990. Thomas Thelford, London, 1993.

Corr D., Accardi M., Graham-Brady L., Shah S. (2007). Digital image correlation analysis of interfacial debonding properties and fracture behavior in concrete [J]. Engineering Fracture Mechanics, 74: 109-121.

Cowell W.L. (1966). Dynamic properties of plain Portland cement concrete [R]. Technical Report No. R447, US Naval Civil Engineering Laboratory, Port Hueneme, California.

Deng Z., Yang H., et.al. (2008). Experimental study on the stress-strain curve of recycled concrete [J]. Concrete, 11: 22-24. (in Chinese)

Dhir P.K., Sangha C.M. (1972). A study of relationships between time, strength, deformation and fracture of plain concrete [J]. Magazine of Concrete Research, 24(81): 197-208.

Dilger W.H., Koch R., Kowalczyk R. (1984). Ductility of plain and confined concrete under different strain rates [J], ACI Journal, 81(l): 73-81.

Domingo-Cabo A., Lázaro C., López-Gayarre F., et al. (2009). Creep and shrinkage of recycled aggregate concrete [J]. Construction and Building Materials, 23: 2545–2553.

Dong Y., Xie H., Zhao P. (1997). Experimental study and constitutive model on concrete under compression with different strain rate [J]. Journal of Hydraulic Engineering, 7: 72-77. (in Chinese)

Du T., Wang W., Liu Z., et al. (2010). The complete stress-strain curve of recycled aggregate concrete under uniaxial compression loading [J]. Journal of Wuhan University of Technology-Materials Science Edition, 25(5): 862-865.

Du X., Jie P., Jin L. (2014). Influence of the interfacial transition zone on concrete failure mode under different loading-rates [J]. Journal of Hydraulic Engineering, 45(S1): 19-23+29. (in Chinese)

Du X., Jin L. (2015). Effect of the interfacial transition zone on the dynamic macroscopic mechanical behavior of concrete [J]. Earthquake Engineering and Engineering Dynamics, 35(1): 11-19. (in Chinese)

Earthquake and explosion resistant engineering research laboratory of Tsinghua University. (1986). The performance of reinforced concrete structural members under impact loading [M]. Beijing: Tsinghua University Press, 1986. (in Chinese)

Eibl J., Schmidt-Hurtienne B. (1999). Strain-rate-sensitive constitutive law for concrete [J]. Journal of Engineering Mechanics, 125(12): 1411-1420.

Elfahal M M., Krauthammer T., Ohno T., et al. (2005). Size effect for normal strength concrete cylinders subjected to axial impact [J]. International Journal of Impact Engineering, 31(4): 461-481.

Elhakam A.A., Mohamed A.E., Awad E. (2012). Influence of self-healing, mixing method and adding silica fume on mechanical properties of recycled aggregates concrete [J]. Construction and Building Materials, 35: 421-427.

Frondistou-Yannas S. (1977). Waste concrete as aggregate for new concrete [J], ACI Journal, 74(8): 373-376.

Geradu J.J.A., Hendriks C.F. (1985). Recycling of road pavement materials in the Netherlands [R]. Rejkswaterstaat communications No. 38, The Hague.

Grote D.L., Park S.W., Zhou M. (2001). Dynamic behavior of concrete at high strain rates and pressures: I. Experimental characterization [J]. International Journal of Impact Engineering, 2001, 25 (9): 869-886.

Guo Z. (2004). Strength and constitutive relation of concrete - principle and Application [M]. Beijing: China Architecture & Building Press, 2004. (in Chinese)

Guo Z., Shi X. (2003). Reinforced Concrete Theory and Analyse [M]. Beijing: Tsinghua University Press. (in Chinese)

Gupta S.M. (2001). Strength Characteristics of concrete made with demolition waste as coarse aggregate [C]. Proceedings of the International Conference on Recent Development in Structural Engineering, Ku rukshetra:364-373.

Harris D.W., Mohorovic C.E., Dolen T.P. (2000). Dynamic properties of mass concrete obtained from dam cores [J]. ACI Materials Journal, 97: 290-296.

Harsh S., Shen Z., Darwin D. (1990). Strain-rate sensitive behavior of cement paste and mortar in compression [J]. ACI Materials Journal, 5(87): 508-516.

Hatano T., Tsutsumi H. (1960). Dynamic compressive deformation and failure of concrete under earthquake load[J]. Proceedings of the Japan Society of Civil Engineering, 67:19-26.

Henrichshen A., Jensen B. (1989). Stykeegenskaber for beton med genanvendelseses-materialer [R]. Internal report.

Hopkinson B. (1914). A method of measuring the pressure in the deformation of high explosives or by the impact of bullets [J]. Proceedings of the Royal Society, 89(612): 411-413.

Hu Q., Song C., Zou C. (2009). Experimental research on the mechanical properties of recycled concrete [J]. Journa of Harbin Institute of Technology, 41(4): 33-36. (in Chinese)

Hu S., Wang D. (2002). Dynamic constitutive relation of concrete under impact [J]. Explosion and Shock Waves, 22(3): 242-446. (in Chinese)

Hu S., Wang D., Liu J. (2001). Experimental study of dynamic mechanical behavior of concrete [J]. Engineering Mechanics, 18(5): 115-119. (in Chinese)

Igarashi S., Bentur A., Mindess S. (1996). Microhardness testing of cementitious materials [J]. Advanced Cement Based Materials, 4(2): 48-57.

Ikeda T., Yamane S. (1988). Strengths of concrete containing recycled aggregate [C]. Proceedings of the Second International RILEM Symposium on Demolition and Reuse of Concrete and Masonry. Tokyo, Japan: 585-594.

Jiang J., Lu X., Ye L. (2005). Finite element analysis of concrete structures [M]. Beijing: Tsinghua University Press0. (in Chinese)

Kashef-Haghighi S., Shao Y.X., Ghoshal S. (2015). Mathematical modeling of CO2 uptake by concrete during accelerated carbonation curing [J]. Cement and Concrete Research, 67: 1-10.

Kawamura M., et al. (1988). Reuse of recycled concrete aggregate for pavement [C]. Proceedings of the Second International RILEM Symposium on Demolition and Reuse of Concrete and Masonry. Tokyo, Japan: 726-735.

Kolsky H. An investigation of the mechanical properties of materials at very high rates of loading [J]. Proceedings of the Physical Society, 1949, 62(11): 676-700.

Kou S.C., Poon C.S. (2010). Properties of concrete prepared with PVA-impregnated recycled concrete aggregate [J]. Cement and Concrete Composites, 32: 649–54.

Kou S.C., Poon C.S., Dixon C. (2007). Influence of fly ash as cement replacement on the properties ofrecycled aggregate concrete [J]. Journal of Materials in Civil Engineering, 19(9): 709-717.

Kou S.C., Poon C.S., Wan H.W. (2012). Properties of concrete prepared with low-grade recycled aggregates [J]. Construction and Building Materials, 36: 881-889.

Kou S.C., Zhan B., Poon C.S. (2014). Use of a CO2 curing step to improve the properties of concrete prepared with recycled aggregates [J]. Cement and Concrete Composites, 45: 22-28.

Lambert D.E., Ross C.A. (2000). Strain rate effect on dynamic fracture and strength [J]. International Journal of Impact Engineering, 24: 985-998.

Lee G.C., Choi H.B. (2013). Study on interfacial transition zone properties of recycled aggregate by micro-hardness test [J]. Construction and Building Materials, 40: 455-460.

Li H., Zhao J., Li T. (2000). Micromechanical modelling of the mechanical properties of a granite under dynamic uniaxial compressive loads [J]. International Journal of Rock Mechanics and Mining Sciences, 37(6): 923-935.

Li H., Zhao J., Li T. (2001). Study of Dynamic Uniaxial Compressive Strength of Rock Material Using Sliding Crack Model [J]. Chinese Journal of Rock Mechanics and Engineering, 20(3): 315-319. (in Chinese)

Li J., Ren X. (2010). A review on the constitutive model for static and dynamic damage of concrete [J]. Advances in Mechanics, (40)3: 284-297. (in Chinese)

Li J., Zhang Q. (2001). Study of Stochastic Damage Constitutive Relationship for Concrete Material [J]. Journal of Tongji University, 29(10): 1135-1141. (in Chinese)

Li L. (2009). Study on Effect of Water Content on Concrete Performance [M]. Beijing: Beijing Jiaotong University. (in Chinese)

Li Q., Meng H. (2003). About the dynamic strength enhancement of concrete-like materials in a split Hopkinson pressure bar test [J]. International Journal of Solids and Structures, 40(2): 343-360.

Li Q., Meng H. (2003). About the dynamics strength enhancement of concrete-like materials in a split Hopkinson pressure bar test [J]. International of Solids and Structures, 2003, 40(2): 343-360.

Li W. (2013). On Multi-Scale Mechanical behaviors of modeled recycled aggregate concrete [D]. Shanghai, Tongji University. (in Chinese)

Li W., Xiao J., Sun Z., et al. (2012). Failure processes of modeled recycled aggregate concrete under uniaxial compression [J]. Cement and Concrete Composites, 34: 1149–1158

Li W., Xiao J., Yuan J. (2011). Stress distribution characteristics of modeled recycled aggregate concrete under uniaxial compression [J]. Journal of Tongji University (Natural Science), 40(6): 906-913. (in Chinese)

Li Z., Wang Q. (2006). Experimental research on effect of loading rate for dynamic fracture toughness of rock [J]. Chinese Journal of Geotechnical Engineering, 12: 2116-2120. (in Chinese)

Liu Q., Xiao J., Sun Z. (2011). Experimental study on the failure mechanism of recycled concrete [J]. Cement and Concrete Research, 41(10):1050-1057

Liu T., Nilson A. (1978). Stress-strain response and fracture of concrete in uniaxial and biaxial compression [J]. ACI Journal, 5(7): 306-312.

Liu W., Xu M., Chen Z. (2014). Parameters Calibration and Verification of Concrete Damage Plasticity Model of ABAQUS [J]. Industrial Construction, S1: 167-171+213. (in Chinese)

Lu Y., Chen X., Teng X., Zhang S. (2014). Dynamic compressive behavior of recycled aggregate concrete based on split Hopkinson pressure bar tests [J]. Latin American Journal of Solids and Structures, 11: 131-141.

Lv P., Song Y. (2002). Dynamic compressive test of concrete and its constitutive model [J]. The Ocean Engineering, 20(2): 43-48. (in Chinese)

Lv P., Song Y., Hou J. (2002). Experimental study and failure criterion of compressive concrete under various loading rates with uniaxial lateral confinement [J]. Engineering Mechanics, 19(5): 67-71. (in Chinese)

Malvar L.J., Ross C.A. (1998). Review of strain rate effects of concrete in tension [J]. ACI Materials Journal, 95(6): 735-739.

Mandal S., Gupta A. (2002). Strength and durability of recycled aggregate concrete [C]. IABSE Symposium Melbourne, Melbourne, Australia, 2002.

Mansur M.A., Chin M.S., Wee T.H. (1999). Stress-strain relationship of high-strength fiber concrete in compression [J]. Journal of Materials in Civil Engineering, 11(1): 21-29.

Mellinger F.M., Birkimer D.L. (1966). Measurement of stress and strain on cylindrical test Specimens of rock and concrete under impact loading [R]. Technical report, U.S. army corps of engineers, Ohio River Division Laboratories, Cincinnati, Ohio, 71:4-46.

Monkman S., ShaoY. (2010). Integration of carbon sequestration into curing process of precast concrete [J]. Canadian Journal of Civil Engineering, 37(2): 302-310.

Morandeau A., Thiery M., Dangla P. Investigation of the carbonation mechanism of CH and C-S-H in terms of kinetics, microstructure changes and moisture properties [J]. Cement and Concrete Research, 2014, 56: 153-170.

Nataraja M.C., Dhang N., Gupta A.P. (1999). Stress-strain curves of steel-fiber reinforced concrete under compression [J]. Cement and Concrete Composites, 21(5-6): 383-390.

Nixon P.J. (1978). Recycled concrete as an aggregate for concrete-a review [J]. Materials and Structures, 11(5): 371-378.

Otsuki N., Miyazato S.I., Yodsudjai W. (2003). Influence of recycled aggregate on interfacial transition zone, strength, chloride penetration and carbonation of concrete [J]. Journal of Materials in Civil Engineering, 15(5): 443-451.

Paliwal B., Ramesh K.T. (2008). An interacting micro-crack damage model for failure of brittle materials under compression [J]. Journal of the Mechanics and Physics of Solids, 56(3): 896-923.

Poon C.S., Shui Z.H., Lam L. (2004). Effect of microstructure of ITZ on compressive strength of concrete prepared with recycled aggregates [J]. Construction and Building Materials, 18(6): 461-468.

Qi C., Qian Q. (2003). Physical Mechanism of Dependence Of Material Strength on Strain Rate For Rock-Like Material [J]. Chinese Journal of Rock Mechanics and Engineering, 22(2): 177-181. (in Chinese)

Rao M.C., Bhattacharyya S.K., Barai S.V. (2011). Behaviour of recycled aggregate concrete under drop weight impact load [J]. Construction and Building Materials, 25(1): 69-80.

Ravindrarajah R., Tam C.T. (1985). Properties of concrete made with crushed concrete as coarse aggregate [J]. Magazine of Concrete Research, 37(130):29-38.

Ravindrarajah R., Tam C.T. (1987). Recycled concrete as fine and coarse aggregates in concrete [J]. Magazine of Concrete Research, 39(141): 214-220.

Reinhardt H.W., Rossi P., van Mier J.G.M. (1990). Joint investigation of concrete at high rates of loading [J]. Materials and Structures, 23(3): 213-216.

Ross C.A., Jerome D.M., Tedesco J.W., Hughes M.L. (1996). Moisture and strain rate effects on concrete strength [J]. ACI Materials Journal, 93(3): 293-300.

Ross C.A., Tedesco J.W., Kuennen S.T. (1995). Effects of strain rate on concrete strength [J]. ACI Materials Journal, 92(5): 37-47.

Rossi P. (1991). Influence of cracking in the presence of free water on the mechanical behavior of concrete [J]. Magazine of Concrete Research, 43(154): 53-57.

Rossi P., Boulay C. (1990). Influence of free water in concrete on the cracking process [J]. Magazine of Concrete Research, 42(152):143-146.

Rossi P., Miex V. (1994). Effect of loading rate on the strength of concrete subjected to uniaxial tension [J]. Material and Structures, 7: 260 -264.

Rossi P., Toutlemonde F. (1996). Effect of loading rate on the tensile behavior of concrete: description of the physical mechanisms [J]. Materials and Structures, 186(29): 116-118.

Rossi P., van Mier J.G.M., Boulay C., et al. (1992). The dynamic behavior of concrete: influence of free water [J]. Materials and Structures, 9(25): 509-514.

Rostasy F.S., Scheuermann J., Sprenger K.H. (1984). Mechanical behaviour of some construction materials subjected to rapid loading and low temperature [J]. Betonwerk, 50(6): 393-401.

Sagoe-Crentsil K.K., Brown T., Taylor A.H. (2001). Performance of concrete made with commercially produced coarse recycled concrete aggregate [J]. Cement and Concrete Research, 31(5): 707-712.

Shah S.P., Winter G. (1966). Inelastic behavior and fracture of concrete [J]. ACI Journal, 1966, 63(9): 925-930.

Shang R.J. (1994). Dynamic constitutive behavior of concrete [D]. Dalian: Dalian University of Technology. (in Chinese)

Shkolnik I.E. (2008). Influence of high strain rates on stress-strain relationship, strength and elastic modulus of concrete [J]. Cement & Concrete Composites, 30(10): 1000-1012.

State General Administration of the People's Republic of China for Quality Supervision and Inspection and Quarantine (AQSIQ) and Standardization Administration of the People's Republic of China (SAC). (2011). GB/T14685. Pebble and crushed stone for construction [S]. Beijing: China Standards Press. (in Chinese)

Sukontasukkul P.，Nimityongskul P.，Mindess S. (2004). Effect of loading rate on damage of concrete [J]. Cement and Concrete Research, 34(11): 2127-2134

Takeda J., Tachikawa H. (1972). Deformation and fracture of concrete subjected to dynamic load [C]. Proceedings of the Conference on Mechanical Behavior of Materials, Kyoto: Society of Materials Science, 267-277.

Tam V.W.Y., Gao X.F., Tam C.M. (2005). Microstructural analysis of recycled aggregate concrete produced from two-stage mixing approach [J]. Cement and Concrete Research, 35: 1195-1203.

Tang T., Saadatmanesh H. (2003). Behavior of concrete beams strengthened with fiber-reinforced polymer laminates under impact loading [J]. Journal of Composites for Construction, 7(3): 209-218.

Tasuji M.E, Slate F.O, Nilson A.H. (1972). Stress-strain response and frscture of concrete in biaxial loading [J]. ACI Journal, 69(5):291-295.

Tedesco J.W., Powell J.C., Ross C.A., et al．(1997). A strain-rate-dependent concrete material model for ADINA [J]. Computers and Structures, 64(5/6): 1053-1067.

Tedesco J.W., Ross C.A., Kuennen S.T. (1993). Experimental and numerical analysis of high strain rate splitting tensile tests [J]. ACI Materials Journal, 90: 162-169.

Tedeseo J.W., Ross C.A. (1994). Numerical Analysis of High strain-Rate Concrete Direct Tension Tests [J]. Computers and Structures, 40(2):313-327

Topcu I.B., Guncan, N.F. (1995). Using waste concrete as aggregate [J]. Cement and Concrete Research, 25(7):1385-1390.

Topçu I.B., Sengel S. (2004). Properties of concretes produced with waste concrete aggregate [J]. Cement and Concrete Research, 34(8): 1307-1312.

Tregger N., Corr D., Graham-Brady L., Shah S. (2006). Modeling the effect of mesoscale randomness on concrete fracture [J]. Probabilistic Engineering Mechanics, 21: 217-225.

Van Mier J.G.M., Shah S.P., Arnaud M., et al. (1997). Strain-softening of concrete in uniaxial compression [J]. Materials ane Structures, 30(4):195–209.

Wang H., Li Q. (2006). Micro-mechanism of static and dynamic strengths for saturated concrete [J]. Journal of Hydraulic Engineering, 37(8): 958-962. (in Chinese)

Wang H., Li Q. (2007). Experiments of the compressive properties of dry and saturated concrete under different loading rates [J]. Journal of Hydroelectric Engineering, 1: 84-89. (in Chinese)

Wang L. (2005). Stress wave Foundation [M]. Beijing: National Defence Industry Press. (in Chinese)

Wang S., Zhang M., Quek S.T. (2011). Effect of specimen size on static strength in dynamic increase factor of high-strength concrete strength from SHPB test [J]. Journal of Testing and Evaluation, 39(5): 898-907.

Wang Z., Liu Y., Shen R. (2008). Stress-strain relationship of steel fiber-reinforced concrete under dynamic compression [J]. Construction and Building Materials, 22(5): 811-819.

Wastein D. (1953). Effect of straining rate on the compressive stress and elastic property of concrete [J]. ACI Journal Proceedings, 49(4): 729-744.

Watson A.J., Hughes B.P. (1985). Compressive strength and ultimate strain of concrete under impact loading [J]. Magazine of concrete Research, 30(105): 189-199.

Wesche K., Schulz R. (1982). Beton aus aufbereitetem Altbeton Technologie und Eigenschaften[J]. Beton, 32(2): 64-68.

Wittmann F.H. (1973).Interaction of hardened cement paste and water [J]. Journal of the American Ceramic Society, 56(8): 409-415.

Wu S., Chen X., Zhou J. (2012). Influence of strain rate and water content on mechanical behavior of dam concrete [J]. Construction and Building Materials, 36(4): 448-457.

Wu S., Zhou J., Chen H. (2010). Unified model and mechanism for dynamic tensile strength increase in concrete base on its microstructure characteristics [J]. Journal of Hydraulic Engineering, 41(4): 419-428. (in Chinese)

Wu X., Li Y., Li H. (2010). Research on the material constants of the HJC dynamic constitutive model for concrete [J]. Chinese Journal of Applied Mechanics, 2: 340-344, 443. (in Chinese)

Xiao J. (2007). Experimental Investigation on Complete Stress-Strain Curve of Recycled Concrete Under Uniaxial Loading [J]. Journal of Tongji University (Natural Science), 35(11): 1445-1449. (in Chinese)

Xiao J. (2008). Recycled concrete [M]. Beijing: China Architecture & Building Press. (in Chinese)

Xiao J., Lan Y. (2006). Investigation on the tensile behavior of recycled aggregate concrete [J]. Journal of Building Materials, 9(2): 154-158. (in Chinese)

Xiao J., Lei B., Wang C. (2008). Concrete waste recycled as products in Wenchuan Earthquake-hit area [C]. The first national conference on recycled concrete research and application, China, Shanghai, 2008: 63-66.

Xiao J., Li J. (2005). Study on relationships between strength indexes of recycled concrete [J]. Journal of Building Materials, 9(2): 197-201. (in Chinese)

Xiao J., Li J., et.al. (2004). Study on compressive strength of recycled aggregate concrete [J]. Journal of Tongji University (Natural Science), 32(12): 1558-1561. (in Chinese)

Xiao J., Li J., Sun Z. (2004). Study on compressive strength of recycled aggregate concrete [J]. Journal of Tongji University (Engineering Science Edition), 32(12): 1558-1561. (in Chinese)

Xiao J., Li J., Zhang Ch. (2005). Mechanical properties of recycled aggregate concrete under uniaxial loading [J]. Cement and Concrete Research, 35(6): 1187-1194.

Xiao J., Li L., Shen L., Poon C.S. (2015). Compressive behaviour of recycled aggregate concrete under impact loading [J]. Cement and Concrete Research, 71: 46-55.

Xiao J., Li W., Corr D.J., Shah S.P. (2013). Effects of interfacial transition zones on the stress -strain behavior of modeled recycled aggregate concrete. Cement and Concrete Research, 52: 82-99.

Xiao J., Li W., Corr D.J., Shah S.P. (2013). Simulation study on the stress distribution in modeled recycled aggregate concrete under uniaxial compression [J]. Journal of Materials in Civil Engineering, 25(4): 504-518.

Xiao J., Li W., Sun Z., et al. (2012). Crack Propagation in Recycled Aggregate Concrete under Uniaxial Compressive Loading [J]. ACI Materials Journal, 109(4): 451-462.

Xiao J., Li W., Sun Z., Lange D.A., Shah S.P. (2013). Properties of interfacial transition zones in recycled aggregate concrete tested by nanoindentation [J]. Cement and Concrete Composites, 2013, 37: 276-292.

Xiao J., Li W., Yuan J. (2011). Meso-level numerical simulation on mechanical properties of modeled recycled concrete under uniaxial compression [J]. Journal of Tongji University (Natural Science), 39(6): 791-797. (in Chinese)

Xiao J., Lin Z., Zhu Jun. (2016). Effects of Recycled Aggregates' Gradation on Compressive Strength of Concrete [J]. Journal of Sichuan University (Engineering Science Edition), 46(4): 154-160. (in Chinese)

Xiao S., Li H., Monteiro P.J.M. (2011). Influence of strain rates and loading histories on the compressive damage behaviour of concrete [J]. Magazine of Concrete Research, 12(63): 915-926.

Xiao S., Lin G., et al. (2001). Effects of strain rate on dynamic behavior of concrete in tension [J]. Journal of Dalian University of Technology, 41(6): 721-725. (in Chinese)

Xiao S., Lin G., et al. (2002). Effect of strain rate on dynamic behavior of concrete in compression [J]. Journal of Harbin University of Civil Engineering and Architecture, 35(5): 35-39. (in Chinese)

Xiao S., Zhang J. (2010). Compressive damage experiment of concrete at different strain rates [J]. China Civil Engineering Journal, 43(3): 40-45. (in Chinese)

Xiao Y., Shan J., Zheng Q., et al. (2009). Experimental studies on concrete filled steel tubes under high strain rate loading [J]. Journal of Materials in Civil Engineering, 21(10): 569-577.

Xuan D., Zhan B., Poon C.S. (2016). Assessment of mechanical properties of concrete incorporating carbonated recycled concrete aggregates [J]. Cement and Concrete Composites, 65: 67-74

Yan D. (2006). Experimental and theoretical study on the dynamic properties of concrete [D]. Dalian: Dalian University of Technology. (in Chinese)

Yan D., Lin G. (2005). Experimental study on the uniaxial dynamic compression properties of concrete [J]. Hebei Water Resources and Hydropower Engineering, 6: 8-10. (in Chinese)

Yan D., Lin G. (2006). Dynamic properties of concrete in direct tension [J]. Cement and Concrete Research, 36(7): 1371-1378.

Yan D., Lin G. (2006). Study on dynamic compressive properties of concrete with different loading paths [J]. Journal of Hydraulic Engineering, 2006, 3:360-364. (in Chinese)

Yan D., Lin G., et.al. (2006). Experimental study of dynamic compressive properties of concrete under different environments [J]. Journal of Dalian University of Technology, 05: 707-711. (in Chinese)

Yoda K., Yoshikane T. (1988). Recycled cement and recycled aggregate concrete in Japan [C]. Proceedings of the second international RILEM symposium on demolition and reuse of concrete and masonry. Tokyo, Japan: 527-536.

Yon J.H., Hawkins N.M., Kobayashi A.S. (1992). Strain-rate sensitivity of concrete mechanical properties [J]. ACI Material Journal, 89: 146-153.

Yurtdas I., Burlion N., Skoczylas F. (2004). Experimental characterization of the drying effect on uniaxial mechanical of mortar [J]. Materials and Structures, 37:170-176.

Zeng S. (2012). Dynamic Experimental Research and Stochastic Damage Constitutive Model for Concrete [D]. Shanghai, Tongji University. (in Chinese)

Zeng S., Li J. (2013). Experimental study on uniaxial compression behavior of concrete under dynamic loading [J]. Journal of Tongji University (Natural Science), 41(1): 7-10. (in Chinese)

Zeng S., Ren X., Li J. (2013). Triaxial behavior of concrete subjected to dynamic compression [J]. Journal of Structural Engineering, 139: 1582-1592.

Zhai Y., Ma W., et.al. (2007). Comparison of Dynamic Capabilities of Granite and Concrete Under Uniaxial Impact Compressive Loading [J]. Chinese Journal of Rock Mechanics and Engineering, 26(4): 762-768. (in Chinese)

Zhai Y., Zhao J., Men Y. (2009). Analysis on the dynamic tension strength of granite and concrete materials under high strain-rate [J]. Journal of Xi'an University of Architecture & Technology (Natural Science Edition), 41(3): 334-339. (in Chinese)

Zhan B., Poon C.S., Liu Q., Kou S.C., Shi C. (2014). Experimental study on CO2 curing for enhancement of recycled aggregate properties [J]. Construction and Building Materials, 67: 3-7.

Zhang J., Shi C., et al. (2015). Performance enhancement of recycled concrete aggregates through carbonation [J]. Journal of Materials in Civil Engineering, 27(11): 04015029.

Zhang Y., Zhu D., et.al. (2015). Dynamic mechanical properties of dry and saturated concretes and their mechanism [J]. Explosion and Shock Waves, 35(6): 864-870. (in Chinese)

Zhang Z., Kou S.,Yu J., et al. (1999). Effects of loading rate on rock fracture [J]. International Journal of Rock Mechanics and Mining Sciences, 36(5): 597-611.

Zheng S., Haussler-Combe U., Eibl J. (1999). New approach to strain rate sensitivity of concrete in compression [J]. Journal of Engineering Mechanics, 125(12): 1403-1410.

Zhou J., Chen X., WU L., Kan X. (2011). Influence of free water content on the compressive mechanical behaviour of cement mortar under high strain rate [J]. Sadhana: Academy Proceeding in Engineering Sciences, 36(3): 357-369.

Zhou J., Ding N. (2014). Moisture effect on compressive behavior of concrete under dynamic loading [J]. Journal of Central South University, 21(12): 4714-4722.

Zielinski A.J., Reinhardt H.W., Kormeling H.A. (1981). Experiments on concrete under impact tensile loading [J]. Materials and Structures, 14(2): 103-112.